Quantum state engineering and stabilization

Zaki Leghtas

ParisTech
INSTITUT DES SCIENCES ET TECHNOLOGIES
PARIS INSTITUTE OF TECHNOLOGY

MINES ParisTech

École doctorale 432: Sciences et Métiers de l'Ingénieur

Doctorat ParisTech

T H È S E

pour obtenir le grade de docteur délivré par

l'École nationale supérieure des mines de Paris

Spécialité Mathématique et Automatique

présentée et soutenue publiquement par

Zaki LEGHTAS

27 Septembre 2012

Préparation et stabilisation de systèmes quantiques

Directeur de thèse: **Pierre ROUCHON**
Co-encadrement de thèse: **Mazyar MIRRAHIMI**

Jury

J.M. CORON, Professeur, Institut universitaire de France	Rapporteur
S. GIRVIN, Professeur, Yale University	Rapporteur
J.M. RAIMOND, Professeur, Ecole Normale Supérieure	Président
C. ALTAFINI, Assistant professeur, SISSA-ISAS	Examinateur
B. HUARD, Chargé de recherche, Ecole Normale Supérieure	Examinateur
M. MIRRAHIMI, Directeur de recherche, INRIA Rocquencourt	Examinateur
P. ROUCHON, Professeur, MINES ParisTech	Examinateur
G. TURINICI, Professeur, Université Paris Dauphine	Examinateur

MINES ParisTech
Centre Automatique et Systèmes
60-62, Boulevard Saint Michel 75272 PARIS cedex 06 FRANCE

THÈSE

ParisTech
INSTITUT DES SCIENCES ET TECHNOLOGIES
PARIS INSTITUTE OF TECHNOLOGY

MINES ParisTech

École doctorale 432: Sciences et Métiers de l'Ingénieur

ParisTech Doctorate

T H E S I S

to obtain the

Doctor's degree from the Ecole nationale supérieure des Mines de Paris

Speciality "Mathematics and Control"

defended in public by

Zaki LEGHTAS

September, 27^{th}, 2012

Quantum state engineering and stabilization

Advisor: **Pierre ROUCHON**
Co-advisor: **Mazyar MIRRAHIMI**

Jury

J.M. CORON, Professor, Institut universitaire de France	Referee
S. GIRVIN, Professor, Yale University	Referee
J.M. RAIMOND, Professor, Ecole Normale Supérieure	Chair
C. ALTAFINI, Assistant professor, SISSA-ISAS	Examiner
B. HUARD, Chargé of research, Ecole Normale Supérieure	Examiner
M. MIRRAHIMI, Director of research, INRIA Rocquencourt	Examiner
P. ROUCHON, Professor, MINES ParisTech	Examiner
G. TURINICI, Professor, Université Paris Dauphine	Examiner

MINES ParisTech
Centre Automatique et Systèmes
60-62, Boulevard Saint Michel 75272 PARIS cedex 06 FRANCE

THÈSE

Acknowledgments

I would like to express my gratitude to Mazyar Mirrahimi and Pierre Rouchon for being remarkable advisors. It was an immense honor to work with them during these last three years, and I hope that this is only the beginning of a much longer collaboration.

I would like to thank Alain Sarlette, with whom I had the pleasure of working with on two of the main projects of my PhD. It is while working with Alain that I took my first steps in adiabatic theory and quantum optics. I am looking forward to our future work together. I would also like to thank Alexei Goun, for teaching me everything I know about experimental femtosecond quantum control, for being so patient and encouraging while we were doing experiments, and for the endless discussions about science we used to have during our lunch breaks.

I would like to thank all my collaborators: Roberto Rey De Castro, Gabriel Turinici, Jean Michel Raimond, Michel Brune, Rob Schoelkopf, Brian Vlastakis, Gerhard Kirchmair and Kurtis Geerlings.

I am very grateful to Herschel Rabitz for inviting me in his research group in Princeton for over a year. I very much enjoyed my time in Princeton, and learnt a lot from discussing with all members of the group. Hersch always encouraged me to pursue my ideas, and allowed me to do experiments in his laboratory. I am also very grateful to Michel Devoret for welcoming me in his lab in Yale for three months, and introducing me to the fascinating world of quantum circuits. I am very excited about pursuing the projects we started over the next couple of years.

I would like to thank Steve Girvin and Jean-Michel Coron for accepting to be my referees, and Benjamin Huard, Jean-Michel Raimond, Claudio Altafini and Gabriel Turinici for accepting to be members of my jury. Their comments and questions helped improve this manuscript, and got me thinking in new directions.

Finally, I would like to thank all members of Sisyphe (INRIA), Qulab and RSL (Yale), and the Rabitz group (Princeton). In particular, I am very grateful to all members of the CAS (Mines ParisTech). The CAS is a truly remarkable place to work in, offering both a very stimulating and pleasant working environment.

Résumé

Cette thèse aborde le problème de préparation et de stabilisation d'états non classiques de systèmes quantiques, ainsi que l'identification d'Hamiltonien. La plupart des méthodes que nous proposons ont été développées en étroite collaboration avec des expérimentateurs. Quelques-unes de ces idées ont déjà été implémentées au laboratoire.

Premièrement, nous avons démontré un résultat d'observabilité pour l'identification d'Hamiltonien. Nous considérons une expérience de contrôle quantique avec des lasers femtoseconde: une observable est mesurée après que le système (typiquement un nuage d'atomes) ait interagi avec un champ laser (notre contrôle). Nous posons le problème d'établir s'il existe un ensemble de contrôles qui fourniraient une information suffisante pour la reconstruction de la matrice de moment dipolaire. Nous démontrons que sous certaines conditions, il existe en effet des contrôles (en analogie avec l'interférométrie de Ramsey) qui rendent le moment dipolaire localement observable. Le reste de la thèse traite des problèmes de préparation et de stabilisation d'états quantiques.

La deuxième contribution est sur le contrôle d'ensemble. Nous proposons un contrôle robuste qui effectue une permutation sur un ensemble de systèmes en échelle. La force de ce résultat qui est basé sur la théorie adiabatique, est que ce contrôle à lui seul, permet d'effectuer une permutation de tout un ensemble de systèmes ayant des paramètres différents. Les résultats sont basés sur une étude mathématique détaillée qui donne des bornes d'erreurs.

Troisièmement, nous nous intéressons à la stabilisation par dissipation contrôlée en électrodynamique quantique en cavité. Nous décrivons une expérience où des atomes interagissent un par un avec un ou deux modes de la cavité. Nous trouvons un contrôle à appliquer durant chaque interaction entre atome et cavité, qui permet de stabiliser les modes de la cavité dans un état cible prédéterminé. En particulier, nous pouvons stabiliser un état intriqué de deux modes de la cavité qui permettrait une violation des inégalités de Bell pour des temps arbitrairement grands. Cette proposition est appuyée par des simulations numériques et une preuve de convergence en dimension infinie (pas de troncature de l'espace d'Hilbert à un nombre de photons fini).

Quatrièmement, nous proposons des contrôles pour la préparation d'états quantiques dans des circuits Josephson (également appelés circuits quantiques). Nous considérons un qubit supraconducteur couplé à un résonateur micro-onde, et nous décrivons une séquence de pulses qui permettrait de construire toute superposition d'états cohérents quasi-orthogonaux dans la cavité, des états intriqués de deux modes de la cavité, et des états intriqués de plusieurs qubits. De récents résultats expérimentaux sont en bon accord avec les prédictions de nos simulations.

La dernière contribution est sur la correction d'erreur quantique. Ceci peut être vu comme la stabilisation d'un espace d'états de dimension deux. Nous proposons d'encoder un bit d'information quantique dans deux états orthogonaux de la cavité. La décohérence induit des sauts qui modifient l'information encodée. Nous pro-

posons une séquence de pulses qui permettrait de rétablir cette information dans l'état de la cavité. Ceci pourrait prolonger la durée de vie d'un qubit de presque un ordre de grandeur. Le grand intérêt de cette proposition est double. Premièrement, elle nécessite un nombre de composants physiques minimal: seulement un qubit fortement couplé (dans le régime dispersif) à un mode de la cavité. Deuxièmement, nous avons des séquences de pulses pour l'encodage d'un qubit dans la cavité, la correction de l'état de la cavité suite à un saut quantique, et enfin le décodage de l'état de la cavité vers l'état du qubit.

Abstract

This thesis tackles the problem of preparing and stabilizing highly non classical states of quantum systems, as well as identifying their Hamiltonian. Most of the methods we propose were developed in close collaboration with experimentalists. Some of these ideas have already been implemented in the laboratory.

First, we derived an observability result for Hamiltonian identification. We consider a typical setting in ultra-fast quantum control experiments where an observable is measured after a system (e.g a cloud of atoms) has interacted with a controlled electric field. We thus pose the problem of whether we can find a set of controls which would provide sufficient information to reconstruct the dipole moment matrix. We prove that under certain conditions, we can find controls (in analogy with Ramsey interferometry) which make the dipole moment matrix locally observable. The rest of the thesis is devoted to quantum state engineering and stabilization.

The second contribution is on ensemble control. We propose a robust control which performs any state permutation on an ensemble of quantum ladder systems. The strength of this result which is based on adiabatic theory, is that this single control performs the same permutation on an ensemble of different systems. The results are based on a detailed asymptotic mathematical analysis giving error bounds.

Third, we address the problem of quantum state stabilization by reservoir engineering in the context of cavity quantum electrodynamics (QED). We describe an experiment where flying atoms successively interact with one or two cavity modes. We find a control to apply during each atom-cavity interaction which would drive and stabilize the cavity modes close to a predefined non-classical target state. In particular, we are able to stabilize an entangled state which would lead to a violation of Bell's inequality for arbitrarily large times. The proposal is supported by numerical simulations and a first mathematical convergence analysis, where the Hilbert space is infinite dimensional (no truncation to a finite number of photons).

Fourth, we introduce a control which performs quantum state preparation in the context of Josephson circuits (also called circuit QED). We consider one superconducting qubit coupled to a microwave resonator and describe a sequence of pulses which would generate any superposition of quasi-orthogonal coherent states, entangled states of two cavity modes and multi-qubit entangled states. Recent preliminary results in the laboratory are in good agreement with our simulation predictions.

The last contribution is to quantum error correction. This may be viewed as the stabilization of a two dimensional manifold. We propose to encode a quantum bit of information in two orthogonal states of a cavity. Decoherence induces jumps out of these two states, thus compromising the encoded information. We describe a sequence of pulses which can restore the cavity state. This lengthens the quantum information lifetime by almost an order of magnitude. The power of this proposal is that it requires a minimal amount of hardware: one qubit coupled to one resonator, and that we have found a full pulse sequence to transfer the qubit state to the cavity, correct against jumps, and transfer the cavity state back to the qubit.

Contents

Chapter 1

Introduction (version française)

Contents

1.1 Physique quantique: de la théorie à la technologie

La physique quantique prédit des effets contre-intuitifs dans la nature. Dès sa conception au début du 20^{me} siècle, il y a eu un grand nombre de controverses sur ses principes fondateurs. Après des décennies de vérifications expérimentales, la physique quantique est aujourd'hui reconnue comme une excellente théorie qui décrit des phénomènes à une multitude d'échelles. Dans la deuxième moitié du siècle dernier, des technologies nécessitant une compréhension détaille de la physique quantique est née. Parmi celles-ci, le transistor, au coeur de l'informatique moderne; l'imagerie par résonance magnétique (IRM), utilisée dans le domaine médical; le laser, avec un nombre incalculable d'applications; les horloges atomiques, qui permettent une mesure du temps d'une précision telle que des technologies comme le GPS ont vu le jour.

Dans les années 1980 et 1990, des scientifiques comme David Deutsch et Peter Shor ont suggéré d'utiliser des propriétés de systèmes quantiques pour effectuer des calculs. Dans son célèbre papier de 1994 [Shor 1994], Shor a démontré qu'il y aurait un gain exponentiel en vitesse de calcul si des systèmes quantiques (plutôt que classiques) étaient utilisés pour la factorisation d'un grand nombre entier en produit de nombres premiers. Quelques années plus tard, Lov Grover a démontré que la physique quantique permettrait un gain quadratique pour la recherche dans une base de données non triées [Grover 1997].

De nos jours, les protocoles de communication sécurisée reposent sur notre incapacité à factoriser de grand nombre entier en produit de nombres premiers. Il n'y a pas de barrière fondamentale qui empêcherait une factorisation rapide. En utilisant des photons dans des états de superpositions (qui sont non classiques)

[Bennett 1984], on pourrait concevoir une communication dont la sureté est garantie par les lois fondamentales de la physique.

Plusieurs expériences de nos jours, nécessitent des mesures de haute précision. L'utilisation d'états quantiques de la lumière comme sonde pourrait rendre ces mesures plus sensibles [Giovannetti 2006]. Par exemple, les interféromètres gravitationnels tentent de mesurer des déplacements relatifs extrêmement petits (de l'ordre de 10^{-20}). L'utilisation d'états intriqués, de superpositions ou comprimés, pourrait aider à atteindre une telle précision.

Toutes ces applications fascinantes nécessitent de pouvoir générer et contrôler des états quantiques. Ceci implique une bonne compréhension des lois de la physique qui gouvernent leur dynamique, et une bonne maitrise des outils pour contrôler cette dynamique. En utilisant des idées issues de la théorie du contrôle, nous étudions des problèmes de préparation et de stabilisation d'états quantiques sur des modèles correspondant à des expériences actuelles.

1.2 Le contrôle quantique

1.2.1 Formulation générale

Un problème de contrôle quantique cohérent peut être modélisé par l'équation de Scrhödinger bilinéaire

$$\begin{aligned} i\hbar\frac{d}{dt}|\psi(t)\rangle &= (\mathbf{H}_0 - \sum_{k=1}^{M} u_k \mathbf{H}_k)|\psi(t)\rangle \,, \\ |\psi(0)\rangle &= |\psi_0\rangle \,. \end{aligned} \tag{1.1}$$

L'état du système (la fonction d'onde) à l'instant t est noté $|\psi(t)\rangle \in \mathcal{H}$. L'espace des états $\mathcal{H}$ est un espace de Hilbert, qui peut être de dimension finie ou infinie. En absence de control, l'Hamiltonien du système est $\mathbf{H}_0$ (aussi appelé l'Hamiltonien libre). L'Hamiltonien est un opérateur auto adjoint sur $\mathcal{H}$. Les contrôles $u_1, \cdots, u_M$ sont des fonctions du temps réelles. Ce sont typiquement des amplitudes de champs électriques ou magnétiques. Ces champs sont couplés au système à travers les Hamiltoniens d'interaction $\mathbf{H}_1, \cdots, \mathbf{H}_M$. Le terme multiplicatif $u_k|\psi\rangle$, rend ce problème non linéaire (plutôt bilinéaire). Pour une introduction détaillée au contrôle quantique, nous recommandons le livre de D. D'Alessandro [D'Alessandro 2008] et le livre de H. Wiseman and G. Milburn [Wiseman 2009].

Nous pouvons regrouper les problèmes abordés en contrôle quantique en trois catégories:

- **L'identification de Hamiltonien:** Prenons des Hamiltoniens $\mathbf{H}_0, \mathbf{H}_1, \cdots, \mathbf{H}_M$ approximativement connus, et une observable O, quels controls $u_1, \cdots, u_M(t)$ faudrait il appliquer afin qu'en mesurant O, nous puissions extraire de l'informations sur $\mathbf{H}_0, \mathbf{H}_1, \cdots, \mathbf{H}_M$? Le résultat d'une mesure à un instant t sur un ensemble de systèmes est $\langle O(t)\rangle = \langle\psi(t)|O|\psi(t)\rangle$.

La mesure $\langle O(t)\rangle$ dépend de $\mathbf{H}_0, \cdots, \mathbf{H}_M$ à travers (1.1). Cette dépendence est non linear, ce qui complique ce problème d'inversion.

- **Commandabilité et préparation d'états:** Considérons que les Hamiltoniens $\mathbf{H}_0, \mathbf{H}_1, \cdots, \mathbf{H}_M$ sont connus. Prenons un état initial $|\psi_0\rangle$ et un état cible $|\psi_T\rangle$, est ce qu'il existe des contrôles $u_1(t), \cdots, u_M(t)$ qui transfèrents le système de $|\psi_0\rangle$ à $|\psi_T\rangle$? Si oui, comment pouvons nous trouver de tels contrôles?

- **La stabilisation d'états quantiques:** Considérons que les Hamiloniens $\mathbf{H}_0, \mathbf{H}_1, \cdots, \mathbf{H}_M$ sont connus. Prenons un état cible $|\psi_T\rangle$ (ou de manière plus générale, un sous espace de l'espace des états) que nous voulons stabiliser. Quels contrôles $u_1(t), \cdots, u_M(t)$ devons-nous appliquer afin que le système reste proche de son état cible (ou espace cible) pour tout temps, en présence of perturbations comme la décohérence.

1.2.2 Vue d'ensemble

Nous présentons une vue d'ensemble non-exhaustive des différentes directions de recherche dans le domaine du contrôle quantique. Des résultats de commandabilité pour des systèmes de dimension infinie ont été introduits dans [Ramakrishna 1995], et sont basés sur des résultats de commandabilités sur des groupes de Lie par V. Jurdjevic and H. Sussman [Jurdjevic 1972]. Ce travail a ouvert le champ à une multitude de travaux qui ont simplifié les conditions nécessaires et/ou suffisantes de commandabilité, en particulier par C. Altafini et G. Turinici [Altafini 2002, Turinici 2001]. Après avoir démontré qu'un système est commandable, il est important d'avoir des méthodes qui trouvent un contrôle pour transférer un système d'un état initial à un état final. A cette fin, plusieures méthodes numériques ont été poroposé, notamment l'algorithme de convergence monotone [Maday 2006][Zhu 1998], ou des méthodes basées sur des fonctions de Lyapunov [Mirrahimi 2005]. Souvent, il est préférable que ces contrôles minimisent une certaine fonction de coût, comme la valeur d'une observable, l'énergie du contrôle, ou sa longueur temporelle [Boscain 2002][Sugny 2007]. Ces contrôles optimaux peuvent être trouvés, par exemple, par des algorithmes génétiques [Judson 1992]. Le contrôle d'un ensemble de systèmes quantiques a été introduit par J.S Li et N. Khaneja [Li 2006], et a des applications intéressantes en résonnance magnétique nucléaire (RMN). La plupart de ces lois de contrôles supposent que l'Hamiltonien du systèmes est bien connu. Ce dernier doit avoir été estimé par la mesure d'une observable. Ceci soulève la question d'observabilité de l'Hamiltonien. Cette question a été abordée par C. Le Bris et d'autres collaborateurs dans [LeBris 2007]. K. Beauchard, J.M Coron, M. Mirrahimi et d'autres collaborateurs se sont intéressés à des problème de commandabilité [Beauchard 2006][Chambrion 2009] et stabilisabilité [Beauchard 2009] en dimension infinie. Des outils d'analyse fonctionnelle et d'équations aux dérivées partielles sont utilisés [Brezis 1983][Coron 2007].

Enfin, un autre vaste domaine de recherche est la stabilisation de systèmes quantiques autour d'un point d'équilibre. Dans le monde classique, la stabilisation est souvent obtenue en mesurant le système, en estimant son état et en appliquant un contrôle pour corriger la différence entre l'état cible et l'état estimé. Plusieurs barrières empêchent l'application directe de cette rétroaction au domaine quantique. La première est fondamentale, et concerne le postulat de la mesure: lorsqu'on mesure un système quantique, on projette inévitablement son état dans un sous-espace propre de l'observable mesurée. Cette grande perturbation de la dynamique due à la mesure doit être prise en compte dans le modèle. La deuxième est pratique: la projection n'est souvent pas la perturbation dominante due à la mesure. La plupart des mesures au laboratoire détruisent complètement l'état du système. Ceci est par exemple le cas de la mesure forte [Reed 2010a], ou la mesure d'un atome de Rydberg dans l'expérience de l'ENS. La troisième, également pratique, est due aux relativement faibles durées de vie des systèmes quantiques. Ces temps sont de l'ordre de 10 μs pour les cavités supraconductrices dans les circuits quantiques, 1 μs pour les qubits supraconducteurs, et 100 ns pour un nuage de Rb. Afin qu'une stabilisation soit efficace, il faut que la mesure, l'estimation et la rétroaction, soient faites dans un temps bien plus court que ces temps de vie. Ceci est difficile sur ordinateur usuel. La théorie initiale de la rétroaction quantique a été établie par H. Wiseman et G. Milburn [Wiseman 1993][Wiseman 1994]. Un grand nombre de travaux en découlent, notamment par H. Mabuchi, A.C Doherty, K. Jacobs, et collaborateurs [Doherty 2000]. La première expérience de rétroaction quantique a récemment été réalisée dans le groupe de S. Haroche [Sayrin 2011], suite à la proposition théorique [Dotsenko 2009]. Ce travail nécessite de traiter de l'information classique avant de rétroagir sur le système. Cette "rétroaction par la mesure" vient s'opposer à la "rétroaction cohérente" [James 2010], où l'on stabilise un système en le couplant à un autre système quantique dissipatif. Cette théorie a été construite par M. James, J. Gough, H. Nurdin et collaborateurs. Ces travaux sont étroitement liés à la stabilisation par "dissipation contrôlée", également appelée "rétroaction autonome". Cette théorie a été introduite par I. Cirac, P. Zoller et collaborateurs [Poyatos 1996]. Il semblerait que cette dissipation contrôlée puisse même servir à réaliser un calculateur quantique robuste [Verstraete 2009].

1.3 Contributions

Dans ce domaine de plus en plus vaste, les contributions de cette thèse sont dans cinq directions:

Premièrement, nous avons démontré un résultat d'observabilité pour l'identification d'Hamiltonien. Nous considérons une expérience type en contrôle quantique avec des lasers femtoseconde: une observable est mesurée après que le système (typiquement un nuage d'atomes) a interagi avec un champ laser (notre contrôle). Nous posons le problème d'établir s'il existe un ensemble de contrôles qui fourniraient une information suffisante pour la reconstruction de la matrice de

moment dipolaire. Nous démontrons que sous certaines conditions, il existe en effet des contrôles (en analogie avec l'interférométrie de Ramsey) qui rendent le moment dipolaire localement observable. Le reste de la thèse traite des problèmes de préparation et de stabilisation d'états quantiques.

La deuxième contribution est sur le contrôle d'ensemble. Nous proposons un contrôle robuste qui effectue une permutation sur un ensemble de systèmes en échelle. La force de ce résultat qui est basé sur la théorie adiabatique, est que ce contrôle à lui seul, permet d'effectuer une permutation de tout un ensemble de systèmes ayant des paramètres différents. Les résultats sont basés sur une étude mathématique détaillée qui donne des bornes d'erreurs.

Troisièmement, nous nous intéressons à la stabilisation par dissipation contrôlée en électrodynamique quantique (QED) en cavité. Nous décrivons une expérience où des atomes interagissent un par un avec un ou deux modes de la cavité. Nous trouvons un contrôle à appliquer durant chaque interaction entre atome et cavité, qui permet de stabiliser les modes de la cavité dans un état cible prédéterminé. En particulier, nous pouvons stabiliser un état intriqué de deux modes de la cavité qui permettrait une violation des inégalités de Bell pour des temps arbitrairement grands. Cette proposition est appuyée par des simulations numériques et une preuve de convergence en dimension infinie (pas de troncature de l'espace d'Hilbert à un nombre de photons fini).

Quatrièmement, nous proposons des contrôles pour la préparation d'états quantiques dans des circuits Josephson (également appelés circuits quantiques). Nous considérons un qubit supraconducteur couplé à un résonateur micro-onde, et nous décrivons une séquence de pulses qui permettrait de construire toute superposition d'états cohérents quasi-orthogonaux dans la cavité, des états intriqués de deux modes de la cavité, et des états intriqués de plusieurs qubits. De récents résultats expérimentaux sont en bon accord avec les prédictions de nos simulations.

La dernière contribution est sur la correction d'erreur quantique. Ceci peut être vu comme la stabilisation d'un espace d'états de dimension deux. Nous proposons d'encoder un bit d'information quantique dans deux états orthogonaux de la cavité. La décohérence induit des sauts qui modifient l'information encodée. Nous proposons une séquence de pulses qui permettrait de rétablir cette information dans l'état de la cavité. Ceci pourrait prolonger la durée de vie d'un qubit de presque un ordre de grandeur. Le grand intérêt de cette proposition est double. Premièrement, elle nécessite un nombre de composants physiques minimal: seulement un qubit fortement couplé (dans le régime dispersif) à un mode de la cavité. Deuxièmement, nous avons des séquences de pulses pour l'encodage d'un qubit dans la cavité, la correction de l'état de la cavité suite à un saut quantique, et enfin le décodage de l'état de la cavité vers l'état du qubit.

Tous les modèles que nous étudions peuvent être décrits par la formulation (1.1) pour des exemples spécifiques de $\mathbf{H}_0, \mathbf{H}_1, \cdots, \mathbf{H}_M$. Il est assez remarquable que des systèmes aussi différents puissent être modélisés par des systèmes spin-ressort similaires [Haroche 2006]. En particulier, nous considérons trois classes de modèles:

- Un système à deux niveaux couplé à un champ électrique classique peut être modélisé en prenant $\mathbf{H}_0 = \omega_q \frac{\sigma_\mathbf{z}}{2}$, $M = 1$ et $\mathbf{H}_1 = \sigma_\mathbf{x}$, où $\sigma_\mathbf{x}, \sigma_\mathbf{y}$ et $\sigma_\mathbf{z}$ sont les matrices de Pauli. On note ω_q la fréquence de l'atome. Un tel modèle est appelé semi-classique car l'atome est modélisé par un système quantique, et le champ par un système classique. Dans les chapitres 3 et 4, nous étudions des systèmes multi-niveaux qui interagissent avec un champ électrique classique.

- Un système à deux niveaux couplé à un champ classique. Ce dernier est modélisé par un oscillateur harmonique. Ceci donne lieu à l'Hamitlonien de Jaynes-Cummings Hamiltonian [Jaynes 1963] $\mathbf{H}_0 = \omega_q \frac{\sigma_\mathbf{z}}{2} + \omega_c \mathbf{a}^\dagger \mathbf{a} + \Omega \sigma_\mathbf{x} \otimes (\mathbf{a} + \mathbf{a}^\dagger)$. On note $\mathbf{a}$ l'opérateur annihilation, ω_c la fréquence de l'oscillateur et Ω la fréquence de couplage entre l'atome et l'oscillateur. Un contrôle est appliqué à l'oscillateur: $\mathbf{H}_1 = \mathbf{a} + \mathbf{a}^\dagger$, et un à l'atome: $\mathbf{H}_2 = \sigma_\mathbf{x}$. Dans le chapitre 6, un modèle similaire est utilisé pour un atome artificiel: a qubit supraconducteur, couplé à un résonateur micro onde.

- Un système à deux niveaux couplé à un oscillateur harmonique, où on s'intéresse uniquement à l'oscillateur harmonique. Afin d'obtenir un système dynamique réduit pour l'oscillateur, on effectue une trace partielle sur l'atome, ce qui donne une équation de Lindblad (i.e une application de Kraus). Dans le chapitre 5, utilise une équation de Lindblad en temps discret, obtenue à partir de l'Hamiltonien de Jaynes et Cummings avec un contrôle uniquement sur l'état du qubit: $\mathbf{H}_1 = \sigma_\mathbf{z}$ and $\mathbf{H}_2 = \sigma_\mathbf{x}$.

1.4 Plan de la thèse

Le contenu de cette thèse est présentée de la manière suivante:

Chapitre 3: Nous commençons par un problème d'identification d'Hamiltonien. Nous démontrons que l'identification d'Hamiltonian à partir de mesures de populations en utilisant une famille de contrôles bien choisis, est un problème bien posé. Ce résultat est basé sur [Leghtas 2012d].

Chapitre 4: Nous procédons ensuite à un problème de préparation d'états. Nous proposons un contrôle qui permet d'effectuer toute permutation d'un système quantique en échelle. Le grand intérêt de cette proposition est que ce même contrôle peut agir sur un ensemble de systèmes avec des paramètres différents, et induire une permutation de chacun de ces systèmes. Ce résultat fut publié dans [Leghtas 2011].

Chapitre 5: Ici, nous nous intéressons à la stabilisation d'états quantiques. Nous décrivons une expérience pour la stabilisation d'états de superposition et d'états intriqués dans un ou deux modes d'une cavité. Ce résultat a fait l'objet de l'article [Sarlette 2012]. Nous suggérons une méthode qui consiste à coupler la cavité à un environnement contrôlé: une série d'atomes uniques traversant la cavité un à

un. Cette méthode ne nécessite pas de feedback en temps réel ce qui rendrait son implémentation au laboratoire relativement simple. Cette dissipation contrôlée induise par les atomes fait converger tout état vers l'état cible. À la fin de ce chapitre, nous démontrons cette convergence en dimension infinie.

Chapitre 6: Ce dernier chapitre commence par une méthode de préparation d'états quantiques. Nous montrons ensuite comment ceci peut être utilisé pour de la correction d'erreur quantique. Nous proposons une suite de pulses qui prépare toute superposition d'états cohérents quasi-orthogonaux dans une cavité micro-onde fortement couplée à un qubit supraconducteur. Ce schéma peut également être adapté pour la préparation d'états intriqués de deux modes de la cavité, et d'états intriqués d'un grand nombre de qubits. Ces résultats sont issus de [Leghtas 2012b]. Nous montrons enfin que ces superpositions d'états cohérents peuvent être utilisées pour de la correction d'erreur quantique [Leghtas 2012c].

Chaque chapitre peut être lu de manière indépendante. La conclusion (chapitre 7) est une ouverture vers d'autres problèmes.

Chapter 2

Introduction

Contents

2.1 Quantum physics: from theory to technology

Quantum physics predicts intriguing and counter-intuitive effects in nature. Since its birth in the early 20^{th} century, there has been a huge amount of controversy around its founding principles. After decades of successful confrontation with experiments, quantum physics is now recognized by many as being in excellent agreement with the laws of nature, at many different scales. In the second half of the last century, technologies requiring a detailed understanding of quantum physics were born. Some of the most important ones include the transistor, at the heart of modern computing; magnetic resonance imaging (MRI) machines, essential in medical research; the laser, with countless applications; and atomic clocks, which provide such a precise measure of time that technologies such as the global positioning system (GPS) were made possible. However, the output of a laser for example, can be very well described by a classical electromagnetic field. The next step of technological progress was then to exploit inherently quantum properties of nature, such as entanglement and delocalization.

In the 1980s and 1990s, scientists like David Deutsch and Peter Shor pursued this effort, and suggested using quantum systems to perform computations. In his famous 1994 paper [Shor 1994], Shor proved that an exponential speed up in computational power would be possible, if quantum systems were used to find the prime factors of a large integer. A few years later, Lov Grover proved that quantum physics can lead to a quadratic speed up for searching in unsorted data [Grover 1997].

Nowadays, secure communication protocols are built on the assumption that we cannot factorize large integers into a product of prime numbers in a short time. There is no physical barrier which prohibits a fast factorization. It was suggested

that photons in superposition states, which are only allowed by quantum mechanics, could be used for secure communication [Bennett 1984]. The security of such a "quantum communication" is guaranteed by the fundamental laws of quantum physics, and not by a current technological limitation.

Cutting edge experiments and advanced technologies are in constant need for more precise measurements. It has been found that using quantum states of light as probes, instead of classical light, can greatly enhance measurement sensitivity. This area of research was coined quantum metrology [Giovannetti 2006] . For example, devices such as gravitational wave interferometers aiming to detect gravitational waves, require measuring extremely small differential displacements (smaller than 10^{-20}). Reaching such sensitivities could be aided by the use of squeezed, superposition and entangled states of light [Giovannetti 2004].

All these exciting applications require the ability to generate quantum states and manipulate them reliably. This necessitates understanding the laws of physics which govern their dynamics, and a detailed insight into how external controls can affect this dynamics. This thesis aims to contribute to this effort by applying ideas drawn from control theory to a set of current experiments.

2.2 Quantum control theory

2.2.1 General formulation

A coherent quantum control problem is usually formulated by the following bilinear Schrödinger equation

$$\begin{aligned} i\hbar\frac{d}{dt}|\psi(t)\rangle &= (\mathbf{H}_0 - \sum_{k=1}^{M} u_k \mathbf{H}_k)|\psi(t)\rangle \ , \\ |\psi(0)\rangle &= |\psi_0\rangle \ . \end{aligned} \tag{2.1}$$

The system state at time t is denoted by the Dirac notation $|\psi(t)\rangle \in \mathcal{H}$, (the wave function). The state space $\mathcal{H}$ is a Hilbert space, which may be of finite or infinite dimension. In absence of control inputs, the system's Hamiltonian is $\mathbf{H}_0$ (also called the free Hamiltonian). A Hamiltonian is a self adjoint operator on $\mathcal{H}$. The control inputs $u_1, \cdots, u_M$ are real functions of time. They are typically electric or magnetic field amplitudes which can be produced at will and constitute our control over the system. These fields couple to the system through the interaction Hamiltonians $\mathbf{H}_1, \cdots, \mathbf{H}_M$. Due to the multiplicative terms $u_k|\psi\rangle$, this is a nonlinear (rather a bilinear) control problem. For a detailed introduction to quantum control, we recommend the book by D. D'Alessandro [D'Alessandro 2008] and the book by H. Wiseman and G. Milburn [Wiseman 2009].

We may group the problems which are tackled in quantum control theory into three categories:

- **Hamiltonian identification:** Given approximately known Hamiltonians $\mathbf{H}_0, \mathbf{H}_1, \cdots, \mathbf{H}_M$, and a measured observable O, what controls $u_1, \cdots, u_M(t)$

should we apply to the system such that by measuring the observable O, we extract information about $\mathbf{H}_0, \mathbf{H}_1, \cdots, \mathbf{H}_M$? The result of a measurement at time t on an ensemble of systems yields $\langle O(t)\rangle = \langle\psi(t)|O|\psi(t)\rangle$. The dependence of $\langle O(t)\rangle$ on $\mathbf{H}_0, \cdots, \mathbf{H}_M$ is through (2.1). This dependence is highly non linear, which hugely complicates the inversion problem.

- **Controllability and quantum state preparation:** Given known Hamiltonians $\mathbf{H}_0, \mathbf{H}_1, \cdots, \mathbf{H}_M$, and known initial and target states $|\psi_0\rangle, |\psi_T\rangle$, do controls $u_1(t), \cdots, u_M(t)$ which drive the system from $|\psi_0\rangle$ to $|\psi_T\rangle$ exist? If the answer is positive, how can we find such controls?

- **Quantum state stabilization:** Given known Hamiltonians $\mathbf{H}_0, \mathbf{H}_1, \cdots, \mathbf{H}_M$ and a target state $|\psi_T\rangle$ (or more generally a target manifold) we wish to stabilize, what controls $u_1(t), \cdots, u_M(t)$ should we apply to maintain the system close to the target state (or target manifold) at all times, in the presence of perturbations such as the effect of decoherence.

2.2.2 Brief Overview

Here we give a brief and highly non-exhaustive overview of the different directions of research in the field of quantum control. Controllability results for finite dimensional quantum systems were introduced in [Ramakrishna 1995] based on results from controllability on Lie groups by V. Jurdjevic and H. Sussman [Jurdjevic 1972]. This work paved the path for a variety of new results simplifying the necessary and/or sufficient controllability conditions, in particular by C. Altafini and G. Turinici [Altafini 2002, Turinici 2001]. The next step after proving that a system is controllable is to actually find a control which takes the system from an initial state to the target state. Several numerical methods have been proposed for this task, such as the monotonic convergent algorithm [Maday 2006][Zhu 1998], or methods based on a Lyapunov function [Mirrahimi 2005]. These controls may need to maximize an observable or minimize a cost function, such as the total energy or the control time [Boscain 2002][Sugny 2007], leading to the field of optimal control of quantum systems. Such an optimal control can be found by combining a learning algorithm to the experimental setting [Judson 1992]. The concept of controlling an ensemble of quantum systems with one single control was introduced by J.S Li and N. Khaneja [Li 2006], and has important implications for nuclear magnetic resonance (NMR). Most of these control strategies assume a good knowledge of the system Hamiltonian. The latter needs to be estimated from a measured observable. This raises the question of whether a measurement record is sufficient to reconstruct the Hamiltonian of a system. Such problems are addressed by C. Le Bris and co workers in [LeBris 2007]. K. Beauchard, J.M Coron, M. Mirrahimi and co-workers have been concerned with the controllability [Beauchard 2006][Chambrion 2009] and stabilizability [Beauchard 2009] of (2.1) in the case where $\mathcal{H}$ is of infinite dimension. Tools from functional analysis and partial differential equations are used to prove the claimed results [Brezis 1983][Coron 2007].

Finally, another large domain of interest is the stabilization of a quantum system around a target steady state. In the classical world, stabilizing a system is usually done by measuring it, estimating its state and based on that information, applying a control which keeps the system close to its target state. Some major difficulties are added in the quantum case. The first is fundamental and concerns the measurement postulate: when a quantum system is measured, it is always projected into an eigenspace of the measured observable [Haroche 2006, Chapter 4]. This large system perturbation due to the measurement necessarily has to be taken into account. The second is practical and concerns the way a measurement is done in the laboratory. Very often, the projection is not the dominant source of perturbation due to the measurement. Indeed, most measurements completely erase the quantum state; this is the case for example in the high power readout of a superconducting qubit [Reed 2010a], or the measurement of a Rybderg atom in the ENS experiment. The third is practical and concerns the very short time scales involved. Many quantum systems have relatively short lifetimes: of the order of 10 μs for superconducting cavities, 1 μs for superconducting qubits, and 100 ns for atomic systems like Rb in the gas phase. In order for a stabilization to be efficient, a whole feedback cycle of: measuring, processing and controlling would need to be performed within these lifetimes. This is far from being easy with a regular desktop computer. The initial theory on quantum feedback is due to H. Wiseman and G. Milburn [Wiseman 1993][Wiseman 1994]. This opened the door to many results, in particular, by H. Mabuchi, A.C Doherty, K. Jacobs, and co-workers [Doherty 2000]. The first experiment closing the loop of feedback by state estimation was performed in the group of S. Haroche [Sayrin 2011], following the theoretical proposal [Dotsenko 2009]. This work assumes measuring the system, classically processing the measurement outcome, and computing the control law to be applied. This "measurement based feedback" is distinct from "coherent" feedback [James 2010], where the feedback loop is performed by connecting the system to another dissipative quantum system. This theory was developed by M. James, J. Gough, H. Nurdin and co-workers. Coherent feedback highly resembles "reservoir engineering", also called "autonomous feedback". This area of research was introduced by I. Cirac, P. Zoller and co-workers [Poyatos 1996]. It has also been suggested that engineering dissipation could be used for robust quantum computation [Verstraete 2009].

2.3 Contributions

In this rapidly growing field of quantum control theory, the contributions of this thesis lie in five areas.

First, we derive an observability result for Hamiltonian identification. We consider a typical setting in ultra-fast quantum control experiments where an observable is measured after a system (e.g a cloud of atoms) has interacted with a controlled electric field. We thus pose the problem of whether we can find a set of controls

which would provide sufficient information to reconstruct the dipole moment matrix ($\mathbf{H}_1$ in the notation of (2.1)). We prove that under certain conditions, we can find controls (in analogy with Ramsey interferometry) which make the dipole moment matrix locally observable. The rest of the thesis is devoted to quantum state engineering and stabilization.

The second contribution is on ensemble control. We propose a robust control which performs any state permutation on an ensemble of quantum ladder systems. The strength of this result which is based on adiabatic theory, is that this single control performs the same permutation on an ensemble of different systems. The results are based on a detailed asymptotic mathematical analysis giving error bounds.

Third, we address the problem of quantum state stabilization by reservoir engineering in the context of cavity quantum electrodynamics (QED). We describe an experiment where flying atoms successively interact with one or two cavity modes. We find a control to apply during each atom-cavity interaction which would drive and stabilize the cavity modes close to a predefined non-classical target state. In particular, we are able to stabilize an entangled state which would lead to a violation of Bell's inequality for arbitrarily large times. This proposal doesn't require any real time data processing and feedback, making it very appealing for experimental implementation. We provide numerical simulations and a first mathematical convergence analysis, where the Hilbert space is infinite dimensional (no truncation to a finite number of photons).

Fourth, we introduce a control which performs quantum state preparation in the context of Josephson circuits (also called circuit QED). We consider one superconducting qubit coupled to a microwave resonator and describe a sequence of pulses which would generate any superposition of coherent states, entangled states of two cavity modes and multi-qubit entangled states. We show that with currently available systems with state of the art coherence times and coupling strengths, we obtain preparation fidelities above 90%. Recent preliminary results in the laboratory are in good agreement with our simulation predictions.

The last contribution is to quantum error correction. This may be viewed as the stabilization of a two dimensional manifold. We propose to encode a quantum bit of information in two orthogonal states of a cavity. Decoherence induces jumps out of these two states, thus compromising the encoded information. We describe a sequence of pulses which can restore the cavity state. This lengthens the quantum information lifetime by almost an order of magnitude. The power of this proposal is that it requires a minimal amount of hardware: one qubit coupled to one resonator, and that we have found a full pulse sequence to transfer the qubit state to the cavity, correct against jumps, and transfer the cavity state back to the qubit.

All the models for which we obtain the above results may be described by the general formulation (2.1) for specific examples of $\mathbf{H}_0, \mathbf{H}_1, \cdots, \mathbf{H}_M$. Quite remarkably, these different systems may be modeled by similar spin-spring systems [Haroche 2006]. In particular, we consider three classes of models:

- A single two level atom coupled to a classical electric field can be modeled

by taking $\mathbf{H}_0 = \omega_q \frac{\sigma_\mathbf{z}}{2}$, $M = 1$ and $\mathbf{H}_1 = \sigma_\mathbf{x}$, where $\sigma_\mathbf{x}, \sigma_\mathbf{y}$ and $\sigma_\mathbf{z}$ denote the Pauli matrices. We denote ω_q the atom frequency. Such a model is called a semi classical-light matter interaction model, where the atom is modeled by a quantum system and the light is modeled by a classical electric field. In chapters 3 and 4, we actually consider multi-level atoms interacting with a classical source of light.

- A single two level atom coupled to a quantized electric field. The latter is modeled by a Harmonic oscillator. This leads to the Jaynes-Cummings Hamiltonian [Jaynes 1963] $\mathbf{H}_0 = \omega_q \frac{\sigma_\mathbf{z}}{2} + \omega_c \mathbf{a}^\dagger \mathbf{a} + \Omega \sigma_\mathbf{x} \otimes (\mathbf{a} + \mathbf{a}^\dagger)$. We denote $\mathbf{a}$ the oscillator's annihilation operator, ω_c its frequency and Ω the coupling strength between the atom and the oscillator. One control is applied to the oscillator leading to $\mathbf{H}_1 = \mathbf{a} + \mathbf{a}^\dagger$, and one to the atom leading to $\mathbf{H}_2 = \sigma_\mathbf{x}$. In chapter 6, a very similar model is applied to an artificial atom: a superconducting qubit, coupled to a microwave resonator.

- A two level atom coupled to a Harmonic oscillator, where the system of interest is the Harmonic oscillator alone. In order to obtain a reduced dynamical model on the oscillator only, we trace out the state of the atom yielding a Lindblad master equation (i.e. a Kraus map). In chapter 5 we use a discrete time Lindblad equation derived from a Jaynes-Cummings Hamiltonian with control on the qubit state only: $\mathbf{H}_1 = \sigma_\mathbf{z}$ and $\mathbf{H}_2 = \sigma_\mathbf{x}$.

2.4 Layout of this dissertation

The content of this thesis has been organized as follows:

Chapter 3: We start with a Hamiltonian identification problem. We prove that identifying the Hamiltonian from population measurements using a family of discriminating control fields is a well posed problem. These results are based on [Leghtas 2012d].

Chapter 4: We then move on to a state preparation problem. We propose a control field which could perform any state permutation on a multi-level system. The power of this scheme is that this one field may act on an ensemble of systems with different parameter values, and permute every single one of them. This result appeared in [Leghtas 2011].

Chapter 5: Here we tackle the problem of quantum state stabilization. Reporting the results of [Sarlette 2012], we describe a scheme for stabilizing superposition states and entangled states in a cavity. In this aim, we suggest tailoring the interaction of the cavity with a controlled environment: a stream of two level atoms. This proposal doesn't require any real time data processing and feedback, making it very appealing for experimental implementation. This controlled dissipation forces

any initial state in the cavity to converge towards the desired target state. The convergence is proved where the cavity state space is an infinite dimensional Hilbert space, having to overcome technical problems such as the non compactness of the unit ball.

Chapter 6: In this final chapter, we start with a state preparation scheme and then see how this can be used to stabilize a whole manifold of states, thus performing quantum error correction. We propose a sequence of pulses which prepares any superposition of non overlapping coherent states in a microwave resonator. This preparation scheme can also be applied to generate entangled states of two modes and entangled states of an arbitrary large number of qubits. This was the subject of a recent paper [Leghtas 2012b]. We then show that these coherent state superpositions can be used for efficient quantum error correction [Leghtas 2012c]. This brings us one step closer to a readily realizable quantum memory.

Each chapter can be read independently. A conclusion in chapter 7 gives an insight on future work.

Chapter 3

Enhanced observability utilizing quantum control

Contents

Ce chapitre traite l'identification d'Hamiltonien pour un système commandable avec des transitions non dégénérées et un état initial connu. On considère un seul contrôle scalaire et une mesure de population à instant T arbitrairement grand. On démontre que la matrice de moment dipolaire est localement observable: pour tout couple de matrices différentes mais suffisamment proches, il existe un contrôle qui permet d'obtenir deux mesures différentes. Ce résultat suggère qu'une simple mesure de population à un seul instant peut être transformée en une source d'information très riche permettant l'identification unique du moment dipolaire, lorsque cette mesure est précédée d'une commande bien choisie. Ce chapitre est basé sur [Leghtas 2012d], qui paraîtra comme une note technique dans IEEE Transactions of Automatic Control. Ce résultat a été obtenu en collaboration avec Gabriel Turinici, Herschel Rabitz et Pierre Rouchon.

This chapter considers Hamiltonian identification for a controllable quantum system with non-degenerate transitions and a known initial state. We assume to have at our disposal a single scalar control input and the population measure of only one state at an (arbitrarily large) final time T. We prove that the quantum dipole moment matrix is locally observable in the following sense: for any two close

but distinct dipole moment matrices, we construct discriminating controls giving two different measurements. This result suggests that what may appear at first to be very restrictive measurements are actually rich for identification, when combined with well designed discriminating controls, to uniquely identify the complete dipole moment of such systems. This chapter is based on [Leghtas 2012d], which is about to appear as a technical note in IEEE transactions of automatic control. This result was obtained in collaboration with Gabriel Turinici, Herschel Rabitz and Pierre Rouchon.

3.1 Introduction

Quantum control has been receiving increasing attention [Brif 2010] and one of its promising applications is to Hamiltonian identification [Warren 1993] by using the ability to actively control a quantum system as a means to gain information about the underlying Hamiltonian governing its dynamics. The underlying premise is that controls may be found which make the measurements not only robust to noise but also highly sensitive to the unknown parameters in the Hamiltonian. Hence, although the performance of laboratory measurements may be constrained, the ability to control a quantum system has the prospect of turning this data into a rich source of information on the system's Hamiltonian.

In this chapter, we consider the problem of identifying the dipole moment (which is assumed to be real) of an $N-$level quantum system, initialized to a known state (ground state), from a single population measurement at one arbitrarily large time T. We suppose an ability to freely control the system with a time dependent electric field $u(t)$. The measurements are obtained by (i) initializing at time $t = 0$ the system's state at a known state $|i\rangle$, (ii) controlling in open loop and without measurement the system with an electric field $u_k(t)$ for $t \in [0, T]$ where $T > 0$, and (iii) measuring at final time T the population of one state $|f\rangle$. This may be repeated for many controls $(u_k)_k$. We prove the existence of controls which make the identification from one population measurement a well posed problem (theorem 3.1). These controls have a simple physical interpretation in analogy with Ramsey interferometry (see Fig. 3.1).

The perspective above combined with control theory is motivated by three practical arguments. First, measuring a state population at one time T is a technique which can have a very high signal to noise ratio (~ 100). Second, technological progress with spatial light modulators (SLM) permits generating a broad variety of controls in the laboratory. Third, ultra short pulsed fields can be well measured in the laboratory [Iaconis 1998]. Hence, we are able to design a variety of precisely known control inputs.

Le Bris *et al* [LeBris 2007] prove the observability of the dipole moment when the population of all states are measured over an arbitrarily large interval of time. Algorithms to reconstruct the dipole from the measured data were proposed using nonlinear observers [Leghtas 2009, Bonnabel 2009]. A different setting is considered

in [Schirmer 2010a, Schirmer 2010b] where it is supposed that one can prepare and measure the system in a set of orthogonal states at various times, and the available data is the probability to measure the system in a certain state when it was prepared in another; Bayesian estimation is used to reconstruct the energy levels, the damping constants and the dipole moment from the measured data. We consider here the less demanding case where the only available measurement is the population of one state at one arbitrarily large time, and the initial state is known and coincides with the ground state. We may summarize the scheme to identify an arbitrary matrix element $\langle l|\mu|k\rangle$ of the dipole moment operator μ by the following:

1. We use the controllability of the system to steer it from the ground state to state $|l\rangle$.
2. "Gently" Rabi flop the transition $|k\rangle \rightarrow |l\rangle$ using the assumed unique transition frequency in a way that does not affect nearby transitions.
3. Finally use the controllability of the system to steer the system to a state which is detectable by the measurement apparatus: population of a state $|f\rangle$.
4. From the measured population, deduce the dipole matrix element.

The chapter is organized as follows. In subsection 3.2 we state the main result in Theorem 3.1, and subsection 3.3 gives the proof of the Theorem and an important lemma on which the main result is based. Finally concluding remarks are presented in subsection 3.4.

3.2 Observability of the quantum dipole moment

3.2.1 Problem setting

We consider a quantum system in a pure state described by the wave function $|\psi\rangle \in \mathcal{S}$. Here $\mathcal{S}$ is the set of N dimensional complex vectors of unit norm. The system interacts with an electric field (the real control input) $u \in \mathcal{U}_T$ for some $T > 0$ with $\mathcal{U}_T \equiv \{f : [0,T] \rightarrow \mathbb{R} \,|\, f \text{ piecewise continuous}\}$. For a given control u we measure the population of the state $|f\rangle$ at time T denoted as $P_{if}(u)$. We denote by $\mathbf{H}_0$ the free Hamiltonian, due to the kinetic and potential energy of the system (Hermitian matrix) and by μ the dipole moment operator, also a Hermitian matrix. In the notation of (2.1), we have $\mu = \mathbf{H}_1$ and $u(t) = u_1(t)$. This choice was made to adapt to the notation used in the mathematical physics community. The initial state $|i\rangle$ and the measured state $|f\rangle$ are eigenvectors of $\mathbf{H}_0$. We consider a semi-classical model for the light-matter interaction, and the dynamics of $|\psi\rangle$ are given by the Schrödinger equation:

$$\begin{aligned} \imath\hbar\frac{d}{dt}|\psi(t)\rangle &= (\mathbf{H}_0 - u(t)\mu)|\psi(t)\rangle \\ |\psi(0)\rangle = |i\rangle \quad &, \quad P_{if}(u) = |\langle f|\psi(T)\rangle|^2 . \end{aligned} \tag{3.1}$$

For all $T > 0$, we suppose that we can create any field $u \in \mathcal{U}_T$ and that we can measure $P_{if}(u)$. For M different fields $\{u_1, .., u_M\}$ we can collect the measurements $\{P_{if}(u_1), .., P_{if}(u_M)\}$. Through (3.1), P_{if} is a function of μ and a functional of u, and when necessary this explicit dependence will be written as $P_{if}(u, \mu)$. The aim of this chapter is to explore the feasibility of estimating the dipole moment μ from the measured data $\{P_{if}(u_1), .., P_{if}(u_M)\}$ using well chosen controls $\{u_1, .., u_M\}$. Below, $P_{if}(u, \mu)$ refers to the measurement achieved on the real system using a control u, and for any $\hat{\mu}$, $P_{if}(u, \hat{\mu})$ is the estimated measurement which is obtained by simulating system (3.1) with the control u and coupling $\hat{\mu}$.

3.2.2 Main result

For all $k \leq N$ we denote $|k\rangle$ as the eigenvector of $\mathbf{H}_0$ with associated eigenvalue E_k. Throughout this chapter, all matrices are written in the basis $(|1\rangle, .., |N\rangle)$. The initial and measured states correspond to some indexes $i, f \in \{1, \ldots, N\}$. For all $k, l \leq N$ we specify $\sigma_x^{lk} \equiv |l\rangle\langle k| + |k\rangle\langle l|$. We define

$$\mathcal{M} \equiv \text{Span}\{\sigma_x^{lk} \backslash k, l \leq N \text{ with } \text{Tr}\left(\mu\sigma_x^{lk}\right) \neq 0\},$$

with Tr being the trace operation. When all non diagonal elements of μ are non-null, $M = \dim(\mathcal{M}) = \frac{N(N-1)}{2}$. The main result is the following:

Theorem 3.1. *Consider a real symmetric matrix μ with zero diagonal entries and a real diagonal matrix $\mathbf{H}_0$ with non-degenerate transitions. Suppose that the system defined in (3.1) is controllable. Then for any positive constant α there exists a time $T > 0$ and M fields $(u_1, .., u_M) \in {\mathcal{U}_T}^M$ such that the cost function*

$$J : \mathcal{M} \ni \hat{\mu} \to \sum_{k=1}^{M} (P_{if}(u_k, \hat{\mu}) - P_{if}(u_k, \mu))^2$$

is in $\mathcal{C}^2(\mathcal{M}, \mathbb{R})$ and locally α-convex[1] around μ.

$\mathcal{C}^k(A, B)$ denotes the set of k times continuously differentiable functions defined over A with values in B. In Section 3.5 we provide the definitions of controllability and a matrix with non-degenerate transitions. Here and throughout this chapter, the norm of matrix μ, noted $||\mu||$ refers to the max norm.
A direct consequence of Theorem 3.1 is the local observability of the dipole moment:

Corollary 3.1. *Under the assumptions of Theorem 3.1, the dipole moment is locally observable in $\mathcal{M}$ (see definition 3.3).*

Proof Take $\alpha > 0$. Theorem 3.1 implies that there exists a time $T > 0$ and M fields $(u_1, .., u_M) \in {\mathcal{U}_T}^M$ such that the cost function J is $\mathcal{C}^2(\mathcal{M}, \mathbb{R})$ and locally α-convex around μ. Hence $\exists r > 0$ such that for all $\hat{\mu} \in \mathcal{M}$ with $||\hat{\mu} - \mu|| \leq r$ and $\hat{\mu} \neq \mu$, $J(\hat{\mu}) > 0$, and hence there exists $u \in \{u_1, .., u_M\}$ such that $P_{if}(u, \hat{\mu}) - P_{if}(u, \mu) \neq 0$.□

[1] The smallest eigenvalue of the Hessian $\nabla^2 J(\mu)$ is larger than α.

Remark 3.1. *The local $\alpha-$convexity is a property stronger than the mere possibility to identify the dipole matrix. It states that the distinction between a dipole candidate $\hat{\mu}$ and the true dipole μ can be observed (through the measurements aggregated in J) to first order in the distance $\|\mu-\hat{\mu}\|$. This first order dependence of the measurement P_{if} with respect to the dipole μ is addressed in more detail in lemma 3.1. For well chosen controls, the J function has a very simple shape around μ and a simple gradient algorithm could be used to identify it.*

The eigenvalues of $\mathbf{H}_0$ are commonly measured through spectroscopy and can be found in reference tables[2] with precisions of order 10^{-7}. The result of theorem 3.1 is also relevant for the problem of discriminating between two molecules with the same free Hamiltonian and different effective dipole operators. In that framework, $\hat{\mu}$ and μ would be the dipole operators of these two molecules (as opposed to one estimated and one true dipole, as considered in this chapter), and the aim is to find controls which produce different data sets for these two different but similar quantum systems. This was experimentally accomplished in [Petersen 2010] where a genetic algorithm is used to find these discriminating controls. A complementary theoretical controllability analysis can be found in [Turinici 2004].

3.3 Proofs

3.3.1 Existence of discriminating controls

We denote $\mu' = \frac{1}{||\mu||}\mu$ the normalized dimensionless dipole moment operator, $\mu'_{lk} \equiv \mathrm{Tr}\left(\mu'\sigma_x^{lk}\right)$ and $\frac{\partial P_{if}}{\partial \mu'_{lk}}(u)$ the partial derivative of $P_{if}(u)$ with respect to μ'_{lk}. Theorem 3.1 is based on the following lemma:

Lemma 3.1. *Suppose that μ is real, symmetric and has only zeros on its diagonal and $\mathbf{H}_0$ is real, diagonal, with non-degenerate transitions (see definition 3.2). Suppose system (3.1) is controllable. Then for all (l,k) with $\mu_{lk} \neq 0$, there exists $\xi_0 > 0$ such that, for all $\xi \in]0, \xi_0[$, there exists a $T > 0$ and $u \in \mathcal{U}_T$ satisfying*

- $\frac{\partial P_{if}}{\partial \mu'_{lk}}(u) = \frac{1}{2\xi} + O(1)$
- $\forall \{m,n\} \neq \{l,k\}$ *with* $\mu_{mn} \neq 0$, $\frac{\partial P_{if}}{\partial \mu'_{mn}}(u) = O(1)$,

where $O(1)$ corresponds to zero order terms with respect to ξ around 0^+.

3.3.2 Proof of Theorem 3.1

To each pair of integers (l_p, k_p), $l_p < k_p$ such that $\mathrm{Tr}\left(\mu'\sigma_x^{l_p k_p}\right) \neq 0$ we associate a unique index $p \in \{1, ..., M\}$, and we define $\sigma_x^p \equiv \sigma_x^{l_p k_p}$ along with $\mu'_p \equiv \mathrm{Tr}\left(\mu'\sigma_x^p\right)$.

According to lemma 3.1, $\exists \xi_0 > 0$ such that $\forall \xi \in]0, \xi_0[$, $\exists\ T_1, .., T_M$ and $(u_1, .., u_M) \in \mathcal{U}_{T_1} \times .. \times \mathcal{U}_{T_M}$ such that: (i) $\forall p \in [1:M]$, $\frac{\partial P_{if}}{\partial \mu'_p}(u_p) = \frac{1}{2\xi} + O(1)$

[2] See for e.g: National Institute of Standards and Technology (NIST) data sheets.

and (ii) $\forall p' \neq p$, $\frac{\partial P_{if}}{\partial \mu'_{p'}}(u_p) = O(1)$. We take $T = \max(T_1, .., T_M)$ and for all $k \in \{1, .., M\}$, we extend the definition of u_k from $[0, T_k]$ to $[0, T]$ by taking $u_k(t) = 0$ for all $t \in]T_k, T]$. We will use $J : \mathcal{M} \to \mathbb{R}$ defined by:

$$J(\hat{\mu}) = \sum_{k=1}^{M} (P_{if}(u_k, \hat{\mu}) - P_{if}(u_k, \mu))^2.$$

For a fixed $T > 0$ and $u \in \mathcal{U}_T$, since $\hat{\mu} \to P_{if}(u, \hat{\mu})$ is in $\mathcal{C}^2(\mathcal{M}, \mathbb{R})$, $\hat{\mu} \to J(\hat{\mu})$ is in $\mathcal{C}^2(\mathcal{M}, \mathbb{R})$. We find

$$\frac{\partial^2 J}{\partial \mu'_p \partial \mu'_{p'}}(\mu) = \sum_{k=1}^{M} \frac{\partial P_{if}}{\partial \mu'_p}(u_k, \mu) \frac{\partial P_{if}}{\partial \mu'_{p'}}(u_k, \mu) \ ,$$

so that for

$$p \in \{1, ..., M\} : \frac{\partial^2 J}{\partial {\mu'_p}^2}(\mu) = \frac{1}{4\xi^2} + O(\frac{1}{\xi}) \ ,$$

and for

$$p \neq p' : \ \frac{\partial^2 J}{\partial \mu'_p \partial \mu'_{p'}}(\mu) = O(\frac{1}{\xi}) \ .$$

We have:

$$\nabla^2 J(\mu) = \frac{1}{4\xi^2} \left(I + O(\xi)\right) \ ,$$

where $\nabla^2 J(\mu)$ is the Hessian of J at μ and I is the identity matrix. The smallest eigenvalue of $\nabla^2 J(\mu)$ scales as $\frac{1}{4\xi^2}(1 + O(\xi))$, hence by taking ξ small enough it can be made larger than α thereby reaching the conclusion above. □

3.3.3 Proof of lemma 3.1

We define the dimensionless time scale $\tau \equiv \frac{1}{\hbar}||\mathbf{H}_0||t$ and also $\top \equiv \frac{1}{\hbar}||\mathbf{H}_0||T$. For two times $\tau, \tau' \in [0, \top]$ we define the propagator $U(\tau', \tau)$ such that $|\psi(\tau')\rangle = U(\tau', \tau)|\psi(\tau)\rangle$. Rewriting (3.1) for $U(\tau, 0)$ we obtain:

$$\begin{aligned} \imath \frac{\partial}{\partial \tau} U(\tau, 0) &= \frac{1}{||\mathbf{H}_0||}(\mathbf{H}_0 - u(\tau)\mu) U(\tau, 0) \\ P_{if}(u) &= |\langle f|U(\top, 0)|i\rangle|^2 \ , U(0, 0) = I \ . \end{aligned} \tag{3.2}$$

The proof of lemma 3.1 has two parts I and II separately treated below.

i) Part I Take two times τ_1, τ_2, $0 < \tau_1 < \tau_2 < \top$. We can write (for any complex z we denote by $\bar{z}$ its complex conjugate): $P_{if}(u) = z\bar{z}$ where $z = \langle f|U(\top, \tau_2)U(\tau_2, \tau_1)U(\tau_1, 0)|i\rangle$.

Denote for any $m, n = 1, ..., M$: $\omega'_{mn} \equiv \frac{E_m - E_n}{||\mathbf{H}_0||}$ and consider the control defined on $[\tau_1, \tau_2]$:

$$u(\tau) = \varepsilon \cos(\omega'_{lk}(\tau - \tau_1)) \ , \tag{3.3}$$

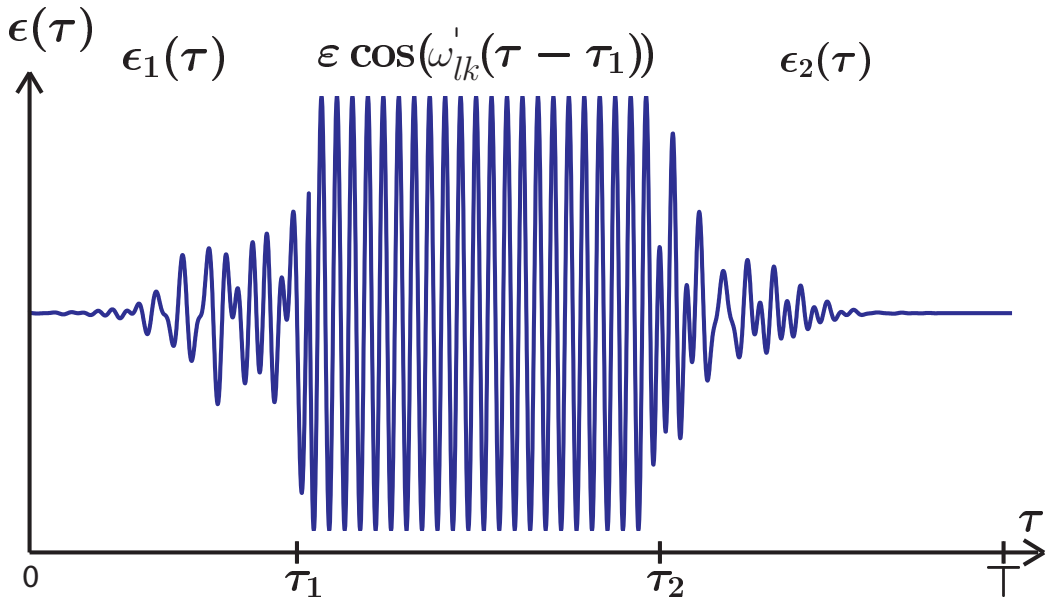

Figure 3.1: A *good* control u has three components (inspired from Ramsey interferometry) to enable the identification of μ_{lk}. The field u_1 is defined over $[0, \tau_1]$ (analog of first Ramsey pulse) to steer the known initial state $|i\rangle$ to $|\psi_1\rangle = |l\rangle$: $|l\rangle = U(\tau_1, 0)|i\rangle$. The field u_2 is defined over $[\tau_2, \top]$ (analog of second Ramsey pulse) is such that $|f\rangle = U(\top, \tau_2)|\psi_2\rangle$ where $|\psi_2\rangle = U(\tau_2, \tau_1)\left(\frac{|l\rangle+\imath|k\rangle}{\sqrt{2}}\right)$ and the propagator $U(\tau_2, \tau_1)$ corresponds, for a long interval $\tau_2 - \tau_1$, to a large number of Rabi oscillations with the control $\varepsilon\cos(\omega'_{lk}(\tau - \tau_1))$ resonant with the $|l\rangle \leftrightarrow |k\rangle$ transition.

where ε is a small strictly positive real parameter. Take $\xi = \frac{||\mu||\varepsilon}{||\mathbf{H}_0||}$. The only remaining degree of freedom in the control over $[\tau_1, \tau_2]$ is ξ, which can be taken arbitrarily small. We define $\mathbf{H}'_0 = \frac{1}{||\mathbf{H}_0||}\mathbf{H}_0$ and $\omega'_{mn} = \langle m|\mathbf{H}'_0|m\rangle - \langle n|\mathbf{H}'_0|n\rangle$. Note that $\omega'_{mn} = -\omega'_{nm}$. We have [Beltrani 2007]

$$\frac{\partial}{\partial \mu'_{lk}} U(\tau_2, \tau_1) = \imath \frac{||\mu||}{||\mathbf{H}_0||} U(\tau_2, \tau_1) \times \int_{\tau_1}^{\tau_2} u(\tau) U^\dagger(\tau, \tau_1) \sigma_x^{lk} U(\tau, \tau_1) d\tau \,. \tag{3.4}$$

We now rewrite (3.2) and (3.4) for the control given in (3.3) on the time interval $[\tau_1, \tau_2]$:

$$\imath \frac{\partial}{\partial \tau} U(\tau, \tau_1) = (\mathbf{H}'_0 - \xi \cos(\omega'_{lk}(\tau - \tau_1))\mu') U(\tau, \tau_1) \tag{3.5}$$

$$\frac{\partial}{\partial \mu'_{lk}} U(\tau_2, \tau_1) = \imath\xi U(\tau_2, \tau_1) \times \int_{\tau_1}^{\tau_2} \cos(\omega'_{lk}(\tau - \tau_1)) U^\dagger(\tau, \tau_1) \sigma_x^{lk} U(\tau, \tau_1) d\tau \,. \tag{3.6}$$

The goal is to show that $\frac{\partial}{\partial \mu'_{lk}} U(\tau_2, \tau_1)$ can be made arbitrarily "large" while $\frac{\partial}{\partial \mu'_{mn}} U(\tau_2, \tau_1)$ stays bounded. Note that all the terms in the integrand of (3.6) are bounded, and a rough estimate of the norm of $\frac{\partial}{\partial \mu'_{lk}} U(\tau_2, \tau_1)$ gives a quantity

proportional to $(\tau_2 - \tau_1)\xi$. Hence, we take $\tau_2 - \tau_1 = \frac{1}{\xi^2}$, implying the need to have expressions for $U(\tau, \tau_1)$ over a time scale on the order of $\frac{1}{\xi^2}$. To this end we state lemma 3.2 which gives such an approximation.

Lemma 3.2. *Consider Eq. (3.5). There exists a Hermitian matrix K and $\xi_0 > 0$ such that, for any $\xi \in]0, \xi_0[$, we have:*

$$\sup_{\tau \in [\tau_1, \tau_1 + \frac{1}{\xi^2}]} ||U(\tau, \tau_1) - e^{-\imath \mathbf{H}_0'(\tau - \tau_1)} e^{\imath(\xi \frac{\mu'_{lk}}{2} \sigma_x^{lk} + \xi^2 K)(\tau - \tau_1)}|| = O(\xi).$$

We continue with the proof of lemma 3.1 and will come back to lemma 3.2 in Section 3.3.4.

Using the expression of $U(\tau, \tau_1)$ given in lemma 3.2, the integrand in (3.6) is:

$$\begin{aligned}\cos(\omega'_{lk}(\tau - \tau_1))U^\dagger(\tau, \tau_1)\sigma_x^{lk}U(\tau, \tau_1) = \\ e^{-\imath(\xi \frac{\mu'_{lk}}{2} \sigma_x^{lk} + \xi^2 K)(\tau - \tau_1)} (\cos(\omega'_{lk}(\tau - \tau_1)) e^{\imath \mathbf{H}_0'(\tau - \tau_1)} \\ \sigma_x^{lk} e^{-\imath \mathbf{H}_0'(\tau - \tau_1)}) e^{\imath(\xi \frac{\mu'_{lk}}{2} \sigma_x^{lk} + \xi^2 K)(\tau - \tau_1)} + O(\xi)\,.\end{aligned}$$

In order to compute (3.6), we need the following result:

$$\begin{aligned}\cos(\omega'_{lk}(\tau - \tau_1)) e^{\imath \mathbf{H}_0'(\tau - \tau_1)} \sigma_x^{lk} e^{-\imath \mathbf{H}_0'(\tau - \tau_1)} &= \tfrac{1}{2}\sigma_x^{lk} + \tfrac{1}{2}\cos(2\omega'_{lk}(\tau - \tau_1))\sigma_x^{lk} \\ &+ \tfrac{1}{2}\sin(2\omega'_{lk}(\tau - \tau_1))\sigma_y^{lk}\,,\end{aligned} \tag{3.7}$$

where we denote $\sigma_y^{lk} = +\imath|l\rangle\langle k| - \imath|k\rangle\langle l|$. In (3.7), the terms oscillating at frequency $2\omega'_{lk}$ independent of ξ will only contribute to $O(\xi)$ in (3.6). We now focus on the contribution of the term with σ_x^{lk} in (3.6) which calls for (see Section 3.5): $\forall \tau$

$$e^{-\imath(\xi \frac{\mu'_{lk}}{2} \sigma_x^{lk} + \xi^2 K)(\tau - \tau_1)} \sigma_x^{lk} e^{\imath(\xi \frac{\mu'_{lk}}{2} \sigma_x^{lk} + \xi^2 K)(\tau - \tau_1)} = \sigma_x^{lk} + O(\xi)\,. \tag{3.8}$$

Introducing (3.8) into (3.6), we find:

$$\frac{\partial}{\partial \mu'_{lk}} U(\tau_2, \tau_1) = \imath \xi U(\tau_2, \tau_1) \left(\frac{\tau_2 - \tau_1}{2} \sigma_x^{lk} + O(1) + (\tau_2 - \tau_1) O(\xi) \right)\,.$$

From now on, we take $\tau_2 = \tau_1 + \frac{1}{\xi^2}$ and obtain:

$$\frac{\partial}{\partial \mu'_{lk}} U(\tau_2, \tau_1) = \imath U(\tau_2, \tau_1)(\tfrac{1}{2\xi}\sigma_x^{lk} + O(1)). \tag{3.9}$$

We define $|\psi_1\rangle \equiv |l\rangle$ and $|\psi_2\rangle \equiv \frac{1}{\sqrt{2}} U(\tau_2, \tau_1)(|l\rangle + \imath|k\rangle)$. Since the system is controllable there exists a time τ_1 and a field $u_1 \in \mathcal{U}_{\tau_1}$ such that $U(\tau_1, 0)|i\rangle = |\psi_1\rangle$, and there exists a time $\top$ and a field u_2 defined over $[\tau_2, \top]$ such that $U^\dagger(\top, \tau_2)|f\rangle = |\psi_2\rangle$. Since the state space is compact (here it is a sphere), we know that if the system is controllable, it is controllable in bounded time, and with bounded controls (see

Theorem 6.5 in [Jurdjevic 1972]). Hence, $\top - \tau_2$ can be chosen bounded for all ξ. Therefore $\frac{\partial}{\partial \mu_{lk}} U(0, \tau_1)$ and $\frac{\partial}{\partial \mu_{lk}} U(\tau_2, \top)$ are bounded. Thus, we have:

$$\frac{\partial}{\partial \mu'_{lk}} P_{if}(u) = 2\Re(\langle f|U(\top,\tau_2)\frac{\partial}{\partial \mu'_{lk}}U(\tau_2,\tau_1)U(\tau_1,0)|i\rangle \\ \langle i|U^\dagger(\tau_1,0)U^\dagger(\tau_2,\tau_1)U^\dagger(\top,\tau_2)|f\rangle) + O(1).$$

We now utilize $U(\tau_1, 0)|i\rangle = |\psi_1\rangle$ and $U^\dagger(\top, \tau_2)|f\rangle = |\psi_2\rangle$ where $|\psi_1\rangle$ and $|\psi_2\rangle$ are defined above, and replace $\frac{\partial}{\partial \mu'_{lk}} U(\tau_2, \tau_1)$ by its expression in (3.9) to find: $\frac{\partial}{\partial \mu'_{lk}} P_{if}(u) = \frac{1}{2\xi} + O(1)$. This expression holds for the control defined as (see Fig. 3.1):

$$u(\tau) = \begin{cases} u_1(\tau), & \text{if } \tau \in [0, \tau_1] \\ \frac{||\mathbf{H}_0||}{||\mu||}\xi \cos(\omega'_{lk}(\tau - \tau_1)), & \text{if } \tau \in]\tau_1, \tau_2[\\ u_2(\tau), & \text{if } \tau \in [\tau_2, \top] \end{cases} \tag{3.10}$$

ii) Part II We now need to prove that $\frac{\partial}{\partial \mu'_{mn}} P_{if}(u) = O(1)$ for $\{m, n\} \neq \{l, k\}$, where u is the control found above in (3.10). As in Eq. (3.6), we have:

$$\frac{\partial}{\partial \mu'_{mn}} U(\tau_2, \tau_1) = \imath\xi U(\tau_2, \tau_1) \times \int_{\tau_1}^{\tau_2} \cos(\omega'_{lk}(\tau - \tau_1)) U^\dagger(\tau, \tau_1)\sigma_x^{mn} U(\tau, \tau_1) d\tau \ , \tag{3.11}$$

and again the result of lemma 3.2 is employed. Eq. (3.11) calls for

$$\begin{aligned} 2\cos(\omega'_{lk}(\tau - \tau_1))e^{\imath \mathbf{H}'_0(\tau-\tau_1)}\sigma_x^{mn}e^{-\imath \mathbf{H}'_0(\tau-\tau_1)} \quad &= \\ \cos((\omega'_{lk} - \omega'_{mn})(\tau - \tau_1))\sigma_x^{mn} - \sin((\omega'_{lk} - \omega'_{mn})(\tau - \tau_1))\sigma_y^{mn} + \\ \cos((\omega'_{lk} + \omega'_{mn})(\tau - \tau_1))\sigma_x^{mn} + \sin((\omega'_{lk} + \omega'_{mn})(\tau - \tau_1))\sigma_y^{mn}. \end{aligned} \tag{3.12}$$

Considering that $\mathbf{H}_0$ has non-degenerate transitions (see definition in Section 3.5) implies that $\omega'_{lk} - \omega'_{mn} \neq 0$ and $\omega'_{lk} + \omega'_{mn} \neq 0$. As the expression in (3.12) oscillates at frequencies independent of ξ, it therefore contributes to $O(\xi)$ in (3.11). Hence, for $\tau_2 - \tau_1 = \frac{1}{\xi^2}$ we can directly conclude that $\frac{\partial}{\partial \mu'_{mn}} P_{if}(u) = O(1)$. □

3.3.4 Proof of lemma 3.2

This proof relies on three consecutive changes of frame that aim to cancel the oscillating terms of order 0 and 1 with respect to ξ. We then derive a specific form of the averaging Theorem (see theorem 4.3.6 in [Sanders 2007] for a general form of the averaging theorem). For the sake of clarity and with no loss of generality, we take $\tau_1 = 0$ and note $U(\tau) \equiv U(\tau, \tau_1)$. Eq. (3.5) may be written in the interaction frame $U_I(\tau) \equiv e^{\imath \mathbf{H}'_0 \tau} U(\tau)$,

$$\frac{\partial}{\partial \tau} U_I(\tau) \quad = \quad \imath\xi \left(\frac{\mu'_{lk}}{2}\sigma_x^{lk} + \frac{\partial}{\partial \tau} H_I(\tau) \right) U_I(\tau)$$

where:

$$\begin{aligned}\frac{\partial}{\partial\tau}H_I(\tau) &= \tfrac{1}{2}\sum_{(m,n)\neq(k,l)}\mu'_{mn}e^{\imath(-\omega'_{kl}+\omega'_{mn})\tau}|m\rangle\langle n| \\ &+ \tfrac{1}{2}\sum_{(m,n)\neq(l,k)}\mu'_{mn}e^{\imath(-\omega'_{lk}+\omega'_{mn})\tau}|m\rangle\langle n|\ ,\end{aligned}$$

and the average of H_I is zero. The average of a time dependent operator $C(\tau)$ is defined as follows (see defintion 4.2.4 in [Sanders 2007]): $\overline{C}=\lim_{\theta\to+\infty}\frac{1}{\theta}\int_0^\theta C(\tau)d\tau$. We now take $U'_I(\tau)=(I-\imath\xi H_I(\tau))U_I(\tau)$. Since $\frac{\partial}{\partial\tau}H_I$ is almost periodic[3], then H_I is also almost periodic and hence bounded for all τ. Hence, there exists $\xi_0>0$, such that $\forall\xi<\xi_0$, $I-\imath\xi H_I(\tau)$ has an inverse and $(I-\imath\xi H_I(\tau))^{-1}=I+\imath\xi H_I(\tau)+O(\xi^2)$. We find:

$$\frac{\partial}{\partial\tau}U'_I(\tau)=\imath\left(\xi\tfrac{\mu'_{lk}}{2}\sigma_x^{lk}-\imath\xi^2\left(\tfrac{\mu'_{lk}}{2}[H_I(\tau),\sigma_x^{lk}]+H_I(\tau)\frac{\partial}{\partial\tau}H_I(\tau)\right)+O(\xi^3)\right)U'_I(\tau).$$

Notice that, with $K=-\imath\overline{H_I\frac{\partial}{\partial\tau}H_I}$ independent of ξ and $\tilde{K}(\tau)$ almost periodic with zero average, we also have: $\frac{\mu'_{lk}}{2}[H_I(\tau),\sigma_x^{lk}]+H_I(\tau)\frac{\partial}{\partial\tau}H_I(\tau)=\imath(K+\frac{\partial}{\partial\tau}\tilde{K}(\tau))$. It is important to note that $\frac{1}{2}\overline{\frac{\partial}{\partial\tau}H_I^2}=0=\overline{H_I\frac{\partial}{\partial\tau}H_I}+\overline{(\frac{\partial}{\partial\tau}H_I)H_I}=\imath(K-K^\dagger)$. Hence $K=K^\dagger$ is Hermitian.

We now take $U''_I(\tau)=(I-\imath\xi^2\tilde{K}(\tau))U'_I(\tau)$. Since $\tilde{K}(\tau)$ is bounded for all τ, then for a sufficiently small ξ, $I-\imath\xi^2\tilde{K}(\tau)$ has an inverse and $(I-\imath\xi^2\tilde{K}(\tau))^{-1}=I+\imath\xi^2\tilde{K}(\tau)+O(\xi^4)$. U''_I satisfies the following equation:

$$\frac{\partial}{\partial\tau}U''_I(\tau)=\imath\left(\xi\tfrac{\mu'_{lk}}{2}\sigma_x^{lk}+\xi^2K+O(\xi^3)\right)U''_I(\tau)\ , \tag{3.13}$$

and we define U_{av} to be the solution to the averaged dynamics ($U_{av}(0)=I$):

$$\frac{\partial}{\partial\tau}U_{av}(\tau)=\imath\left(\xi\tfrac{\mu'_{lk}}{2}\sigma_x^{lk}+\xi^2K\right)U_{av}(\tau)\ . \tag{3.14}$$

We can directly solve (3.14): $U_{av}(\tau)=e^{\imath\left(\xi\frac{\mu'_{lk}}{2}\sigma_x^{lk}+\xi^2K\right)\tau}$. Subtracting (3.13) from (3.14), we find, using Gronwall's lemma, that for all $\tau<\frac{1}{\xi^2}$ one has $U''_I(\tau)=U_{av}(\tau)+O(\xi)$. Also note that to go from U_I to U''_I we have used two consecutive changes of variables which are close to the identity, hence: $\forall\tau\ U''_I(\tau)=U_I(\tau)+O(\xi)$. Finally, since $e^{-\imath\mathbf{H}'_0\tau}$ is an isometry, we have:

$$U(\tau)=e^{-\imath\mathbf{H}'_0\tau}e^{\imath(\xi\frac{\mu'_{lk}}{2}\sigma_x^{lk}+\xi^2K)\tau}+O(\xi)\text{ for all }\tau\leq\tfrac{1}{\xi^2}\ .\square$$

3.4 Conclusion

Identification of the real dipole moment matrix is shown to be well posed for a controllable finite dimensional quantum system with non-degenerate transitions and using as measurements only one population at a final time T. The results also provide a theoretical foundation to optimal discrimination experiments.

[3] It can be written as $\sum_{k=1}^{M}e^{i\omega_k\tau}A_k$

3.5 Definitions and computation

Definition 3.1. *We say that system (3.1) is controllable [D'Alessandro 2008] if for all* $|\psi_1\rangle, |\psi_2\rangle \in \mathcal{S}$ *there exists a time* t *and a control* $u \in \mathcal{U}_t$ *such that for* $|\psi(0)\rangle = |\psi_1\rangle$, *(3.1) leads to* $|\psi(t)\rangle = |\psi_2\rangle$.

Definition 3.2. *Let* $\mathbf{H}_0$ *and* μ *be* $N \times N$ *Hermitian matrices. We denote* $E_1, .., E_N$ *the eigenvalues of* $\mathbf{H}_0$ *and* $|1\rangle, .., |N\rangle$ *its corresponding eigenvectors. We say that* $\mathbf{H}_0$ *has non-degenerate transitions [Turinici 2003] if* $\forall (l,k) \neq (m,n)$, $l \neq k$ *and* $m \neq n$, *such that* $\langle l|\mu|k\rangle \neq 0$ *and* $\langle m|\mu|n\rangle \neq 0$, *we have* $E_l - E_k \neq E_m - E_n$.

Definition 3.3. *Take system (3.1). Let us denote* $\mathcal{M}$ *as the space to which* μ *belongs. We say that* μ *is locally observable in* $\mathcal{M}$ *if there exists* $r > 0$ *such that for all* $\hat{\mu} \in \mathcal{M}$ *with* $0 < ||\hat{\mu} - \mu|| \leq r$ *and* $\hat{\mu} \neq \mu$, *there exists* $T > 0$ *and* $u \in \mathcal{U}_T$ *such that* $P_{if}(u, \hat{\mu}) \neq P_{if}(u, \mu)$.

Computation: Here, we compute

$$\Sigma_x^{lk}(\tau) = e^{-i(\xi \frac{\mu'_{lk}}{2} \sigma_x^{lk} + \xi^2 K)(\tau - \tau_1)} \sigma_x^{lk} e^{i(\xi \frac{\mu'_{lk}}{2} \sigma_x^{lk} + \xi^2 K)(\tau - \tau_1)} .$$

We have $\mu'_{lk} \neq 0$ and $\sigma_x^{lk} + \xi \frac{2K}{\mu'_{lk}}$ is Hermitian. Hence, there exists a unitary matrix P_ξ and a real diagonal matrix Δ_ξ such that $\sigma_x^{lk} + \xi \frac{2K}{\mu'_{lk}} = P_\xi \Delta_\xi P_\xi^\dagger$. The function $\xi \in [0, \xi_0] \to \sigma_x^{lk} + \xi \frac{2K}{\mu'_{lk}}$ is analytic, therefore the eigenvectors of $\sigma_x^{lk} + \xi \frac{2K}{\mu'_{lk}}$ can be continued analytically as a function of ξ (see Theorem 6.1 in chapter II, §6 section 1 and 2 in [Kato 1966]). Hence, $P_\xi = P_0 + O(\xi)$ where P_0 is such that $P_0^\dagger \sigma_x^{lk} P_0 = \sigma_z^{lk}$ is real and diagonal ($\sigma_z^{lk} = |l\rangle\langle l| - |k\rangle\langle k|$). We find, $\forall \tau$: $\Sigma_x^{lk}(\tau) = \sigma_x^{lk} + O(\xi)$, where $O(\xi)$ is a first order term in ξ and a bounded function of τ.

Chapter 4

Adiabatic passage and ensemble control

Contents

Ce chapitre est sur le transfert de population entre états propres du Hamiltonien, dans un système quantique en échelle, contrôlé par un champ électrique. Nous montrons que ce problème peut être traité dans le cadre du passage adiabatique, dont l'efficacité pour le contrôle d'ensemble de systèmes est bien connue. Nous commençons par démontrer la robustesse du champ "chirpé", qui est utilisé par les expérimentateurs pour transférer la population de l'état fondamental vers l'état le plus excité, sur un ensemble de systèmes différents. Nous proposons ensuite des nouvelles lois de commandes robustes qui induisent toute permutation de populations d'états propres d'un ensemble de systèmes. Ces contrôles combinent le balayage en fréquence et la modulation d'amplitude. Ces propositions sont appuyées par des simulations et des preuves donnant des bornes d'erreurs. Ce travail a été réalisé en collaboration

avec Alain Sarlette et Pierre Rouchon, et est paru dans la revue Journal of Physics B [Leghtas 2011].

This chapter considers population transfer between eigenstates of a finite quantum ladder controlled by a classical electric field. Using an appropriate change of variables, we show that this setting can be set in the framework of adiabatic passage, which is known to facilitate ensemble control of quantum systems. Building on this insight, we present a mathematical proof of robustness for a control protocol – chirped pulse – practiced by experimentalists to drive an ensemble of quantum systems from the ground state to the most excited state. We then propose new adiabatic control protocols using a single chirped and amplitude shaped pulse, to robustly perform any permutation of eigenstate populations, on an ensemble of systems with imprecisely known coupling strengths. Such adiabatic control protocols are illustrated by simulations achieving all 24 permutations for a 4-level ladder. This chapter reports the results obtained in collaboration with Alain Sarlette and Pierre Rouchon, and published in Journal of Physics B [Leghtas 2011].

4.1 Introduction

Population transfer from eigenstate k to eigenstate l of a quantum system refers to finding a control input such that the projection of the final system state on eigenstate l of the free Hamiltonian has the same norm as the projection of the initial system state on eigenstate k. Applications of population transfer range from population inversion [Nussenzweig 1993], where k and l are the lowest and highest energy eigenstates, to quantum information processing [Nielsen 2000, Averin 1998, Aharonov 2007], where logic gates would (selectively) permute the populations of several eigenstates. In many applications, including those mentioned, relative insensitivity to variations in system parameters is important for robustness purposes.

In the present chapter, we show how control inputs designed on the basis of adiabatic passage can implement any given permutation of eigenstate populations for a finite anharmonic quantum ladder. The latter is a quantum system with a finite number of unequally spaced energy levels, where only consecutive levels are coupled. The controls we use are chirped pulses [Chelkowski 1990] with appropriately modulated amplitudes and exploit the idea of eigenvalue crossing [Yatsenko 2002]. The ladder consists of a free Hamiltonian with approximately equidistant eigenvalues and where the control input couples eigenstates associated with consecutive eigenvalues. A striking robustness feature is that our control fields must only satisfy a set of key properties and achieve population transfer independently of the values of dipole moments coupling consecutive levels of the ladder. This is a major difference with respect to early non-adiabatic approaches to molecular ladder dissociation using chirped pulses [Chelkowski 1990]. Adiabatic passage through eigenvalue crossings has also very recently been used to prove approximate controllability in finite time

of an infinite dimensional quantum system [Boscain 2011].

In this sense, we achieve a specific form of *ensemble control*. Ensemble control in its most general form wants a single given input to drive an ensemble of systems, with different values of some parameter p, from given p-dependent initial state to given p-dependent final state [Li 2009, definition 1]. Currently, solutions to this general problem are essentially restricted to two-level systems, achieving approximate ensemble control in finite time and exact ensemble control in infinite time [Li 2009, Li 2006, Beauchard 2010]. They rely on accurate knowledge of laser-system coupling strengths and accurately tailored inputs, involving e.g. exact instantaneous "π-amplitude-impulses". In our setting, system parameters need not be exactly known and the input must only satisfy a few key properties. In turn, regarding initial-to-final-state transformations, we are limited to population permutations (with arbitrary relative phases between components of different eigenstates) that are constant as a function of system parameters. Driving an ensemble of 2-level systems from a common initial to a common final state has also been much studied in the NMR context, e.g. with geometric methods [Li 2006].

Adiabatic passage is a control strategy that builds on the adiabatic evolution property: A system state initially close to an eigenstate of a time-varying Hamiltonian $\mathbf{H}(t)$ approximately follows the time-varying eigenstate of $\mathbf{H}(t)$ if it varies slowly enough; the slower $\mathbf{H}(t)$ varies, the better the adiabatic approximation. A thorough formal study of adiabatic evolution can be found in [Avron 1987, Avron 1999, Teufel 2003], on which we build the proofs of our results. Adiabatic evolution has been standard since the early days of quantum mechanics [Messiah 1958], e.g. when interpreting system evolution in terms of "avoided eigenvalue crossings". In a ladder control context, population inversion in two-level systems by a "chirped" pulse — where frequencies of a Gaussian laser pulse are spread out in time — is known by experimentalists and theoretically explained in the adiabatic framework [Allen 1987]. This is the most basic case of our control, section 4.3 with $N = 2$. Many experimentalists have then focused on *multiple-laser techniques*, individually addressing pairwise couplings in an N-level system; this includes stimulated Raman adiabatic passage (STIRAP), see e.g. [Oreg 1984, Shapiro 2009, Vitanov 2001]. For N-level ladder systems specifically, the possibility of population transfer from the lowest to the highest energy eigenstates with a single *chirped* laser pulse has been recognized and exploited in "adiabatic rapid passage" experiments [Hulet 1983, Nussenzweig 1993, Maas 1999, Vitanov 2001]. An analysis of N-level adiabatic molecular dissociation with chirped pulses is given in [Guérin 1997] based on the Floquet representation. In the present chapter we provide a simple mathematical proof of population inversion with avoided crossings (gap condition) based on Favard's Theorem [Favard 1935] and on the roots of orthogonal polynomials [Szegö 1967], and extend the framework by adding amplitude control to perform not only population inversion but all different permutations of free Hamiltonian eigenstates.

The chapter is organized as follows. Section 4.3 gives the formal statement and section 4.6 the proof for N-level population inversion with "adiabatic rapid

passage", actually proving how initial population of level k is finally transferred to level $N-k-1$ in adiabatic approximation. The key point for using adiabatic passage is a change of frame that depends on time-varying control input phase; it is detailed in section 4.2 after formal description of the ladder system. The proof then applies the standard "adiabatic theorem with spectral gap condition", where time-varying eigenvalues are shown to remain separated for all times. The inversion is insensitive to exact energy values of the individual levels in the ladder. Section 4.4 proposes adiabatic control inputs to transfer population between two arbitrary eigenstates. It requires the control field to vanish at specific times which depend on (some) energy levels of the *anharmonic* ladder, such that we select a pair of time-varying eigenvalues to cross. System evolution is then ruled by the "adiabatic theorem without spectral gap condition". A complementary study of system behavior in the neighborhood of two crossing eigenvalues and valid for more general systems than ladder ones, can be found in [Boscain 2010]. We provide a formal proof of the control's effect and highlight its ensemble/robustness features in section 4.6. Section 4.5 finally shows how any permutation of eigenstate populations can be achieved in this adiabatic passage framework. Each control protocol is illustrated by a simulation at the end of the corresponding section.

Notation: We use the Dirac bra-ket notations: $|\psi\rangle \in \mathbb{C}^N$ denotes a complex vector, $\langle\psi| = |\psi\rangle^\dagger$ is its Hermitian transpose, and $\langle .|.\rangle : \mathbb{C}^N \times \mathbb{C}^N \to \mathbb{C} : (|\psi_1\rangle, |\psi_2\rangle) \to \langle\psi_1|\psi_2\rangle = \langle\psi_1||\psi_2\rangle$ is the Hermitian scalar product. For $z \in \mathbb{C}$ we note $\Re(z)$ its real part and z^* its conjugate. $\mathcal{H}_N$ is the set of $N \times N$ Hermitian matrices, where $N \in \mathbb{N}$. We note $\mathbf{I}$ the $N \times N$ identity matrix. For any matrix $A \in \mathbb{C}^{N\times N}$, we denote its Frobenius (or Hilbert-Schmidt) norm $\|A\| = \sqrt{\mathrm{Tr}\,(A^\dagger A)}$ where $\mathrm{Tr}\,(\cdot)$ denotes trace. For $\mathbf{H} \in \mathcal{H}_N$, it holds $\|\mathbf{H}\| = \sqrt{\sum_{i=0}^{N-1} \lambda_i^2}$ where $\lambda_0, \ldots, \lambda_{N-1}$ are the (real) eigenvalues of $\mathbf{H}$. For $\mathbf{H} \in \mathcal{H}_N$ and λ an eigenvalue of $\mathbf{H}$, we denote $\mathbf{P}_\lambda \in \mathcal{H}_N$ the orthogonal projector on the eigenspace of $\mathbf{H}$ associated to the eigenvalue λ. If $\mathbf{H}$ has M distinct eigenvalues $\{\lambda_0, .., \lambda_{M-1}\}$, with $M \leq N$, then $\mathbf{H} = \sum_{k=0}^{N-1} \lambda_k \mathbf{P}_{\lambda_k}$ is the spectral decomposition of $\mathbf{H}$. If $M = N$, then $\mathbf{H}$ is called *non degenerate* and each $\mathbf{P}_{\lambda_k}$ is a rank-one projector. When $M < N$ we say that $\mathbf{H}$ is degenerate; then some $\mathbf{P}_{\lambda_k}$ have rank larger than 1.
$\mathbb{S}^1$ denotes the unit circle equivalent to $\mathbb{R}$ modulo 2π. For J an interval of $\mathbb{R}$, the derivative of a differentiable function $f : J \to \mathbb{S}^1$ is a function from J to $\mathbb{R}$. For all $n \in \mathbb{N}$, we denote $\mathcal{C}^n(J, K)$ the set of n times continuously differentiable functions from J to K, where J is an interval of $\mathbb{R}$ and K is an interval of $\mathbb{R}$ or $\mathbb{S}^1$. A multi-component function is n times continuously differentiable, e.g. $\mathbf{H}(s) \in \mathcal{C}^n(J, \mathcal{H}_N)$, if all its components belong to $\mathcal{C}^n(J, K)$. For $f \in \mathcal{C}^1(J, K \subseteq \mathbb{R}^n)$, we note $f'(y) \in \mathcal{C}^0(J, \mathbb{R}^n)$ the value at $y \in J$ of the derivative of f. $\mathbb{R}_{>0}$ is the set of strictly positive real numbers; we use analog notation with $\geq$, $\leq$ or $<$. $\mathbb{N}_a^b$ is the set of integers from a to b, both boundaries included. When writing $c_0, \ldots, c_{N-1} \in \mathcal{S}$ we mean that c_k belongs to the set $\mathcal{S}$ for each $k \in \mathbb{N}_0^{N\text{-}1}$. Infimum and supremum of a set are noted inf and sup respectively.

4.2 Problem setting

4.2.1 Standard formulation

Consider a quantum system with wavefunction $|\psi\rangle \in \mathbb{C}^N$, $\langle\psi|\psi\rangle = 1$, $N \in \mathbb{N}$, whose dynamics is governed by the Schrödinger equation (with $\hbar = 1$)

$$i\,\frac{d}{dt}|\psi(t)\rangle = \left(\mathbf{H}_0 + u(t)\mathbf{H}_1\right)|\psi(t)\rangle\,. \tag{4.1}$$

The Hamiltonians $\mathbf{H}_0 \in \mathcal{H}_N$ and $\mathbf{H}_1 \in \mathcal{H}_N$ respectively characterize free and control-induced evolution, $u(t)$ being a real scalar control. In the present chapter, we consider a quantum ladder for which the Hamiltonians, in the eigenbasis $\{|0\rangle, \ldots, |N-1\rangle\}$ of $\mathbf{H}_0$, take the form

$$\mathbf{H}_0 = \sum_{k=0}^{N-1} k(\omega_0 + \Delta_k)\,|k\rangle\langle k| \tag{4.2}$$

$$\mathbf{H}_1 = \sum_{k=0}^{N-2} \mu_k\left(|k\rangle\langle k+1| + |k+1\rangle\langle k|\right), \tag{4.3}$$

with $\omega_0 \in \mathbb{R}_{>0}$; $\Delta_0, \ldots, \Delta_{N-1} \in \mathbb{R}$; and $\mu_0, \ldots, \mu_{N-2} \in \mathbb{R}_{>0}$. We assume that system (4.1) features two very different orders of magnitude,

$$||u(t)\mathbf{H}_1|| \approx |\Delta_k| \ll \omega_0 \quad \text{for all } k \text{ and all } t\,. \tag{4.4}$$

Physically, $\mathbf{H}_0$ is the free Hamiltonian of a quantum ladder with mean resonant frequency ω_0 and anharmonicities Δ_k. We call eigenstates $|0\rangle, \ldots, |N-1\rangle$ of $\mathbf{H}_0$ the *levels* of the ladder. $\mathbf{H}_1$ is the dipole moment matrix and models couplings between consecutive eigenstates; it is therefore tridiagonal with zero diagonal elements, and can be taken real positive and symmetric without loss of generality[1]. Condition (4.4) expresses that control amplitude is relatively weak and that the ladder is close to a harmonic one, i.e. eigenvalues of $\mathbf{H}_0$ associated to consecutive eigenstates are close to equidistant. This allows to exploit resonant transitions between all consecutive

[1] The orthonormal basis of eigenvectors of $\mathbf{H}_0$: $\{|k\rangle\}_{k=0,\cdots,N-1}$ is defined up to a phase on each $|k\rangle$. This phase can be chosen arbitrarily. We assume that the system is a quantum ladder, i.e. that $\mathbf{H}_1$ is tridiagonal in the basis $\{|k\rangle\}_{k=0,\cdots,N-1}$, hence it can be written:

$$\mathbf{H}_1 = \sum_{k=0}^{N-2} \mu_k\left(|k\rangle\langle k+1|\right) + c.c\,,$$

where the μ_ks are, a-priori, complex numbers. Now, we may perform the change of frame $|k\rangle \to e^{i\eta_k}|k\rangle$, where the η_ks are real. In this new basis, $\mathbf{H}_1$ is written

$$\mathbf{H}_1 = \sum_{k=0}^{N-2} e^{i(\eta_{k+1}-\eta_k)}\mu_k\left(|k\rangle\langle k+1|\right) + c.c\,.$$

We arbitrarily pick $\eta_0 = 0$, and for all $k \geq 0$, $\eta_{k+1} = \eta_k - arg(\mu_k)$. This cancels the phase of each μ_k and $\mathbf{H}_1$ has only real positive matrix elements in this basis.

eigenstates with a control of carrier frequency ω_0. We consider a typical such control with a small positive parameter ε,

$$u(t) = 2\,\Re\left(e^{i\omega_0 t}E(t)\right)\ , \quad E(t) = A(\varepsilon t)e^{\frac{i}{\varepsilon}\theta(\varepsilon t)} \tag{4.5}$$

$$\text{with } \|\frac{d}{dt}E(t)\| \ll \omega_0\ , \tag{4.6}$$

where $A(t) \in \mathbb{R}$ and $\theta(t) \in \mathbb{S}^1$ for all $t \in \mathbb{R}_{\geq 0}$. The parameter ε governs the rate of variations in the envelope $A(\varepsilon t)$ and frequency $\frac{d}{dt}\frac{1}{\varepsilon}\theta(\varepsilon t) = \theta'(\varepsilon t)$ of $E(t)$; we show in the next sections how taking ε small allows us to apply adiabatic passage properties. The slow but nonzero frequency variation is a key element for our control strategy. Physically, control fields like (4.5) are obtained e.g. by "shaping" a single laser pulse [Weiner 2000].

The rotating wave approximation (RWA), standard in quantum systems modeling, consists in writing (4.1) with the change of variable $|\phi(t)\rangle = \left(\sum_{k=0}^{N-1} e^{ik\omega_0 t}\,|k\rangle\langle k|\right)\,|\psi(t)\rangle$ and neglecting fast oscillating terms, to keep only those that vary at frequencies $\ll \omega_0$. It can be justified by averaging theory [Sanders 2007] thanks to inequalities (4.4),(4.6). Within this approximation, $|\phi\rangle$ follows the dynamics

$$i\frac{d}{dt}|\phi(t)\rangle = (\bar{\mathbf{H}}_I + \widetilde{\mathbf{H}}_I(t))\,|\phi(t)\rangle \tag{4.7}$$

where

$$\begin{aligned}\bar{\mathbf{H}}_I &= \sum_{k=0}^{N-1} k\Delta_k\,|k\rangle\langle k| \\ \widetilde{\mathbf{H}}_I(t) &= \sum_{k=0}^{N-2} \mu_k(E(t)|k\rangle\langle k+1| + E^*(t)|k+1\rangle\langle k|)\ .\end{aligned}$$

4.2.2 Change of frame

Hamiltonian $\widetilde{\mathbf{H}}_I(t)$ contains a control field whose phase $\frac{1}{\varepsilon}\theta(\varepsilon t)$ varies on timescales of order one. The key idea to apply adiabatic passage to the N-level system is an appropriate further change of frame on (4.7), such that all explicit time-dependence in the resulting dynamics involves timescales of order ε. To this end, we extend the change of frame given in [Allen 1987, Section 4.6] for the two-level case and define $|\xi(t)\rangle = \sum_{k=0}^{N-1} e^{k\frac{i}{\varepsilon}\theta(\varepsilon t)}\,|k\rangle\langle k|\ |\phi(t)\rangle$. The two changes of frames come down to writing the system dynamics in the frame imposed by the field phase $\omega_0 t + \theta(\varepsilon t)/\varepsilon$. Dynamics (4.7) becomes

$$i\frac{d}{dt}|\xi(t)\rangle = (\mathbf{H}_R(\omega(\varepsilon t)) + A(\varepsilon t)\mathbf{H}_1)\,|\xi(t)\rangle \tag{4.8}$$

with $\omega = \theta'$, $\mathbf{H}_1$ given by (4.3) and

$$\mathbf{H}_R(v) = \sum_{k=0}^{N-1} k(\Delta_k - v)\,|k\rangle\langle k| \quad \text{for all } v \in \mathbb{R}\ . \tag{4.9}$$

Define the propagator U^ε to be a time-dependent N by N unitary matrix such that the solution of (4.8) is given by $|\xi(t)\rangle = U^\varepsilon(t)|\xi(0)\rangle$ for all t and for all $|\xi(0)\rangle$. Then U^ε follows the dynamics

$$i\varepsilon\frac{d}{ds}U^\varepsilon(s) \;=\; \mathbf{H}(s)\,U^\varepsilon(s)\;,\quad U^\varepsilon(0)=\mathbf{I} \tag{4.10}$$

$$\text{with}\qquad \mathbf{H}(s) \;=\; \mathbf{H}_R(\omega(s)) + A(s)\mathbf{H}_1 \tag{4.11}$$

in the time scale $s=\varepsilon t$. In the following, we study system (4.10) for s in the interval $[0,1]$ and with $A(s)$ and $\omega(s)$ as controls. Our goal is to achieve:

(a) *Adiabatic approximate eigenstate permutations:*

$$\lim_{\varepsilon\to 0^+}\ \max_{k\in G}\ \|\,U^\varepsilon(1)|k\rangle\langle k|U^\varepsilon(1)^\dagger - |\sigma(k)\rangle\langle\sigma(k)|\,\| = 0 \tag{4.12}$$

for given $G\subseteq \mathbb{N}_0^{N\text{-}1}$ and given permutation σ of $(0,\dots,N-1)$.

(b) *Ensemble control:* a single control (A,ω) achieves such eigenstate permutation on an ensemble of systems with different parameter values; the parameters are the dipole moments $(\mu_0,\dots,\mu_{N-2})$ and, in some cases, the anharmonicities $(\Delta_0,\dots,\Delta_{N-1})$.

(c) *Robust control inputs:* the above holds for any (A,ω) that satisfy a set of key properties, and do not necessitate having a perfect shape for (A,ω).

Remark 4.1. *Writing (4.12) in terms of $|k\rangle\langle k|$, the projector on eigenspace $\{\beta\,|k\rangle : \beta\in\mathbb{C}\}$, expresses that the goal is really population transfer, i.e. we allow $U^\varepsilon(1)|k\rangle \approx e^{i\chi_k}|\sigma(k)\rangle$ with arbitrary phases $\chi_k\in\mathbb{S}^1$. Both frame changes — for RWA in section 4.2.1 and θ-dependent in section 4.2.2 — involve only phase changes on eigenstates. Therefore, for all t and for all $|k\rangle$,*

$$\begin{aligned}\||\psi(t)\rangle\langle\psi(t)| - |k\rangle\langle k|\| &= \||\phi(t)\rangle\langle\phi(t)| - |k\rangle\langle k|\| \\ &= \||\xi(t)\rangle\langle\xi(t)| - |k\rangle\langle k|\|\;.\end{aligned}$$

4.3 Robust ensemble transfer from $|k\rangle$ to $|N-k-1\rangle$

In this section we consider a control protocol – chirped pulse – used by physicists to drive a system from the lowest eigenspace, spanned by $|0\rangle$, to the highest eigenspace, spanned by $|N-1\rangle$, of the free Hamiltonian $\mathbf{H}_0$ given in (4.2). In fact we prove that a general (robust) class of control inputs transfers population from eigenstate $|k\rangle$ to eigenstate $|N-k-1\rangle$, for all k, on an ensemble of systems with different values of parameters $\mu_0,\dots,\mu_{N-2}$ (dipole moments) and $\Delta_0,\dots,\Delta_{N-1}$ (anharmonicities).

The key requirements on the control are (i) to use a sufficiently chirped pulse — condition (b) in Theorem 4.1 — and (ii) to avoid all eigenvalue crossings — condition (c) in Theorem 4.1.

4.3.1 Transfer Theorem

For $k = 0, \ldots, N-1$, we denote the eigenvalues of $\mathbf{H}_R(\omega(s))$ by $\lambda_k^R(s) = \langle k|\mathbf{H}_R(\omega(s))|k\rangle = k(\Delta_k - \omega(s))$.

Theorem 4.1. *For given $\Delta > 0$, $\mu_{max} > \mu_{min} > 0$, consider $\mathcal{S}$ an ensemble of systems of type (4.10) with $\mu_j \in [\mu_{min}, \mu_{max}]$ for all $j \in \mathbb{N}_0^{N\text{-}2}$ and $\Delta_j \in [-\Delta, \Delta]$ for all $j \in \mathbb{N}_0^{N\text{-}1}$. Take controls A and ω with:*

(a) A and $\omega \in \mathcal{C}^2([0,1], \mathbb{R})$

(b) $\omega(0)$ and $\omega(1)$ are such that, for all systems in $\mathcal{S}$,

$$\begin{aligned} &\lambda_0^R(0) < \ldots < \lambda_{N-1}^R(0) \quad \textit{and} \\ &\lambda_0^R(1) > \ldots > \lambda_{N-1}^R(1) \end{aligned} \tag{4.13}$$

(c) $A(0) = A(1) = 0$ and $A(s) \neq 0$ for $s \in]0,1[$

Then $\exists$ a constant $C > 0$ such that, for all $\varepsilon > 0$,

$$\sup_{\substack{\mathcal{S} \\ k \in \mathbb{N}_0^{N\text{-}1}}} \| U^\varepsilon(1)|k\rangle\langle k|U^\varepsilon(1)^\dagger - |N-k-1\rangle\langle N-k-1| \| \quad \leq \quad C\varepsilon\,.$$

The proof of this theorem is given in section 4.6; we there actually replace the simple condition (c) on A by a more general one: $A(0) = A(1) = 0$ and $A(s) \neq 0$ for all $s \in \mathcal{I}^\omega(\mathcal{S})$, where

$$\mathcal{I}^\omega \quad = \quad \{s \in [0,1] : \mathbf{H}_R(\omega(s)) \textit{ is degenerate for some system } \in \mathcal{S}\}\,. \tag{4.14}$$

The argument is based on the facts that the system approximately follows eigenstates of $\mathbf{H}(s)$ for small enough ε (adiabatic theorem), eigenvalues of $\mathbf{H}_R$ are inverted between $s = 0$ and $s = 1$ thanks to $\omega(s)$ (chirping), and nonzero $A(s)$ avoids all crossings for eigenvalues of $\mathbf{H}(s)$ such that e.g. the initial highest-energy level $|N-1\rangle$ connects to the final highest-energy level $|0\rangle$ (see Lemma 4.1 in section 4.6). Theorem 4.1 implies that for a given control satisfying the assumptions, taking ε small enough allows one to invert the state populations of a whole ensemble of systems featuring different parameter values. Note that however, the phases in the resulting states depend on the parameter values. The control inputs only need to satisfy a few weak conditions and are therefore robust to many perturbations. These insensitivity properties of the adiabatic passage protocol have long been recognized by experimentalists. They commonly use the following type of control, see e.g. [Vitanov 2001].

Example 1. *A function ω satisfying the inequalities (4.13) is e.g. $\omega(s) = \alpha(s - \frac{1}{2})$, for a large enough positive α; such ω is said to perform a frequency sweep. Typically, such inputs are obtained by a "chirped" Gaussian laser pulse, which takes the form $E(t) = E_0 \int_{-\infty}^{+\infty} e^{-\zeta^2\tau^2}\, e^{i\kappa\zeta^2}\, e^{-i\zeta t}\, d\zeta$ where $\kappa \neq 0$ characterizes chirping.*

Theorem 4.1 still holds if inequality (4.13) is replaced by

$$\lambda_0^R(0) > \ldots > \lambda_{N-1}^R(0) \text{ and } \lambda_0^R(1) < \ldots < \lambda_{N-1}^R(1)\,,$$

i.e. the direction of the frequency sweep in Example 1 can be inverted (taking a large enough *negative* α). However, for a given system, choosing one inequality over the other may allow to get a lower value for the constant hidden in the "order of magnitudes" result. This brings a mathematical foundation to the experimental observations made e.g. in [Maas 1999].

4.3.2 Simulations

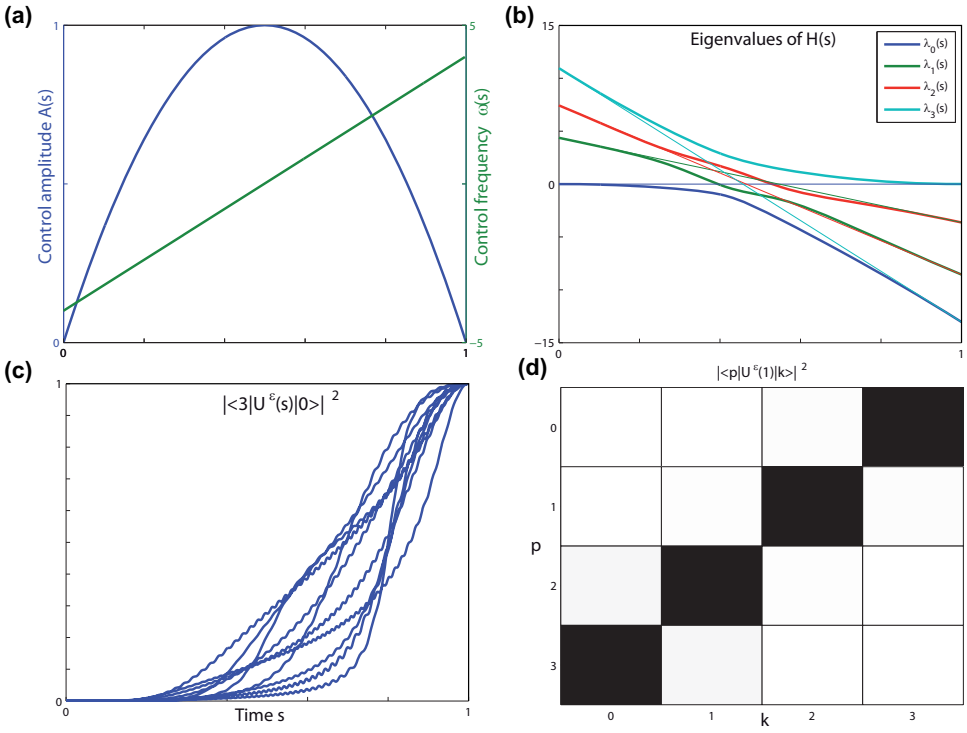

Figure 4.1: Control scheme transferring $|k\rangle$ to $|N-k-1\rangle$. (a) control inputs $A(s)$, $\omega(s)$. (b) s-dependent eigenvalues of $\mathbf{H}(s)$ (thick lines) and of $\mathbf{H}_R(\omega(s))$ (thin lines). (c) population on level $|3\rangle$ for 10 systems whose parameters μ_0, μ_1, μ_2 and $\Delta_1, \Delta_2, \Delta_3$ were randomly picked respectively in $[1,5]$ and $[-0.4, 0.4]$, and all starting at the initial state $|0\rangle$. (d) squared norm of the matrix elements of $U^\varepsilon(1)$, represented in shading from white (value 0) to black (value 1).

We simulate system (4.10) with a control satisfying assumptions (a), (b) and (c) of Theorem 4.1. We consider a 4-level quantum ladder (so $N = 4$). We take $\varepsilon = 10^{-2}$, $\Delta_0, \ldots, \Delta_3 \in [-\Delta, \Delta] = [-0.4, 0.4]$ and $\mu_0, \mu_1, \mu_2 \in [\mu_{min}, \mu_{max}] = [1, 5]$. The control is $\omega(s) = 8(s - \frac{1}{2})$ and $A(s) = s(1-s)$, represented on Fig.4.1.a. In Fig.4.1.b, we show how the eigenvalues of $\mathbf{H}(s)$ (thick lines) avoid crossing For the

illustrated random choice of detunings, the eigenvalues of $\mathbf{H}_R(\omega(s))$ (thin lines) are very close to concurrent between $s = 0.5$ and $s = 0.6$. This poses no problem for the adiabatic transfer from $|k\rangle$ to $|N-k-1\rangle$. The successful transfer is illustrated on Fig.4.1.d, which shows the squared norm of the projection of $U^\varepsilon(1)|k\rangle$ onto $|p\rangle$, for all pairs $(|k\rangle, |p\rangle)$ of eigenvectors of $\mathbf{H}_0$; this is equivalent to the squared norm of element on row p, column k of matrix $U^\varepsilon(1)$ that acts by left-multiplication on initial column-vectors, for $U^\varepsilon(1)$ expressed in basis $(|0\rangle, \ldots, |3\rangle)$. Fig. 4.1.c shows ensemble control on ten systems with different random values of $\Delta_0, \ldots, \Delta_3$ and μ_0, μ_1, μ_2.

4.4 Robust ensemble transfer from $|l\rangle$ to $|p\rangle$

In this section we propose a new robust control protocol to drive a system from the eigenspace (of free Hamiltonian $\mathbf{H}_0$) spanned by $|l\rangle$ to the eigenspace spanned by $|p\rangle$, for any given l and p in $\mathbb{N}_0^{N\text{-}1}$. The population transfer works on an ensemble of systems with different values of $\mu_0, \ldots, \mu_{N-2}$ (dipole moments), and for a general class of inputs where zero-crossings of $A(s)$ must coincide with degeneracies of $\mathbf{H}_R(\omega(s))$; the latter depend on $\omega(s)$ and (some of the) anharmonicities $\Delta_0, \ldots, \Delta_{N-1}$, which must hence be fixed.

4.4.1 From $|0\rangle$ to any $|p\rangle$

For the sake of clarity, we start by giving sufficient conditions on A and ω for the particular population transfer from $|0\rangle$ to arbitrary level $|p\rangle$. Section 4.4.2 generalizes the result to arbitrary initial state $|l\rangle$. Consider the following assumptions:

(A1) $\mathcal{S}$ is an ensemble of systems of type (4.10) with $\mu_j \in [\mu_{min}, \mu_{max}]$ for all $j \in \mathbb{N}_0^{N\text{-}2}$, for some given $\mu_{max} > \mu_{min} > 0$, and with given sequence of detunings $(\Delta_0, \ldots, \Delta_{N-1})$, such that the set $\{k(\Delta_k - v) \colon k \in \mathbb{N}_0^{N\text{-}1}\}$ contains at least $N-1$ distinct values for any $v \in \mathbb{R}$;

(A2) ω is analytic and $\frac{d}{ds}\omega(s) > \gamma > 0$ for all $s \in [0,1]$;

(A3) $\omega(0)$ and $\omega(1)$ are such that (4.13) holds.

For any m and n in $\mathbb{N}_0^{N\text{-}1}$ with $m < n$, we note $s(m,n)$ the unique time[2] where $\lambda_m^R(s(m,n)) = \lambda_n^R(s(m,n))$.

As all systems in $\mathcal{S}$ have the same sequence of detunings, they feature the same eigenvalues $\lambda_0^R, \ldots, \lambda_{N-1}^R$ of $\mathbf{H}_R$ and hence the same set of $s(m,n)$. The set of all $s(m,n)$ equals $\mathcal{I}^\omega$ defined in (4.14), with dependence on particular system $\in \mathcal{S}$ becoming irrelevant. The end of (A1) further implies that $\mathbf{H}_R$ has at most one pair of equal eigenvalues for any $s \in [0,1]$ i.e. $(m,n) \neq (j,k)$ implies $s(m,n) \neq s(j,k)$, hence $\mathcal{I}^\omega$ contains $N(N-1)/2$ distinct values. Further define $\mathcal{I}_0^\omega = \{s_1, \ldots, s_{N-1}\} \subset \mathcal{I}^\omega$

[2] If assumptions (A1) to (A3) hold, then the existence and uniqueness of $s(m,n)$ is ensured for all m and $n > m$: see Fig.4.2.b or Fig.4.3.c

the $N-1$ points where $\lambda_0^R(s) = \lambda_n^R(s)$ for some $n \in \mathbb{N}_1^{N\text{-}1}$, numbered such that $s_1 < s_2 < \ldots < s_{N-1}$. Thus, for each $s_k \in \mathcal{I}_0^\omega$ there exists a unique $n \in \mathbb{N}_1^{N\text{-}1}$ such that $s_k = s(0,n)$.

The key requirements on the control to achieve population transfer from $|0\rangle$ to $|p\rangle$ are (i) to use a sufficiently chirped pulse frequency (condition (A3)) and (ii) to shape the pulse amplitude in order to appropriately provoke ((c) in Theorem 4.2) or avoid ((b),(d) in Theorem 4.2) crossing of eigenvalues of $\mathbf{H}$.

Theorem 4.2. *Consider $\mathcal{S}$ an ensemble of systems satisfying (A1) with a control ω satisfying (A2) and (A3). Take $p \in \{0,\ldots,N-1\}$ and consider a control A with the following properties:*

(a) A is analytic over $[0,1]$ and $A(0) = A(1) = 0$.

(b) $A(s) \neq 0$ for all $s \in \mathcal{I}^\omega \backslash \mathcal{I}_0^\omega$.

(c) $A(s_k) = 0$ for all $s_k \in \mathcal{I}_0^\omega$ with $k \leq N-p-1$.

(d) $A(s_k) \neq 0$ for all $s_k \in \mathcal{I}_0^\omega$ with $k \geq N-p$.

Then $\exists$ a constant $C > 0$ such that, for all $\varepsilon > 0$,

$$\sup_{\mathcal{S}} \parallel U^\varepsilon(1)|0\rangle\langle 0|U^\varepsilon(1)^\dagger - |p\rangle\langle p| \parallel \quad \leq \quad C\sqrt{\varepsilon}\,.$$

The proof, given in section 4.6, shows that at eigenvalue crossing points the system adiabatically follows the eigenvector corresponding to the *crossing* branch.

4.4.2 From any $|l\rangle$ to any $|p\rangle$

Under assumptions (A1) to (A3), we denote $\mathcal{I}_{k+}^\omega(s) = \{s(m,n) \in \mathcal{I}^\omega : m = k,\ n > k \text{ and } s(m,n) > s\}$ and $\mathcal{I}_{k-}^\omega(s) = \{s(m,n) \in \mathcal{I}^\omega : m < k,\ n = k \text{ and } s(m,n) > s\}$, for any $k \in \mathbb{N}_0^{N\text{-}1}$. Further let $q_{k\pm}(s) = \inf(\mathcal{I}_{k\pm}^\omega(s))$ and define $g_{k\pm}(s)$ by $s(k, g_{k+}(s)) = q_{k+}(s)$ and $s(g_{k-}(s), k) = q_{k-}(s)$ respectively. For $p \leq N-l-1$, construct $\mathcal{I}_{lp}^\omega$ with the following algorithm.

1. $d := 0$; $x := 0$; $k := l$; $\mathcal{I}_{lp}^\omega := \emptyset$;
2. **while** $d < N-l-p-1$ **do**
3. **while** [$\mathcal{I}_{k-}^\omega(x) \neq \emptyset$ **and** $q_{k-}(x) < q_{k+}(x)$] **do**
4. $k := g_{k-}(x)$; $x := q_{k-}(x)$;
5. **end while**
6. $\mathcal{I}_{lp}^\omega := \mathcal{I}_{lp}^\omega \cup \{q_{k+}(x)\}$; $d := d+1$; $x := q_{k+}(x)$;
7. **end while**

The algorithm is verified to always successfully complete[3]. For $p \geq N-l-1$, we can define $\mathcal{I}^{\omega}_{lp}$ with a similar algorithm but where '$<$' is changed to '$>$' on line 2 and indices $_{k-}$, $_{k+}$ are switched. Then $\mathcal{I}^{\omega}_{lp}$ contains $|N-l-p-1|$ elements.

Corollary 4.1. *Consider $\mathcal{S}$ an ensemble of systems satisfying (A1) with a control ω satisfying (A2) and (A3). Take l, p in $\mathbb{N}_0^{N\text{-}1}$ and consider a control A with the following properties:*

(a) A is analytic over $[0,1]$ and $A(0) = A(1) = 0$.

(b) $A(s) = 0$ for all $s \in \mathcal{I}^{\omega}_{lp}$.

(c) $A(s) \neq 0$ for all $s \in \mathcal{I}^{\omega} \setminus \mathcal{I}^{\omega}_{lp}$.

Then $\exists$ a constant $C > 0$ such that, for all $\varepsilon > 0$,

$$\sup_{\mathcal{S}} \parallel U^{\varepsilon}(1)|l\rangle\langle l|U^{\varepsilon}(1)^{\dagger} - |p\rangle\langle p| \parallel \quad \leq \quad C\sqrt{\varepsilon}\,.$$

Assumption (A1) ensures that each eigenvalue crossing / anti-crossing can be addressed individually. This ensures that any transfer can be implemented in any situation, but it is in general not necessary for a given system and transfer, as (simultaneous) crossings of some eigenvalue branches are irrelevant. The control proposed for Theorem 4.2 or Corollary 4.1 is just one amongst many possibilities of "eigenvalue crossing designs". Indeed, depending on (l,p) and on the particular arrangement of the $s(m,n)$, one can find other subsets $\mathcal{J}_{lp} \subset \mathcal{I}^{\omega}$ such that taking $A(s) = 0$ if and only if $s \in \mathcal{J}_{lp}$, permutes the eigenvalues in such a way that $\lambda_l(1) = \lambda_p^R(1)$. The controls that we propose are optimal in the sense that they require a minimal number of pairwise crossings, that is of nullings of A at accurate points. Variant annihilation subsets $\mathcal{J}_{lp}$ may be useful (i) to avoid some crossing points $s(m,n)$ or eigenvalue branches (e.g. because corresponding Δ_m or Δ_n is poorly known, or because $s(m,n)$ is close to some other point in $\mathcal{I}^{\omega}$), (ii) to optimize adiabatic convergence as a function of ε, or (iii) to simultaneously perform population transfers between several eigenstates, as we do in section 4.5.

Another approach [Thomas 2005] for transferring $|l\rangle$ to $|p\rangle$ is to use $A(s)$ Gaussian, i.e. without any nulls, but reduce $\omega(s)$ to a specific range. Indeed, under the above assumptions, it is possible to choose $\omega_{\min}$ and $\omega_{\max}$ such that $l(\Delta_l - \bar{v}) = p(\Delta_p - \bar{v})$ for some $\bar{v} \in [\omega_{\min}, \omega_{\max}]$ and $\mathbf{H}_R(v)$ is non-degenerate for all $v \in [\omega_{\min}, \omega_{\max}] \setminus \{\bar{v}\}$. Then taking $\omega(s)$ monotone between $\omega_{\min}$ and $\omega_{\max}$ just induces one avoided crossing that exchanges $|l\rangle$ and $|p\rangle$. Pictorially, this is like selecting a particular narrow vertical slice on Fig.4.1.b. Depending on the specific system under study and whether it is experimentally easier to precisely modulate the amplitude or the phase of a field, one method may be more suitable than

[3] Indeed by construction, the cardinality of $\mathcal{I}^{\omega}_{k+}(x)$ equals $N-l-d-1$ (except *during* the update on line 6) and the cardinality of $\mathcal{I}^{\omega}_{k-}(x)$ decreases by one each time line 4 is applied; thus it is impossible to keep applying line 4 infinitely, and line 6 is always well-defined (that is $\mathcal{I}^{\omega}_{k+}(x) \neq \emptyset$) for $d < N-l-1$.

the other. A main advantage of our method is that, unlike the method proposed in [Thomas 2005], it can be extended to achieve any permutation of eigenstates as is shown in section 4.5.

4.4.3 Simulations

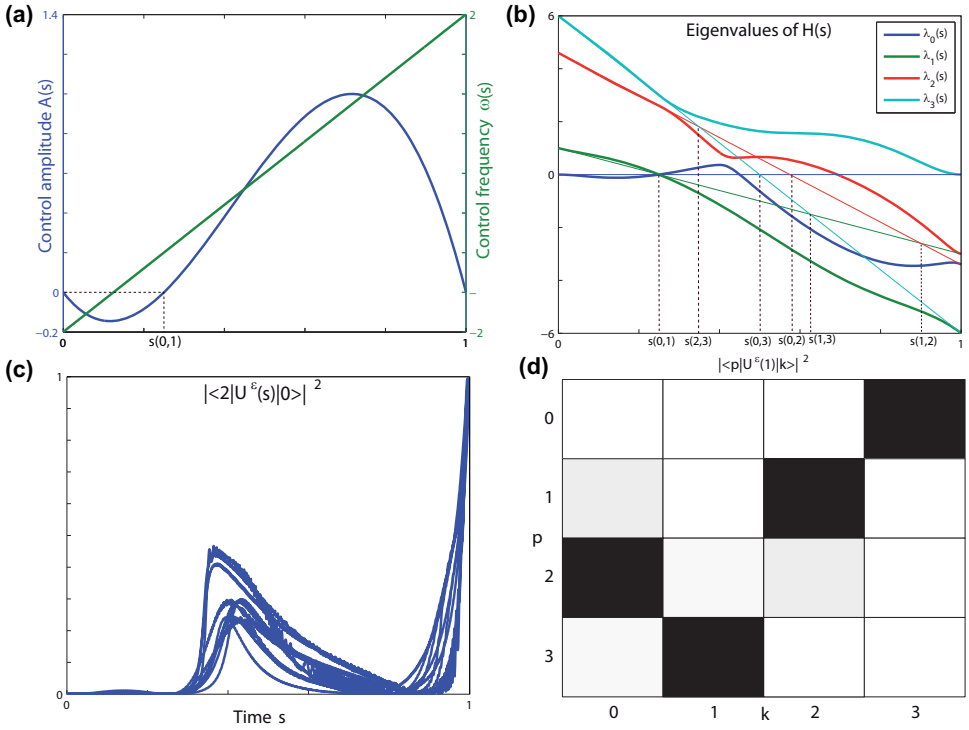

Figure 4.2: Control scheme transferring $|0\rangle$ to $|2\rangle$; subplots analogue to Fig.4.1, except that $\Delta_1, \Delta_2, \Delta_3$ remain fixed for (c). A(s) vanishes at $s = 0.25$ so that λ_0 and λ_1 cross instead of avoiding crossing.

As in section 4.3.2 we simulate (4.10) for a 4-level quantum ladder (so $N = 4$) with $\mu_0, \mu_1, \mu_2 \in [\mu_{min}, \mu_{max}] = [1, 5]$. We now take $\varepsilon = 10^{-3}$ and in accordance with the statement of Theorem 4.2 we fix the anharmonicities, taking $\Delta_1 = -1$, $\Delta_2 = 0.3$, $\Delta_3 = 0$ (the value of Δ_0, multiplied by $k = 0$, is irrelevant). We target in particular a transfer from $|0\rangle$ to $|2\rangle$. The algorithm of section 4.4.2 reduces to the simple case of Theorem 4.2, requesting a single zero of $A(s)$ at $s = \inf\{s(0,1), s(0,2), s(0,3)\} = s(0,1) = 0.25$ in addition to $A(0) = A(1) = 0$. We take $A(s) = s(1-s)(s-0.25)$ and $\omega(s) = 4(s - \frac{1}{2})$, represented on Fig.4.2.a. In Fig.4.2.b, we show how the eigenvalues $\lambda_k(s)$ of $\mathbf{H}(s)$ cross or not (thick lines); the eigenvalues of $\mathbf{H}_R(\omega(s))$ (thin lines) define points $s(m,n)$ for our control design. Fig.4.2.d confirms achievement of the intended result by showing the squared norm of components of matrix $U^\varepsilon(1)$ in basis $(|0\rangle, \ldots, |3\rangle)$: we indeed have $|\langle p|U^\varepsilon(1)|k\rangle|^2 \approx 1$ for $(p,k) = (2,0)$ (other values incidental). Fig.4.2.c illustrates ensemble control on

ten systems with different random values of μ_0, μ_1, μ_2. Since for this particular case the control only exploits a precise crossing point $s(0,1) = 0.25$, we might actually allow ensembles of systems with different Δ_2, Δ_3.

4.5 Robust ensemble permutation of populations

In this section we describe the most general result of the chapter, adiabatically transferring $(|0\rangle\langle 0|, \ldots, |N-1\rangle\langle N-1|)$ to $(|\sigma(0)\rangle\langle\sigma(0)|, \ldots, |\sigma(N-1)\rangle\langle\sigma(N-1)|)$, where σ is any permutation of $\mathbb{N}_0^{N\text{-}1}$. As in section 4.4, the population permutation works on an ensemble of systems with different values of $\mu_0, \ldots, \mu_{N-2}$ (dipole moments), and for a general class of inputs where zero-crossings of $A(s)$ must coincide with degeneracies of $\mathbf{H}_R(\omega(s))$; the latter depend on $\omega(s)$ and require anharmonicities $\Delta_0, \ldots, \Delta_{N-1}$ to be fixed and known. We prove existence of an appropriate control by recurrence on N. In fact this recurrence method can be used to design $A(s)$, as we illustrate in section 4.5.2.

4.5.1 Permutation theorem

Theorem 4.3. *Consider $\mathcal{S}$ an ensemble of systems satisfying (A1) with a control ω satisfying (A2) and (A3). Take σ to be any permutation of $\mathbb{N}_0^{N\text{-}1}$. Then there exists a subset $\mathcal{I}_A \subseteq \mathcal{I}^\omega$ for which, taking control A to satisfy*

(a) A analytic over $[0,1]$ and $A(0) = A(1) = 0$,

(b) $A(s) = 0$ for all $s \in \mathcal{I}_A$,

(c) $A(s) \neq 0$ for all $s \in \mathcal{I}^\omega \setminus \mathcal{I}_A$,

implies: $\exists$ a constant $C > 0$ such that, for all $\varepsilon > 0$,

$$\sup_{\substack{\mathcal{S} \\ k \in \mathbb{N}_0^{N\text{-}1}}} \| U^\varepsilon(1)|k\rangle\langle k|U^\varepsilon(1)^\dagger - |\sigma(k)\rangle\langle\sigma(k)| \| \quad \leq \quad C\sqrt{\varepsilon}\,.$$

Since the proof of this Theorem is constructive and necessary for the understanding of the example below, we present it here.

Proof 4.1 (of Theorem 4.3)**.** *The formal arguments (sup, adiabatic propagator) are presented in detail in the proof of Theorem 4.1 in section 4.6. We focus on the construction of the control $A(s)$ by following analytic eigenvalue branches of $\mathbf{H}(s)$.*

The property is obvious for $N = 2$: either $(\sigma(0), \sigma(1)) = (1, 0)$, which follows Theorem 4.1 just requiring $A(s(0,1)) \neq 0$; or $(\sigma(0), \sigma(1)) = (0, 1)$, which follows Theorem 4.2 transferring $|0\rangle$ to $|p\rangle = |0\rangle$ with one crossing[4], i.e. just requiring $A(s(0,1)) = 0$.

[4]Indeed, $\{\mathbf{P}_{\lambda_0(1)}, \mathbf{P}_{\lambda_1(1)}\} = \{|0\rangle\langle 0|, |1\rangle\langle 1|\}$ then automatically implies transferring $|1\rangle\langle 1|$ to $\mathbf{P}_{\lambda_1(1)} = |1\rangle\langle 1|$.

Assume that we can achieve any permutation of $\mathbb{N}_0^{K\text{-}1}$ *for* $N = K$*, and we are given a permutation* σ *of* $\mathbb{N}_0^K$ *for* $N = K+1$ *where* $\sigma(l) = K$ *and* $\sigma(K) = p$*.*
• *If* $l = p = K$*, i.e.* $\sigma(K) = K$*, then first build the remaining permutation on levels* $|0\rangle, \ldots, |K-1\rangle$ *by neglecting level* $|K\rangle$*. This uses the result for* $N = K$*; it just requires* $A(s) = 0$ *for some* $s = s(m,n)$ *and* $A(s) \neq 0$ *for some other* $s = s(m,n)$*, with* $m, n < K$*. Now take a particular such* $A(s)$ *where in addition,* $A(s) = 0$ *for all* $s \in \{s(m,K) : m \in \mathbb{N}_0^{K\text{-}1}\}$*. Then* $\lambda_K(s)$*, starting at* $\lambda_K(0) = \lambda_K^R(0)$*, exactly follows the same crossings as* $\lambda_K^R(s)$ *to end up as* $\lambda_K(1) = \lambda_K^R(1)$*; the other levels remain unperturbed, so* σ *is achieved.*
• *If* $l \neq K \neq p$*, then first construct* $\overline{A}(s)$ *by applying the result of the preceding point to* $\overline{\sigma}$*, defined by*

$$\overline{\sigma}(l) = p\,;\;\; \overline{\sigma}(K) = K\,;\;\; \overline{\sigma}(k) = \sigma(k) \text{ for all } k \notin \{l, K\}\,.$$

$\overline{A}(s)$ *performs the target permutation, except that* K *remains on* K *and* l *goes to* p*. From (4.13) eigenvalue branch* $\lambda_K(s)$ *necessarily crosses, at some* $\overline{s} \in \{s(m,K) : m \in \mathbb{N}_0^{K\text{-}1}\}$*, the analytic eigenvalue branch that starts at* $\lambda_l(0) = \lambda_l^R(0)$ *and ends at* $\lambda_l(1) = \lambda_p^R(0)$*. Define* $A(s)$ *to have the same zeros as* $\overline{A}(s)$ *except that* $A(\overline{s}) \neq 0$*. This just transforms the crossing at* $\overline{s}$ *into an anti-crossing, such that the analytic branch coming from* $\lambda_K(0)$ *(resp.* $\lambda_l(0)$*) now connects to the analytic branch going to* $\lambda_p(1)$ *(resp.* $\lambda_K(1)$*). Thus* $A(s)$ *achieves the target permutation* σ*.* □

Each "eigenvalue crossing design" choice $\mathcal{I}_A$ yields a particular permutation $\sigma_{\mathcal{I}_A}$. For $N > 2$, the number $2^{N(N-1)/2}$ of possible $\mathcal{I}_\mathcal{A}$ (i.e. subsets of $\mathcal{I}^\omega$) is strictly larger than the number $N!$ of permutations. Thus there are still several $\mathcal{I}_\mathcal{A}$ that yield the same σ. Unlike in section 4.4, building $A(s)$ as in the proof of Theorem 4.3 does not necessarily yield a minimal cardinality of $\mathcal{I}_\mathcal{A}$ for given σ.

4.5.2 Example and simulations

We first illustrate the control design by recurrence based on the proof of Theorem 4.3. Consider target permutation $\sigma(0,1,2,3) = (2,0,3,1)$. First we reduce it down to an elementary permutation. Start with $K = N-1 = 3$ and note $(l,p) = (2,1)$ because $\sigma(2) = K$ and $\sigma(K) = 1$; we thus define $\overline{\sigma}(0,1,l=2,3) = (2,0,p=1,3)$ and impose $\overline{A}(s) = 0$ for $s \in \{s(0,3), s(1,3), s(2,3)\}$ reducing the permutation to $0,1,2$. Then we take $\overline{K} = N-1 = 2$ and note $(\overline{l},\overline{p}) = (0,1)$ because $\overline{\sigma}(0) = \overline{K}$ and $\overline{\sigma}(\overline{K}) = 1$; we thus define $\overline{\overline{\sigma}}(\overline{l} = 0,1,2,3) = \overline{\overline{\sigma}}(\overline{p} = 1,0,2,3)$ and impose $\overline{\overline{A}}(s) = 0$ for $s \in \{s(0,2), s(1,2)\}$ reducing the permutation to $0,1$. To implement $\overline{\overline{\sigma}}$ we need $\overline{\overline{A}}(s(0,1)) \neq 0$. Now we progressively move up to permutations on more levels, removing one $^-$ at a time from our objects. The reader is encouraged to follow crossings/anti-crossings under the different controls by referring to Fig.4.3.c, corresponding to our chirping choice $\omega(s) = 4(s - \frac{1}{2})$. Under $\overline{\overline{A}}$ the analytic branch from $|\overline{l}\rangle = |0\rangle$ to $|\overline{p}\rangle = |1\rangle$ meets the branch staying on $|\overline{K}\rangle = |2\rangle$ at $\overline{\overline{s}} = s(1,2)$. We therefore impose $\overline{A}(s(1,2)) \neq 0$ unlike for $\overline{\overline{A}}$, and for the rest copy the requirements of $\overline{\overline{A}}$: $\overline{A}(s(0,1)) \neq 0$, $\overline{A}(s(0,2)) = 0$. Now under $\overline{A}$ the branch from $|l\rangle = |2\rangle$ to $|p\rangle = |1\rangle$

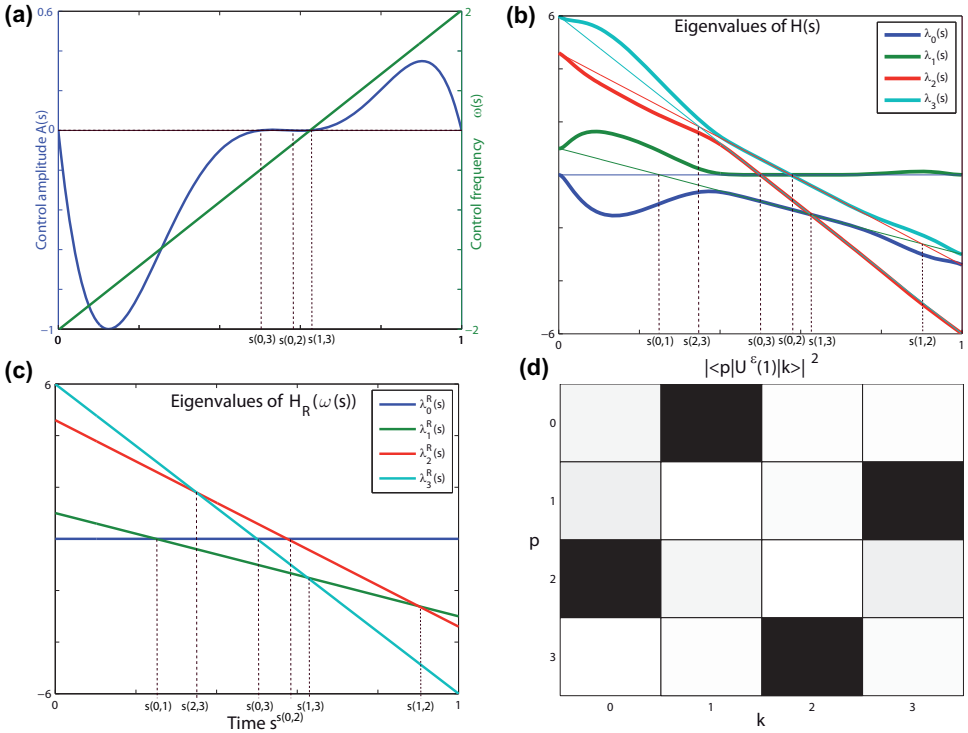

Figure 4.3: Control scheme generating permutation $\sigma(0,1,2,3) = (2,0,3,1)$ and simulation result. Subplots (a),(b),(d) analogue to Fig.4.1). Subplot (c) shows the eigenvalues of $\mathbf{H}_R(\omega(s))$, used to design $\mathcal{I}_A$ (see text). The points $s \in \mathcal{I}_A$ where $A(s) = 0$ are marked on (a).

crosses the branch staying on $|K\rangle = |3\rangle$ at $\overline{s} = s(2,3)$. We therefore get requirements for our actual control A by imposing $A(s(2,3)) \neq 0$ unlike for $\overline{A}$, for the rest copying the requirements of $\overline{A}$, i.e. $A(s) = 0$ for $s \in \{s(0,3), s(1,3), s(0,2)\}$ and $A(s) \neq 0$ for $s \in \{s(0,1), s(1,2)\}$. To satisfy these requirements, we take the polynomial control $A(s) = s(1-s)(s-s(0,3))(s-s(1,3))(s-s(0,2))$, represented on Fig.4.3.a. Fig.4.3.b shows how the eigenvalues of $\mathbf{H}(s)$ cross and anti-cross depending on whether $A(s)$ vanishes or not. The squared norm components of $U^\varepsilon(1)$ resulting from a simulation of (4.10) with this control and $\varepsilon = 10^{-3}$ are shown on Fig.4.3.d on a white-to-black scale, confirming achievement of permutation $\sigma(0,1,2,3) = (2,0,3,1)$.

Fig.4.4 shows the same squared norm components of $U^\varepsilon(1)$ in gray-shades for 24 cases, corresponding to different control inputs $A(s)$ designed for all 24 possible permutations of the set $(0,1,2,3)$. The controls $A(s)$ are built as the product of (i) a polynomial vanishing on $\mathcal{I}_A \cup \{0,1\}$ and only there, and (ii) a set of functions $(1 + g(s - s(m,n)))$, with $g(s - s(m,n))$ Gaussians centered on all $s \in \mathcal{I}_\omega \setminus \mathcal{I}_A$; the role of the latter is to amplify $A(s)$ in the vicinity of intended "anti-crossings", improving convergence of the adiabatic limit as a function of ε. Fig.4.4 corresponds to the choice $\varepsilon = 10^{-3}$.

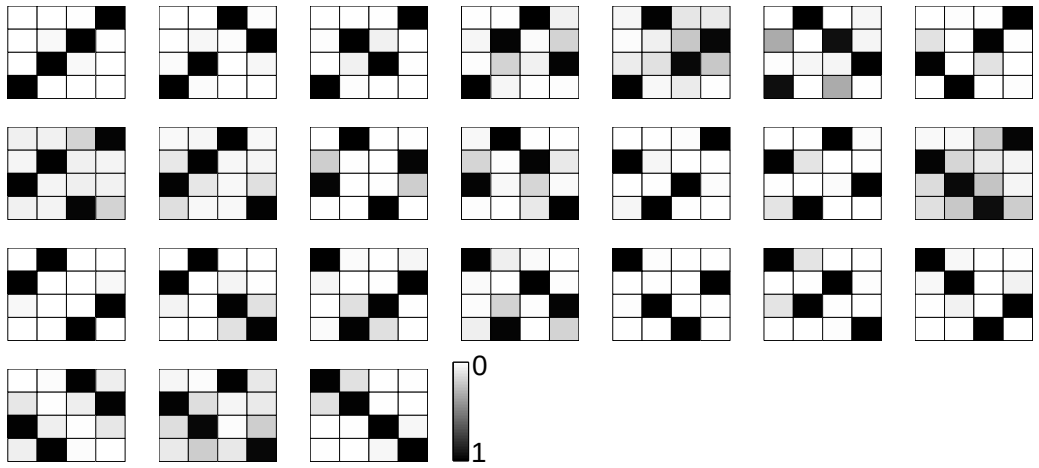

Figure 4.4: Simulation results of (4.10) for 24 different controls $A(s)$ following Theorem 4.3 to achieve each one of the 24 permutations of $(0, 1, 2, 3)$ with adiabatic passage. Shading represents squared norm of elements of matrix $U^{\varepsilon}(1)$ expressed in basis $|0\rangle, \ldots, |3\rangle$, from white (value 0) to black (value 1). In other words, each subplot may be read as a 4×4 matrix where the black patches are ones and the white patches are zeros; gray patches indicate intermediate values, reflecting that the unitary propagator obtained by integrating (4.10) is not exactly a permutation matrix for the finite $\varepsilon = 10^{-3}$.

4.6 Proofs

In this section we give the proofs of all the formal results presented in previous sections.

4.6.1 Proof of Theorem 4.1

We start the proof by recalling the following result [Nagao 1993].

Lemma 4.1. *Let $\mathbf{D}_N$ be a real tridiagonal and symmetric $N \times N$ matrix defined by*

$$\mathbf{D}_N = \sum_{k=0}^{N-1} a_k |k\rangle\langle k| + \sum_{k=0}^{N-2} c_k (|k\rangle\langle k+1| + |k+1\rangle\langle k|) \tag{4.15}$$

in some orthonormal basis $(|0\rangle, \ldots, |N-1\rangle)$. If $c_k \neq 0$ for all $k \in \mathbb{N}_0^{N\text{-}2}$, then $\mathbf{D}_N$ is non degenerate.

Proof 4.2 (of Lemma 4.1)**.** *Denote Q_n the characteristic polynomial of $\mathbf{D}_n$, which is defined as (4.15) with N replaced by n, for all $n \in \{1, \ldots, N\}$. The sequence of polynomials $(Q_n)_n$ verifies the following recurrence relation: for $n \geq 2$,*

$$Q_n(x) = (x - a_{n-1}) Q_{n-1}(x) - (c_{n-2})^2 Q_{n-2}(x)\,, \tag{4.16}$$

with $Q_0(x) = 1$ and $Q_1(x) = x - a_0$. According to Favard's Theorem [Favard 1935], a sequence satisfying (4.16) where $(c_{n-2})^2 > 0$ for all n, is a sequence of orthogonal polynomials. Furthermore, from [Szegö 1967, Theorem 3.3.1], every polynomial Q_n in a sequence of orthogonal polynomials has n real and distinct zeros; this is in particular true for $n = N$, therefore $\mathbf{D}_N$ is non degenerate. □

Proof 4.3 (of Theorem 4.1)**.** *We prove the result for any single system in $\mathcal{S}$ and conclude that it remains true for the sup over $\mathcal{S}$. Indeed, the application*

$$\begin{aligned}(\mu_0, \ldots, \mu_{N-2}, \Delta_0, \ldots, \Delta_{N-1}) \\ \rightarrow \quad \| \, U^\varepsilon(1)|k\rangle\langle k|U^\varepsilon(1)^\dagger - |N-k-1\rangle\langle N-k-1| \, \|\end{aligned}$$

reaches its sup over the allowed compact space since the state of a (sufficiently regular) dynamical system at a finite time depends continuously on system parameters (see e.g. [Khalil 2001, theorem 3.5]). The proof for one system is in two steps: first we prove that the hypotheses of the adiabatic theorem with gap condition are verified, then we apply the theorem to compute the image at $s = 1$ of the initial projector $|k\rangle\langle k|$ in the adiabatic approximation.

Step 1: *By hypothesis (a), we have $\mathbf{H}(s) \in \mathcal{C}^2([0,1], \mathcal{H}_N)$ and therefore continuous over $[0,1]$. From [Kato 1966, section II.5.2], it is then possible to find N continuous functions $\lambda_0(s), \ldots, \lambda_{N-1}(s)$ such that $\lambda_0(s) \leq \ldots \leq \lambda_{N-1}(s)$ for all $s \in [0,1]$ are the eigenvalues of $\mathbf{H}(s)$. In terms of associated eigenspace projections, note that $\{\mathbf{P}_{\lambda_k(s)} : k \in \mathbb{N}_0^{N\text{-}1}\} = \{|k\rangle\langle k| : k \in \mathbb{N}_0^{N\text{-}1}\}$ every time $A(s) = 0$, by the uniqueness of the spectral decomposition of a non degenerate matrix. However, the pairwise correspondence depends on the value of $\omega(s)$. In particular, by hypotheses (b) and (c),*

$$\mathbf{P}_{\lambda_k(0)} = |k\rangle\langle k| \quad \text{and} \quad \mathbf{P}_{\lambda_k(1)} = |N-k-1\rangle\langle N-k-1| \tag{4.17}$$

for all k. For a given $s \in [0,1]$,
- *either $A(s) \neq 0$, then $\mathbf{H}(s)$ has N distinct eigenvalues according to Lemma 4.1;*
- *or $A(s) = 0$, then $\mathbf{H}(s) = \mathbf{H}_R(\omega(s))$ and it must have N distinct eigenvalues by hypothesis (c). Hence,*

$$\lambda_0(s) < .. < \lambda_{N-1}(s) \text{ for all } s \in [0,1]\,. \tag{4.18}$$

Then by continuity over the compact interval $[0,1]$, there exists $\delta > 0$ such that $\lambda_k(s) + \delta < \lambda_{k+1}(s)$ for all $k \in \mathbb{N}_0^{N\text{-}2}$ and for all $s \in [0,1]$: each $\lambda_k(s)$ is at all times surrounded by a "spectral gap" of amplitude δ in which there is no other eigenvalue. We can therefore apply the adiabatic theorem with gap condition (see [Teufel 2003, Theorem 2.2]) to eigenvalue $\lambda_k(s)$, for any particular $k \in \mathbb{N}_0^{N\text{-}1}$, as is done in the following.

Step 2: *The adiabatic theorem ensures that $\mathbf{P}_{\lambda_k(s)} \in \mathcal{C}^2([0,1], \mathcal{H}_N)$. Define the "adiabatic Hamiltonian"*

$$\mathbf{H}_{a,k}(s) = \mathbf{H}(s) - i\varepsilon \mathbf{P}_{\lambda_k(s)} \frac{d}{ds} \mathbf{P}_{\lambda_k(s)} - i\varepsilon \mathbf{P}^\perp_{\lambda_k(s)} \frac{d}{ds} \mathbf{P}^\perp_{\lambda_k(s)} \tag{4.19}$$

where $\mathbf{P}^{\perp}_{\lambda_k(s)} = \mathbf{I} - \mathbf{P}_{\lambda_k(s)}$*, and the "adiabatic propagator"* $U^{\varepsilon}_{a,k}$ *which satisfies, for all* $s \in [0,1]$*,*

$$i\varepsilon \frac{d}{ds} U^{\varepsilon}_{a,k}(s) = \mathbf{H}_{a,k}(s)\, U^{\varepsilon}_{a,k}(s) \quad \text{with } U^{\varepsilon}_{a,k}(0) = \mathbf{I}\,. \tag{4.20}$$

One verifies that this construction ensures

$$U^{\varepsilon}_{a,k}(s)\mathbf{P}_{\lambda_k(0)}U^{\varepsilon}_{a,k}(s)^{\dagger} = \mathbf{P}_{\lambda_k(s)} \tag{4.21}$$

for all $s \in [0,1]$*. The adiabatic theorem states the existence of a constant* $C_1 > 0$ *such that*

$$||U^{\varepsilon}(s) - U^{\varepsilon}_{a,k}(s)|| \leq C_1\varepsilon \quad \text{for all } \ s \in [0,1]\,,$$

in particular for $s = 1$*. This implies*

$$\begin{aligned}
&\|U^{\varepsilon}(1)|k\rangle\langle k|U^{\varepsilon}(1)^{\dagger} - U^{\varepsilon}_{a,k}(1)|k\rangle\langle k|U^{\varepsilon}_{a,k}(1)^{\dagger}\| \\
&\quad\leq \ \|(U^{\varepsilon}(1) - U^{\varepsilon}_{a,k}(1))|k\rangle\langle k|U^{\varepsilon}(1)^{\dagger}\| \\
&\qquad + \ \|U^{\varepsilon}_{a,k}(1)|k\rangle\langle k|(U^{\varepsilon}(1) - U^{\varepsilon}_{a,k}(1))^{\dagger}\| \\
&\quad\leq \ \|U^{\varepsilon}(1) - U^{\varepsilon}_{a,k}(1)\| \ \ \| \, |k\rangle\langle k| \, \| \ \ (\|U^{\varepsilon}_{a,k}(1)\| + \|U^{\varepsilon}(1)\|) \\
&\quad\leq \ C_1\varepsilon \ \cdot \ 1 \ \cdot \ 2\sqrt{N}
\end{aligned}$$

since $\|U\| = \sqrt{Tr\,(U^{\dagger}U)} = \sqrt{Tr\,(\mathbf{I})}$ *for any unitary matrix* U*. Combining this with (4.17),(4.21) yields the result, where* $C = 2C_1\sqrt{N}$*.* □

4.6.2 Proof of Theorem 4.2 and corollary 4.1

We start by proving a Lemma about the behavior of time-dependent eigenvalues crossing each other.

Lemma 4.2. *Assume that* $\mathbf{H}(s)$ *as defined in (4.11) depends analytically on the real parameter* s *on an interval* $\mathcal{I} \subset \mathbb{R}$*, with* $\frac{d}{ds}\omega(s) > \gamma > 0$ *for all* $s \in \mathcal{I}$*. Suppose that* $\mathbf{H}_R(\omega(s))$ *is non degenerate on* $\mathcal{I}$ *except for a simple degeneracy at* $\bar{s} \in \mathcal{I}$*, i.e.* $\mathbf{H}_R(\omega(\bar{s}))$ *has* $N-1$ *distinct eigenvalues and* $\mathbf{H}_R(\omega(s))$ *has* N *distinct eigenvalues for* $s \in \mathcal{I} \setminus \{\bar{s}\}$*. If* $A(\bar{s}) = 0$*, then:*

(a) There exist N *unique functions* $\lambda_0, \ldots, \lambda_{N-1}$ *analytic over* $\mathcal{I}$*, with* $\lambda_0(s) < \ldots < \lambda_{N-1}(s)$ *for all* $s < \bar{s}$*, and such that* $\{\lambda_0(s), \ldots, \lambda_{N-1}(s)\}$ *are the eigenvalues of* $\mathbf{H}(s)$ *for all* $s \in \mathcal{I}$*.*

(b) Let k *be such that* $\lambda_k(\bar{s}) = \lambda_{k+1}(\bar{s})$*. Then for all* $s > \bar{s}$ *we have*

$$\lambda_0(s) < \ldots < \lambda_{k+1}(s) < \lambda_k(s) < \ldots < \lambda_{N-1}(s)\,.$$

Proof 4.4 (of Lemma 4.2)**.** *Point (a) is a direct consequence of [Kato 1966, Theorem 6.1]. The order of the analytic eigenvalues is obviously preserved over time intervals where* $\mathbf{H}(s)$ *is non degenerate; by Lemma 4.1, these intervals are* $\{s < \bar{s}\}$

and $\{s > \bar{s}\}$. *The issue is what happens at* $s = \bar{s}$. *In the following, we show that* $\lambda_k'(\bar{s}) \neq \lambda_{k+1}'(\bar{s})$. *Since the eigenvalues are analytic and* $\lambda_k(\bar{s}) = \lambda_{k+1}(\bar{s})$, *a Taylor expansion then yields the conclusion of (b).*

We lead calculations similar to those of [Messiah 1958, section XVI.II.8]. According to [Kato 1966, section II.6.2], since $\mathbf{H}$ *is analytic over* $\mathcal{I}$ *and* $\mathbf{H}(s) \in \mathcal{H}_N$ *for all* $s \in \mathcal{I}$, *there exist rank one orthogonal spectral projections* $\mathbf{P}_{\lambda_0(s)}, \ldots, \mathbf{P}_{\lambda_{N-1}(s)}$ *which are analytic over* $\mathcal{I}$. *Computing the derivative of*

$$\mathbf{H}(s)\mathbf{P}_{\lambda_k(s)} = \lambda_k(s)\mathbf{P}_{\lambda_k(s)} \tag{4.22}$$

with respect to s *at* $s = \bar{s}$, *we get*

$$\mathbf{H}'(\bar{s})\mathbf{P}_{\lambda_k(\bar{s})} + \mathbf{H}(\bar{s})\mathbf{P}'_{\lambda_k(\bar{s})} = \lambda_k'(\bar{s})\mathbf{P}_{\lambda_k(\bar{s})} + \lambda_k(\bar{s})\mathbf{P}'_{\lambda_k(\bar{s})} \ .$$

Multiplying the last equation by $(\mathbf{P}_{\lambda_k(\bar{s})} + \mathbf{P}_{\lambda_{k+1}(\bar{s})})$ *from the left, using (4.22) and the fact that* $\mathbf{P}_{\lambda_k}$ *and* $\mathbf{P}_{\lambda_{k+1}}$ *are two orthogonal projectors (*$\mathbf{P}_{\lambda_k}^2 = \mathbf{P}_{\lambda_k}$, $\mathbf{P}_{\lambda_{k+1}}^2 = \mathbf{P}_{\lambda_{k+1}}$ *and* $\mathbf{P}_{\lambda_k}\mathbf{P}_{\lambda_{k+1}} = 0$*), we get* $(\mathbf{P}_{\lambda_k(\bar{s})} + \mathbf{P}_{\lambda_{k+1}(\bar{s})})\mathbf{H}'(\bar{s})\mathbf{P}_{\lambda_k(\bar{s})} = \lambda_k'(\bar{s})\mathbf{P}_{\lambda_k(\bar{s})}$. *Noting that* $\mathbf{P}_{\lambda_k(\bar{s})} = (\mathbf{P}_{\lambda_k(\bar{s})} + \mathbf{P}_{\lambda_{k+1}(\bar{s})})\mathbf{P}_{\lambda_k(\bar{s})}$, *we get*

$$\begin{aligned}(\mathbf{P}_{\lambda_k(\bar{s})} + \mathbf{P}_{\lambda_{k+1}(\bar{s})})\mathbf{H}'(\bar{s})(\mathbf{P}_{\lambda_k(\bar{s})} + \mathbf{P}_{\lambda_{k+1}(\bar{s})})\mathbf{P}_{\lambda_k(\bar{s})} \\ = \lambda_k'(\bar{s})\mathbf{P}_{\lambda_k(\bar{s})} \ .\end{aligned}$$

The analog holds with k *and* $k{+}1$ *switched. This implies that* $\{\lambda_k'(\bar{s}), \lambda_{k+1}'(\bar{s})\}$ *are the eigenvalues of the* 2×2 *matrix obtained by restricting operator* $\mathbf{H}'(\bar{s})$ *to the column space of* $(\mathbf{P}_{\lambda_k(\bar{s})} + \mathbf{P}_{\lambda_{k+1}(\bar{s})})$. *Since* $A(\bar{s}) = 0$ *we have* $\mathbf{H}(\bar{s}) = \mathbf{H}_R(\omega(\bar{s}))$. *Denoting* $|m\rangle$ *and* $|n\rangle$ *the two eigenvectors of* $\mathbf{H}_R$ *corresponding to eigenvalue* $\lambda_k(\bar{s}) = \lambda_{k+1}(\bar{s})$, *we have* $\mathbf{P}_{\lambda_k(\bar{s})} + \mathbf{P}_{\lambda_{k+1}(\bar{s})} = |m\rangle\langle m| + |n\rangle\langle n|$. *Defining*

$$\big(\mathbf{H}'(\bar{s})\big)_{mn} = \begin{pmatrix} \langle m|\mathbf{H}'(\bar{s})|m\rangle & \langle m|\mathbf{H}'(\bar{s})|n\rangle \\ \langle n|\mathbf{H}'(\bar{s})|m\rangle & \langle n|\mathbf{H}'(\bar{s})|n\rangle \end{pmatrix}$$

and computing

$$\mathbf{H}'(\bar{s}) = \omega'(\bar{s})\frac{d}{dv}\mathbf{H}_R(v)\,|_{v=\omega(\bar{s})} + A'(\bar{s})\mathbf{H}_1 \ , \ \textit{we get}$$

$$\big(\mathbf{H}'(\bar{s})\big)_{mn} = \begin{pmatrix} -m\omega'(\bar{s}) & A'(\bar{s})\mu_{mn} \\ A'(\bar{s})\mu_{mn} & -n\omega'(\bar{s}) \end{pmatrix} \tag{4.23}$$

where $\mu_{mn} = \langle m|\mathbf{H}_1|n\rangle$. *Thus* $\mu_{mn} = 0$ *if* $|m-n| > 1$ *and* $\mu_{mn} \neq 0$ *if* $|m-n| = 1$. *In both cases, since* $\omega'(\bar{s}) \neq 0$ *and* $m \neq n$, *the matrix in (4.23) has* 2 *real and distinct eigenvalues, corresponding to* $\lambda_k'(\bar{s}) \neq \lambda_{k+1}'(\bar{s})$. □

Proof 4.5 (of Theorem 4.2)**.** *Taking* $A(s) = 0$ *at some points where* $\mathbf{H}_R$ *is degenerate means that eigenvalues of* $\mathbf{H}(s)$ *will not remain distinct at those points. We therefore use the adiabatic theorem without spectral gap condition, see [Teufel 2003, corollary 2.5]. Like for Theorem 4.1, we prove the result for one system* $\in \mathcal{S}$ *and conclude the result for the sup. The proof is again in two steps. First we state how*

the adiabatic theorem can be applied; then we compute the image at $s = 1$ of initial state $|k\rangle\langle k|$ in adiabatic approximation.

Step 1: *Since* $\mathbf{H}$ *is Hermitian, analytic over* $[0,1]$ *and simply degenerate at isolated points, we can apply Lemma 4.2(a) repeatedly to conclude that there is a unique set of functions* $\lambda_0, \ldots, \lambda_{N-1}$ *analytic over* $\mathcal{I}$*, with* $\lambda_0(0) < \ldots < \lambda_{N-1}(0)$*, and such that* $\{\lambda_0(s), \ldots, \lambda_{N-1}(s)\}$ *are the eigenvalues of* $\mathbf{H}(s)$ *for all* $s \in \mathcal{I}$*. Moreover, according to [Kato 1966, section II.6.2], there is a unique set of associated rank-one projectors* $\mathbf{P}_{\lambda_0(s)}, \ldots, \mathbf{P}_{\lambda_{N-1}(s)}$ *which are analytic over* $\mathcal{I}$*. In particular, given assumption (A3) and as* $\mathbf{H}(s) = \mathbf{H}_R(\omega(s))$ *for* $s \in \{0,1\}$*, we have* $(\lambda_k(0), \mathbf{P}_{\lambda_k(0)}) = (\lambda_k^R(0), |k\rangle\langle k|)$ *for all* k *and* $\{(\lambda_0(1), \mathbf{P}_{\lambda_0(1)}), \ldots, (\lambda_{N-1}(1), \mathbf{P}_{\lambda_{N-1}(1)})\} = \{(\lambda_0^R(1), |0\rangle\langle 0|), \ldots, (\lambda_{N-1}^R(1), |N-1\rangle\langle N-1|)\}$*. Note however that, unlike for Theorem 4.1, the pairwise correspondence between elements of the latter sets is not obvious a priori, because here eigenvalues of* $\mathbf{H}(s)$ *do not remain distinct on* $[0,1]$*. A second difficulty is to assess how the system's state evolves when eigenvalues become degenerate. This second part is answered by the adiabatic theorem witout gap condition. Introduce, as in Theorem 4.1, the adiabatic Hamiltonian* $\mathbf{H}_{a,0}$ *and adiabatic propagator* $U_{a,0}^\varepsilon$*, given by (4.19) and (4.20) respectively with* $k = 0$*. Then by construction* $U_{a,0}^\varepsilon(1)|0\rangle\langle 0|U_{a,0}^\varepsilon(1)^\dagger = U_{a,0}^\varepsilon(1)\mathbf{P}_{\lambda_0(0)}U_{a,0}^\varepsilon(1)^\dagger = \mathbf{P}_{\lambda_0(1)}$*. The adiabatic theorem states that* $\exists C$ *such that*

$$\| U^\varepsilon(s)|k\rangle\langle k|U^\varepsilon(s)^\dagger - U_{a,0}^\varepsilon(s)|k\rangle\langle k|U_{a,0}^\varepsilon(s)^\dagger \| \leq C\sqrt{\varepsilon} \tag{4.24}$$

for all $|k\rangle \in \{|0\rangle, \ldots, |N-1\rangle\}$*. Thus the actual system adiabatically follows the analytic* $\mathbf{P}_{\lambda_k(s)}$*, from* $\mathbf{P}_{\lambda_0(0)} = |0\rangle\langle 0|$ *up to* $\mathbf{P}_{\lambda_0(1)}$ *in particular.*

Step 2: *We now compute* $\mathbf{P}_{\lambda_0(1)}$*. Define a small interval* $I_{mn} = [\tau_{mn}^o, \tau_{mn}^f] \subset [0,1]$ *around each point* $s(m,n)$ *such that all* I_{mn} *are disjoint. If* $A(s(m,n)) \neq 0$*, then as shown in Theorem 4.1,* $\mathbf{H}(s)$ *is non degenerate for all* $s \in I_{mn}$*, such that for any* j,k *with* $\lambda_j(\tau_{mn}^o) < \lambda_k(\tau_{mn}^o)$ *we have* $\lambda_j(\tau_{mn}^f) < \lambda_k(\tau_{mn}^f)$*. On the other hand, if we take* $A(s(m,n)) = 0$*, then two eigenvalues intersect at* $s = s(m,n)$ *and the analytic branches cross so that their order changes as stated in Lemma 4.2(b). To avoid separate treatment of limit cases, we define* $s_0 = 0$ *and* $s_N = 1$*. Now by construction:*

- $\lambda_j(0) = \lambda_j^R(0)$ *for all* $j \in \mathbb{N}_0^{N\text{-}1}$.
- *For* $k \in \mathbb{N}_1^N$*,* $\lambda_0^R(s)$ *is the* k^{th} *smallest eigenvalue of* $\mathbf{H}_R(\omega(s))$ *when* $s \in (s_{k-1}, s_k)$.
- *As long as* $A(s_0) = \ldots = A(s_{k-1}) = 0$*, that is for* $k \leq N-p$*,* $\lambda_0(s)$ *follows the same crossings as* $\lambda_0^R(s)$*; therefore it is the* k^{th} *smallest eigenvalue of* $\mathbf{H}(s)$ *when* $s \in (s_{k-1}, s_k)$.
- *For* $s > s_{N-p-1}$*, we have* $A(s) \neq 0$ *so the* $\lambda_k(s)$ *keep the same order, i.e.* $\lambda_0(s)$ *remains the* $(N-p)^{th}$ *smallest eigenvalue of* $\mathbf{H}(s)$.

- *In particular for $s = 1$, from (4.13) we identify $\lambda_0(1) = \lambda^R_{N-(N-p)}(1) = \lambda^R_p(1)$, such that $\mathbf{P}_{\lambda_0(1)} = |p\rangle\langle p|$ by uniqueness of the spectral decomposition.* □

Remark 4.2. *To apply the adiabatic Theorem [Teufel 2003, corollary 2.5], it is sufficient to have $\mathbf{P}_{\lambda_0(s)} \in \mathcal{C}^2([0,1],\mathcal{H}_N)$. However, a condition like $\mathbf{H}(s) \in \mathcal{C}^2([0,1],\mathcal{H}_N)$ does not ensure the existence of $\mathbf{P}_{\lambda_0(s)},\dots,\mathbf{P}_{\lambda_{N-1}(s)} \in \mathcal{C}^2([0,1],\mathcal{H}_N)$, see [Kato 1966, example 5.3]. It is only for analytic $\mathbf{H}(s)$ that we can guarantee analytic $\mathbf{P}_{\lambda_0(s)}$, which then in particular belongs to $\mathcal{C}^2([0,1],\mathcal{H}_N)$.*

Proof 4.6 (of corollary 4.1)**.** *The arguments are the same as in the proof of Theorem 4.2. We concentrate on tracking the analytic eigenvalue branches $\lambda_0(s),\dots,\lambda_{N-1}(s)$ of $\mathbf{H}(s)$ to establish their pairwise correspondence with eigenvalues $\lambda^R_0(s),\dots,\lambda^R_{N-1}(s)$ of $\mathbf{H}_R(\omega(s))$ at $s = 1$. We prove the result for $p < N-l-1$; the case $p > N-l-1$ is treated similarly, while $p = N-l-1$, implying $\mathcal{I}^\omega_{lp} = \emptyset$, is the case covered by Theorem 4.1. Denote $s_1 < \ldots < s_{N-l-p-1}$ the elements of $\mathcal{I}^\omega_{lp}$, and $s_0 = 0$, $s_{N-l-p} = 1$.*

The algorithm constructs $\mathcal{I}^\omega_{lp}$ such that the $(l+d)^{th}$ and $(l+d+1)^{th}$ smallest eigenvalues of $\mathbf{H}_R(\omega(s))$ become equal at s_d, for each $d \in \mathbb{N}_1^{N-l-p-1}$. Taking $A(s_d) = 0$ implies $\mathbf{H}(s_d) = \mathbf{H}_R(\omega(s_d))$ so the same eigenvalue equalities hold for $\mathbf{H}(s)$ at $s = s_d$. Moreover from point (c) and Lemma 4.1 all eigenvalues of $\mathbf{H}(s)$ remain distinct for $s \notin \mathcal{I}^\omega_{lp}$. Therefore the analytic eigenvalue branch $\lambda_l(s)$, starting with $\lambda_l(0) = \lambda^R_l(0)$, exactly evolves through crossings at $s_1,\dots,s_{N-l-p-1}$ such that it is the $(l+d+1)^{th}$ smallest eigenvalue of $\mathbf{H}(s)$ for $s \in (s_d, s_{d+1})$. In particular, $\lambda_l(1)$ is the $(N-p)^{th}$ smallest eigenvalue of $\mathbf{H}(1) = \mathbf{H}_R(\omega(1))$, which from (A2) means $\lambda_l(1) = \lambda^R_p(1)$ such that $\mathbf{P}_{\lambda_l(1)} = |p\rangle\langle p|$. □

4.7 Summary and discussion

This chapter shows how adiabatic passage can be applied to a quantum ladder system to achieve permutations of populations on the ladder levels with a single laser pulse. We explicitly propose control inputs whose precise functional dependence on time is not important as long as they satisfy a few key features, most notably vanishing or not at specific times. This makes our strategy robust against multiplicative input disturbances. Another important advantage of our adiabatic strategy is its ability to simultaneously control an ensemble of systems with different dipole moment values.

Theorems in the present chapter provide a proof of concept in idealized situations. Several practical issues deserve a more quantitative investigation in future work. Probably the most important aspect is to characterize precision of the adiabatic approximation as a function of ε. Indeed, for small ε the actual control time $t = \frac{s}{\varepsilon}$ gets long; this further implies that, at constant power $A^2(s)$, the energy given to the system gets large. Beyond performance requirements, this also invalidates our model at infinitesimal ε (e.g. regarding finite lifetime of the levels). Although orders of magnitude are given for the adiabatic limit, variations in the proportionality

constant can lead to significant discrepancies. Investigating them, as well as "optimal paths" minimizing non-adiabatic losses [Guérin 2002], could yield guidelines for choosing amongst several possible "eigenvalue crossing designs". Both precision of adiabatic approximation and modeling assumptions (e.g. RWA) also limit the range of "ensemble" properties in practice.

It may appear surprising at first sight that two different evolutions are selected just by taking $A(\overline{s}) = 0$ or $A(\overline{s}) \neq 0$ at a precise instant $\overline{s}$. The elucidation is that this dichotomy only holds at the limit $\varepsilon \to 0^+$. For a given ε, the larger $|A|$ in the neighborhood of $s = \overline{s}$, the more the evolution deviates from the $A(\overline{s}) = 0$ case. Nevertheless, for small ε, the relevant neighborhood around $\overline{s}$ for selecting population transfer or not indeed gets small. Our scheme might therefore allow selective population permutation as a function of $\{\Delta_0, \ldots, \Delta_{N-1}\}$ on an ensemble of systems, in a scheme resembling resonance selection. Take $A(\overline{s}) = 0$ for $\overline{s} \in \mathcal{I}^\omega$ of a nominal system. If a system has detunings very close to nominal, then two of its $\lambda_k^R(s)$ cross at a point $\widetilde{s}$ close to $\overline{s}$, where $A(\widetilde{s}) \approx 0$, such that for moderate ε its final state will be close to the adiabatic result of the nominal system with $A(\overline{s}) = 0$. If a system has detunings more different from nominal, then all its crossings of $\lambda_k^R(s)$ occur at points where A significantly differs from zero, and with moderate ε its final state will be closer to the adiabatic result of the nominal system with $A(\overline{s}) \neq 0$. A quantitative statement of this idea requires further investigation.

Chapter 5

Stabilizing non-classical states in cavity QED

Contents

Nous analysons une méthode de stabilisation d'états non classiques dans une cavité par dissipation contrôlée, initialement proposée par Sarlette et al [Phys. Rev. Lett. ***107****, 010402 (2011)]. Nous généralisons la méthode pour la protection d'états intriqués de deux modes de la cavité. Le réservoir qui induit la dissipation est composé d'atomes qui interagissent les uns après les autres avec la cavité. Cette interaction est d'abord dispersive, puis résonnante, puis dispersive à nouveau. Nous étudions en détail la compétition entre la décohérence et l'effet de cette dissipation contrôlée induite par le réservoir d'atomes. Nous montrons que cette méthode est robuste aux imperfections expérimentales, et qu'elle pourrait être implémentée au laboratoire dans un futur proche, soit dans le domaine de l'électrodynamique quantique en cavité, soit dans celui des circuits quantiques. Ce chapitre est basé sur un papier écrit en collaboration avec Alain Sarlette, Michel Brune, Jean-Michel Raimond et Pierre Rouchon. Il a été récemment accepté pour publication dans Physical Review A [Sarlette 2012]. Ici, nous détaillons certains calculs et dans la section 5.2, nous démontrons un résultat de convergence en dimension infinie. Ma contribution*

principale à ce projet a été la stabilisation d'états intriqués de deux modes de la cavité (section 5.1.6), ainsi que la preuve de convergence (section 5.2).

We analyze a quantum reservoir engineering method, originally introduced by Sarlette *et al* [Phys. Rev. Lett. **107**, 010402 (2011)], for the stabilization of non-classical field states in high quality cavities. We generalize the method to the protection of mesoscopic entangled field states shared by two non-degenerate field modes. The reservoir is made up of a stream of atoms undergoing successive composite interactions with the cavity, each combining resonant with non-resonant parts. We gain detailed insight into the competition between the engineered reservoir and decoherence. We show that the operation is quite insensitive to experimental imperfections and that it could thus be implemented in the near future, either in the context of microwave Cavity Quantum Electrodynamics or in that of circuit-QED. This chapter is built on a paper we wrote in collaboration with Alain Sarlette, Michel Brune, Jean-Michel Raimond and Pierre Rouchon. It was recently accepted for publication in Physical Review A [Sarlette 2012]. Here, extra details and computations are given. Moreover, in section 5.2, we have included a convergence proof where the state space is an infinite dimensional Hilbert space . My main contribution to this project is the stabilization of the two-mode entangled state (section 5.1.6) and the convergence proof (section 5.2).

5.1 Proposal to stabilize non-classical states of one- and two-mode radiation fields by reservoir engineering

Nonclassical electromagnetic field states are extremely important, both for a fundamental understanding of the quantum properties of light and for their possible use in practical applications. For instance, squeezed states (SS) have fluctuations of one of their quadratures below those of the vacuum state, or of a classical coherent state [Dowling 2008]. They thus lead to interesting methods for high-precision measurements and metrology [Giovannetti 2004]. They are for instance planned to be used for reducing the noise of the gravitational wave interferometers below the standard quantum limit [Goda 2008].

Mesoscopic field state superpositions (MFSS) are also the focus of an intense interest. They involve a quantum superposition of two quasi-classical coherent components with different complex amplitudes. These counter-intuitive states bridge the gap between the quantum and the classical worlds and shed light on the decoherence process responsible for the conspicuous lack of superpositions at our scale [Haroche 2006].

Finally, entangled superpositions of mesoscopic states (ESMS) shared by several field modes are even more intriguing. They violate generalized Bell inequalities [Banaszek 1999], illustrating the fundamentally non-local nature of quantum phyics. However, their non-local character is rapidly erased by a fast decoherence

process [Milman 2005], driving them back into a statistical mixture that can be undestood in terms of a classical local hidden variable model. This interplay of decoherence and nonlocality opens fascinating perspectives for exploring the limits of the quantum.

In principle, the SS and MFSS could be simply prepared in the optical domain by letting a coherent laser pulse propagate in a non-linear medium, whose index of refraction is a linear function of the light pulse intensity (Kerr medium) [Yurke 1986]. The field evolves from initial coherent state $|\alpha\rangle$ under the action of the Kerr Hamiltonian $\mathbf{H}_K$:

$$\mathbf{H}_K = \zeta_K \mathbf{N} + \gamma_K \mathbf{N}^2 . \tag{5.1}$$

Here $\mathbf{N}$ is the photon number operator, ζ_K is proportional to the linear index and γ_K is the Kerr frequency describing the strength of the non-linearity. In the following, we use units such that $\hbar = 1$. Note that the collisional interaction Hamiltonian for an $\mathbf{N}$-atom sample in a tightly confining potential or in an optical lattice is similar to $\mathbf{H}_K$ [Will 2010].

Depending on the interaction time t_K, the final state $e^{-i\,t_K \mathbf{H}_K}|\alpha\rangle$ spans a number of nonclassical forms [Haroche 2006, Section 7.2], including:

(i) squeezed states for $t_K\gamma_K \ll \pi$;

(ii) states with 'banana'-shaped Wigner function for slightly larger $t_K\gamma_K$;

(iii) mesoscopic field state superpositions $|k_\alpha\rangle$ with k equally spaced components for $t_K\gamma_K = \pi/k$ [1].

(iv) in particular, a MFSS of two coherent states with opposite amplitudes:

$$|c_{\tilde{\alpha}}\rangle \quad = \quad (|\tilde{\alpha}\rangle + i\,|\text{-}\tilde{\alpha}\rangle)/\sqrt{2}\,, \tag{5.2}$$

with $\tilde{\alpha} = \alpha\, e^{-i\zeta_K t_K}$, for $t_K\gamma_K = \frac{\pi}{2}$.

The top panels on Figure 5.1 present the Wigner functions of the states (i)-(iv) for a mean photon number $|\alpha|^2 = 2.7$.

This preparation method by a *deterministic unitary evolution* is simple in its principle, but its implementation is extraordinarily difficult for propagating light fields, due to the weakness of the Kerr nonlinearity [Rosenbluh 1991].

Other methods for the production of these nonclassical states have been proposed or realized in the context of trapped ions [Monroe 1996, Myatt 2000] or Cavity Quantum Electrodynamics (CQED) [Haroche 2006, Brune 1992, Brune 1996, Deléglise 2008, Davidovich 1993, Villas-Bôas 2003, Solano 2003, de Matos Filho 1996]. Both systems implement the 'spin-spring' model, the simplest nontrivial quantum situation of a two-level system coupled to a harmonic oscillator, embodied by the harmonic motion of the ion or by a single field mode. The proposed nonclassical state production methods are either deterministic or rely on

[1] The components are well separated only in the case $k < \pi\alpha$ [Haroche 2006, Section 7.2]

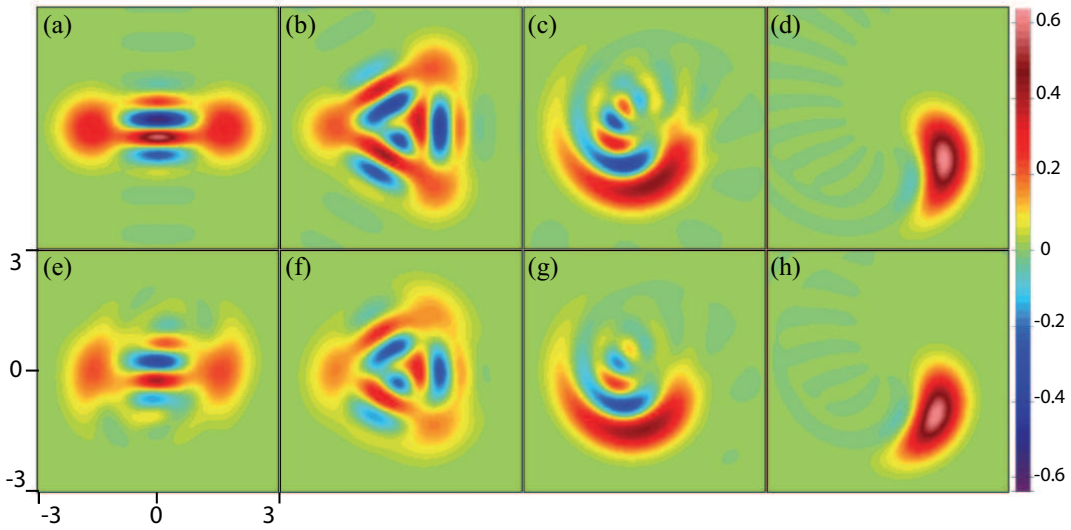

Figure 5.1: (a-d) Wigner functions of nonclassical field states $e^{-i\,t_K \mathbf{H}_K}|\alpha\rangle$ generated by propagation of an initial coherent state through a Kerr medium, (a) 2-component MFSS given by Eq. (5.2) for $t_K\gamma_K = \pi/2$; (b) 3-component MFSS for $t_K\gamma_K = \pi/3$; (c) 'banana'-state, for $t_K\gamma_K = 0.28$; and (d) squeezed state, for $t_K\gamma_K = 0.08 \ll \pi$. (e-h): similar states stabilized, despite decoherence, by the atomic reservoir as explained in the remainder of this Section. Frame (e) corresponds to the reference two-component MFSS most lengthily discussed in the rest of this Section.

a *detection-conditioned* scheme. The latter expand the possibilities of the former by applying a measurement operation after a unitary evolution towards an intermediate target state. Measurement back-action generates different final states conditioned by the stochastic detection outcome [Ourjoumtsev 2007]. In the microwave CQED context, detection-conditioned preparation of MFSS and ESMS can be achieved by the dispersive interaction of an initial coherent field state with a two-level atom, initially prepared in a state superposition, followed by the detection of the atomic state in an appropriate basis [Haroche 2006, Brune 1996].

All these preparation techniques do not solve, however, the problem of *stabilizing* ("protecting") a selected nonclassical state for long times in spite of the unavoidable coupling of the system $\mathcal{S}$ to its environment $\mathcal{E}$. *Reservoir engineering* can be used to stabilize target quantum states by strongly coupling $\mathcal{S}$ to an "engineered" environment, or reservoir $\mathcal{R}$, a large quantum system with many degrees of freedom. The reservoir is designed so that, when acting alone, it drives $\mathcal{S}$, whatever its intial state, towards a unique target 'pointer state', a stable state of $\mathcal{S}$ coupled to $\mathcal{R}$ [Zurek 1981, Zurek 2003]. The state of $\mathcal{S}$ remains close to this pointer state even in the presence of $\mathcal{E}$, provided $\mathcal{R}$ is more strongly coupled to $\mathcal{S}$ than $\mathcal{E}$. An engineered reservoir thus achieves much more than the preparation of a target state. It effectively *stabilizes* the system close to it for arbitrarily long times.

Reservoir engineering is experimentally challenging. Reservoirs made up of lasers and magnetic fields for trapped-ion oscillators have been proposed [Poyatos 1996, de Matos Filho 1996, Carvalho 2001] and demonstrated [Barreiro 2011]. Recently, a reservoir has been used to generate entanglement of spin states of macroscopic atomic ensembles [Krauter 2011].

In the context of CQED, the reservoir may be a stream of atoms interacting with the trapped field. An early proposal [Slosser 1989] relied on the so-called 'trapping state conditions' for the micromaser [Rempe 1990], which require a very fine tuning of the parameters and can only be properly achieved in the case of a zero-temperature environment. Reservoirs composed of atoms in combination with external fields have also been proposed to stabilize one-mode squeezed states [Werlang 2008] and two-mode squeezed vacuum entanglement [Pielawa 2007].

In [Sarlette 2011], we proposed a robust reservoir engineering method for CQED. It generates and stabilizes nonclassical states of a single mode of the radiation field, including SS and MFSS. The reservoir is made up of a stream of 2-level atoms, each prepared in a coherent superposition of its basis states. They interact one at a time with the field according to the Jaynes-Cummings model before being discarded, a procedure reminiscent of the "reset" operation performed in other contexts [Reed 2010b, Barreiro 2011]. The key idea is to use a tailored composite interaction of each atom with the field: dispersive, then resonant, then dispersive again. The pointer states of this composite interaction are precisely those, $e^{-it_K \mathbf{H}_K}|\alpha\rangle$, resulting from the action of a Kerr Hamiltonian acting upon an initially coherent state.

This method is quite general and could be implemented in a variety of CQED settings, particularly in the active context of circuit QED [Devoret 2004] or in that

of microwave CQED, with circular Rydberg atoms and superconducting Fabry Perot cavities. For the sake of definiteness, we shall focus in this Section on the microwave CQED case, and particularly on the current ENS CQED experiment whose scheme is depicted on Fig. 5.2. The bottom panels of Fig. 5.1 present the results of numerical simulations of the ENS experiment, with interaction parameters chosen to reproduce the states generated by the Kerr Hamiltonian (top panels).

The present Section is intended to provide an in-depth description of this single-mode reservoir engineering procedure, with a detailed analysis of the physical mechanism of state stabilization. We also discuss the competition between the engineered reservoir and the ordinary cavity enviroment, giving simple insights into the finite final fidelity of the prepared state.

We finally extend the scheme proposed in [Sarlette 2011] to the stabilization of entangled superpositions of mesoscopic states of two field modes. The atoms of the reservoir undergo a tailored interaction with two modes of the same cavity, combining dispersive and resonant parts for each mode. This proposal opens interesting perspectives for studying the interplay between entanglement, non-locality and decoherence in the context of mesoscopic quantum states.

This Section is organized as follows. We consider the single-mode case for most of this Section and extend it to two modes in Section 5.1.6. Section 5.1.1 describes the experimental scheme and the principle of the method. Section 5.1.2 discusses, as a building block for the next Sections, how a stream of atoms resonant with one field mode stabilizes approximately a coherent field state. Section 5.1.3 introduces the composite interaction: non-resonant, resonant and non-resonant again. In this Section, we treat the non-resonant interactions in the dispersive regime of a large atom-cavity detuning. We thus get a simple qualitative insight into the mechanism generating non-classical states. Section 5.1.4 details the more realistic case of intermediate atom-cavity detuning. We show that the main features of Section 5.1.3 are recovered, exhibiting the robustness of the method. Section 5.1.5 analyzes the effect of decoherence due to the cavity damping and imprecisions on the experimental parameters. We find that the method is also robust against realistically large imperfections. Section 5.1.6 presents the stabilization of two-mode ESMS. Finally, detailed computations are given in Section 5.1.8.

5.1.1 General description

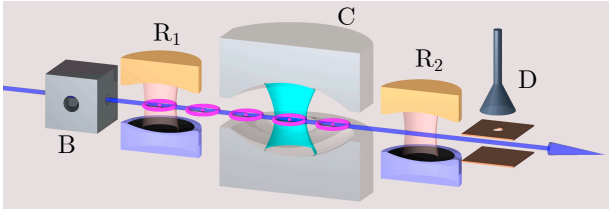

Figure 5.2: Scheme of the current ENS CQED experiment.

The scheme of the ENS experiment is depicted on Fig. 5.2 (see [Haroche 2006, Deléglise 2008] for details). A microwave field of frequency ω_c is trapped in the superconducting cavity C (damping time $T_c = 65$ ms). Atoms are sent one after the other through C. They cross its standing wave gaussian mode at a constant, adjustable velocity v. The mode interacts with the transition between the two atomic levels $|g\rangle$ and $|e\rangle$ (circular Rydberg states with principal quantum numbers 50 and 51). A static electric field applied across the cavity mirrors is used to adjust the atomic transition frequency ω_0 and hence the atom-cavity detuning $\delta = \omega_0 - \omega_c \ll \omega_c$ via the Stark effect. Varying the electric field during the atom-field interaction makes it possible to engineer the detuning profile $\delta(t)$. Zero and small δ values are used for the resonant and non-resonant parts of the interaction. Making δ very large allows us to effectively turn off the atom-field interaction.

We describe the atom and field states in a frame rotating at frequency ω_c. The atoms are prepared in state $|g\rangle$ in B, by a time-resolved laser and radiofrequency excitation of a velocity-selected thermal rubidium atomic beam. Before entering C, the atoms are prepared in a coherent superposition of $|g\rangle$ and $|e\rangle$ in the low-quality cavity R_1, driven by a classical microwave source ("first Ramsey zone") at frequency ω_c. Without loss of generality, we can choose the phase reference for all atoms so that they enter the cavity in the initial state $|u_{\rm at}\rangle = \cos(u/2)|g\rangle + \sin(u/2)|e\rangle$ with $u > 0$. In a Bloch sphere representation with $|e\rangle$ at the north pole, $|u_{\rm at}\rangle$ corresponds to a vector at an angle u with the north-south vertical axis.

A second classical microwave pulse in the second Ramsey zone R_2 is followed by a detection in the $\{|e\rangle, |g\rangle\}$ basis in the field-ionization detector D. This amounts to a projective measurement of the atomic state at the exit of C, in a basis that can be chosen arbitrarily by properly setting the microwave pulse in R_2. For the engineered reservoir operation, the result of this final atomic state detection is irrelevant. Detection results are however necessary in other phases of the experiment. In particular, they will be used to reconstruct the field state generated by the engineered reservoir, using a method described in [Deléglise 2008].

Let us first consider atom-cavity interaction for an atom that crosses cavity axis at $t = 0$. The atom-field interaction is ruled by the Jaynes-Cummings Hamiltonian $\mathbf{H}_{JC}$. Neglecting far off-resonant terms (rotating wave approximation, negligible interaction with other cavity modes), we have:

$$\mathbf{H}_{JC} = \frac{\delta(t)}{2}(|e\rangle\langle e| - |g\rangle\langle g|) + i\frac{\Omega(s)}{2}(\,|g\rangle\langle e|\,\mathbf{a}^\dagger - |e\rangle\langle g|\,\mathbf{a}\,)\,, \tag{5.3}$$

where $\Omega(s)$ is the atom-cavity coupling strength (vacuum Rabi frequency) at position $s = vt$ along the atomic trajectory; $\mathbf{a}$ is the photon annihilation operator in C. The photon number operator $\mathbf{N} = \mathbf{a}^\dagger\mathbf{a} = \sum_n\ n\ |n\rangle\langle n|$ defines the Fock states basis $\{|n\rangle\}$.

The coupling strength $\Omega(s)$ is determined by the atomic transtion parameters and by the cavity mode geometry. It is written here as $\Omega(s) = \Omega_0\ e^{-s^2/w^2}$, with $\Omega_0/2\pi = 50$ kHz and $w = 6$ mm for the ENS setup. To get a finite total interaction duration T, we assume that the coupling cancels when $|s| > 1.5\,w$. The total

interaction time of the atom with the field is thus $T = 3w/v$. We have checked numerically that this truncation of the interaction time has negligible effects.

The evolution operator, or propagator $\mathbf{U}$ associated with $\mathbf{H}_{JC}$ expresses the transformation that the joint atom-cavity state undergoes during their interaction. The Schrödinger equation for $\mathbf{U}$, starting at the initial time $t = t_0$ is:

$$\frac{d}{dt}\mathbf{U}(t) = -i\,\mathbf{H}_{JC}(t)\,\mathbf{U}(t) \quad \text{with} \quad \mathbf{U}(t_0) = \mathbf{I}\,, \tag{5.4}$$

where $\mathbf{I}$ is the identity operator. We note $\mathbf{U}_T$ the propagator obtained by integration of Eq. (5.4) over one full atom-cavity interaction, that lasts from $-T/2$ to $T/2$.

We represent the action of $\mathbf{U}_T$ over the field state by the operators $\mathbf{M}_g^{\mathbf{U}_T}$ and $\mathbf{M}_e^{\mathbf{U}_T}$, such that:

$$\mathbf{U}_T\,(|u_{\rm at}\rangle|\psi\rangle) \;\; = \;\; |g\rangle\,\mathbf{M}_g^{\mathbf{U}_T}|\psi\rangle + |e\rangle\,\mathbf{M}_e^{\mathbf{U}_T}|\psi\rangle\;,$$

for any pure initial field state $|\psi\rangle$. Tracing over the final atomic state, the modification of the field density operator due to the interaction with the atom is thus finally given by the Kraus map [Kraus 1983]

$$\rho \to \mathbf{M}_g^{\mathbf{U}_T}\rho\mathbf{M}_g^{\mathbf{U}_T\,\dagger} + \mathbf{M}_e^{\mathbf{U}_T}\rho\mathbf{M}_e^{\mathbf{U}_T\,\dagger}\,. \tag{5.5}$$

For the reservoir action, we let a stream of atoms consecutively interact with the field and always use the same parameter set (detuning profile, atom velocity v and initial state $|u_{\rm at}\rangle = \cos(u/2)|g\rangle + \sin(u/2)|e\rangle$). Thus each atom affects the field according to Eq. (5.5). The interaction of C with the $(k+1)$th atomic sample begins as soon as that with the kth sample ends. Successive atoms are thus separated by the time interval T. We denote by ρ_k the cavity state just after interacting with the kth atom and tracing over its irrelevant final state. The field density operator ρ_k is thus given by:

$$\rho_k = \mathbf{M}_g^{\mathbf{U}_T}\rho_{k\text{-}1}\mathbf{M}_g^{\mathbf{U}_T\,\dagger} + \mathbf{M}_e^{\mathbf{U}_T}\rho_{k\text{-}1}\mathbf{M}_e^{\mathbf{U}_T\,\dagger}\,. \tag{5.6}$$

We aim to stabilize a pure pointer state $\rho_\infty = |\psi_\infty\rangle\langle\psi_\infty|$, which must be a fixed point of this Kraus map. The right-hand side of Eq. (5.6), with $\rho_{k\text{-}1} = \rho_\infty$, is a statistical mixture of two pure states. It is then a pure state only if its two terms are proportional to each other. Thus, $|\psi_\infty\rangle$ must be an eigenstate of both $\mathbf{M}_g^{\mathbf{U}_T}$ and $\mathbf{M}_e^{\mathbf{U}_T}$. State stabilization by reservoir engineering amounts to tailoring a Kraus map for the field from a constrained physical setting.

We have shown in [Sarlette 2011] that it is possible to engineer the atom-cavity interaction so that the Kraus map leaves invariant the states $\approx e^{-i\,t_K\mathbf{H}_K}|\alpha\rangle$, in which α and $\gamma_K\,t_K$ in Eq.(5.1) can be chosen at will. Explicitly, we build $\mathbf{U}_T$ by sandwiching a resonant interaction ($\delta = 0$ for $t \in [-t_r/2, t_r/2]$) symmetrically between two dispersive interactions with opposite detuning: $\delta = \delta_0$ before the resonant interaction, $\delta = -\delta_0$ thereafter. We choose a positive δ_0 value for the sake of definiteness.

This timing is illustrated on Fig. 5.3. Each resonant or dispersive interaction phase is characterized by a set of parameters that we denote $q = (t_1, t_2, v, \delta_0)$ where t_1 is start time, t_2 is stop time. The corresponding propagators are denoted $\mathbf{U}_q$.

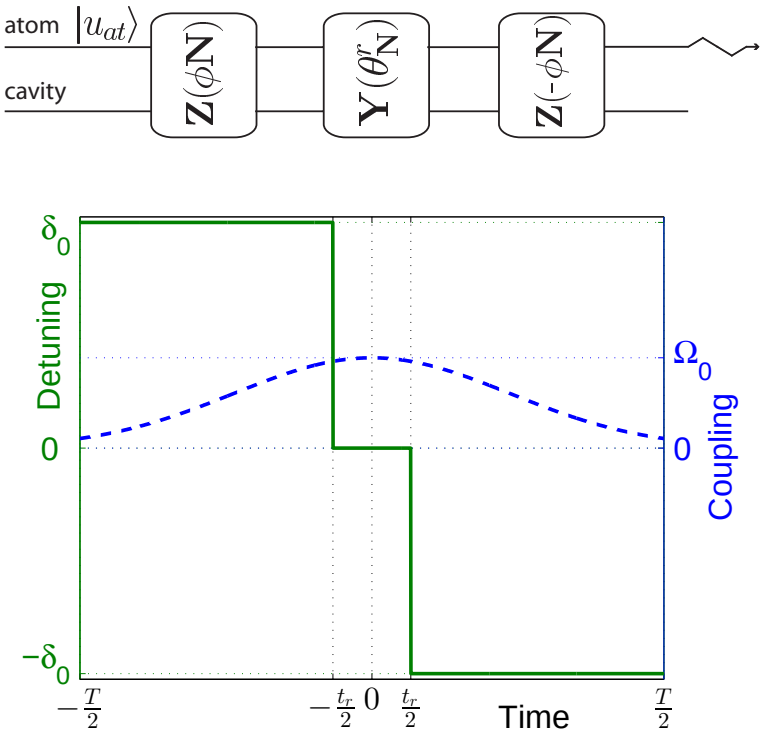

Figure 5.3: Time profile of δ (difference between the tunable frequency ω_0 of the atomic transition and the fixed frequency ω_c of the single cavity mode; bottom frame, full line) and $\Omega(vt)$ (bottom frame, dashed line) during cavity crossing by one atomic sample; we take $t = 0$ when the atom is at cavity center. Top frame: scheme of the propagators corresponding to the successive steps in the composite interaction.

To compute these evolution operators, we use the fact that each two-dimensional subspace spanned by $(|g,\, n+1\rangle, |e,\, n\rangle)$ is invariant under the action of $\mathbf{H}_{JC}$. The state $|g,0\rangle$ does not take part in the evolution. We can thus view the action of $\mathbf{U}_q$ as photon-number-dependent rotations acting on a set of Bloch spheres B_n $(n = 0, 1, ...)$, with $|g, n+1\rangle$ at the south-pole and $|e, n\rangle$ at the north-pole defining their Z-axes. These rotations can be decomposed as general rotations around the X-, Y- and Z-axes of the Bloch spheres. We use the notation $f_{\mathbf{N}} = f(\mathbf{N}) = \sum_n f(n)\,|n\rangle\langle n| = \sum_n f_n\,|n\rangle\langle n|$ for arbitrary functions f of n, with the fundamental property

$$\mathbf{a}\, f(\mathbf{N}) = f(\mathbf{N}+\mathbf{I})\, \mathbf{a}\,. \tag{5.7}$$

We can then cast these rotations as:

$$\begin{aligned}
\mathbf{X}(f_{\mathbf{N}}) &= |g\rangle\langle g|\,\cos(f_{\mathbf{N}}/2) + |e\rangle\langle e|\,\cos(f_{\mathbf{N}+\mathbf{I}}/2) \\
&\quad -i|e\rangle\langle g|\,\mathbf{a}\frac{\sin(f_{\mathbf{N}}/2)}{\sqrt{\mathbf{N}}} - i|g\rangle\langle e|\,\frac{\sin(f_{\mathbf{N}}/2)}{\sqrt{\mathbf{N}}}\,\mathbf{a}^\dagger\,, \qquad (5.8)\\
\mathbf{Y}(f_{\mathbf{N}}) &= |g\rangle\langle g|\,\cos(f_{\mathbf{N}}/2) + |e\rangle\langle e|\,\cos(f_{\mathbf{N}+\mathbf{I}}/2) \\
&\quad -|e\rangle\langle g|\,\mathbf{a}\frac{\sin(f_{\mathbf{N}}/2)}{\sqrt{\mathbf{N}}} + |g\rangle\langle e|\,\frac{\sin(f_{\mathbf{N}}/2)}{\sqrt{\mathbf{N}}}\,\mathbf{a}^\dagger\,, \qquad (5.9)\\
\mathbf{Z}(f_{\mathbf{N}}) &= |g\rangle\langle g|\,e^{i\,f_{\mathbf{N}}/2} + |e\rangle\langle e|\,e^{-i\,f_{\mathbf{N}+\mathbf{I}}/2}\,. \qquad (5.10)
\end{aligned}$$

As shown in Sections 5.1.2 and 5.1.3, $\mathbf{Y}(f_{\mathbf{N}})$ with $f(n)$ proportional to $\sqrt{n+1}$ corresponds to a resonant interaction and $\mathbf{Z}(f_{\mathbf{N}})$ with $f(n)$ proportional to n corresponds to a non-resonant interaction in the dispersive regime $\delta \gg \Omega$. See Section 5.1.8.1 for more details.

5.1.2 Engineered reservoir for coherent state stabilization

The coherent state $|\alpha\rangle$ is obtained by the action of the displacement operator $\mathbf{D}_\alpha = e^{\alpha\,\mathbf{a}^\dagger - \alpha^\dagger\,\mathbf{a}}$ on the vacuum [Haroche 2006]:

$$|\alpha\rangle = \mathbf{D}_\alpha\,|0\rangle\; = e^{-|\alpha|^2/2}\sum_n \frac{\alpha^n}{\sqrt{n!}}|n\rangle\,. \tag{5.11}$$

We show here how a short resonant interaction ($\delta = 0$) with weakly excited atoms provides an engineered reservoir, whose pointer state is close to a coherent state [Sarlette 2011].

Stabilization of coherent states is not an amazing feat. A classical radiation source weakly coupled to the cavity directly generates a coherent state. This is a routine operation in microwave CQED experiments. However, the situation described in this Section is an essential building block for the stabilization of more complex nonclassical states, as shown below. Moreover, it is an interesting micromaser situation [Slosser 1989, Casagrande 2002], in which the small excitation of the atoms leads to a finite energy in the steady state even though the cavity is assumed to be lossless.

We consider a resonant interaction over a time interval t_r, corresponding to the parameter set $r = (-t_r/2, t_r/2, v, 0)$. Following Section 5.1.8.1, the associated propagator is:

$$\begin{aligned} \mathbf{U}_r &= \mathbf{Y}(\theta^r_{\mathbf{N}}) \\ &= |g\rangle\langle g|\,\cos(\theta^r_{\mathbf{N}}/2) + |e\rangle\langle e|\,\cos(\theta^r_{\mathbf{N+I}}/2) \\ &\quad -|e\rangle\langle g|\,\mathbf{a}\frac{\sin(\theta^r_{\mathbf{N}}/2)}{\sqrt{\mathbf{N}}} + |g\rangle\langle e|\,\frac{\sin(\theta^r_{\mathbf{N}}/2)}{\sqrt{\mathbf{N}}}\,\mathbf{a}^\dagger\,, \end{aligned} \tag{5.12}$$

with

$$\theta^r_n = \theta_r\sqrt{n}, \quad \theta_r = \int_{-t_r/2}^{t_r/2} \Omega(vt)\,dt\,. \tag{5.13}$$

This readily yields:

$$\begin{aligned} \mathbf{M}_g^{\mathbf{U}_r} &= \cos(\tfrac{u}{2})\,\cos(\theta^r_{\mathbf{N}}/2) + \sin(\tfrac{u}{2})\,\frac{\sin(\theta^r_{\mathbf{N}}/2)}{\sqrt{\mathbf{N}}}\,\mathbf{a}^\dagger \\ \mathbf{M}_e^{\mathbf{U}_r} &= \sin(\tfrac{u}{2})\,\cos(\theta^r_{\mathbf{N+I}}/2) - \cos(\tfrac{u}{2})\,\mathbf{a}\frac{\sin(\theta^r_{\mathbf{N}}/2)}{\sqrt{\mathbf{N}}}\,. \end{aligned} \tag{5.14}$$

A pointer state of this resonant reservoir must be an eigenstate of both $\mathbf{M}_g$ and $\mathbf{M}_e$ given by Eq.(5.14). Let us expand it over the Fock states basis, $|\psi_\infty\rangle = \sum \psi_n|n\rangle$. We get a condition on the coefficients ψ_n, for $n = 0, 1, 2, ...$:

$$\sin(\theta^r_{n+1}/2)\,\psi_{n+1} = \tan\tfrac{u}{2}\,(1+\cos(\theta^r_{n+1}/2)\,)\,\psi_n\,. \tag{5.15}$$

This relation allows to compute all the ψ_n starting from $\psi_0 \neq 0$, except if $\sin(\theta^r_m/2) = 0$ for some m. This condition corresponds to the existence of a trapping state $|m-1\rangle$ [Filipovicz 1986], which is then uncoupled from $|m\rangle$. The Hilbert subspaces corresponding to the photon numbers $\leq (m-1)$ and to those $\geq m$ are then decoupled, such that the steady state depends on the initial conditions. Since all states considered in the remainder of this Section have an energy lower than 20 photons, we arbitrarily truncate the Hilbert space to $n \leq n_{\max} = 50$. We can thus avoid trapping states by choosing small θ_r values such that $\sin(\theta^r_{n+1}/2) \neq 0$ for all $0 \leq n \leq n_{\max}$. Dividing (5.15) by $\sin(\theta^r_{n+1}/2)$ then gives the recurrence:

$$\psi_{n+1} = \frac{\tan(u/2)}{\tan(\theta^r_{n+1}/4)}\,\psi_n\,, \tag{5.16}$$

which defines a unique normalized pointer state.

For $(\theta^r_{n_{\max}}/4)^2 \ll 1$, the recurrence (5.16) reduces to $\psi_{n+1} \approx \frac{4\tan(u/2)}{\theta_r\sqrt{n+1}}\,\psi_n$, which defines a coherent state $|\alpha_\infty\rangle$ with $\alpha_\infty = \frac{4\tan(u/2)}{\theta_r}$ (compare with the last member of Eq. (5.11)).

This value of α_∞ can be retrieved by a simplified reasoning as in [Sarlette 2011]. Assume that the cavity already contains a large coherent field of amplitude $\alpha \gg 1$. The incoming atoms then undergo a resonant Rabi rotation in this field, with an atomic Bloch vector initially pointing towards the south pole of the Bloch sphere.

The Bloch vector rotates by an angle $-\theta_r\alpha$, such that if $\theta_r\alpha < 2u$ (resp. $\theta_r\alpha > 2u$) the final atomic state has a lower (resp. larger) energy than the initial one, i.e. in average gives energy to (resp. draws energy from) the field. This energy exchange thus stabilizes a field with amplitude $\alpha_\infty = 2u/\theta_r$.

We have numerically examined the fidelity $F = |\langle\psi_\infty|\alpha_*\rangle|^2$ of the pointer state $|\psi_\infty\rangle$ defined by Eq. (5.16) with respect to a coherent state $|\alpha_*\rangle$ of the same mean photon number $|\alpha_*|^2 = \langle\psi_\infty|\mathbf{N}|\psi_\infty\rangle$. Fig. 5.4(a) represents that mean photon number in gray scale, for a range of parameters u, θ_r delimited such that the fidelity F is larger than 99%. We limit the plot to $\theta_r < (2\pi)/\sqrt{n_{\max}} \approx 0.88$ to avoid trapping states, and to $\theta_r > 5\tan(u/2)/\sqrt{n_{\max}}$ to remain in the truncated Hilbert space (top left corner cut off). The coherent state approximation for $|\psi_\infty\rangle$ remarkably holds for a range of u and θ_r much larger than that predictable from the qualitative discussion above.

Convergence towards $|\alpha_\infty\rangle$ can be simply analyzed in the limit of small u, θ_r. Expansion of Eq. (5.14) to second order in u, $\theta_{\mathbf{N}}^r$ yields the Kraus map:

$$\begin{aligned}\rho_{k+1} \;\approx\; & \rho_k + \frac{u\theta_r}{4}\left([\mathbf{a}^\dagger, \rho_k] - [\mathbf{a}, \rho_k]\right) \\ & -\frac{\theta_r^2}{8}\left(\mathbf{N}\rho_k + \rho_k\mathbf{N} - 2\mathbf{a}\rho_k\mathbf{a}^\dagger\right) .\end{aligned} \tag{5.17}$$

It can be simplified by letting $\tilde{\rho} = \mathbf{D}_{-\alpha_\infty}\,\rho\,\mathbf{D}_{\alpha_\infty}$ such that $\rho = |\alpha_\infty\rangle\langle\alpha_\infty|$ corresponds to $\tilde{\rho} = |0\rangle\langle 0|$. A few calculations show that Eq. (5.17) transforms into

$$\tilde{\rho}_{k+1} = \tilde{\rho}_k - \frac{\theta_r^2}{8}\left(\mathbf{N}\tilde{\rho}_k + \tilde{\rho}_k\mathbf{N} - 2\mathbf{a}\tilde{\rho}_k\mathbf{a}^\dagger\right). \tag{5.18}$$

This is a finite difference version of the standard Lindlblad equation, describing the damping of an harmonic oscillator coupled to a zero temperature bath. It efficiently drives any initial state towards the vacuum, with a relaxation rate proportional to θ_r^2. This analogy shows that the initial map [Eq. (5.17)] drives any initial cavity state towards a coherent state $|\alpha_\infty\rangle$ with $\alpha_\infty = 2u/\theta_r$. Smaller θ_r values, i.e. shorter interaction times of each atom with the field lead to a higher energy pointer state (for a given u), but to a lower convergence rate (independently of u).

Similar conclusions are directly reached from Eq. (5.17) by assuming that the field is, at each step during its evolution towards the equilibrium, in a coherent state with amplitude α_k. Using simple second-order approximations in u, θ_r [2], we find that this amplitude evolves as:

$$\alpha_{k+1} = (1 - \theta_r^2/8)\alpha_k + u\theta_r/4\,. \tag{5.19}$$

[2] Explicitly, we have (all $|\cdot\rangle$ denote coherent states)

$$\begin{aligned}\varepsilon\mathbf{N}|\beta\rangle &= |(1+\varepsilon)\beta\rangle - |\beta\rangle + |\beta|^2\Re(\varepsilon)|\beta\rangle \\ \varepsilon\mathbf{a}^\dagger|\beta\rangle &= |\beta+\varepsilon\rangle - |\beta\rangle + \Re(\varepsilon\beta^\dagger)|\beta\rangle \\ \sum_\nu a_\nu|\beta+\varepsilon_\nu\rangle &= \left(\sum_\nu a_\nu\right)|\tfrac{\sum_\nu a_\nu(\beta+\varepsilon_\nu)}{\sum_\nu a_\nu}\rangle\,,\end{aligned}$$

up to second order terms in $|\varepsilon|$, $|\varepsilon_\nu|$, with $\varepsilon, \varepsilon_\nu, a_\nu \in \mathbb{C}$ and $\sum_\nu a_\nu \neq 0$.

This first-order system has the explicit solution $\alpha_k = (1-\theta_r^2/8)^k(\alpha_0-\alpha_\infty)+\alpha_\infty$ starting from α_0 at $k=0$. Noting that $\log|\langle\alpha_\infty|\alpha_k\rangle|^2 = -|\alpha_k-\alpha_\infty|^2$, the fidelity indicator $\log|\log|\langle\alpha_\infty|\alpha_k\rangle|^2| = \log|\alpha_0-\alpha_\infty|^2 - \lambda_{\rm conv}\,k$ decreases linearly in k towards $-\infty$. The slope $\lambda_{\rm conv} = 2|\log(1-\theta_r^2/8)|$ measures the exponential convergence speed of $|\alpha_k-\alpha_\infty|^2$, which increases with θ_r and is independent of u.

Numerical simulations of Eq. (5.6) with the exact Kraus map [Eq. (5.14)] vindicate this approximate analysis. Figure 5.4(b) shows the evolution of $\log|\log\langle\psi_\infty|\rho_k|\psi_\infty\rangle|$ as a function of the number of atom-field interactions k, starting from the vacuum $\rho_0=|0\rangle\langle 0|$, with the real Kraus map associated with $\mathbf{U}_r$. The evolution is linear, as predicted by the simplified model. We have checked that this linearity holds for a large range of parameter values: it is only for large θ_rs that the curve bends slightly upwards for the first few ks. This allows us to use the slope $\lambda_{\rm conv}$ of that approximate line as a measure of convergence speed. Fig. 5.4(c) shows the dependency of $\lambda_{\rm conv}$ in θ_r, for two different u values: $u=0.1$ (dotted curve) and $u=1$ [dashed curve, which does not extend to low θ_r values, according to the accessible domain on Fig. 5.4(a)]. They closely follow the simplified model (full line), which is independent of u and slightly overestimates the convergence speed.

5.1.3 Kerr Hamiltonian simulation in the dispersive regime

We now discuss the case of a full composite interaction, with the detuning profile $\delta(t)$ represented on Fig. 5.3. The full propagator

$$\mathbf{U}_T = \mathbf{U}_{d_2}\,\mathbf{U}_r\,\mathbf{U}_{d_1}\,, \tag{5.20}$$

is the concatenation of three unitary operators corresponding first to the dispersive interaction with $d_1=(-T/2,-t_r/2,v,\delta_0)$ as the atom enters the cavity, then to the resonant one with $q=r$ around cavity center, then to the last dispersive interaction with $d_2=(t_r/2,T/2,v,-\delta_0)$ as the atom leaves the cavity. The exact expression of $\mathbf{U}_r$ is given by Eq. (5.12). The dispersive propagators $\mathbf{U}_{d_1}$ and $\mathbf{U}_{d_2}$ are computed in Section 5.1.8.1, assuming that δ_0 and v satisfy the adiabatic approximation condition [Eq. (5.50)]. This condition merely expresses that the interaction Hamiltonian $\mathbf{H}_{JC}$ varies slowly (through $\Omega(vt)$) in comparison to the differences between its eigenfrequencies. Thus, each initial eigenstate of $\mathbf{H}_{JC}$ remains an eigenstate and only accumulates a phase proportional to its eigenenergy.

To get a simple insight in the physics of the stabilization of nonclassical states, the present Section focuses (like [Sarlette 2011]) on the simple case in which the two nonresonant interactions take place in the dispersive regime, i.e. $\delta_0 \gg \Omega_0$. This avoids spurious population transfers in the dispersive phase, as atomic levels dressed by the cavity field almost coincide with the bare levels $|e\rangle$ and $|g\rangle$. The dispersive propagators, deduced from Eq. (5.56) in Section 5.1.8.1, then write:

$$\begin{aligned} \mathbf{U}_{d_1} &\approx \mathbf{U}_{d_2}^\dagger \approx \mathbf{Z}(\phi_{\mathbf{N}}^d) \\ \text{with } \phi_{\mathbf{N}}^d &= \phi_\gamma \mathbf{N} + \phi_\zeta\,, \end{aligned} \tag{5.21}$$

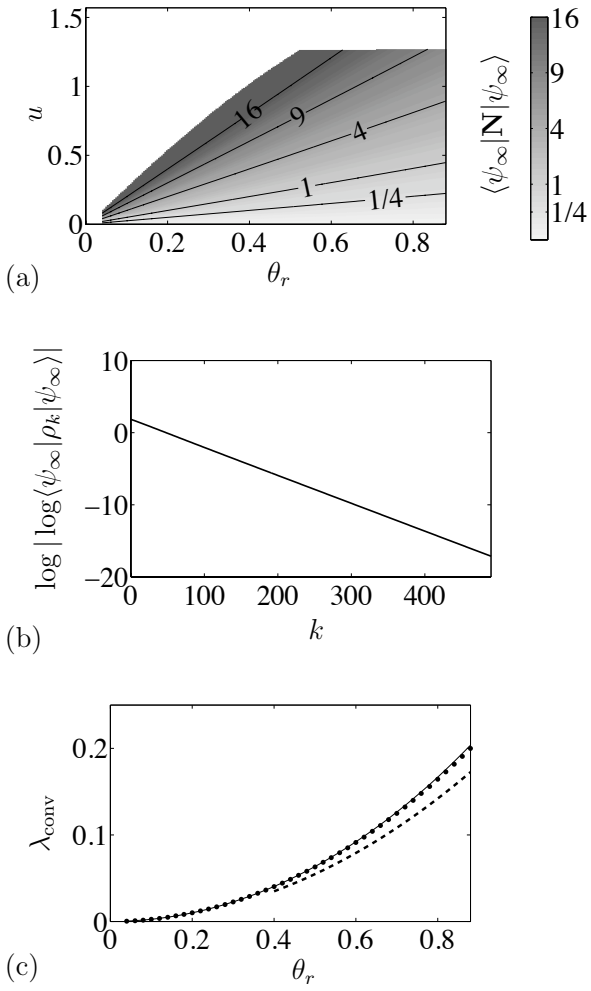

Figure 5.4: Reservoir with interaction $\mathbf{U}_r$. (a) Mean photon number $\langle\psi_\infty|\mathbf{N}|\psi_\infty\rangle$ of the pointer state $|\psi_\infty\rangle$. Grayscale axis is linear in $\sqrt{\langle\psi_\infty|\mathbf{N}|\psi_\infty\rangle}$. The shaded zone is delimited such that the corresponding states have at least a 99% fidelity $|\langle\psi_\infty|\alpha_*\rangle|^2$ to a coherent state $|\alpha_*\rangle$ of same mean photon number $|\alpha_*|^2 = \langle\psi_\infty|\mathbf{N}|\psi_\infty\rangle$. On the top left corner, pointer states have significant population outside the truncated Hilbert space. On the top right part, $|\langle\psi_\infty|\alpha_*\rangle|^2$ drops to $\sim 98\%$ as u approaches $\pi/2$. (b) Evolution of the fidelity indicator $\log|\log\langle\psi_\infty|\rho_k|\psi_\infty\rangle|$ as a function of the number of atom-field interactions (i.e. Kraus map iterations) k, starting from vacuum $\rho_0 = |0\rangle\langle 0|$. We have arbitrarily set $u = 0.5$ and $\theta_r = 0.4$, for which $\langle\psi_\infty|\mathbf{N}|\psi_\infty\rangle = 6.21$. (c) Convergence rate λ_{conv} as a function of θ_r for $u = 0.1$ (dotted curve) and $u = 1$ (dashed curve). Dependency on u is small. We also represent (full curve) the analytic result of the simplified model [Eq. (5.19)]. This model slightly overestimates the convergence speed.

where $\phi_\gamma = 1/(2\,\delta_0)\,\int_{-T/2}^{-t_r/2}\Omega^2(vt)\,dt$ is a phase shift per photon and $\phi_\zeta = \delta_0(T - t_r)/2$ reflects the free atom evolution in the interaction representation at cavity frequency.

The full propagator can then be written

$$\begin{aligned}\mathbf{U}_T \approx \mathbf{U}_d &= \mathbf{Z}(-\phi^d_{\mathbf{N}})\ \mathbf{U}_r\ \mathbf{Z}(\phi^d_{\mathbf{N}}) \\ &= |g\rangle\langle g|\,\cos\theta^r_{\mathbf{N}}/2 + |e\rangle\langle e|\,\cos\theta^r_{\mathbf{N+I}}/2 \\ &\quad -|e\rangle\langle g|\,\mathbf{a}\,\frac{\sin\theta^r_{\mathbf{N}}/2}{\sqrt{\mathbf{N}}}\,e^{i(\phi_\gamma\mathbf{N}+\phi_\zeta)} \\ &\quad +|g\rangle\langle e|\,\frac{\sin\theta^r_{\mathbf{N}}/2}{\sqrt{\mathbf{N}}}\,e^{-i(\phi_\gamma\mathbf{N}+\phi_\zeta)}\,\mathbf{a}^\dagger\ , \end{aligned} \tag{5.22}$$

where $\theta^r_{\mathbf{N}}$ is defined by Eq. (5.13). The two opposite dispersive interactions have no net effect when the atom remains in the same state during the resonant interaction $\mathbf{U}_r$. In contrast, $\mathbf{Z}$ does not commute with terms in which the atomic level changes in the resonant phase. For these terms, the dispersive phase shifts add up. The global evolution $\mathbf{U}_d$ thus associates a phase shift to each term of $\mathbf{U}_r$ that changes the field energy. An increasing field energy corresponds to a decrease of the field phase and vice versa. These correlated phase and amplitude shifts suggest that $\mathbf{U}_d$ might stabilize a coherent state distorted by amplitude-dependent phase shifts, a situation similar to that encountered during the propagation through a Kerr medium.

The action of the atom can indeed be expressed by an operator acting on the field only. Let us define the Hermitian operator $h^d_{\mathbf{N}}$ by:

$$h^d_{\mathbf{N}} = \phi_\gamma(\mathbf{N}^2 + \mathbf{N})/2 + \phi_\zeta\mathbf{N}\,. \tag{5.23}$$

With the commutation identity [Eq. (5.7)] we have $e^{-ih^d_{\mathbf{N}}}\,\mathbf{a}\,e^{ih^d_{\mathbf{N}}} = \mathbf{a}\,e^{i(\phi_\gamma\mathbf{N}+\phi_\zeta)}$ and

$$\mathbf{U}_d = e^{-ih^d_{\mathbf{N}}}\,\mathbf{U}_r\,e^{ih^d_{\mathbf{N}}}\ . \tag{5.24}$$

Thus, $\mathbf{U}_d$ is equivalent to $\mathbf{U}_r$ modulo a basis change on the field state alone defined by the unitary operator $e^{-ih^d_{\mathbf{N}}}$.

In other words, when ρ evolves under the Kraus map associated to $(\mathbf{M}_g^{\mathbf{U}_d}\,,\ \mathbf{M}_e^{\mathbf{U}_d})$, $\rho^h = e^{ih^d_{\mathbf{N}}}\ \rho\ e^{-ih^d_{\mathbf{N}}}$, evolves under the Kraus map associated to $(\mathbf{M}_g^{\mathbf{U}_r}\,,\ \mathbf{M}_e^{\mathbf{U}_r})$. It follows from Section 5.1.2 that ρ^h converges towards a coherent pointer state $|\alpha_\infty\rangle$. Therefore, ρ converges with the same convergence rate towards a nonclassical pointer state $\exp[-ih^d_{\mathbf{N}}]\,|\alpha_\infty\rangle$.

The effective Hamiltonian $h^d_{\mathbf{N}}/t_K$ is equal to the Kerr Hamiltonian $\mathbf{H}_K$, with $\gamma_K t_K = \phi_\gamma/2$ and $\zeta_K t_K = (\phi_\zeta + \phi_\gamma/2)$. The engineered reservoir thus stabilizes the nonclassical pointer states $e^{-it_K\mathbf{H}_K}\,|\alpha_\infty\rangle$ which would be produced by propagation through a Kerr medium (see Fig. 5.1). Tuning T and δ_0 allows us to choose ϕ_γ at will. We can thus prepare and stabilize a whole class of such states, as described in the introduction of this Section. In particular, for $\phi_\gamma = \pi$, we get the MFSS $|c_{\tilde\alpha_\infty}\rangle = (|\tilde\alpha_\infty\rangle + i\,|\text{-}\tilde\alpha_\infty\rangle)/\sqrt{2}$ with $\tilde\alpha_\infty = e^{-i\,(\phi_\zeta+\pi/2)}\,\alpha_\infty$. Note that the stabilization of this two-component MFSS is the most demanding experimentally, since it requires the longest dispersive interaction time.

The discussions in this Section only apply in the limit of small Ω/δ_0. Reaching a significant value of ϕ_γ in this case requires a large dispersive interaction time $(T-t_r)/2$, that can be prohibitive. First, in the experimental context of Fig. 5.2, $T = 3w/v$ is limited by the minimal achievable atomic velocity (a few tens of m/s in the ENS setup). Second, a larger T means less frequent atom-field interaction and thus a weaker reservoir, implying a less efficient protection of the target state against decoherence induced by cavity relaxation.

5.1.4 Regime of arbitrary detunings

We thus discuss now dispersive interaction with moderate Ω/δ_0 values; which allows one to reach significant dispersive effects within moderate interaction times. We therefore use a more precise expression of the propagator for the nonresonant interactions (parameter sets d_1 and d_2), by applying the adiabatic approximation to the actual dressed states (instead of $|g,n+1\rangle$ and $|e,n\rangle$ as in Eq. (5.21) when assuming $\delta_0 \gg \Omega_0$). Developments detailed in Section 5.1.8.1 lead to:

$$\mathbf{U}_T \approx \mathbf{U}_c = \mathbf{Z}(-\phi_\mathbf{N})\,\mathbf{X}(\xi_\mathbf{N})\,\mathbf{Y}(\theta^r_\mathbf{N})\,\mathbf{X}(\xi_\mathbf{N})\,\mathbf{Z}(\phi_\mathbf{N})\;, \tag{5.25}$$

with

$$\phi_n = \delta_0 \int_{-T/2}^{-t_r/2} \sqrt{1+n\,(\Omega(vt)/\delta_0)^2}\;dt\;, \tag{5.26}$$

$$\tan\xi_n = \tfrac{\Omega(vt_r/2)\sqrt{n}}{\delta_0} \quad \text{with } \xi_n \in (\tfrac{-\pi}{2},\tfrac{\pi}{2})\;. \tag{5.27}$$

We recognize in this expression the central resonant interaction evolution operator, $\mathbf{Y}(\theta^r_\mathbf{N})$, and the two phase-shift operations accumulated during the non-resonant interactions ($\mathbf{Z}(-\phi_\mathbf{N})$ and $\mathbf{Z}(\phi_\mathbf{N})$). Note that here, unlike in Section 5.1.3, ϕ_n is a nonlinear function of n. The remaining two $\mathbf{X}(\xi_\mathbf{N})$ operators reflect the fact that the atomic energy eigenstates do not coincide with the dressed levels at $\pm t_r/2$, when the atomic frequency is suddenly switched. Note that we neglect two similar transformations which appear in principle when the atom gets first coupled to the mode and finally decoupled from it, since the atom-field coupling is then quite negligible.

Some tedious but simple computations exploiting Eq. (5.7) allow us to write:

$$\begin{aligned}\mathbf{U}_c = {} & |g\rangle\langle g|\,\cos(\theta^c_\mathbf{N}/2) + |e\rangle\langle e|\,\cos(\theta^c_{\mathbf{N}+\mathbf{I}}/2) \\ & -|e\rangle\langle g|\,\mathbf{a}\frac{\sin(\theta^c_\mathbf{N}/2)}{\sqrt{\mathbf{N}}}\;e^{i\phi^c_\mathbf{N}} \\ & +|g\rangle\langle e|\,e^{-i\phi^c_\mathbf{N}}\;\frac{\sin(\theta^c_\mathbf{N}/2)}{\sqrt{\mathbf{N}}}\,\mathbf{a}^\dagger\;.\end{aligned} \tag{5.28}$$

Here, $\theta^c_n \in [0,2\pi)$ is defined by

$$\cos(\theta^c_n/2) = \cos(\theta^r_n/2)\;\cos\xi_n\;. \tag{5.29}$$

Introducing [3]

$$\chi_n^c = \arg[\sin(\theta_n^r/2) - i\cos(\theta_n^r/2)\sin\xi_n\,]\,, \tag{5.30}$$

we define the composite phase as $\phi_{\mathbf{N}}^c = \phi_{\mathbf{N}} + \chi_{\mathbf{N}}^c$.

Comparing Eqs. (5.28) and (5.22), we finally get:

$$\mathbf{U}_c = \mathbf{Z}(-\phi_{\mathbf{N}}^c)\ \mathbf{Y}(\theta_{\mathbf{N}}^c)\ \mathbf{Z}(\phi_{\mathbf{N}}^c)\,. \tag{5.31}$$

This expression of $\mathbf{U}_c$ has the same general form as that used in the dispersive case (Section 5.1.3). Angles $\theta_{\mathbf{N}}^c$, $\phi_{\mathbf{N}}^c$ replace $\theta_{\mathbf{N}}^r$, $\phi_{\mathbf{N}}^d$ respectively. We now show that with these adaptations, most of the conclusions of the previous Sections still hold. The reservoir in realistic situations indeed stabilizes the nonclassical states $|\psi\rangle \approx e^{-it_K\mathbf{H}_K}\,|\alpha\rangle$.

5.1.4.1 Effects of $\mathbf{Y}(\theta_{\mathbf{N}}^c)$ and $\mathbf{Z}(\pm\phi_{\mathbf{N}}^c)$

Let us first consider a reservoir of atoms whose interaction with the cavity would be described by $\mathbf{Y}(\theta_{\mathbf{N}}^c)$. Note that this situation is not physical: the $\mathbf{Y}(\theta_{\mathbf{N}}^c)$ evolution operator is no more than a convenient mathematical factor appearing in the expression of the complete evolution operator $\mathbf{U}_c$.

In analogy with Section 5.1.2, the pointer state $|\psi_\infty\rangle = \sum \psi_n|n\rangle$ corresponding to this fictitious interaction is defined by the recurrence relation:

$$\psi_{n+1} \;=\; \frac{\tan(u/2)}{\tan(\theta_{n+1}^c/4)}\,\psi_n\,, \tag{5.32}$$

for $n = 0, 1, 2, \ldots$. Equation (5.29) ensures $|\cos(\theta_{n+1}^c/2)| < 1\ \forall n$, therefore $0 < \theta_{n+1}^c/4 < \pi/2$. Moreover $\lim_{n\mapsto+\infty}\theta_n^c = \pi$, such that Eq. (5.32) always yields a well-defined finite energy state as soon as $|\tan(u/2)| < 1$ i.e. $|u| < \pi/2$. For large n values, the recurrence (5.32) is approximated by $\psi_{n+1} = \tan\frac{u}{2}\,\psi_n$ and ψ_n converges exponentially towards 0 with $\sum_n\ n\,\psi_n^2$ finite. The energy exchange resulting from the rapid variation of the atomic frequency near the cavity center thus removes the possibility of trapping states.

Note that even in the absence of the central resonant interaction, with $\theta_n^r = 0$ in Eq. (5.29), relation (5.32) defines a unique pointer state with finite energy. It is thus in principle possible to simplify our scheme by using only two dispersive phases with opposite detunings. In this case, energy would be transferred from the qubit to the cavity during these non-fully-dispersive interactions, where the qubit-cavity detuning is larger, but of the same order, as the coupling Ω.

For θ_r and Ω_r/δ_0 small, $2\tan(\theta_n^c/4) \approx \theta_n^c/2 \approx \theta_c\sqrt{n}/2$ with $\theta_c = \sqrt{\theta_r^2 + (\frac{2\Omega_r}{\delta_0})^2}$. The pointer state is thus close to a coherent state $|\alpha_\infty\rangle$, as in Section 5.1.2, with the amplitude $\alpha_\infty = 4\tan(u/2)\,/\,\theta_c$. Convergence arguments similar to those of Section 5.1.2 (effective Lindblad master equation) can be given. The convergence rate is

[3] Note that for all $n > 0$, phase χ_n^c is well-defined because $|\xi_n| \in (0, \pi/2)$. For $n = 0$, the term multiplying the undefined χ_0^c vanishes in Eq. (5.28).

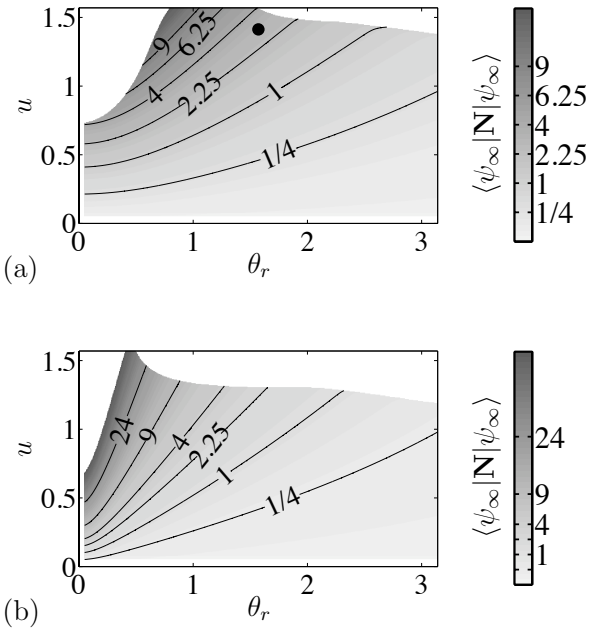

Figure 5.5: Mean photon number $\langle\psi_\infty|\mathbf{N}|\psi_\infty\rangle$ of the pointer state $|\psi_\infty\rangle$ stabilized by $\mathbf{Y}(\theta^c_\mathbf{N})$, with $\delta_0 = 2.2\,\Omega_r$ (a) and $\delta_0 = 10\,\Omega_r$ (b). Grayscale axis is linear in $\sqrt{\langle\psi_\infty|\mathbf{N}|\psi_\infty\rangle}$. The 2-component MFSS on Fig. 5.1 uses $u = 0.9\pi/2$ and $\theta_r = \pi/2$ with $\delta_0 = 2.2\,\Omega_r$, corresponding to the black dot on (a), for which $\langle\psi_\infty|\mathbf{N}|\psi_\infty\rangle = 2.96$. The shaded zone is delimited such that all corresponding states have at least 99% fidelity $|\langle\psi_\infty|\alpha_*\rangle|^2$ to a coherent state $|\alpha_*\rangle$ of the same mean photon number ($|\alpha_*|^2 = \langle\psi_\infty|\mathbf{N}|\psi_\infty\rangle$).

now proportional to θ_c^2. We conjecture that this convergence is valid for any u with $0 \leq u < \pi/2$, $\theta_r \geq 0$, $\Omega_r > 0$ and $\delta_0 > 0$.

Figure 5.5 presents numerical estimations of the field pointer state $|\psi_\infty\rangle$ stabilized by a hypotetical reservoir using interaction $\mathbf{Y}(\theta^c_\mathbf{N})$. For all represented parameter values, fidelity $|\langle\psi_\infty|\alpha_*\rangle|^2$ to a coherent state $|\alpha_*\rangle$ of the same mean photon number ($|\alpha_*|^2 = \langle\psi_\infty|\mathbf{N}|\psi_\infty\rangle$), is at least 99%. That mean photon number is represented by the grayscale. The larger value $\Omega_r/\delta_0 = 1/2.2$ used on Fig. 5.5(a), does not allow to reach as high mean photon numbers as the value $\Omega_r/\delta_0 = 1/10$ of Fig. 5.5(b). Small Ω_r/δ_0 however are more subject to undesired population of the high-lying Fock states, reminiscent of the trapping states, for large θ_r and u. This explains the smaller domain where fidelity is larger than 99%. With the particular values used for Fig. 5.1(e) (black dot on Fig. 5.5(a), with $\Omega_r/\delta_0 = 1/2.2$, $\theta = \pi/2$ and $u = 0.45\pi$), fidelity to a coherent state is almost 99.9% and $\langle\psi_\infty|\mathbf{N}|\psi_\infty\rangle = 2.96$.

We now examine the influence of the $\mathbf{Z}(\pm\phi^c_\mathbf{N})$ operators on the pointer state defined by $\mathbf{Y}(\theta^c_\mathbf{N})$. A first observation is that it does not modify the photon number populations, since it commutes with $\mathbf{N}$. Thus, the energy of the field pointer state,

for a reservoir with composite interaction, is entirely determined by the parameters in $\mathbf{Y}(\theta^c_{\mathbf{N}})$, as represented for example on Fig. 5.5. Let us define the Hermitian operator $h^c_{\mathbf{N}}$ by the recurrence relation:

$$h^c_{n+1} - h^c_n = \phi^c_{n+1} \ , \tag{5.33}$$

for $n = 0, 1, 2, ...$, with an arbitrary h^c_0. Using Eq. (5.7) as in Section 5.1.3 yields

$$\mathbf{U}_c = e^{-ih^c_{\mathbf{N}}} \ \mathbf{Y}(\theta^c_{\mathbf{N}}) \ e^{ih^c_{\mathbf{N}}} \ . \tag{5.34}$$

The pointer states of $\mathbf{U}_c$ are those of $\mathbf{Y}(\theta^c_{\mathbf{N}})$ transformed by the unitary $e^{-ih^c_{\mathbf{N}}}$. The choice of h^c_0 for solving Eq. (5.33) is thus physically irrelevant, as it corresponds in Eq. (5.34) to two constant opposite phases that cancel out. The operator $h^c_{\mathbf{N}}$ here plays exactly the role of $h^d_{\mathbf{N}}$ in Section 5.1.3. The only difference is that, as ϕ^c_n is nonlinear, h^c_n is defined with the discrete integral (5.33). If ϕ^c_n is nearly linear in n over the relevant photon numbers [dominant photon numbers in the pointer state $|\psi_\infty\rangle$ associated to $\mathbf{Y}(\theta^c_{\mathbf{N}})$], then h^c_n is nearly quadratic and the situation of Section 5.1.4 is recovered. The reservoir stabilizes nonclassical pointer states $|\psi^c_\infty\rangle = e^{-ih^c_{\mathbf{N}}}|\psi_\infty\rangle \approx e^{-it_K\mathbf{H}_K}|\alpha\rangle$ with t_K depending on the parameters governing ϕ^c_n.

5.1.4.2 Choice of the reservoir operating point

We now use this detailed description of the reservoir to justify the choice of operating parameters leading to the generation of the two component MFSS presented in figure 5.1(e): $u = 0.45\,\pi$, $\theta_r = \pi/2$, $v = 70$ m/s, $\delta = 2.2\,\Omega_0$. Note that the state in Fig. 5.1(e), with ≈ 2.7 photons on the average has been computed with a finite cavity lifetime $T_c = 65$ ms. The same computation in an ideal cavity leads to an average photon number equal to 2.96, see Fig. 5.5. The *two-component* MFSS corresponds to the largest effect of the dispersive interaction, and hence to the most demanding experimental conditions.

The chosen parameters are the result of a tradeoff between contradictory requirements. First, the composite phase shift ϕ^c_n must be nearly linear in n over the useful photon number range, with a slope of π per photon. Second, the time of convergence towards the steady state needs to be much shorter than the decoherence time ($T_c/5.6$) of the target state due to unavoidable cavity relaxation. Linearity of ϕ^c_n improves with larger δ_0/Ω_r. The π phase shift per photon condition then requires very long atom-cavity interaction time, in clear contradiction with the second requirement.

The tradeoff is further examined in Fig. 5.6. Figure 5.6(a) evaluates the linearity of ϕ^c_n by showing $D\phi^c_n = \phi^c_{n+1} - \phi^c_n = h^c_{n+1} + h^c_{n-1} - 2h^c_n$ for different parameter values. Once again θ_r has little influence and we set it to $\pi/2$. For each value of Ω_r/δ_0, we adjust v to have $D\phi^c_n = \pi$ for the same mean photon number $n = 2.96$ (by interpolation). That value is chosen to cover the parameter values of Fig. 5.1(e), represented by a black dot on Figs. 5.5 and 5.6. As expected, $D\phi^c_n$ is quite constant

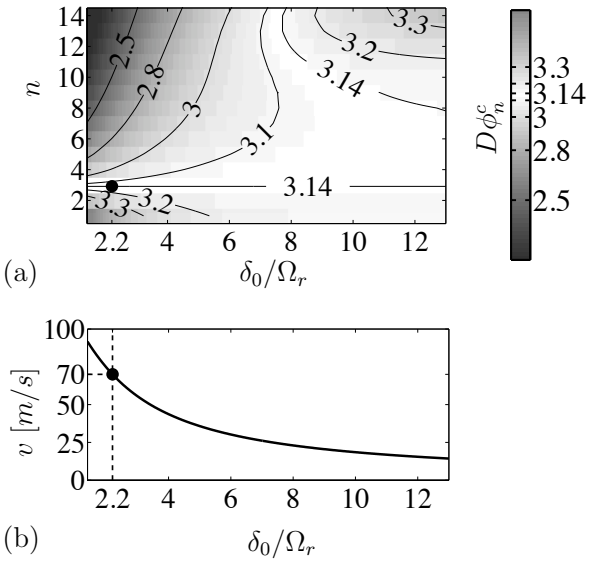

Figure 5.6: (a) Kerr-effect-inducing $D\phi_n^c = \phi_{n+1}^c - \phi_n^c$ as a function of photon number n. Since ϕ_0^c is undefined, we start with $D\phi_1^c$. We set $\theta_r = \pi/2$. (b) Corresponding velocities v: for each δ_0/Ω_r, we adjust v to have $D\phi_n^c = \pi$ at $n = 2.96$. That value is chosen to cover the parameter values $v = 70$ m/s, $\delta_0/\Omega_r = 1/2.2$ (black dots) used for the 2-component MFSS in Fig. 5.1. An ideal h_n^c, proportional to $\mathbf{H}_K$, requires $D\phi_n^c$ constant in n. Small δ_0/Ω_r values are disadvantageous for this criterion, but allow higher velocity and hence more frequent reservoir atoms for a same mean $D\phi^c$.

for moderate photon numbers in the dispersive region $\delta_0/\Omega_r \gg 1$. This corresponds however to unrealistically small atomic velocities, represented on Fig. 5.6(b). In the region of low δ_0/Ω_r values, a $D\phi_n^c \approx \pi$ at $n = 2.96$ can be reached with larger v, but $D\phi_n^c$ varies more rapidly with n. This variation is nevertheless sufficiently weak in the range $2 \leq n \leq 5$ for $\delta_0/\Omega_r \approx 2.2$, corresponding to the $v = 70$ m/s that is used for Fig. 5.1(e).

Let us now examine the overall reservoir fidelity and the convergence rate λ_{conv} from the vacuum towards the target state, as defined in Fig. 5.4. We choose as free reservoir parameters θ_r and δ_0/Ω_r. This choice sets the value of v [see Fig. 5.6(b)]. Then u is adjusted so that the target mean photon number is 2.96 (see Fig. 5.5(a)). Figure 5.7(a) shows the ratio λ_{conv}/T, where T is the total interaction time of each atom with the cavity. This ratio is the real convergence rate in s^{-1} units. For Fig. 5.1(e), since the expected target state decoherence time is of order $65/5.6 \approx 10$ ms, we choose a parameter set $\delta_0/\Omega_r = 2.2$ and $\theta_r = \pi/2$, corresponding to a 1400 s^{-1} convergence rate (black dot on Fig. 5.7(a)). The fidelity with respect to an ideal MFSS with the same energy is shown on Fig.5.7(b). Our choice of parameters does not correspond to a maximum fidelity due to the variation of $D\phi_n^c$ in the useful n value range (see Fig. 5.6(a)). However, we get an excellent 95%

fidelity.

Figures 5.8 left and right respectively present the Wigner functions of the steady state MFSS obtained with this parameter choice, and of a theoretical superposition of two coherent states with opposite phases and same total energy. The slight distortions of the quasi coherent components in the pointer state MFSS are due to the non-linearity of the phase shift ϕ_n^c.

5.1.5 Decoherence and experimental imperfections

The choice of operating parameters performed above has been based on a rough estimate of the action of decoherence. We now show how the reservoir allows us to stabilize MFSS with a high fidelity, in presence of cavity relaxation due to a zero-temperature environment (Section 5.1.5.1). In Section 5.1.5.2, we study the robustness of the scheme against other experimental imperfections by numerical simulations.

5.1.5.1 Cavity relaxation

First, we consider the field evolution with a simplified model. It is obtained from equation (5.19) for a coherent evolution, sandwiched between two dispersive transformations (Eq. (5.21)):

$$\begin{aligned} \alpha_{k+1} &= (1-\theta_r^2/8)\alpha_k + u\theta_r/4 \\ \rho_k'^h &= |\alpha_k\rangle\langle\alpha_k| \\ \rho_k' &= e^{-i\pi/2\ \mathbf{N}^2}\rho_k'^h e^{i\pi/2\ \mathbf{N}^2}\ . \end{aligned} \tag{5.35}$$

In a Monte-Carlo approach, the evolution of the field density matrix due to cavity relaxation can be represented as a succession of quantum jumps described by the annihilation operator $\mathbf{a}$, occurring at random times and interrupting a non-unitary deterministic evolution of the field state [Molmer 1993].

The action of $\mathbf{a}$ on an MFSS $|c_\alpha\rangle$ is:

$$\mathbf{a}|c_\alpha\rangle \propto |c_{-\alpha}\rangle\,.$$

Since the loss of photons in the environment cannot be detected, an initial $|c_\alpha\rangle$ state rapidly evolves in the absence of the reservoir into a statistical mixture of $|c_\alpha\rangle$ and $|c_{-\alpha}\rangle$, i.e. into a mixture of $|\alpha\rangle$ and $|\text{-}\alpha\rangle$. When the reservoir is present, it drives $|c_{-\alpha}\rangle$ back to $|c_\alpha\rangle$ after each jump. If the reservoir-induced convergence time is much shorter than the average interval between two jumps, then the field is mostly close to $|c_\alpha\rangle$.

This simple description suggests to seek a solution for the steady state with decoherence under the form $\rho_\infty'^h = \int \mu(z)|z\rangle\langle z|\,dz$. This is a statistical mixture of coherent states $|z\rangle$ with real amplitudes z weighted by $\mu(z)$.

In the absence of cavity relaxation, the evolution of $\rho_k'^h$ in the simplified model [Eq. (5.35)] can be viewed as a discretization of the Lindblad master equation:

$$\tfrac{d}{dt}\rho'^h = [\beta\mathbf{a}^\dagger - \beta^\dagger\mathbf{a},\, \rho'^h] - \tfrac{\kappa}{2}(\mathbf{N}\rho'^h + \rho'^h\mathbf{N} - 2\mathbf{a}\rho'^h\mathbf{a}^\dagger)\,, \tag{5.36}$$

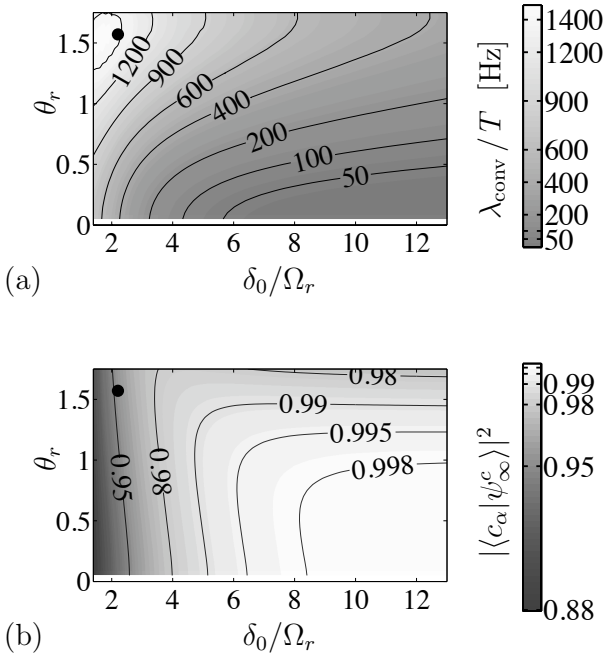

Figure 5.7: (a): Convergence rate $\lambda_{\rm conv}/T$ giving the slope, in time units (s^{-1}), of the convergence towards the reservoir pointer state $|\psi^c_\infty\rangle$, according to $\log|\log\langle\psi^c_\infty|\rho_k|\psi^c_\infty\rangle| = \log|\log\langle\psi^c_\infty|\rho_0|\psi^c_\infty\rangle| - \lambda_{\rm conv}\,k$ (see Fig. 5.4). For each θ_r and Ω_r/δ_0, we adjust v as in Fig. 5.6 to keep $D\phi^c_n \approx \pi$, and u to keep $\langle\psi^c_\infty|\mathbf{N}|\psi^c_\infty\rangle = 2.96$; this reference comes from the values $\theta_r = \pi/2$, $u = 0.45\pi$, $\Omega_r/\delta_0 = 2.2$, $v = 70$ m/s (black dot) used for Fig. 5.1(e). Time $T = 3w/v$ between consecutive atoms changes as we adjust v. (b): Fidelity of the same $|\psi^c_\infty\rangle$ to a 2-component MFSS $|c'_{\alpha_\infty}\rangle = (|\alpha_\infty\rangle + ie^{i\beta}\,|\text{-}\alpha_\infty\rangle)/\sqrt{2}$, where we tune α_∞ and $0 \le \beta < \pi$ to optimize fidelity. It turns out that $|\beta| < 0.005$ for most parameter values, while $|\alpha_\infty|^2$ decreases as fidelity decreases, below 2.7 for the lowest values of Ω_r/δ_0. The black dot marks the case of the 2-component MFSS in Fig. 5.1. For θ_r values larger than those represented, no u value stabilizes a mean photon number 2.96, see also Fig. 5.5. The two plots together illustrate a tradeoff between fidelity in absence of decoherence and convergence speed.

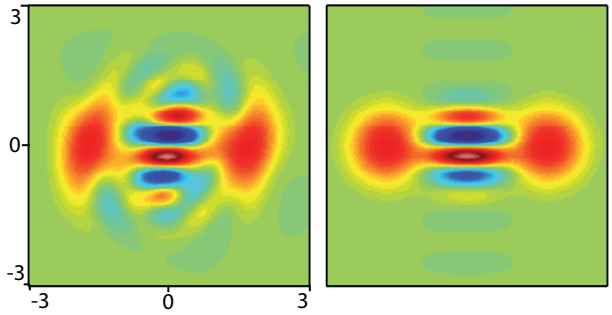

Figure 5.8: Wigner function illustrating a stabilized 2-component MFSS (colorbar as in Fig. 5.1). Left: $|\psi_\infty^c\rangle\langle\psi_\infty^c|$, pointer state of our reservoir with composite interaction. Parameter values are $\theta_r = \pi/2$, $u = 0.45\pi$, $\delta_0 = 2.2\Omega_0$, $v = 70$ m/s, i.e. those used for figure 5.1(e), except T_c set to infinity here. Right: target state $|c_\alpha\rangle\langle c_\alpha|$.

with $\beta\, dt = u\theta_r/4$ and $\kappa\, dt = \theta_r^2/4$. Eq. (5.36) describes the evolution of the field mode coupled with a classical source with an amplitude β and damped at a rate κ. At long times, ρ' converges towards a coherent state $|\alpha_\infty\rangle$ with $\alpha_\infty = 2\beta/\kappa$, see e.g. [Haroche 2006]. Note that in Eq.(5.36), the damping rate κ is induced by *the atomic reservoir* and not by cavity relaxation. Since ρ'^h follows (5.36), ρ' follows

$$\frac{d}{dt}\rho' \;=\; \beta[\mathbf{a}^\dagger e^{-i\pi\mathbf{N}} \;-\; e^{i\pi\mathbf{N}}\mathbf{a},\, \rho'] \;-\; \tfrac{\kappa}{2}(\mathbf{N}\rho' \;+\; \rho'\mathbf{N} \;-\; 2e^{i\pi\mathbf{N}}\mathbf{a}\rho'\mathbf{a}^\dagger e^{-i\pi\mathbf{N}}) \quad ,$$

where we can assume, up to a change of phase, that β is real and positive.

We now add to this simple model a thermal environment at zero temperature that induces decoherence of the field with the cavity lifetime $T_c = 1/\kappa_c$. This adds the usual Lindblad terms to the second member of the previous equation and ρ' now obeys:

$$\begin{aligned}\frac{d}{dt}\rho' = \beta[\mathbf{a}^\dagger e^{-i\pi\mathbf{N}} - e^{i\pi\mathbf{N}}\mathbf{a},\, \rho'] \\ - \tfrac{\kappa}{2}(\mathbf{N}\rho' + \rho'\mathbf{N} - 2e^{i\pi\mathbf{N}}\mathbf{a}\rho'\mathbf{a}^\dagger e^{-i\pi\mathbf{N}}) \\ - \tfrac{\kappa_c}{2}(\mathbf{N}\rho' + \rho'\mathbf{N} - 2\mathbf{a}\rho'\mathbf{a}^\dagger)\,. \quad (5.37)\end{aligned}$$

In the Kerr representation, ρ'^h then evolves according to:

$$\begin{aligned}\frac{d}{dt}\rho'^h = \beta[\mathbf{a}^\dagger - \mathbf{a},\, \rho'^h] \\ - \tfrac{\kappa+\kappa_c}{2}(\mathbf{N}\rho'^h + \rho'^h\mathbf{N} - 2\mathbf{a}\rho'^h\mathbf{a}^\dagger) \\ - \kappa_c(\mathbf{a}\rho'^h\mathbf{a}^\dagger - e^{i\pi\mathbf{N}}\mathbf{a}\rho'^h\mathbf{a}^\dagger e^{-i\pi\mathbf{N}})\,. \quad (5.38)\end{aligned}$$

Without the terms in the third line of Eq. (5.38), we would get Eq. (5.36) with κ replaced by $\kappa + \kappa_c$. This would yield a coherent steady state of amplitude $\alpha_\infty^c = \alpha_\infty/(1+\eta)$ with $\eta = (4T)/(\theta_r^2\, T_c)$. The whole equation (5.38) leaves invariant

the set of mixtures of coherent states with real amplitudes in $[-\alpha_\infty^c, \alpha_\infty^c]$. We therefore search for the stationary solution under the form:

$$\rho'^h_\infty = \int_{-\alpha_\infty^c}^{\alpha_\infty^c} \mu(z)|z\rangle\langle z|\, dz\,. \tag{5.39}$$

As shown in Section 5.1.8.3, this yields a solution:

$$\mu(z) = \mu_0 \frac{\left(((\alpha_\infty^c)^2 - z^2)^{(\alpha_\infty^c)^2}\ e^{z^2}\right)^{r_c}}{\alpha_\infty^c - z}\ , \tag{5.40}$$

with $r_c = 2\kappa_c/(\kappa+\kappa_c)$. The normalization factor $\mu_0 > 0$ ensures that $\int_{-\alpha_\infty^c}^{\alpha_\infty^c} \mu(z)dz = 1$. In any case, $\mu(-\alpha_\infty^c) = 0$. For small κ_c, we have $\lim_{z\mapsto\alpha_\infty^c} \mu(z) = +\infty$ and ρ'^h_∞ is close to the coherent state $|\alpha_\infty^c\rangle$. For large κ_c, α_∞^c tends to zero and thus the field steady-state becomes close to the vacuum.

We now compare this simplified model to the actual reservoir in the presence of relaxation. Figure 5.9 illustrates the reservoir-induced convergence after a quantum jump. The leftmost column shows the Wigner function of ρ' during this recovery process for the simplified model (5.35). We start as $|c_\alpha\rangle$ (upper left frame). Immediately after a jump (second frame in the leftmost column), the state is $|c_{-\alpha}\rangle$. Successive snapshots of the recovery procedure are presented in the next frames. We neglect here the action of cavity relaxation during this recovery process. Note that after ≈ 4 reservoir atoms, the state is the vacuum, from which $|c_\alpha\rangle$ is gradually recovered.

The second column depicts the evolution of ρ'^h. In this representation, the initial state is the coherent state $|\alpha\rangle$ (first frame). It jumps to $|\text{-}\alpha\rangle$ (second frame), and then gradually evolves back towards $|\alpha\rangle$ according to Eq. (5.19), staying coherent at all time.

On the third column, we show the Wigner functions of the actual cavity state ρ induced by our reservoir, whose dynamics is governed by the Kraus map associated to $\mathbf{U}_c$. The last column shows the evolution of $\rho^h = e^{ih^c_{\mathbf{N}}}\,\rho\, e^{-ih^c_{\mathbf{N}}}$. We observe that ρ^h and ρ'^h follow qualitatively the same path. The main difference is a notable distortion of ρ^h when the field amplitude is near zero.

In figure 5.10, we plot the two marginal distributions of the Wigner functions for ρ'^h_∞ and ρ^h_∞ along the real and complex quadratures. The reservoir steady states ρ'^h_∞ and ρ^h_∞ approximately correspond to the quantum Monte Carlo average of the trajectories depicted in Fig. 5.9. Figure 5.10 features dominant peaks which suggest that the field is mostly close to the target. The distortions with respect to a coherent state visible on the fourth column of Fig. 5.9, lead to a plateau or bump on the marginal distributions of ρ^h_∞. We nevertheless observe that our simplified model [Eq.(5.37)] captures the main features of the influence of decoherence.

5.1.5.2 Experimental uncertainties

We have performed extensive numerical simulations to assess the robustness of the reservoir versus uncertainties in the experimental settings. The evolution operators

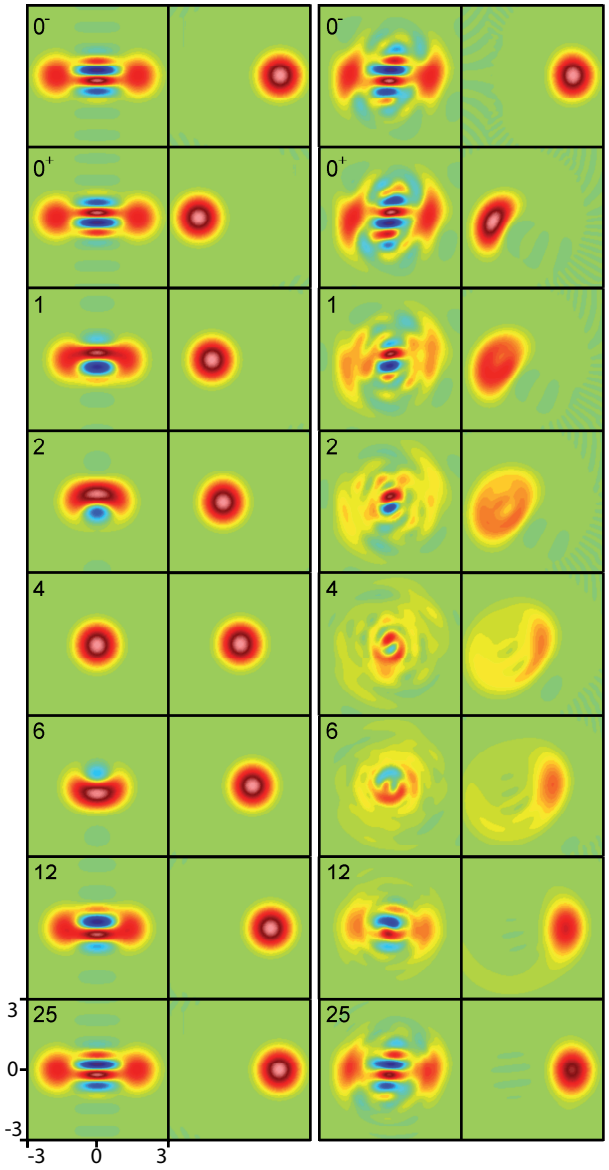

Figure 5.9: Evolution of the cavity field coupled to a reservoir stabilizing a 2-component MFSS, immediately after a relaxation-induced photon loss. Parameter values are those used for Fig. 5.8. The frames are labelled by the number of atomic interactions. A photon loss out of the reservoir pointer state occurs between frames labelled 0^- and 0^+. Left two columns: simplified model, described by Eq. (5.35). We show the Wigner functions of both the cavity state, ρ', on column 1 and of ρ'^h on column 2. Right two columns: same plots for the actual reservoir characterized by $\mathbf{U}_c$ (ρ on column 3 and ρ^h on column 4).

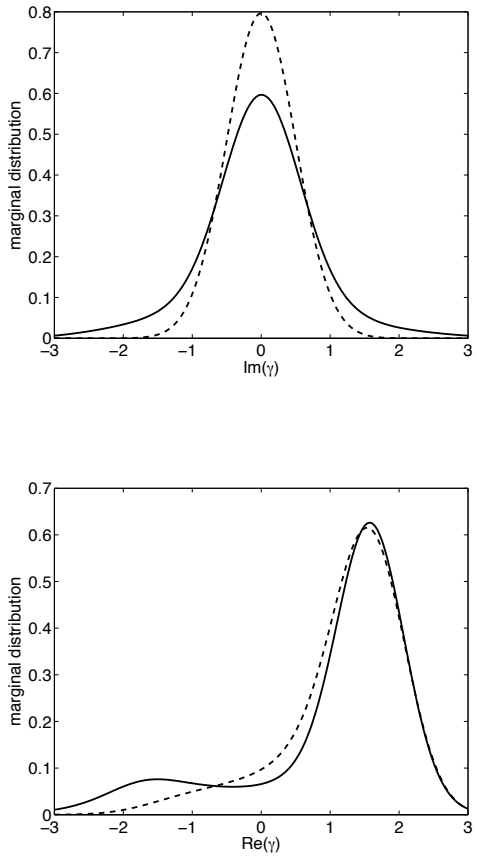

Figure 5.10: Steady state of the cavity field coupled to the atomic reservoir and to a relaxation-inducing environment with T_c =65 ms. Top [resp: bottom]: marginal distribution of the Wigner function along the imaginary [resp: real] quadrature for the simplified model (dashed line) and for our reservoir (solid line). These states correspond to the quantum Monte Carlo average of the sequence presented in Fig. 5.9.

during the interaction are computed exactly from the Hamiltonian $\mathbf{H}_{JC}$ [Eq. (5.3)], using the quantum optics package for MATLAB [Tan 1999]. The Hilbert space is truncated to the 60 first Fock states. We take into account separately the atom-cavity coupling determined by $\mathbf{H}_{JC}$ and the relaxation of the cavity mode (modeled in the standard Lindblad form). This simplifying approach holds since $T \ll T_c$.

We use as a reference the generation of a two-component MFSS containing 2.7 photons on the average (thermal environment with $T_c = 65$ ms and a mean number $n_t = 0.05$ of blackbody photons per mode, $\delta = 2.2\,\Omega_0$, $v = 70$ m/s, $u = 0.45\pi$, $t_r = 5$ μs, see Fig. 5.1(e)). We take into account the randomness of the Rydberg state preparation [Sarlette 2011]. In each atomic sample, we excite a random number of atoms obeying a Poisson law with an average p_{at}. We take a low value $p_{at} = 0.3$ such that, in a first approximation, we only get samples containing zero or one atom (we examine later in this Section the influence of samples containing two atoms). Note that these are the conditions used for figure 5.1(e). In each case, we compute, for a slight change in the experimental settings, the variation of the fidelity of the pointer state w.r.t. an ideal optimized two-component MFSS. For the reference set of parameters, the steady-state fidelity is 70%.

For velocities in the $66 \leq v \leq 74$ m/s interval, the fidelity is only slightly altered, varying from 65% to 70%. It is thus insensitive to a velocity dispersion in the 10% range, well below the values achieved in the experiment.

The fidelity is also quite insensitive to a slight mismatch in the values of the detuning for the two dispersive interactions. Assuming that δ takes the value $a_1 \times 2.2\,\Omega_0$ in the first dispersive period and $-a_2 \times 2.2\,\Omega_0$ in the second, the fidelity drops by at most 10% when a_1 and a_2 vary by up to 10%. The latter cover far more than the actual uncertainty on the atomic frequency.

We have slightly offset the timing of the resonant interaction, shifting it in time by δt and keeping t_r constant. A shift of up to 1 μs (well above the 10 ns timing accuracy) has no effect on the fidelity at the 1% level. The fidelity is also quite insensitive to a finite rise time for the voltage controlling the atomic Stark effect in the cavity, and hence to a finite commutation time for the detuning δ. Using an exponential relaxation model, and setting t_r to maintain a constant θ_r value, we find that the fidelity is unchanged for commutation times up to 200 ns, in the range of accessible values.

We have also studied the sensitivity to the atomic samples containing two atoms at the same time. We decide randomly for each sample the actual number of atoms, N_a, according to a Poisson distribution with the average value p_{at}, truncated above $N_a = 2$. For two-atom samples, we integrate the exact equations of motion, assuming an identical coupling of both atoms to the mode. This condition is realized in the experiment, since the maximum separation between the atoms in a sample is, below 1 mm in C, much smaller than the wavelength – 6 mm – or than the mode waist w.

We observe that the two-atom events do have an impact on the fidelity. For $p_{at} = 0.3$, the energy of the prepared cat decreases down to 2.4 photons on the average and the fidelity is reduced to 66%. For larger p_{at} values, the decrease is

more important and the fidelity reduces to 34% for $p_{at} = 0.5$ (for larger p_{at}, the simulation should also include 3-atom samples).

If we consider an unrealistic reservoir involving samples containing always two atoms, we get as steady-state a large two-component cat, with 4.8 photons on the average and a fidelity of 65%. In the real situation, this two-atom engineered reservoir interferes destructively with the operation of the one-atom samples, leading to reduced average energy and fidelity.

When we reduce p_{at} below 0.3, the fidelity and the energy also decrease, since the reservoir is then less efficient to counteract decoherence. For $p_{at} = 0.2$, we get a 1.9 photons state with a fidelity of only 54%. Optimizing the average number of atoms per sample is thus important to achieve an efficient engineered reservoir.

Note finally that the phase of the MFSS coherent components is determined by the phase of the atomic state superposition when the resonant interaction period begins. Since the atom is detuned from the mode during the dispersive interactions, this phase rotates at frequency $\pm\delta_0$ during the time interval $-T/2 \leq t \leq -t_r/2$. The timing of Stark shifts, that determines the atom-field interactions, should thus define $(T - t_r)/2$ with an uncertainty much smaller than $1/\delta_0$ to avoid spurious rotations of this phase. With detunings in the 100 kHz to few MHz range, this timing accuracy is easily achieved.

5.1.6 A reservoir for two-mode entangled states

Our reservoir engineering strategy can be adapted to protect entangled state superpositions of two cavity modes, which violate a Bell inequality. Preparation of entangled states of two cavity modes, without protection, was considered in [Milman 2005, Rauschenbeutel 2001]. An approximate reservoir for entangling large atomic ensembles is proposed and realized in [Krauter 2011]. In ion traps, reservoir engineering has recently been used to stabilize a Bell state and a GHZ state of four qubits [Barreiro 2011].

We present here a scheme in which the two modes belong to the same cavity (two TEM modes of orthogonal polarization, whose degeneracy is lifted by an appropriate mirror shape). Extension to two separate cavities would require atoms going back and forth between them, a feat not easily achieved in the present context of the ENS experiments.

5.1.6.1 Model and target

We consider two modes a and b of the cavity of respective frequencies $\omega_a < \omega_b$. We denote by $\mathbf{b}$ [resp. $\mathbf{a}$] the photon annihilation operator for mode b [resp. mode a] and $\mathbf{N}_b = \mathbf{b}^\dagger\mathbf{b}$ [resp: $\mathbf{N}_a = \mathbf{a}^\dagger\mathbf{a}$] the associated photon number operators. A separable joint state of the two modes is written $|\psi_a, \psi_b\rangle$. The atomic qubit (transition frequency $\omega_0 \approx \omega_a, \omega_b$) interacts with the modes according to the Jaynes-Cummings

Hamiltonian, which is written, in a frame rotating at the frequency $\omega_m = (\omega_a+\omega_b)/2$:

$$\begin{aligned}\overline{\mathbf{H}}_{JC} &= \Delta\,(\mathbf{N}_b - \mathbf{N}_a) + \frac{\delta(t)}{2}(|e\rangle\langle e| - |g\rangle\langle g|) \\ &\quad + i\frac{\Omega(s)}{2}(|g\rangle\langle e|(\mathbf{a}^\dagger + \mathbf{b}^\dagger) - |e\rangle\langle g|(\mathbf{a}+\mathbf{b}))\ ,\end{aligned} \tag{5.41}$$

where $\Delta = (\omega_b - \omega_a)/2 > 0$ and $\delta(t) = \omega_0(t) - \omega_m$. Here again, $\delta(t)$ can be adjusted by controlling ω_0 through the Stark effect. We assume that the couping $\Omega(s)$ is the same with both modes, a restriction that could be easily relaxed.

We denote by $\overline{\mathbf{U}}$ the unitary evolution operator associated to $\overline{\mathbf{H}}_{JC}$ (the overline here denotes two-mode operators), which is the solution of the Schrödinger equation:

$$\frac{d}{dt}\overline{\mathbf{U}}(t) = -i\overline{\mathbf{H}}_{JC}(t)\,\overline{\mathbf{U}}(t) \quad \text{with} \quad \overline{\mathbf{U}}(t_0) = \mathbf{I}\ . \tag{5.42}$$

We denote by $\overline{\mathbf{U}}_q$ the two-mode evolution operator corresponding to the parameter set q, and $(\mathbf{M}_g^{\overline{\mathbf{U}}_q}, \mathbf{M}_e^{\overline{\mathbf{U}}_q})$ the associated Kraus operators. Approximate analytical expressions of $\overline{\mathbf{U}}_q$ for the relevant parameter sets are given in Section 5.1.8.1. Operators $\overline{\mathbf{Z}}$ and $\overline{\mathbf{Y}}$ generalizing for each mode the ones introduced in the previous Sections are also defined in Section 5.1.8.1.

Let us consider first the successive resonant interaction of the atoms, initially prepared in $|u_{at}\rangle = \cos(u/2)|g\rangle + \sin(u/2)|e\rangle$, with the modes b and a. The corresponding propagator is $\overline{\mathbf{U}}_r = \overline{\mathbf{Y}}(\theta^r_{\mathbf{N}_a})\overline{\mathbf{Y}}(\theta^r_{\mathbf{N}_b})$. The associated Kraus map $\left(\mathbf{M}_g^{\overline{\mathbf{U}}_r}, \mathbf{M}_e^{\overline{\mathbf{U}}_r}\right)$ stabilizes a tensor product of two coherent states $|\text{-}\alpha, \alpha\rangle$, where $\alpha = 2u/\theta_r$ for small enough u and θ_r.

An initial coherent state product $|\alpha, \beta\rangle$ propagated under the Hamiltonian

$$\overline{\mathbf{H}}'_K = \overline{\gamma}_K(\mathbf{N}_a + \mathbf{N}_b)^2 + \zeta_a\mathbf{N}_a + \zeta_b\mathbf{N}_b \tag{5.43}$$

for a time $t_K = \frac{\pi}{k\overline{\gamma}_K}$, k small integer, gets transformed into

$$e^{-it_K\overline{\mathbf{H}}'_K}|\alpha, \beta\rangle = \frac{1}{\sqrt{k}}\sum_{m=1}^{k} r_m\ |e^{-i2m\pi/k}\tilde{\alpha},\ e^{-i2m\pi/k}\tilde{\beta}\rangle \tag{5.44}$$

with $r_m = \frac{1}{\sqrt{k}}\ \sum_{n=1}^{k}\ e^{2imn\pi/k}\, e^{-i(n^2+kn)\pi/k}$, $\tilde{\alpha} = -e^{-i\zeta_a t_K}\alpha$ and $\tilde{\beta} = -e^{-i\zeta_b t_K}\beta$. In particular, for $t_K\gamma_K = \pi/2$, the state

$$|\overline{c}_{\tilde{\alpha},\tilde{\beta}}\rangle = (|\tilde{\alpha}, \tilde{\beta}\rangle - i|-\tilde{\alpha}, -\tilde{\beta}\rangle)/\sqrt{2}$$

is entangled for any $\alpha, \beta > 0$, see e.g. [Banaszek 1999]. Remarkably, a state $|\overline{c}_{\alpha,\beta}\rangle$ is also obtained when propagating an initial coherent state product for a time $t_K = \frac{\pi}{2\overline{\gamma}_K}$ under Hamiltonian

$$\overline{\mathbf{H}}_K = \overline{\gamma}_K(\mathbf{N}_a - \mathbf{N}_b)^2 + \zeta_a\mathbf{N}_a + \zeta_b\mathbf{N}_b \tag{5.45}$$

since $\frac{\pi}{2}(\mathbf{N}_a+\mathbf{N}_b)^2-\frac{\pi}{2}(\mathbf{N}_a-\mathbf{N}_b)^2 = 2\pi\mathbf{N}_a\mathbf{N}_b$. In particular, for $\zeta_a = 0$ and $\zeta_b = 2\gamma_K$ an initial state $|\text{-}\alpha,\alpha\rangle$ would get transformed into:

$$|\overline{c}_\alpha\rangle = (|\alpha,\alpha\rangle - i|\text{-}\alpha,\text{-}\alpha\rangle)/\sqrt{2}\,. \tag{5.46}$$

In the following we show how to stabilize an ESMS of two field modes with the two-level atom reservoir setup used for the single-mode case. A first method, which is the strict analog of the single-mode case, could mimic the action of $\overline{\mathbf{H}}'_K$ on a coherent state product. In the large Δ limit, it allows one to stabilize any k-component ESMS, but requires 4 dispersive interactions which can yield prohibitively large interaction times for low k. The atom's frequency would be successively set to $\omega_b+\delta_0, \omega_a+\delta_0, \omega_b, \omega_a, \omega_b-\delta_0, \omega_a-\delta_0$. We would need to be in a regime where $\Delta \gg \delta_0 \gg \Omega_0$. A second method mimics the action of $\overline{\mathbf{H}}_K$ in special conditions with 2 dispersive interactions only, allowing to stabilize $|\overline{c}_\alpha\rangle$ more efficiently. We have chosen to detail the second method since although it only stabilizes a 2 component ESMS, it allows violation of Bell's inequality for a cavity lifetime only a few times larger than the best reported so far [Kuhr 2007].

In the next Section, we show that the action of $\overline{\mathbf{H}}_K$ can be simulated by sandwiching the resonant interaction $\overline{\mathbf{U}}_r$ between two dispersive interactions. The corresponding reservoir thus stabilizes $|\overline{c}_\alpha\rangle$.

5.1.6.2 Composite interaction

The detuning profile $\delta(t)$ used to stabilize $|\overline{c}_\alpha\rangle$ is represented in Fig. 5.11 (bottom part). The atomic frequency is first set at ω_m ($\delta = 0$), between $t = -T/2$ and $t = -t_r$. The atom interacts non-resonantly with both modes, with opposite detunings. We restrict in this Section to the dispersive regime. The corresponding evolution operator is $\overline{\mathbf{Z}}(\overline{\phi}(\mathbf{N}_b - \mathbf{N}_a))$ (see Section 5.1.8.1), describing opposite phase shifts of the two modes driven by the atom, with a phase shift per photon $\overline{\phi}$.

The atom is then successively set at resonance with b and a for a time t_r. During these short time intervals, we neglect the residual dispersive interaction with the other mode. The second dispersive interaction with the two modes is performed by setting again $\delta = 0$ from t_r to $T/2$. With this sequence, the phase shifts produced in the dispersive interactions would add up for the terms where the atom undergoes $|e\rangle\langle e|$ and $|g\rangle\langle g|$ during the resonant parts. Instead, as in the single mode case, these phase shifts must cancel out. We thus apply on the atom at t_r a π pulse on the $|e\rangle \rightarrow |g\rangle$ transition. This almost-instantaneous pulse on the atom while it is in the cavity can be achieved by injecting a field through the space between the cavity mirrors. The field frequency ω_e, very different from ω_c, does not affect the cavity field. On the other hand, the atomic transition frequency ω_0 is Stark-shifted close to ω_e for the (very short) duration of this pulse.

The phases of modes a and b evolve at the frequencies $\pm\Delta$. In order to cancel the build-up of these phases during reservoir operation, we constrain the total time T between successive resonant interactions to $T\Delta = 0$ modulo 2π. This condition is easily achieved with the Stark atomic tuning.

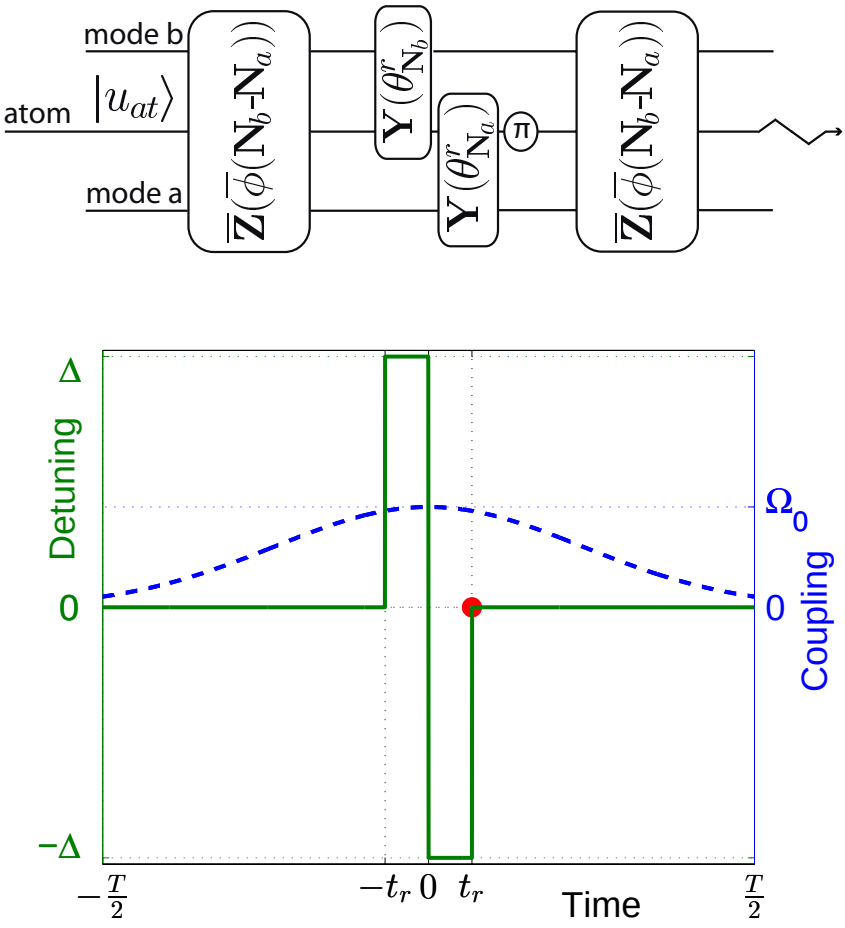

Figure 5.11: Timing of the composite interaction of the atom with the two cavity modes a and b at frequencies $\omega_b > \omega_a$. Bottom frame, solid line: time profile of δ (difference between the atomic frequency ω_0 and the mean frequency ω_m of the two cavity modes) during cavity crossing by one atomic sample. For $\delta = 0, +\Delta, -\Delta$ respectively, ω_0 coincides with $\omega_m = \frac{\omega_b+\omega_a}{2}$, ω_b, ω_a. The π pulse on the atomic state is represented here as a red dot. Bottom frame, dashed line: coupling strength $\Omega(vt)$ with $t = 0$ when the atom is at cavity center. Top frame: scheme of the propagators corresponding to the successive steps in the composite interaction.

This leads, up to irrelevant rotations, to the propagator (see Section 5.1.8.1 for a detailed calculation):

$$\begin{aligned}\overline{\mathbf{U}}_T \approx \overline{\mathbf{U}}_{\bar{c}}^{\text{eff}} &= \overline{\mathbf{Z}}(\overline{\phi}(\mathbf{N}_b - \mathbf{N}_a))\overline{\mathbf{Y}}(\theta^r_{\mathbf{N}_a}) \\ &\quad \overline{\mathbf{Y}}(\theta^r_{\mathbf{N}_b})\overline{\mathbf{Z}}(\overline{\phi}(\mathbf{N}_a - \mathbf{N}_b)) \ . \end{aligned} \tag{5.47}$$

Setting the dispersive interactions to produce a $\overline{\phi} = \pi$ phase shift per photon, we get

$$\overline{\mathbf{U}}_{\bar{c}}^{\text{eff}} = e^{-it_K\overline{\mathbf{H}}_K}\overline{\mathbf{Y}}(\theta^r_{\mathbf{N}_a})\overline{\mathbf{Y}}(\theta^r_{\mathbf{N}_b})e^{it_K\overline{\mathbf{H}}_K} \ ,$$

with $t_K\overline{\gamma}_K = \pi/2$. The resulting atomic reservoir thus stabilizes the entangled pointer state $|\bar{c}_\alpha\rangle$. Adapted detuning profiles $\delta(t)$ yield the same propagators when the interaction strength is not the same on both modes[4]. Generalization to entangled states with more than two coherent components in each mode is straightforward, using slightly more complex detuning sequences. Indeed the latter must then be chosen to have additive instead of opposite dispersive effects on the two modes.

5.1.6.3 Entanglement and the Bell inequality

The entanglement of the photon state produced by the reservoir can be proved by a violation of a Bell inequality adapted to this two-mode case [Banaszek 1999, Milman 2005]. The Bell signal is:

$$\mathcal{B}(\gamma_a, \gamma_b, \gamma'_a, \gamma'_b) = \tfrac{\pi^2}{4}|\overline{W}(\gamma'_a, \gamma'_b) + \overline{W}(\gamma_a, \gamma'_b) + \overline{W}(\gamma'_a, \gamma_b) - \overline{W}(\gamma_a, \gamma_b)| \ , \tag{5.48}$$

where $\overline{W}(\gamma_a, \gamma_b)$ is the two-mode Wigner function. It is defined as:

$$\overline{W}(\gamma_a, \gamma_b) = \tfrac{4}{\pi^2}\text{Tr}\left(\mathbf{D}^a_{-\gamma_a}\mathbf{D}^b_{-\gamma_b}\,\rho\,\mathbf{D}^a_{\gamma_a}\mathbf{D}^b_{\gamma_b}\overline{\mathbf{P}}\right) \ ,$$

where $\overline{\mathbf{P}} = e^{i\pi(\mathbf{N}_a+\mathbf{N}_b)}$ is a joint parity operator and $\mathbf{D}^a_{\gamma_a}$ and $\mathbf{D}^b_{\gamma_b}$ are the displacement operators for modes a and b respectively. In a local realistic model, $\mathcal{B}$ is always smaller than 2. A value larger than 2 for some $(\gamma_a, \gamma_b, \gamma'_a, \gamma'_b)$ amplitudes is a proof that ρ is not separable. Let us give a brief explanation for this. The Bell signal in (5.48) may be written as

$$\mathcal{B} = |\langle\mathbf{O}_1\mathbf{O}_2\rangle + \langle\mathbf{O}_2\mathbf{O}_3\rangle + \langle\mathbf{O}_1\mathbf{O}_4\rangle - \langle\mathbf{O}_4\mathbf{O}_3\rangle|$$

where $\langle\mathbf{O}_k\mathbf{O}_j\rangle = \text{Tr}\,(\rho\mathbf{O}_k\mathbf{O}_j)$ is the expectation value of the observable $\mathbf{O}_k \otimes \mathbf{O}_j$ when the system is in state ρ, and

$$\mathbf{O}_1 = \mathbf{D}^a_{\gamma'_a}\mathbf{P_a}\mathbf{D}^a_{-\gamma'_a} \qquad \mathbf{O}_2 = \mathbf{D}^b_{\gamma'_b}\mathbf{P_b}\mathbf{D}^b_{-\gamma'_b}$$

[4] Consider interaction strength $\Omega_a(s) = \Omega(s)$ with mode a and $\Omega_b(s) = \lambda\Omega(s)$ with mode b, where $\lambda \neq 1$. Adjusting the resonant interaction times to get the same coherent state amplitude in both modes is straightforward. Equal dispersive phases are obtained by setting $\delta(t) \approx \bar{\delta}_0 = \Delta\frac{1-\lambda^2}{1+\lambda^2} \neq 0$ for $t \in (-T/2, -t_r/2) \cup (t_r/2, T/2)$. Indeed, to first order approximation in Ω_0/Δ, this choice shifts the eigenvalues of the Hamiltonian by equal amounts $\Omega_a(s)/\sqrt{1+\frac{\bar{\delta}_0}{\Delta}} = \Omega_b(s)/\sqrt{1-\frac{\bar{\delta}_0}{\Delta}}$ for the two modes.

$$\mathbf{O}_3 = \mathbf{D}^a_{\gamma_a}\mathbf{P_a}\mathbf{D}^a_{-\gamma_a} \qquad \mathbf{O}_4 = \mathbf{D}^b_{\gamma_b}\mathbf{P_b}\mathbf{D}^b_{-\gamma_b} \ .$$

We have defined the parity operators for each mode $\mathbf{P}_a = e^{i\pi\mathbf{N}_a}$ and $\mathbf{P}_b = e^{i\pi\mathbf{N}_b}$. A computation like that of the CHSH inequality follows [Nielsen 2000, page 115]. The result o_k of a measurement of the observable $\mathbf{O}_k$ yields one of its eigenvalues. Since $\mathbf{O}_k^2 = \mathbf{I}$, these eigenvalues are 1 and -1. Assume that before each measurement, the four observables $(\mathbf{O}_1, \mathbf{O}_2, \mathbf{O}_3, \mathbf{O}_4)$ (even the ones which are not measured) have a definite value (o_1, o_2, o_3, o_4) with probability $p(o_1, o_2, o_3, o_4)$. Then we have

$$\begin{aligned}
\mathcal{B} &= |\langle \mathbf{O}_1\mathbf{O}_2\rangle + \langle \mathbf{O}_2\mathbf{O}_3\rangle + \langle \mathbf{O}_1\mathbf{O}_4\rangle - \langle \mathbf{O}_4\mathbf{O}_3\rangle| \\
&= |\sum_{o_1,o_2,o_3,o_4} p(o_1,o_2,o_3,o_4)o_1o_2 + \sum_{o_1,o_2,o_3,o_4} p(o_1,o_2,o_3,o_4)o_2o_3 \\
&+ \sum_{o_1,o_2,o_3,o_4} p(o_1,o_2,o_3,o_4)o_1o_4 + \sum_{o_1,o_2,o_3,o_4} p(o_1,o_2,o_3,o_4)o_3o_4| \\
&= |\sum_{o_1,o_2,o_3,o_4} p(o_1,o_2,o_3,o_4)(o_1o_2 + o_2o_3 + o_1o_4 - o_3o_4)| \ .
\end{aligned}$$

Notice that $b = o_1o_2+o_2o_3+o_1o_4-o_4o_3 = (o_1+o_3)o_2+(o_1-o_3)o_4$. Since $o_1, o_3 = \pm 1$, we either have $o_1 + o_3 = 0$ or $o_1 - o_3 = 0$. Hence $b = \pm 2$. And hence, the absolute value of the average will necessarily satisfy

$$\mathcal{B} \leq 2 \ .$$

Now let us show that for an entangled state of the form $|\overline{c}_\alpha\rangle = (|\alpha,\alpha\rangle - i|\text{-}\alpha,\text{-}\alpha\rangle)/\sqrt{2}$, we can find $\gamma_a, \gamma_b, \gamma'_a$ and γ'_b such that the bell signal violates the latter inequality: $\mathcal{B} > 2$. We take $\rho = |\overline{c}_\alpha\rangle\langle\overline{c}_\alpha|$, and hence we have

$$\begin{aligned}
\tfrac{\pi^2}{4}\overline{W}(\gamma_a,\gamma_b) &= \tfrac{1}{2}\langle\alpha|\mathbf{D}^a_{\gamma_a}e^{i\pi\mathbf{N}_a}\mathbf{D}^a_{-\gamma_a}|\alpha\rangle\langle\alpha|\mathbf{D}^b_{\gamma_b}e^{i\pi\mathbf{N}_b}\mathbf{D}^b_{-\gamma_b}|\alpha\rangle \\
&+ \tfrac{1}{2}\langle-\alpha|\mathbf{D}^a_{\gamma_a}e^{i\pi\mathbf{N}_a}\mathbf{D}^a_{-\gamma_a}|-\alpha\rangle\langle-\alpha|\mathbf{D}^b_{\gamma_b}e^{i\pi\mathbf{N}_b}\mathbf{D}^b_{-\gamma_b}|-\alpha\rangle \\
&+ \Re(i\langle-\alpha|\mathbf{D}^a_{\gamma_a}e^{i\pi\mathbf{N}_a}\mathbf{D}^a_{-\gamma_a}|\alpha\rangle\langle-\alpha|\mathbf{D}^b_{\gamma_b}e^{i\pi\mathbf{N}_b}\mathbf{D}^b_{-\gamma_b}|\alpha\rangle)
\end{aligned}$$

The first two lines in this equation correspond to the Wigner function of a coherent state in each mode. A statistical mixture of $|\alpha,\alpha\rangle$ and $|-\alpha,-\alpha\rangle$ would lead to the same terms. The last line however, is a signature of coherence between the two components. We thus expect that this is the term which will enable the violation of the Bell inequality. To compute these terms, we will need the following relations [Haroche 2006, Section 3.1.3]

$$\begin{aligned}
\mathbf{D}_\gamma|\alpha\rangle &= e^{(\gamma\alpha^\dagger - \gamma^\dagger\alpha)/2}|\alpha+\gamma\rangle \\
\langle\alpha|\beta\rangle &= e^{-\frac{1}{2}(|\alpha|^2+|\beta|^2)}e^{\alpha^\dagger\beta} \ .
\end{aligned}$$

Simulations show that for real α, the Bell inequality is violated for pure imaginary $\gamma_a, \gamma'_a, \gamma_b, \gamma'_b$. Hence, we take a real α and constrain our search to pure imaginary amplitudes, which we denote $\gamma_a = i\xi_a$ where ξ_a is now real. The same holds for the three other amplitudes. We have

$$\langle\alpha|\mathbf{D}^a_{\xi_a}e^{i\pi\mathbf{N}_a}\mathbf{D}^a_{-\xi_a}|\alpha\rangle = e^{-2(\alpha^2+\xi_a^2)} \ ,$$

and

$$\Re(i\langle-\alpha|\mathbf{D}^a_{\xi_a}e^{i\pi\mathbf{N}_a}\mathbf{D}^a_{-\xi_a}|\alpha\rangle\langle-\alpha|\mathbf{D}^b_{\xi_b}e^{i\pi\mathbf{N}_b}\mathbf{D}^b_{-\xi_b}|\alpha\rangle) = e^{-2(\xi_a^2+\xi_b^2)}\sin(4(\xi_a+\xi_b)\alpha)\ .$$

This yields

$$\tfrac{\pi^2}{4}\overline{W}(\gamma_a,\gamma_b) = e^{-(4\alpha^2+2\xi_a^2+2\xi_b^2)} + e^{-2(\xi_a^2+\xi_b^2)}\sin(4(\xi_a+\xi_b)\alpha)\ .$$

As expected, the first term in this equation can be neglected for large enough α. A re-scaling $\xi_a, \xi_b \to 4\alpha\xi_a, 4\alpha\xi_b$ yields

$$\tfrac{\pi^2}{4}\overline{W}(\gamma_a,\gamma_b) = e^{-\frac{1}{8\alpha^2}(\xi_a^2+\xi_b^2)}\sin(\xi_a+\xi_b) \approx \sin(\xi_a+\xi_b)\ ,$$

for large enough α. The Bell signal may now simply be written as

$$\mathcal{B} = |\sin(\xi'_a+\xi'_b) + \sin(\xi'_a+\xi_b) + \sin(\xi_a+\xi'_b) - \sin(\xi_a+\xi_b)|\ .$$

For $\xi_a = \xi_b = 0$ and $\xi'_a = \xi'_b = \pi/3$, we find $\mathcal{B} = 3\sqrt{3}/2 \approx 2.6 > 2$. This corresponds to $\gamma_a = \gamma_b = 0$, and $\gamma'_a = \gamma'_b = i(\pi/3)/(4\alpha) \approx 1/4$, for $\alpha = 1$. This is consistent with the simulation of Fig. 5.13 which we explain in the next section. The white dots on this figure show the amplitudes $\gamma_a, \gamma_b, \gamma'_a$ and γ'_b which are found to maximize the Bell signal.

5.1.6.4 Numerical simulations

We numerically solve Eq. (5.42) and iterate the corresponding Kraus maps starting from the vacuum state with $u = \pi/4$ and $\theta_r = \pi/2$, such that the entangled field modes amplitude α is of the order of 1. Decoherence is modeled as the separate coupling of each field mode with a thermal environment, with the same damping time T_c and the same temperature ($n_t = 0.05$). The interaction strength $\Omega(s)$ of the atom with each mode has the same Gaussian profile as in the single-mode case, with $\Omega_0/2\pi = 50$ kHz. In the computations, the field Hilbert space is truncated to the 10 first Fock states for each mode.

Figure 5.12 shows (solid line) the evolution of the fidelity $\langle\overline{c}_\alpha|\rho|\overline{c}_\alpha\rangle$ of the two-mode cavity state ρ w.r.t. an entangled two-component MFSS $|\overline{c}_\alpha\rangle$ with $|\alpha|^2 = 0.67$ photons on average, starting from the vacuum. The reference state is numerically optimized to maximize its fidelity w.r.t. the reservoir stationary state ($\approx \rho_{200}$). We find $0.67 < 2u/\theta_r = 1$ because of finite cavity lifetime. We have chosen $\Delta = 8\,\Omega_0$, $T_c = 650$ ms. The atomic velocity is $v = 22$ m/s and each atomic sample has a probability $p_{at} = 0.3$ to contain one atom (we neglect here two-atom samples). The engineered reservoir is efficient, since the optimal fidelity is $\approx 89\%$. This value is reached after ≈ 30 samples, corresponding to only 10 atoms on average. To illustrate the protection of the state, we interrupt the reservoir after 200 atomic samples. As shown in Figure 5.12, the fidelity w.r.t. the target state rapidly decreases.

Figure 5.13 shows a cut of the two-mode Wigner function of ρ_{200} in the plane $\Re(\gamma_a) = \Re(\gamma_b) = 0$ in which maximum violation of the inequality is expected

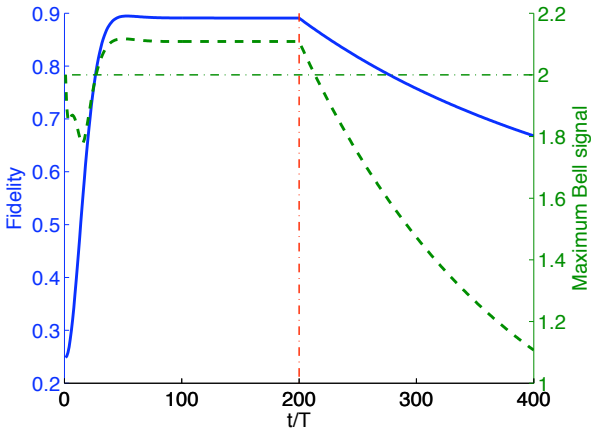

Figure 5.12: Simulation of the reservoir stabilizing a two-mode entangled state. Solid line: fidelity of ρ, the cavity state starting at vacuum, w.r.t. an ideal optimized entangled state of the two modes $|\overline{c}_\alpha\rangle$, as a function of time in units of the sample interaction time T. The reservoir operates up to $t/T = 200$ and is then switched off. Dashed line: maximum Bell signal $\mathcal{B}^{\max}$ as a function of time. A $\mathcal{B}^{\max}$ value above the thin dash-dotted line ($\mathcal{B}^{\max} = 2$) proves entanglement of ρ.

[Banaszek 1999]. A numerical optimization of the Bell signal in this plane provides the four amplitudes shown as white dots. We have performed similar optimizations of $\mathcal{B}$ after each atomic sample interaction and plotted the maximum Bell signal $\mathcal{B}^{\max}$ as a dashed line in figure 5.12. It reaches $\approx 2.1 > 2$ which implies that the reservoir stabilizes a provably entangled state of the modes. When the reservoir is switched off after 200 interactions, decoherence causes a rapid decrease of $\mathcal{B}^{\max}$.

Figure 5.14 shows the maximum Bell signal $\mathcal{B}^{\max}$ of the steady state as a function of T_c, for three detuning and atomic velocity values. The Bell inequality is violated for all these settings when $T_c > 450$ ms. The crossing of the different curves illustrates the competition between two effects. For small T_c, the Bell signal is larger when Δ is smaller, since a small Δ corresponds to a relatively large velocity and thus to a smaller total interaction duration T. Thus the reservoir is a more efficient protection against decoherence when Δ is small. For very large T_c, cavity damping becomes negligible w.r.t. the dispersive approximation error introduced in the reservoir action, for which large Δ values are preferred.

The T_c values required for a violation are certainly difficult to reach, but they are only ≈ 3 times larger than the best damping time reported so far [Kuhr 2007]. Stabilizing field states violating a Bell inequality may thus be within reach of the next generation of experiments.

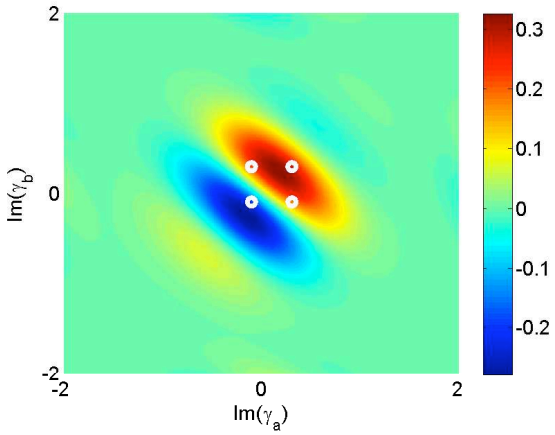

Figure 5.13: Cut in the plane ($\Re(\gamma_a) = \Re(\gamma_b) = 0$) of the two-mode Wigner function $\overline{W}(\gamma_a, \gamma_b)$ of ρ_{200}. The fringes and negative values for $\overline{W}$ are a signature of the "quantumness" of the stabilized state. The white dots show the points used to maximize the violation of Bell's inequality.

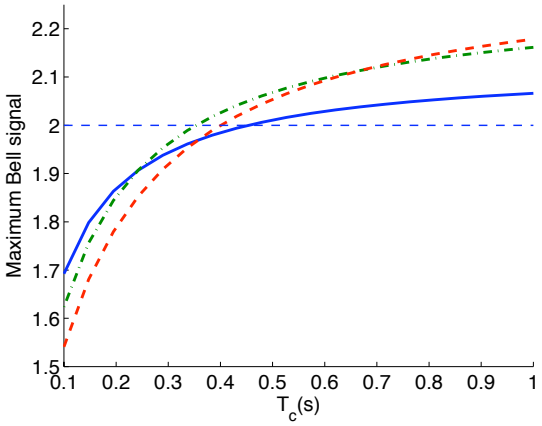

Figure 5.14: Maximum Bell signal $\mathcal{B}^{\max}$ of ρ_{200} as a function of the cavity lifetime T_c for $\Delta/2\pi = 300$ kHz, $v = 30$ m/s (solid blue line); $\Delta/2\pi = 400$ kHz, $v = 22$ m/s (dashed-dotted green line); $\Delta/2\pi = 500$ kHz, $v = 18$ m/s (dashed red line).

5.1.7 Summary and discussion

We have proposed simple engineered reservoirs stabilizing a wide variety of non-classical field states in one and two quantum cavity modes. These reservoirs efficiently counteract the standard relaxation of the cavities and offer promising perspectives for studies and applications of mesoscopic field state superpositions.

We have gained a detailed insight into the reservoir mechanisms, and particu-

larly into the way it corrects for decoherence-induced quantum jumps of the field. We have performed extensive numerical simulations justifying the approximations used in [Sarlette 2011] and assessing the robustness of the method to experimental imperfections.

We have discussed here, for the sake of definiteness, the reservoir operation in the context of the microwave-CQED experiments performed with circular Rydberg atoms and superconducting cavities at ENS. We have shown that many quantum states protected by our reservoir could realistically be observed in this context. Clearly, the method could be straightforwardly extended to other spin/spring systems, in cavity QED and trapped ions contexts. It is particularly appealing for the thriving field of circuit-QED [Devoret 2004]. Resettable superconducting qubits [Reed 2010b] interacting with one or two cavity modes could be used to implement our proposal. With two separate cavities interacting with one qubit, it would become possible to stabilize a non-local entangled mesoscopic superposition and to study the fascinating interplay between decoherence and non-locality.

5.1.8 Detailed computations

5.1.8.1 Propagators

This section details the computation of the propagators associated to the atom-cavity interaction in the various settings used in the main text. These propagators are computed using an adiabatic approximation. We start this section by clarifying this approximation. Consider the general problem of solving [Teufel 2003]:

$$i\varepsilon\frac{d}{dt}\mathbf{U}^{\varepsilon}(t)=\mathbf{H}(t)\mathbf{U}^{\varepsilon}(t)\;, \tag{5.49}$$

where ε is a small parameter, $\mathbf{U}^{\varepsilon}$ is a unitary operator initialized at $\mathbf{U}^{\varepsilon}(0)=\mathbf{I}$, and $\mathbf{H}(t)$ is a time-dependent hermitian operator. In general, $\mathbf{H}(t_1)$ and $\mathbf{H}(t_2)$ do not commute for different times t_1 and t_2, which makes the above differential equation non-trivial. For a given projector $\mathbf{P}(t)$ on an eigenspace of $\mathbf{H}(t)$, we start by defining $\mathbf{H}_a(t)$ and $\mathbf{U}_a^{\varepsilon}(t)$:

$$\begin{aligned} i\varepsilon\frac{d}{dt}\mathbf{U}_a^{\varepsilon} &= \mathbf{H}_a\mathbf{U}_a^{\varepsilon}\;,\\ \mathbf{H}_a &= \mathbf{H}-i\varepsilon\mathbf{P}\frac{d}{dt}\mathbf{P}-i\varepsilon\mathbf{P}^{\perp}\frac{d}{dt}\mathbf{P}\;. \end{aligned}$$

The adiabatic theorem states that if $t\rightarrow\mathbf{H}(t)$ is $\mathcal{C}^2$ (twice continuously differentiable) and the eigenvalue $\lambda(t)$ corresponding to the projector $\mathbf{P}(t)$ satisfies the gap condition [Teufel 2003, equation (1.5)], then $t\rightarrow\mathbf{P}(t)$ is $\mathcal{C}^2$ and there exists a constant C, such that for all t

$$||\mathbf{U}^{\varepsilon}(t)-\mathbf{U}_a^{\varepsilon}(t)||\leq C\varepsilon t\;.$$

In practice, we would like to have a simple expression for $\mathbf{U}_a^{\varepsilon}$. The latter has the interesting property of transforming, exactly, a projector at time 0 into a projector

at time t:

$$\mathbf{U}_a^\varepsilon(t)\mathbf{P}(0)\mathbf{U}_a^\varepsilon(t)^\dagger = \mathbf{P}(t) \ .$$

As pointed out in [Teufel 2003, Remark 1.3], the generalization where many parts of the spectrum are mutually separated by a gap is straightforward. In particular, we consider the simple case where $\mathbf{H}$ has N separated eigenvalues (N is the dimension of the Hilbert space), and hence, each projector $\mathbf{P}_1, \cdots, \mathbf{P}_N$ is of rank one. We therefore search for a solution of the form:

$$\mathbf{U}_a^\varepsilon(t) = \sum_{n=1}^{N} e^{i\phi_n(t)} |V_n(t)\rangle\langle V_n(0)| \ ,$$

where $\mathbf{P}_n(t) = |V_n(t)\rangle\langle V_n(t)|$, and $\mathbf{P}_n(0) = |V_n(0)\rangle\langle V_n(0)|$. Recall that $\mathbf{H}(t)|V_n(t)\rangle = \lambda_n(t)|V_n(t)\rangle$. To fully determine $\mathbf{U}_a^\varepsilon$, we need to find ϕ_n. To this end, we insert this expression in the Schrödinger equation with

$$\mathbf{H}_a = \mathbf{H} - i\varepsilon \sum_{n=1}^{N} \mathbf{P}_n \frac{d}{dt}\mathbf{P}_n \ .$$

Multiplying by $\langle V_n(t)|$ on the left and $|V_n(0)\rangle$ on the right, we find

$$\frac{d}{dt}\phi_n(t) = -\lambda_n(t)/\varepsilon + i\left\langle V_n(t)|\frac{d}{dt}V_n(t)\right\rangle \ .$$

We have

$$\mathbf{U}_a^\varepsilon(t) = \sum_{n=1}^{N} e^{-i\frac{1}{\varepsilon}\int_0^t \lambda_n(s)ds} e^{-\int_0^t \left\langle V_n(s)|\frac{dV_n(s)}{ds}\right\rangle} |V_n(t)\rangle\langle V_n(0)| \ .$$

Notice that this expression of $\mathbf{U}_a^\varepsilon(t)$ is invariant under the transformation $|V_n(t)\rangle \to e^{i\theta_n(t)}|V_n(t)\rangle$, where $\theta_n(.)$ is a smooth function. This "Gauge choice freedom" is expected since each eigenvector $|V_n(t)\rangle$ is only defined up to a global phase. The term $\frac{1}{\varepsilon}\int_0^t \lambda_n(s)ds$ is commonly called the dynamical phase, while the term $\int_0^t \left\langle V_n(s)|\frac{dV_n(s)}{ds}\right\rangle$ is related to the Berry phase [Shapere 1989]. In the case where for all time we have $\left\langle V_n(s)|\frac{dV_n(s)}{ds}\right\rangle = 0$, the expression of $\mathbf{U}_a^\varepsilon$ simplifies to the one we commonly use:

$$\mathbf{U}_a^\varepsilon(t) = \sum_{n=1}^{N} e^{-i\frac{1}{\varepsilon}\int_0^t \lambda_n(s)ds} |V_n(t)\rangle\langle V_n(0)| \ .$$

When does this condition hold? Take a basis of the Hilbert space $|0\rangle, .., |N\rangle$. For all time an eigenvector $|V(t)\rangle$ can be written: $|V(t)\rangle = \sum_k r_k(t)e^{i\theta_k(t)}|k\rangle$ (r_k and θ_k are real smooth functions). Besides we have $\sum_k r_k^2 = 1$, hence $\sum_k r_k(t)\frac{d}{dt}r_k(t) = 0$. Hence $\left\langle V(t)|\frac{d}{dt}V(t)\right\rangle = i\sum_k r_k^2(t)\frac{d}{dt}\theta_k(t)$. Whenever the phases θ_k are time independent, $\left\langle V(t)|\frac{d}{dt}V(t)\right\rangle = 0$. This is the case for the eigenvectors $(|-,n\rangle_t, |+,n\rangle_t)$ that diagonalize $\mathbf{H}_{JC}(t)$ in the present work (see below (5.51)), which shows that we don't acquire a Berry phase [Shapere 1989].

Single-mode case: For a resonant interaction [$\delta(t) = 0$], Eq. (5.4) is written:

$$\frac{d}{dt}\mathbf{U}(t) = \frac{\Omega(s)}{2}\left(|g\rangle\langle e|\,\mathbf{a}^\dagger - |e\rangle\langle g|\,\mathbf{a}\right)\mathbf{U}(t)\ ,$$

with $s = vt$ if we set the time origin such that the atom crosses the cavity axis at $t = 0$. For each Bloch sphere B_n associated with the invariant space spanned by $(|g, n+1\rangle, |e, n\rangle)$, this interaction induces a Rabi rotation at an angular rate $\sqrt{n}\Omega(s)$ around the Y axis. We therefore define the unitary operator $\mathbf{Y}(f_\mathbf{N})$ [Eq. (5.9)] performing a rotation around Y by an angle $f(n)$, where $f(n)$ is an arbitrary function of n. The resonant interaction propagator is thus given by Eq. (5.12).

For the interaction between t_1 and t_2 with a constant nonzero detuning $\delta(t) = \overline{\delta} \neq 0$[5], the Gaussian variation of $\Omega(vt)$ precludes an exact integration of Eq. (5.4). However, assuming that $\Omega(vt)$ varies slowly enough, the coupled atom-field system evolves adiabatically. An initial eigenstate of $\mathbf{H}_{JC}(t_1)$ (a "dressed state") then remains, for any time t, close to an eigenstate of $\mathbf{H}_{JC}(t)$ [Haroche 2006]. This adiabatic approximation is valid provided:

$$\left|\frac{2v}{w\Omega_0\sqrt{n+1}}se^{-s^2}\right| \ll \left(\frac{\overline{\delta}}{\Omega_0\sqrt{n+1}}\right)^2 + e^{-2s^2}, \quad \forall s \in \left(\tfrac{t_1 v}{w}, \tfrac{t_2 v}{w}\right)\ , \tag{5.50}$$

for all n in the relevant photon number range [Messiah 1964, Section XVII-13].

The dressed states $(|-, n\rangle_t, |+, n\rangle_t)$ that diagonalize $\mathbf{H}_{JC}(t)$ for each $n = 1, 2, ...$ satisfy

$$\mathbf{H}_{JC}(t)\,|\pm, n\rangle_t = \pm\frac{\overline{\delta}}{2}\sqrt{1 + (n+1)\left(\frac{\Omega(vt)}{\overline{\delta}}\right)^2}\,|\pm, n\rangle_t\ ,$$

and are explicitly written

$$\begin{aligned} |-, n\rangle_t &= \cos(\xi_n^{(t)}/2)\,|g, n+1\rangle + i\sin(\xi_n^{(t)}/2)\,|e, n\rangle \\ |+, n\rangle_t &= i\sin(\xi_n^{(t)}/2)\,|g, n+1\rangle + \cos(\xi_n^{(t)}/2)\,|e, n\rangle\ , \end{aligned} \tag{5.51}$$

where we define $\xi_n^{(t)}$ by

$$\tan\xi_n^{(t)} = \frac{\Omega(vt/2)\sqrt{n}}{\overline{\delta}} \quad \text{with } \xi_n^{(t)} \in \left(\tfrac{-\pi}{2}, \tfrac{\pi}{2}\right)\ . \tag{5.52}$$

The propagator $\mathbf{U}_q$ corresponding to the parameter set $q = (t_1, t_2, v, \overline{\delta})$ is thus

$$\mathbf{U}_q = \sum_n |-, n\rangle_{t_2}\langle -, n|_{t_1}\ e^{\frac{i}{2}\phi^q_{n+1}} + |+, n\rangle_{t_2}\langle +, n|_{t_1}\ e^{\frac{-i}{2}\phi^q_{n+1}}\ , \tag{5.53}$$

where the accumulated phase ϕ_n^q is given by:

$$\phi_n^q = \overline{\delta}\int_{t_1}^{t_2}\sqrt{1 + n(\Omega(vt)/\overline{\delta})^2}\,dt\ . \tag{5.54}$$

[5]The following developments also carry through with (slowly) continuously varying $\delta(t)$. For pedagogical reasons, we have chosen to explain the experiment with piecewise constant δ. We therefore directly particularize the notation to $\delta(t) = \overline{\delta}$ constant.

The restriction of $\mathbf{U}_q$ on the Bloch sphere B_n can then be written as:

$$\begin{aligned}
&|-,n\rangle_{t_2}\langle -,n|_{t_1}\ e^{\frac{i}{2}\phi^q_{n+1}}\ +\ |+,n\rangle_{t_2}\langle +,n|_{t_1}\ e^{\frac{-i}{2}\phi^q_{n+1}}\\
=\ &(|-,n\rangle_{t_2}\langle g,n+1|\ +\ |+,n\rangle_{t_2}\langle e,n|)\\
&\times(|g,n+1\rangle\langle g,n+1|\ e^{\frac{i}{2}\phi^q_{n+1}}\ +\ |e,n\rangle\langle e,n|\ e^{\frac{-i}{2}\phi^q_{n+1}})\\
&\times(|-,n\rangle_{t_1}\langle g,n+1|\ +\ |+,n\rangle_{t_1}\langle e,n|)^\dagger\ . \qquad (5.55)
\end{aligned}$$

The transformation $(|-,n\rangle_t\langle g,n+1|\ +\ |+,n\rangle_t\langle e,n|)$ is a rotation around the X-axis of B_n by an angle $-\xi^{(t)}_{n+1}$. The transformation $(|g,n+1\rangle\langle g,n+1|\ e^{i\phi^q_{n+1}/2} + |e,n\rangle\langle e,n|\ e^{-i\phi^q_{n+1}/2})$ is a rotation around the Z-axis of B_n by an angle ϕ^q_{n+1}. We thus introduce in Eqs. (5.8),(5.10) the unitary operators $\mathbf{X}(f_\mathbf{N})$ and $\mathbf{Z}(f_\mathbf{N})$ representing these rotations on each Bloch sphere B_n. Noting that $\mathbf{X}(-f_\mathbf{N})^\dagger = \mathbf{X}(f_\mathbf{N})$, we can finally write (5.53) in the compact form:

$$\mathbf{U}_q = \mathbf{X}(-\xi^{(t_2)}_\mathbf{N})\ \mathbf{Z}(\phi^q_\mathbf{N})\ \mathbf{X}(\xi^{(t_1)}_\mathbf{N})\ . \qquad (5.56)$$

At the start and end of the complete composite interaction, the atom-cavity coupling is weak: $\Omega^2(\pm vT/2) = \Omega_0^2/100$. We can thus take $\mathbf{X}(-\xi^{(-T/2)}_\mathbf{N}) = \mathbf{X}(\xi^{(T/2)}_\mathbf{N}) = \mathbf{I}$ in Section 5.1.4 since $\xi^{(\pm T/2)}_\mathbf{N} \approx 0$. This leads to Eq. (5.25).

In the large detuning regime studied in Section 5.1.3, we can even neglect all the $\mathbf{X}$ operators in $\mathbf{U}_q$ compared to the large dispersive phase shift operator $\mathbf{Z}(\phi^q_\mathbf{N})$.

Two-mode case: In the two-mode case, it is not possible to get an exact expression for the dressed states. We thus restrict either to a resonant interaction with one of the modes or to a dispersive interaction with both, assuming a large detuning 2Δ between modes a and b. In the resonant case, we neglect the residual dispersive interaction with the other mode. For the non-resonant interaction, we use simple first-order dispersive expressions. In both cases, simulations integrating Eq. (5.42) explicitly confirm the validity of our approximations.

We start by giving some explicit formulas for the eigenvectors and eigenvalues of $\overline{\mathbf{H}}_{JC}/\Delta$. These are computed using perturbation theory [Messiah 1964]. Using the adiabatic approximation, we are then able to give an expression for the propagator. From (5.41), we have

$$\overline{\mathbf{H}}_{JC}/\Delta = (\mathbf{N}_b - \mathbf{N}_a) + i\varepsilon(-|g\rangle\langle e|(\mathbf{a}^\dagger + \mathbf{b}^\dagger) + |e\rangle\langle g|(\mathbf{a}+\mathbf{b}))\ ,$$

where $\varepsilon = -\frac{\Omega(s)}{2\Delta}$ and we have taken $\delta = 0$.

We first split the total Hilbert space $\mathcal{H}$ into the direct sum of finite dimensional subspaces in which the total energy in the two modes and the atom is conserved. For any two integers m, n, we denote $|g,m,n\rangle$ the state where the atom is $|g\rangle$ and the two modes are in the Fock states $|m\rangle$ and $|n\rangle$. The same holds when the atom is in $|e\rangle$. We denote $|g,m,n\rangle^\varepsilon$ the eigenvector of $\overline{\mathbf{H}}_{JC}/\Delta$ which would overlap with $|g,m,n\rangle$ if we take $\varepsilon \to 0$ analytically.

$$\mathcal{H} = \bigoplus_{E\in\mathbb{N}} \mathrm{span}\{|g,E,0\rangle^\varepsilon, |e,E-1,0\rangle^\varepsilon, |g,E-1,1\rangle^\varepsilon, .., |g,1,E-1\rangle^\varepsilon, |e,0,E-1\rangle^\varepsilon, |g,0,E\rangle^\varepsilon\}\ .$$

The eigenvectors are given, for all $E \in \mathbb{N}$, by

$$\begin{aligned}
|g,E,0\rangle^\varepsilon &= |g,E,0\rangle - i\varepsilon\sqrt{E}|e,E-1,0\rangle + O(\varepsilon^2) \\
|g,0,E\rangle^\varepsilon &= |g,0,E\rangle + i\varepsilon\sqrt{E}|e,0,E-1\rangle + O(\varepsilon^2) \\
|g,n,E-n\rangle^\varepsilon &= |g,n,E-n\rangle - i\varepsilon\sqrt{n}|e,n-1,E-n\rangle \\
&+ i\varepsilon\sqrt{E-n}|e,n,E-n-1\rangle + O(\varepsilon^2) \\
&\quad \forall n \in \{1,..,E-1\} \\
|e,n-1,E-n\rangle^\varepsilon &= |e,n-1,E-n\rangle - i\varepsilon\sqrt{n}|g,n,E-n\rangle \\
&+ i\varepsilon\sqrt{E-n+1}|g,n-1,E-n+1\rangle + O(\varepsilon^2) \\
&\quad \forall n \in \{1,..,E\}\ . \qquad (5.57)
\end{aligned}$$

The corresponding eigenvalues are

$$\bigcup_{E\in\mathbb{N}} \{\lambda^\varepsilon_{g,E,0}, \lambda^\varepsilon_{e,E-1,0}, \lambda^\varepsilon_{g,E-1,1}, .., \lambda^\varepsilon_{g,1,E-1}, \lambda^\varepsilon_{e,0,E-1}, \lambda^\varepsilon_{g,0,E}\}$$

where, for all $E \in \mathbb{N}$:

$$\begin{aligned}
\lambda^\varepsilon_{g,E,0} &= -E - \varepsilon^2 E + O(\varepsilon^4) \\
\lambda^\varepsilon_{g,0,E} &= E + \varepsilon^2 E + O(\varepsilon^4) \\
\lambda^\varepsilon_{g,n,E-n} &= E - 2n + \varepsilon^2(E-2n) + O(\varepsilon^4) \\
&\quad \forall n \in \{1,..,E-1\} \\
\lambda^\varepsilon_{e,n-1,E-n} &= E - 2n + 1 + \varepsilon^2(2n-E-1) + O(\varepsilon^4) \\
&\quad \forall n \in \{1,..,E\}\ . \qquad (5.58)
\end{aligned}$$

Let us first investigate the resonant case, with $\delta = \pm\Delta$. A simple adaptation of the single mode results leads to:

$$\begin{aligned}
\overline{\mathbf{U}}_q &= e^{-i\Delta(\mathbf{N}_b-\mathbf{N}_a)(t_2-t_1)}\, \overline{\mathbf{Z}}(\Delta(t_2-t_1))\, \overline{\mathbf{Y}}(\theta^q_{\mathbf{N}_b}) \\
&\quad \text{for } q = (t_1,t_2,v,\Delta) \qquad (5.59) \\
\overline{\mathbf{U}}_q &= e^{-i\Delta(\mathbf{N}_b-\mathbf{N}_a)(t_2-t_1)}\, \overline{\mathbf{Z}}(\Delta(t_1-t_2))\, \overline{\mathbf{Y}}(\theta^q_{\mathbf{N}_a}) \\
&\quad \text{for } q = (t_1,t_2,v,-\Delta)\ , \qquad (5.60)
\end{aligned}$$

where $\overline{\mathbf{Y}}(\theta^q_{\mathbf{N}_a})$, for instance, is the tensor product of $\mathbf{Y}(\theta^q_{\mathbf{N}_a})$ acting on the pair atom-mode a, with the identity acting on b. We define a generalized two-mode phase rotation by:

$$\overline{\mathbf{Z}}(f_{\mathbf{N}_a,\mathbf{N}_b}) = |g\rangle\langle g|\, e^{\frac{i}{2} f_{\mathbf{N}_a,\mathbf{N}_b}} + |e\rangle\langle e|\, e^{\frac{-i}{2} f_{(\mathbf{N}_a+\mathbf{I}),(\mathbf{N}_b+\mathbf{I})}}\ , \qquad (5.61)$$

where the operator $f_{\mathbf{N}_a,\mathbf{N}_b}$ is diagonal in the joint Fock state basis of the two modes with $f_{\mathbf{N}_a,\mathbf{N}_b}|n_a,n_b\rangle = f(n_a,n_b)|n_a,n_b\rangle$. In Eqs. (5.59) and (5.60), $\overline{\mathbf{Z}}$ is used with a constant argument $f_{\mathbf{N}_a,\mathbf{N}_b} = \pm\Delta(t_2-t_1)$.

We now consider the dispersive interaction corresponding here to $\delta = 0$. Applying second-order perturbation theory in Ω_0/Δ (see Eqs. (5.57)(5.58)), we get for $q = (t_1, t_2, v, 0)$:

$$\overline{\mathbf{U}}_q \;=\; e^{-i\Delta(\mathbf{N}_b - \mathbf{N}_a)(t_2 - t_1)}\, \overline{\mathbf{Z}}(\overline{\phi}^q(\mathbf{N}_b - \mathbf{N}_a))\,, \tag{5.62}$$

with $\overline{\phi}^q = \frac{1}{2\Delta}\int_{t_1}^{t_2} \Omega^2(vt)\, dt$.

Using Eqs. (5.59),(5.60),(5.62) and the commutation relation (5.7), we get an approximate evolution operator with the sequence defined in Section 5.1.6 (with $T\Delta = 0$ modulo 2π):

$$\begin{aligned}\overline{\mathbf{U}}_T \approx \overline{\mathbf{U}}_{\bar{c}}^{\text{eff}} \;=\;& \overline{\mathbf{U}}_\pi\, \overline{\mathbf{Z}}(-\Delta(T/2 + t_r)) \\ & \overline{\mathbf{Z}}(\overline{\phi}(\mathbf{N}_b - \mathbf{N}_a))\, \overline{\mathbf{Y}}(\theta^r_{\mathbf{N}_a})\, \overline{\mathbf{Y}}(\theta^r_{\mathbf{N}_b}) \\ & \overline{\mathbf{Z}}(\overline{\phi}(\mathbf{N}_a - \mathbf{N}_b))\, \overline{\mathbf{Z}}(\text{-}\Delta(T/2 - t_r))\,,\end{aligned} \tag{5.63}$$

with

$$\overline{\phi} \;=\; \frac{1}{2\Delta}\int_{-T/2}^{-t_r} \Omega^2(vt)\, dt\,. \tag{5.64}$$

The first line in Eq. (5.63) has no effect on the Kraus map since it is a rotation on the atom only after it has interacted with the modes. The operator $\overline{\mathbf{Z}}(-\Delta(T/2 - t_r))$ can simply be compensated by properly setting the phase of the Ramsey pulse, preparing now each atom in $\overline{\mathbf{Z}}(\Delta(T/2 - t_r))|u_{at}\rangle$. These considerations lead to the effective propagator given in Eq. (5.47).

5.1.8.2 Simulation details

In this section we give some details on how we numerically simulate the reservoir in order to obtain the results of Section 5.1.6.4.

Interaction with the environment is modeled by the following Kraus operators [Haroche 2006, page 186] :

$$\begin{aligned}\mathbf{M}^a_{\text{loss}} &= \sqrt{T\kappa_{\text{loss}}}\mathbf{a} & \mathbf{M}^b_{\text{loss}} &= \sqrt{T\kappa_{\text{loss}}}\mathbf{b} \\ \mathbf{M}^a_{\text{gain}} &= \sqrt{T\kappa_{\text{gain}}}\mathbf{a}^\dagger & \mathbf{M}^b_{\text{gain}} &= \sqrt{T\kappa_{\text{gain}}}\mathbf{b}^\dagger\end{aligned}$$

$$\begin{aligned}\mathbf{M}_{\text{no}} \;=\;& \mathbf{I} - \frac{1}{2}({\mathbf{M}^a_{\text{loss}}}^\dagger\mathbf{M}^a_{\text{loss}} + {\mathbf{M}^b_{\text{loss}}}^\dagger\mathbf{M}^a_{\text{loss}} \\ & + {\mathbf{M}^a_{\text{gain}}}^\dagger\mathbf{M}^a_{\text{gain}} + {\mathbf{M}^b_{\text{gain}}}^\dagger\mathbf{M}^b_{\text{gain}})\,,\end{aligned}$$

$$\text{where } \kappa_{\text{loss}} = (1 + n_{\text{t}})/Tc\,, \qquad \kappa_{\text{gain}} = n_t/Tc\,.$$

These operators model the loss and gain of a photon in each mode due to cavity damping and thermal photons respectively. We neglect the contribution of events such as the simultaneous absorption or emission of a photon in both modes at the same time, and the absorption or emission of two photons and more in each mode

during T. These events occur with a probability of higher order in $\kappa_{\text{loss}}T, \kappa_{\text{gain}}T$ and can therefore be neglected. We also neglect the pure dephasing of the cavity, since its frequency is extremely stable on the time scale of the experiment we propose. $\mathbf{M}_{\text{no}}$ is constructed such that, neglecting second order terms in $T\kappa_{\text{loss}}$ and $T\kappa_{\text{gain}}$, we verify the identity

$$\begin{aligned}\mathbf{I} &= \mathbf{M}^{a}_{\text{loss}}{}^{\dagger}\mathbf{M}^{a}_{\text{loss}} + \mathbf{M}^{b}_{\text{loss}}{}^{\dagger}\mathbf{M}^{b}_{\text{loss}} + \mathbf{M}^{a}_{\text{gain}}{}^{\dagger}\mathbf{M}^{a}_{\text{gain}} \\ &+ \mathbf{M}^{b}_{\text{gain}}{}^{\dagger}\mathbf{M}^{b}_{\text{gain}} + \mathbf{M}^{\dagger}_{\text{no}}\mathbf{M}_{\text{no}} \ .\end{aligned}$$

We also take into account the fact that only about $p_{at} \approx 1/3$ of samples are occupied by an atom. Hence, at each cavity-sample interaction step, with probability $1 - p_{at}$, the cavity is simply damped by the environment, and with probability p_{at}, an atom is present in the sample and applies the Kraus map $(\mathbf{M}_{\mathbf{g}}^{\overline{\mathbf{U}}_{\mathbf{T}}}, \mathbf{M}_{\mathbf{e}}^{\overline{\mathbf{U}}_{\mathbf{T}}})$ to the cavity. This leads us to solving the following Kraus map:

$$\begin{aligned}\rho_{k+1/2} &= (1-p_{at})\rho_k + p_{at}(\mathbf{M}_{\mathbf{g}}^{\overline{\mathbf{U}}_{\mathbf{T}}}\rho_k\mathbf{M}_{\mathbf{g}}^{\overline{\mathbf{U}}_{\mathbf{T}}}{}^{\dagger} + \mathbf{M}_{\mathbf{e}}^{\overline{\mathbf{U}}_{\mathbf{T}}}\rho_k\mathbf{M}_{\mathbf{e}}^{\overline{\mathbf{U}}_{\mathbf{T}}}{}^{\dagger}) \ , \\ \rho_{k+1} &= \mathbf{M}^{a}_{\text{loss}}\rho_{k+1/2}\mathbf{M}^{a}_{\text{loss}}{}^{\dagger} + \mathbf{M}^{b}_{\text{loss}}\rho_{k+1/2}\mathbf{M}^{b}_{\text{loss}}{}^{\dagger} \\ &+ \mathbf{M}^{a}_{\text{gain}}\rho_{k+1/2}\mathbf{M}^{a}_{\text{gain}}{}^{\dagger} + \mathbf{M}^{b}_{\text{gain}}\rho_{k+1/2}\mathbf{M}^{b}_{\text{gain}}{}^{\dagger} \\ &+ \mathbf{M}_{\text{no}}\rho_{k+1/2}\mathbf{M}_{\text{no}}{}^{\dagger} \ .\end{aligned} \tag{5.65}$$

Note that a more rigorous solution would be to solve at each step k, a Lindblad equation on the atom-cavity system including cavity decoherence. At the end of each interaction, we can trace out the atomic state and recover the cavity density matrix. This would capture the possibility of a quantum jump of the cavity while it is interacting with the atom. Here, we decouple the coherent evolution due to the interaction with the atom (from k to $k+1/2$) and the damping (from $k+1/2$ to $k+1$). This decoupling saves us a lot of computational time. Indeed, $\mathbf{M}_{\mathbf{g}}^{\overline{\mathbf{U}}_{\mathbf{T}}}$ and $\mathbf{M}_{\mathbf{e}}^{\overline{\mathbf{U}}_{\mathbf{T}}}$ are computed once by solving the Schrödinger equation, and then we simply iterate (5.65). We checked numerically that our simplified scheme gives the right result. A possible explanation is the following. If a quantum jump occurs in the presence or absence of an atom, the cavity jumps to a different state. However, since the reservoir seems to drive all states to the target state with convergence times much smaller than T_c, whether an atom was present or not shouldn't matter.

5.1.8.3 Equilibrium of reservoir with damping

If ρ'^{h}_{∞} of the form (5.39) is a stationary solution of (5.38) then we have:

$$\begin{aligned}\int_{-\alpha^c_\infty}^{\alpha^c_\infty} \mu(z)\left(\beta - \tfrac{\kappa+\kappa_c}{2}z\right)\left((\mathbf{a}^\dagger - z)|z\rangle\langle z| + |z\rangle\langle z|(\mathbf{a}-z)\right)\,dz \\ + \int_{-\alpha^c_\infty}^{\alpha^c_\infty} \kappa_c(\mu(-z)-\mu(z))z^2|z\rangle\langle z|\,dz = 0 \ ,\end{aligned}$$

(using $\mathbf{a}|z\rangle = z|z\rangle$, $e^{i\pi\mathbf{N}}\mathbf{a}|z\rangle = z|\text{-}z\rangle$ and their Hermitian conjugates). For any real ξ, multiplying on the left by coherent state $\langle\xi|$ and on the right by $|\xi\rangle$ yields

$$\int_{-\alpha_\infty^c}^{\alpha_\infty^c} 2\mu(z)\left(\beta - \tfrac{\kappa+\kappa_c}{2}z\right)(\xi - z)e^{-(\xi-z)^2}\,dz + \int_{-\alpha_\infty^c}^{\alpha_\infty^c} \kappa_c z^2(\mu(-z)-\mu(z))e^{-(\xi-z)^2}\,dz = 0\,,$$

since $|\,\langle\xi|z\rangle\,|^2 = e^{-(\xi-z)^2}$, ξ and z being real. An integration by parts of the first integral yields

$$\left[\mu(z)\left(\beta - \tfrac{\kappa+\kappa_c}{2}z\right)e^{-(\xi-z)^2}\right]_{z=-\alpha_\infty^c}^{z=\alpha_\infty^c} - \int_{-\alpha_\infty^c}^{\alpha_\infty^c}\left(\tfrac{d}{dz}\left(\mu(z)\left(\beta - \tfrac{\kappa+\kappa_c}{2}z\right)\right)\right)e^{-(\xi-z)^2}\,dz + \int_{-\alpha_\infty^c}^{\alpha_\infty^c}\kappa_c z^2(\mu(-z)-\mu(z))e^{-(\xi-z)^2}\,dz = 0\,.$$

One solution is a μ which verifies: (we conjecture that since the latter equation holds for any real ξ, this is the only possibility)

$$\kappa_c z^2(\mu(-z)-\mu(z)) - \tfrac{d}{dz}\left(\mu(z)\left(\beta - \tfrac{\kappa+\kappa_c}{2}z\right)\right) = 0$$

for $z \in (-\alpha_\infty^c, \alpha_\infty^c)$ with the boundary conditions $\lim_{z\mapsto\alpha_\infty^c}\mu(z)(z-\alpha_\infty^c) = 0$ and $\mu(-\alpha_\infty^c) = 0$.

To solve this differential equation for $z \in [-\alpha_\infty^c, \alpha_\infty^c]$, we decompose μ into its even and odd parts: these parts satisfy two first-order coupled differential equations that can be integrated directly to give formula (5.40) for $\mu(z)$.

5.2 A first convergence proof

In this section, we provide a mathematical result proving that the engineered reservoir of atoms we considered previously forces the cavity to converge to the desired cat state.

We consider the dynamics followed by one mode of the cavity when interacting with a stream of flying atoms. The interaction we consider here corresponds to that of Section 5.1.4, where we consider the resonant interaction time to be zero: $t_r = 0$. Dropping the latter assumption adds technical difficulties to the proof which we have not yet been able to overcome. Thus, each atom enters the cavity with a frequency detuned w.r.t the cavity frequency by $\Delta = \Omega_0/\varepsilon$. When the atom is in the cavity center, its frequency is shifted to a detuning of $-\Delta$. The propagator associated to such an interaction is given in (5.25), where $\theta^r_{\mathbf{N}} = 0$ and hence $\mathbf{Y}(\theta^r_{\mathbf{N}}) = \mathbf{I}$. In order to simplify computations by having a real operator, we replace $\mathbf{X}(\xi_{\mathbf{N}})$ by $\mathbf{Y}(\xi_{\mathbf{N}})$. Moreover, note that $\mathbf{Y}(\xi_{\mathbf{N}})\mathbf{Y}(\xi_{\mathbf{N}}) = \mathbf{Y}(2\xi_{\mathbf{N}})$. We thus consider a propagator of the form $\mathbf{Z}(-\phi_{\mathbf{N}})\mathbf{Y}(2\xi_{\mathbf{N}})\mathbf{Z}(\phi_{\mathbf{N}})$. We have also proven that taking a Kerr Hamiltonian $h_{\mathbf{N}} \sim \phi_\gamma \mathbf{N}^2$, we have $\mathbf{Z}(-\phi_{\mathbf{N}})\mathbf{Y}(2\xi_{\mathbf{N}})\mathbf{Z}(\phi_{\mathbf{N}}) = e^{-ih^c_{\mathbf{N}}}\mathbf{Y}(2\xi_{\mathbf{N}})e^{ih^c_{\mathbf{N}}}$. Hence, we prove the convergence of a dynamical system evolving under a Kraus map associated to $\mathbf{Y}(2\xi_{\mathbf{N}})$ to a pointer state $|\bar{\psi}\rangle\langle\bar{\psi}|$, which proves the convergence of the Kraus map associated to $\mathbf{Z}(-\phi_{\mathbf{N}})\mathbf{Y}(2\xi_{\mathbf{N}})\mathbf{Z}(\phi_{\mathbf{N}})$ to $e^{-ih^c_{\mathbf{N}}}|\bar{\psi}\rangle\langle\bar{\psi}|e^{ih^c_{\mathbf{N}}}$.

The main difficulty here is that we take the cavity state space to be infinite dimensional, rather than truncating to a finite dimensional space using a Galerkin approximation which would greatly simplify the proof. Infinite dimensional Banach spaces lose a key property compared to finite dimensional ones: the compactness of their unit ball. This complicates any convergence proof since bounded sequences do not necessarily admit converging subsequences. Many methods have been proposed to overcome this difficulty, in particular, proving the pre-compactness of the trajectories. That is, that there exists a compact set which is invariant under the system's dynamics. This is the path we have followed. We start by posing the problem, next we formulate the main result in theorem 5.1. This result is based on the two lemmas 5.1 and 5.2. Finally, we give the proofs of the theorem and the two lemmas.

5.2.1 Problem setting

We model the cavity state space with the Hilbert space $\mathcal{H}$ spanned by the Hilbert basis $\{|n\rangle\}_{n\geq 0}$:

$$\mathcal{H} = \{\sum_{n\geq 0} \psi_n |n\rangle \text{ where } \psi_n \in \mathbb{C} \text{ and } \sum_{n\geq 0} |\psi_n|^2 < \infty\} .$$

For all n, $|n\rangle$ is called a Fock state: a cavity state with exactly n photons. For all $|\psi\rangle = \sum_{n\geq 0} \psi_n |n\rangle$ and $|\phi\rangle = \sum_{n\geq 0} \phi_n |n\rangle$ in $\mathcal{H}$, the scalar product on $\mathcal{H}$ corresponds to $< \phi, \psi >= \sum_{n\geq 0} \phi_n^* \psi_n \in \mathbb{C}$.

An important linear operator on $\mathcal{H}$ is the annihilation operator $\mathbf{a}$. It is defined as follows: $\mathbf{a}|0\rangle = 0$ and for all $n \geq 1$ $\mathbf{a}|n\rangle = \sqrt{n}|n-1\rangle$. We have the important

commutation relation:

$$[\mathbf{a}, \mathbf{a}^\dagger] = \mathbf{I} \, .$$

From $\mathbf{a}$, we define the photon number operator $\mathbf{N} = \mathbf{a}^\dagger \mathbf{a}$ which acts as follows: for all $n \geq 0$ $\mathbf{N}|n\rangle = n|n\rangle$. For any analytic function f of $\mathbb{R}$, we use the notation $f_{\mathbf{N}}$ to denote the linear operator on $\mathcal{H}$ acting as follows: for all $n \geq 0$, $f_{\mathbf{N}}|n\rangle = f(n)|n\rangle$. We recall the fundamental relation:

$$\mathbf{a}\, f(\mathbf{N}) = f(\mathbf{N} + \mathbf{I})\, \mathbf{a} \, .$$

Let $\mathcal{L}(\mathcal{H})$ be the set of continuous linear operators from $\mathcal{H}$ to $\mathcal{H}$. We define the trace operator:

$$\mathrm{Tr} : \ \rho \in D(\mathrm{Tr}) \subset \mathcal{L}(\mathcal{H}) \rightarrow \mathrm{Tr}\,(\rho) = \sum_{n \geq 0} \langle n|\rho|n\rangle \, .$$

Here, $D(\mathrm{Tr})$ is the domain of $\mathrm{Tr}(.)$: a subset of $\mathcal{L}(\mathcal{H})$ on which the series $\sum \langle n|\rho|n\rangle$ is absolutely convergent. Now consider the set of Hilbert-Schmidt operators:

$$\mathcal{O}_{HS} = \{\rho \in \mathcal{L}(\mathcal{H}), \ \rho^\dagger \rho \in D(\mathrm{Tr})\} \, .$$

Notice that since $\rho^\dagger \rho$ is positive, $\rho^\dagger \rho \in D(\mathrm{Tr})$ is equivalent to $\mathrm{Tr}\left(\rho^\dagger \rho\right) < \infty$. We have that

$$\left(\mathcal{O}_{HS}, (A, B) \in {\mathcal{O}_{HS}}^2 \rightarrow \mathrm{Tr}\left(A^\dagger B\right)\right) \text{ is a Hilbert space} \, .$$

We define the linear operator $\mathbb{K}$ on $\mathcal{O}_{HS}$, also called a Kraus map:

$$\mathbb{K} : \mathcal{O}_{HS} \ni \rho \rightarrow \mathbf{M}_g \rho \mathbf{M}_g^\dagger + \mathbf{M}_e \rho \mathbf{M}_e^\dagger \in \mathcal{O}_{HS} \, . \tag{5.66}$$

The Kraus operators $\mathbf{M}_g$ and $\mathbf{M}_e$ are those associated to $\mathbf{Y}(2\xi_{\mathbf{N}})$. We have (see (5.14))

$$\begin{aligned} \mathbf{M}_g &= \cos(u/2)\cos(\xi_{\mathbf{N}}) + \sin(u/2)\frac{\sin(\xi_{\mathbf{N}})}{\sqrt{\mathbf{N}}}\mathbf{a}^\dagger \, , \\ \mathbf{M}_e &= \sin(u/2)\cos(\xi_{\mathbf{N}+1}) - \cos(u/2)\mathbf{a}\frac{\sin(\xi_{\mathbf{N}})}{\sqrt{\mathbf{N}}} \, . \end{aligned} \tag{5.67}$$

Recall that (see (5.27)) $\cos(\xi_{\mathbf{N}}) = 1/\sqrt{1+\varepsilon^2\mathbf{N}}$, $\sin(\xi_{\mathbf{N}}) = \varepsilon\sqrt{\mathbf{N}}/\sqrt{1+\varepsilon^2\mathbf{N}}$ and $\xi_{\mathbf{N}} \in (-\frac{\pi}{2}, \frac{\pi}{2})$.

Operators $\mathbf{M}_g$ and $\mathbf{M}_e$ satisfy the important relation (needed to preserve $\mathrm{Tr}\,(\rho) = 1$ under the Kraus map):

$$\mathbf{M}_g^\dagger \mathbf{M}_g + \mathbf{M}_e^\dagger \mathbf{M}_e = \mathbf{I} \, .$$

From the latter equation, we have that $\mathbf{M}_g$ and $\mathbf{M}_e$ are bounded over $\mathcal{O}_{HS}$, and hence $\mathbb{K}$ is bounded over $\mathcal{O}_{HS}$. Hence, as claimed in (5.66), we have $\mathbb{K}(\mathcal{O}_{HS}) \subset \mathcal{O}_{HS}$.

We therefore know that there exists $K > 0$ such that for all $\rho \in \mathcal{O}_{HS}$ $||\mathbb{K}(\rho)|| \leq K||\rho||$, let us show that we can in fact take $K = 2$. Take $\rho \in \mathcal{O}_{HS}$, we have:

$$\begin{aligned} ||\mathbb{K}(\rho)||^2 &= ||\mathbf{M}_g\rho\mathbf{M}_g^\dagger + \mathbf{M}_e\rho\mathbf{M}_e^\dagger||^2 \\ &\leq 2\left(||\mathbf{M}_g\rho\mathbf{M}_g^\dagger||^2 + ||\mathbf{M}_e\rho\mathbf{M}_e^\dagger||^2\right) . \end{aligned}$$

Besides,

$$\begin{aligned} ||\mathbf{M}_g\rho\mathbf{M}_g^\dagger||^2 &= \mathrm{Tr}\left(\mathbf{M}_g\rho^\dagger\mathbf{M}_g^\dagger\mathbf{M}_g\rho\mathbf{M}_g^\dagger\right) \\ &= \mathrm{Tr}\left(\left(\rho^\dagger\mathbf{M}_g^\dagger\mathbf{M}_g\rho\right)\mathbf{M}_g^\dagger\mathbf{M}_g\right) \\ &= \mathrm{Tr}\left(\rho^\dagger\mathbf{M}_g^\dagger\mathbf{M}_g\rho\right) - \mathrm{Tr}\left(\left(\rho^\dagger\mathbf{M}_g^\dagger\mathbf{M}_g\rho\right)\mathbf{M}_e^\dagger\mathbf{M}_e\right) \\ &= \mathrm{Tr}\left(\rho^\dagger\rho\right) - \mathrm{Tr}\left(\rho^\dagger\mathbf{M}_e^\dagger\mathbf{M}_e\rho\right) - \mathrm{Tr}\left(\mathbf{M}_e\rho^\dagger\mathbf{M}_g^\dagger\mathbf{M}_g\rho\mathbf{M}_e^\dagger\right) \\ &\leq \mathrm{Tr}\left(\rho^\dagger\rho\right) , \end{aligned}$$

since $\rho^\dagger\mathbf{M}_e^\dagger\mathbf{M}_e\rho \geq 0$ and $\mathbf{M}_e\rho^\dagger\mathbf{M}_g^\dagger\mathbf{M}_g\rho\mathbf{M}_e^\dagger \geq 0$. The same holds for

$$||\mathbf{M}_e\rho\mathbf{M}_e^\dagger||^2 \leq \mathrm{Tr}\left(\rho^\dagger\rho\right) .$$

From this, we have

$$||\mathbb{K}(\rho)|| \leq 2||\rho|| .$$

In analogy with Section 5.1.2, we find that:

- $\mathbf{M}_g$ and $\mathbf{M}_e$ have a unique common eigenvector $|\bar{\psi}\rangle$ if and only if $\tan(u/2) < 1$. In the following we take u such that $\gamma = \tan(u/2) < 1$.
- Expanding $|\bar{\psi}\rangle$ on the Fock basis $|\bar{\psi}\rangle = \sum_{n=0}^{\infty}\bar{\psi}_n|n\rangle$, the sequence $(\bar{\psi}_n)_n$ satisfies
$$\forall n \geq 0 \qquad \bar{\psi}_{n+1} = \tan(u/2)\frac{\varepsilon\sqrt{n+1}}{\sqrt{1+\varepsilon^2(n+1)}-1}\,\bar{\psi}_n$$
and $\bar{\psi}_0$ is such that $\langle\bar{\psi}|\bar{\psi}\rangle = 1$ (with arbitrary phase).
- The associated eigenvalues are:
$$\begin{aligned} \mathbf{M}_g|\bar{\psi}\rangle &= \cos(u/2)|\bar{\psi}\rangle \\ \mathbf{M}_e|\bar{\psi}\rangle &= -\sin(u/2)|\bar{\psi}\rangle \end{aligned} \tag{5.68}$$

Consider the set of density operators

$$\mathcal{D} = \{\rho \in \mathcal{O}_{HS}, \rho^\dagger = \rho, \mathrm{Tr}\,(\rho) = 1, \rho \geq 0\} .$$

This is the set of physically permitted states of an open quantum system. Notice that $\mathbb{K}(\mathcal{D}) \subset \mathcal{D}$. Finally for all $A > 0$ consider the set

$$\mathcal{V}_A = \{\rho \in \mathcal{D}, \sum_n \sigma_n\langle n|\rho|n\rangle \leq A\} ,$$

where $\sigma_n = \sum_{k=0}^{n-1} \alpha_k$, and $(\alpha_k)_{k\geq 0}$ are defined next. Let $\gamma = \tan(\frac{u}{2})$ and take $n_0 = \text{int}\left(\left(\frac{2\gamma}{\varepsilon(1-\gamma^2)}\right)^2\right) + 1$, where int denotes the integer part. For all $n \leq n_0$ we take $\alpha_n = 0$ and for all $n > n_0$ we take $\alpha_n = \frac{1+\varepsilon^2(n+1)}{n+1}$. For all n, $\sigma_n \geq 0$, $(\sigma_n)_{n\geq 0}$ is an increasing sequence, and $\lim_{n\to\infty} \sigma_n = +\infty$.

5.2.2 Main result

Theorem 5.1. *Take $A > 0$, $\rho_0 \in \mathcal{V}_A$ and for all $k \geq 0$ $\rho_{k+1} = \mathbb{K}(\rho_k)$. We have $\lim_{k\to\infty} Tr\left((\rho_k - |\bar{\psi}\rangle\langle\bar{\psi}|)^2\right) = 0$.*

The theorem is based on the Lyapunov function $\rho \to \langle\bar{\psi}|\rho|\bar{\psi}\rangle$, and the two following lemmas:

Lemma 5.1. *Take $A > 0$, $\rho_0 \in \mathcal{V}_A$ and for all $k \geq 0$ $\rho_{k+1} = \mathbb{K}(\rho_k)$. We have for all $k \geq 0$, $\rho_k \in \mathcal{V}_A$.*

Lemma 5.2. *Take $A > 0$. The set $\mathcal{V}_A$ is compact for the topology inherited from $\mathcal{O}_{HS}$: For all sequence $(\rho_k)_{k\geq 0} \in \mathcal{V}_A$, $\exists\ q : \mathbb{N} \to \mathbb{N}$ and $\rho_\infty \in \mathcal{V}_A$ such that $Tr\left((\rho_{q(k)} - \rho_\infty)^2\right) \to 0$.*

Notice that for any sequence $(\rho_k)_{k\geq 0}$ initialized at a state ρ_0 of finite energy, we have strong convergence towards $|\bar{\psi}\rangle\langle\bar{\psi}|$. Indeed, for all $n \geq 0$, we have $\alpha_n \leq 1 + \varepsilon^2$, and hence $\sigma_n \leq (1 + \varepsilon^2)n$. Take $\rho_0 \in \mathcal{D}$, such that ρ_0 has finite energy: $\sum_{n\geq 0} n\rho_0^{nn} = E_0 < +\infty$. We have $\sum_{n\geq 0} \sigma_n \rho_0^{nn} \leq (1+\varepsilon^2)E_0$. Hence $\rho_0 \in \mathcal{V}_A$ where $A = (1+\varepsilon^2)E_0$. And according to theorem 5.1, $(\rho_k)_{k\geq 0}$ converges strongly towards $|\bar{\psi}\rangle\langle\bar{\psi}|$.

5.2.3 Proofs

5.2.3.1 Proof of Theorem 5.1

Take $A > 0$, $\rho_0 \in \mathcal{V}_A$ and for all $k \geq 0$ $\rho_{k+1} = \mathbb{K}(\rho_k)$. We want to prove that $\lim_{k\to\infty} \text{Tr}\left((\rho_k - |\bar{\psi}\rangle\langle\bar{\psi}|)^2\right) = 0$. According to lemma 5.1, for all $k \geq 0$, $\rho_k \in \mathcal{V}_A$. According to lemma 5.2, $\mathcal{V}_A$ is compact, and hence there exists a sequence q and $\rho_\infty \in \mathcal{V}_A$ such that $\text{Tr}\left((\rho_{q(k)} - \rho_\infty)^2\right) \to 0$. Here we prove that necessarily $\rho_\infty = |\bar{\psi}\rangle\langle\bar{\psi}|$. Since $\mathcal{V}_A$ is compact, this would prove the sought result.

To this end we use the fidelity between ρ and the pure state $|\bar{\psi}\rangle\langle\bar{\psi}|$ as a Lyapunov function (in standard terminology, the Lyapunov function would be $1 - V$):

$$V : \rho \in \mathcal{D} \to \langle\bar{\psi}|\rho|\bar{\psi}\rangle \in \mathbb{R}^+ .$$

It is well known that the fidelity increases under the action of a Kraus map [Nielsen 2000, theorem 9.6]. In particular, for the Kraus map (5.66), we have

$$V(\rho_{k+1}) = V(\rho_k) + \langle\bar{\chi}|\rho_k|\bar{\chi}\rangle ,$$

where $|\bar{\chi}\rangle = (\sin(u/2)\mathbf{M}_g^\dagger + \cos(u/2)\mathbf{M}_e^\dagger)|\bar{\psi}\rangle$. Where we have used the fact that $\left(\cos(u/2)\mathbf{M}_g^\dagger - \sin(u/2)\mathbf{M}_e^\dagger\right)|\bar{\psi}\rangle = |\bar{\psi}\rangle$. Since ρ_k is positive, $\langle\bar{\chi}|\rho_k|\bar{\chi}\rangle \geq 0$.

Thus, $k \to V(\rho_k)$ is increasing, since it is bounded by 1, it converges. Consequently $\langle\bar{\chi}|\rho_k|\bar{\chi}\rangle$ converges to 0. Hence $\langle\bar{\chi}|\rho_\infty|\bar{\chi}\rangle = 0$. Since $\mathbf{M}_g$ and $\mathbf{M}_e$ are bounded over the unit ball of $\mathcal{O}_{HS}$, $\mathbb{K}$ is bounded and hence continuous over $\mathcal{O}_{HS}$. Therefore, $\lim_{k\to\infty} \mathrm{Tr}\left((\mathbb{K}(\rho_{q(k)}) - \mathbb{K}(\rho_\infty))^2\right) = 0$, hence $\langle\bar{\chi}|\mathbb{K}(\rho_\infty)|\bar{\chi}\rangle = 0$, thus

$$\langle\bar{\chi}|\mathbf{M}_g\rho_\infty\mathbf{M}_g^\dagger|\bar{\chi}\rangle = 0\ , \qquad \langle\bar{\chi}|\mathbf{M}_e\rho_\infty\mathbf{M}_e^\dagger|\bar{\chi}\rangle = 0\ .$$

By iteration, we see that necessarily, ρ_∞ is orthogonal to any iterates of $\mathbf{M}_g^\dagger$ and $\mathbf{M}_e^\dagger$ on $|\bar{\chi}\rangle$. Consider a non zero eigenvector $|\phi_\infty\rangle$ of ρ_∞: $\rho_\infty|\phi_\infty\rangle = \lambda|\phi_\infty\rangle$, $\lambda > 0$. Necessarily, $|\phi_\infty\rangle$ is orthogonal to any iterates of $\mathbf{M}_g^\dagger$ and $\mathbf{M}_e^\dagger$ on $|\bar{\chi}\rangle$. We may decompose $|\phi_\infty\rangle$ over $|\bar{\psi}\rangle$ and the orthogonal subspace to $|\bar{\psi}\rangle$, we note $|\phi_\infty^\perp\rangle$ the projection of $|\phi_\infty\rangle$ over the orthogonal subspace to $|\bar{\psi}\rangle$. Since $|\bar{\psi}\rangle$ is orthogonal to all iterates of $\mathbf{M}_g^\dagger$ and $\mathbf{M}_e^\dagger$ over $|\bar{\chi}\rangle$, $|\phi_\infty\rangle$ is orthogonal to these iterates if and only if $|\phi_\infty^\perp\rangle$ also is. Moreover, we have

$$(\cos(\tfrac{u}{2})\mathbf{M}_g^\dagger - \sin(\tfrac{u}{2})\mathbf{M}_e^\dagger)|\bar{\psi}\rangle = |\bar{\psi}\rangle \text{ and } (\sin(\tfrac{u}{2})\mathbf{M}_g^\dagger + \cos(\tfrac{u}{2})\mathbf{M}_e^\dagger)|\bar{\psi}\rangle = |\bar{\chi}\rangle\ ,$$

consequently, $|\phi_\infty^\perp\rangle$ is orthogonal to all the iterates of $\mathbf{M}_g^\dagger$ and $\mathbf{M}_e^\dagger$ on $|\bar{\psi}\rangle$. Let us now prove that this implies $|\phi_\infty^\perp\rangle = 0$: this will show that $|\phi_\infty\rangle$ is collinear to $|\bar{\psi}\rangle$, and since, $\rho_\infty \in \mathcal{V}_A$, we have $\mathrm{Tr}\,(\rho_\infty) = 1$ and hence $\rho_\infty = |\bar{\psi}\rangle\langle\bar{\psi}|$. This would prove that the accumulation set of ρ_k is equal to the single element ρ_∞ and hence we have strong convergence of all the trajectories starting in $\mathcal{V}_A$ towards $|\bar{\psi}\rangle\langle\bar{\psi}|$.

From $\mathbf{M}_g|\bar{\psi}\rangle = \cos(\frac{u}{2})|\bar{\psi}\rangle$ and $\mathbf{M}_e|\bar{\psi}\rangle = -\sin(\frac{u}{2})|\bar{\psi}\rangle$, we get

$$\frac{\sin(\xi_{\mathbf{N}})}{\sqrt{\mathbf{N}}}\mathbf{a}^\dagger|\bar{\psi}\rangle = \frac{\cos(\frac{u}{2})}{\sin(\frac{u}{2})}(1-\cos(\xi_{\mathbf{N}}))|\bar{\psi}\rangle, \qquad \mathbf{a}\frac{\sin(\xi_{\mathbf{N}})}{\sqrt{\mathbf{N}}}|\bar{\psi}\rangle = \frac{\sin(\frac{u}{2})}{\cos(\frac{u}{2})}(1+\cos(\xi_{\mathbf{N}+1}))|\bar{\psi}\rangle.$$

Since $\mathbf{M}_g^\dagger = \cos(u/2)\cos(\xi_{\mathbf{N}}) + \sin(u/2)\mathbf{a}\frac{\sin(\xi_{\mathbf{N}})}{\sqrt{\mathbf{N}}}$ and $\mathbf{M}_e^\dagger = \sin(u/2)\cos(\xi_{\mathbf{N}+1}) - \cos(u/2)\frac{\sin(\xi_{\mathbf{N}})}{\sqrt{\mathbf{N}}}\mathbf{a}^\dagger$, we have

$$\begin{aligned}
\mathbf{M}_g^\dagger|\bar{\psi}\rangle &= \frac{1}{\cos(\frac{u}{2})}\left(\cos^2(\tfrac{u}{2})\cos(\xi_{\mathbf{N}}) + \sin^2(\tfrac{u}{2})(1+\cos(\xi_{\mathbf{N}+1}))\right)|\bar{\psi}\rangle \\
\mathbf{M}_e^\dagger|\bar{\psi}\rangle &= \frac{1}{\sin(\frac{u}{2})}\left(\sin^2(\tfrac{u}{2})\cos(\xi_{\mathbf{N}+1}) - \cos^2(\tfrac{u}{2})(1-\cos(\xi_{\mathbf{N}}))\right)|\bar{\psi}\rangle
\end{aligned}$$

Thus $\cos(\xi_{\mathbf{N}})|\bar{\psi}\rangle$ and $\cos(\xi_{\mathbf{N}+1})|\bar{\psi}\rangle$ are linear combinations of $|\bar{\psi}\rangle$, $\mathbf{M}_g^\dagger|\bar{\psi}\rangle$ and $\mathbf{M}_e^\dagger|\bar{\psi}\rangle$. Since $|\phi_\infty^\perp\rangle$ is orthogonal to $|\bar{\psi}\rangle$, $\mathbf{M}_g^\dagger|\bar{\psi}\rangle$ and $\mathbf{M}_e^\dagger|\bar{\psi}\rangle$, it is also orthogonal to $\cos(\xi_{\mathbf{N}})|\bar{\psi}\rangle$ and $\cos(\xi_{\mathbf{N}+1})|\bar{\psi}\rangle$.

Let us prove that $|\phi_\infty^\perp\rangle$ is orthogonal to $\cos^r(\xi_{\mathbf{N}})|\bar{\psi}\rangle$ and $\cos^r(\xi_{\mathbf{N}+1})|\bar{\psi}\rangle$, for any integer r. It is sufficient to prove that $\cos^r(\xi_{\mathbf{N}})|\bar{\psi}\rangle$ and $\cos^r(\xi_{\mathbf{N}+1})|\bar{\psi}\rangle$ are linear combinations of iterates of $\mathbf{M}_g^\dagger$ and $\mathbf{M}_e^\dagger$ on $|\bar{\psi}\rangle$. This is true for $r = 1$, assume it is

true for r and let's prove it is true for $r+1$. We have

$$\begin{aligned}
\mathbf{M}_g^\dagger \cos^r(\xi_{\mathbf{N}})|\bar{\psi}\rangle &= \left(\cos(u/2)\cos^{r+1}(\xi_{\mathbf{N}}) + \sin(u/2)\cos^r(\xi_{\mathbf{N}+1})\mathbf{a}\frac{\sin(\xi_{\mathbf{N}})}{\sqrt{\mathbf{N}}}\right)|\bar{\psi}\rangle \\
&= \frac{1}{\cos(\frac{u}{2})}\left(\cos^2(u/2)\cos^{r+1}(\xi_{\mathbf{N}}) + \sin^2(u/2)(\cos^{r+1}(\xi_{\mathbf{N}+1}) + \cos^r(\xi_{\mathbf{N}+1}))\right)|\bar{\psi}\rangle \\
\mathbf{M}_e^\dagger \cos^r(\xi_{\mathbf{N}+1})|\bar{\psi}\rangle &= \left(\sin(u/2)\cos^{r+1}(\xi_{\mathbf{N}+1}) - \cos(u/2)\cos^r(\xi_{\mathbf{N}})\frac{\sin(\xi_{\mathbf{N}})}{\sqrt{\mathbf{N}}}\mathbf{a}^\dagger\right)|\bar{\psi}\rangle \\
&= \frac{1}{\sin(\frac{u}{2})}\left(\sin^2(u/2)\cos^{r+1}(\xi_{\mathbf{N}+1}) - \cos^2(u/2)(\cos^r(\xi_{\mathbf{N}}) - \cos^{r+1}(\xi_{\mathbf{N}}))\right)|\bar{\psi}\rangle\ .
\end{aligned} \tag{5.69}$$

Recall that $\cos^r(\xi_{\mathbf{N}})|\bar{\psi}\rangle$, $\cos^r(\xi_{\mathbf{N}+1})|\bar{\psi}\rangle$, $\mathbf{M}_g^\dagger\cos^r(\xi_{\mathbf{N}})|\bar{\psi}\rangle$ and $\mathbf{M}_e^\dagger\cos^r(\xi_{\mathbf{N}+1})|\bar{\psi}\rangle$ are linear combinations of iterates of $\mathbf{M}_g^\dagger$ and $\mathbf{M}_e^\dagger$ over $|\bar{\psi}\rangle$. Hence, $\cos^{r+1}(\xi_{\mathbf{N}})|\bar{\psi}\rangle$ and $\cos^r(\xi_{\mathbf{N}+1})|\bar{\psi}\rangle$ are also linear combinations of iterates of $\mathbf{M}_g^\dagger$ and $\mathbf{M}_e^\dagger$ over $|\bar{\psi}\rangle$.

We have proved that for any r, $|\phi_\infty^\perp\rangle$ is orthogonal to $\cos^r(\xi_{\mathbf{N}})|\bar{\psi}\rangle$. Noting $|\phi_\infty^\perp\rangle = \sum_{n\geq 0} x_n|n\rangle$, $x_n \in \mathbb{C}$, $\sum_n |x_n|^2 \leq 1$, we have, for all $r > 0$:

$$\sum_{n\geq 0} x_n\bar{\psi}_n \cos^r(\xi_n) = 0\ .$$

Since $\xi_0 = 0$, we have

$$\forall r > 0 \qquad x_0\bar{\psi}_0 + \sum_{n\geq 1} x_n\bar{\psi}_n\cos^r(\xi_n) = 0\ .$$

Moreover, $\cos(\xi_n) = \frac{1}{\sqrt{1+\varepsilon^2 n}} < \frac{1}{\sqrt{1+\varepsilon^2}} < 1$ for all $n \geq 1$. Hence $\left|\sum_{n\geq 1} x_n\bar{\psi}_n\cos^r(\xi_n)\right| \leq \frac{1}{\sqrt{1+\varepsilon^{2^r}}}\sum_{n\geq 1}|x_n\bar{\psi}_n|$ where $\sum_{n\geq 1}|x_n\bar{\psi}_n|$ is finite since $\sum_{n\geq 0}|x_n|^2 \leq 1$ and $\sum_{n\geq 0}|\bar{\psi}_n|^2 \leq 1$. Hence, taking the limit where $r \to \infty$, we get $x_0\bar{\psi}_0 = 0$. Since $\bar{\psi}_0 \neq 0$, we conclude $x_0 = 0$. For x_1, the reasoning is similar. Since $\cos(\xi_1) \neq 0$, we have

$$\forall r > 0, \qquad x_1\bar{\psi}_1 + \sum_{n\geq 2}\left(\frac{\cos(\xi_n)}{\cos(\xi_1)}\right)^r x_n\bar{\psi}_n = 0.$$

We have $\frac{\cos(\xi_n)}{\cos(\xi_1)} < \frac{\sqrt{1+\varepsilon^2}}{\sqrt{1+2\varepsilon^2}} < 1$ for all $n \geq 2$, hence, taking the limit $r \to \infty$, we get $x_2\bar{\psi}_2 = 0$. Since for all n $\bar{\psi}_n \neq 0$, and $\cos(\xi_n)$ is strictly decreasing, we repeat this reasoning and deduce $x_n = 0$ for all $n \geq 0$. From this we conclude that the only non null eigenvector of ρ_∞ is $|\bar{\psi}\rangle$, and hence $\rho_\infty = \lambda|\bar{\psi}\rangle\langle\bar{\psi}|$ where $\lambda \neq 0$. Since $\rho_\infty \in \mathcal{V}_A$, we have $\mathrm{Tr}\,(\rho_\infty) = 1$ and hence $\lambda = 1$. This concludes the proof.

5.2.3.2 Proof of Lemma 5.1

We define

$$f(\rho) = \sum_{n=0}^{\infty}\sigma_n\langle n|\rho|n\rangle\ .$$

We are going to prove that for any $\rho \in \mathcal{D}$, $f(\mathbb{K}(\rho)) \leq f(\rho)$. Since $\mathbb{K}(\mathcal{D}) \subset \mathcal{D}$, this proves that if we take $\rho_0 \in \mathcal{V}_A$, for all k, $\rho_k \in \mathcal{V}_A$. We have $\mathbb{K}(\rho) = \mathbf{M}_g \rho \mathbf{M}_g^\dagger + \mathbf{M}_e \rho \mathbf{M}_e^\dagger$, hence

$$\begin{aligned}
f(\mathbb{K}(\rho)) &= \sum_{n\geq 0} \sigma_n \left(\langle n|\mathbf{M}_g \rho \mathbf{M}_g^\dagger|n\rangle + \langle n|\mathbf{M}_e \rho \mathbf{M}_e^\dagger|n\rangle \right) \\
&= \sum_{n\geq 0} \sigma_n \left(\frac{\cos^2(\frac{u}{2})}{1+\varepsilon^2 n} + \frac{\sin^2(\frac{u}{2})}{1+\varepsilon^2+\varepsilon^2 n} \right) \langle n|\rho|n\rangle \\
&+ \varepsilon^2 \sin^2(\tfrac{u}{2}) \sum_{n=1} \left(\sigma_n \frac{n}{1+\varepsilon^2 n} \langle n-1|\rho|n-1\rangle \right) \\
&+ \varepsilon^2 \cos^2(\tfrac{u}{2}) \sum_{n=0} \left(\sigma_n \frac{n+1}{1+\varepsilon^2+\varepsilon^2 n} \langle n+1|\rho|n+1\rangle \right) \\
&+ \varepsilon \sin(u) \sum_{n=1} \left(\sigma_n \frac{\sqrt{n}}{1+\varepsilon^2 n} \Re(\langle n|\rho|n-1\rangle) \right) \\
&- \varepsilon \sin(u) \sum_{n=0} \left(\sigma_n \frac{\sqrt{n+1}}{1+\varepsilon^2+\varepsilon^2 n} \Re(\langle n+1|\rho|n\rangle) \right) .
\end{aligned}$$

This can be written as

$$\begin{aligned}
f(\mathbb{K}(\rho)) &= f(\rho) \\
&- \sum_{n\geq 0} \sigma_n \left(\cos^2(\tfrac{u}{2}) \frac{\varepsilon^2 n}{1+\varepsilon^2 n} + \sin^2(\tfrac{u}{2}) \frac{\varepsilon^2(n+1)}{1+\varepsilon^2+\varepsilon^2 n} \right) \langle n|\rho|n\rangle \\
&+ \varepsilon^2 \sin^2(\tfrac{u}{2}) \sum_{n=0} \left(\sigma_{n+1} \frac{n+1}{1+\varepsilon^2(n+1)} \langle n|\rho|n\rangle \right) \\
&+ \varepsilon^2 \cos^2(\tfrac{u}{2}) \sum_{n=1} \left(\sigma_{n-1} \frac{n}{1+\varepsilon^2 n} \langle n|\rho|n\rangle \right) \\
&+ \varepsilon \sin(u) \sum_{n=1} (\sigma_n - \sigma_{n-1}) \frac{\sqrt{n}}{1+\varepsilon^2 n} \Re(\langle n|\rho|n-1\rangle) ,
\end{aligned}$$

Using $\sigma_n = \sum_{k=0}^{n-1} \alpha_k$, and noting $\gamma = \tan(u/2)$, we get

$$\begin{aligned}
\frac{f(\mathbb{K}(\rho)) - f(\rho)}{\varepsilon \cos^2(\frac{u}{2})} &= \varepsilon \alpha_0 \gamma^2 \frac{1}{1+\varepsilon^2} \langle 0|\rho|0\rangle \\
&+ \varepsilon \sum_{n\geq 1} \left(-\alpha_{n-1} \frac{n}{1+\varepsilon^2 n} + \alpha_n \gamma^2 \frac{n+1}{1+\varepsilon^2(n+1)} \right) \langle n|\rho|n\rangle \\
&+ 2\gamma \sum_{n\geq 1} \alpha_{n-1} \frac{\sqrt{n}}{1+\varepsilon^2 n} \Re(\langle n|\rho|n-1\rangle) .
\end{aligned}$$

Take $n_0 = \text{int}\left(\left(\frac{2\gamma}{\varepsilon(1-\gamma^2)} \right)^2 \right) + 1$, where int denotes the integer part. For all $n \leq n_0$ we take $\alpha_n = 0$ and for all $n > n_0$ we take $\alpha_n = \frac{1+\varepsilon^2(n+1)}{n+1}$. We have

$$\begin{aligned}\frac{f(\mathbb{K}(\rho))-f(\rho)}{\varepsilon\cos^2(\frac{u}{2})} &= \varepsilon\sum_{n\geq n_0}(-1+\gamma^2)\langle n|\rho|n\rangle \\ &+ 2\gamma\sum_{n\geq n_0}\frac{1}{\sqrt{n}}\Re(\langle n|\rho|n-1\rangle) \\ &\leq \varepsilon(\gamma^2-1)+2\frac{\gamma}{\sqrt{n_0}}\sum_{n=n_0}|\Re(\langle n|\rho|n-1\rangle)|\,.\end{aligned}$$

For all $\rho\geq 0$ and $n\geq 1$, we have

$$|\Re(\langle n|\rho|n-1\rangle)|\leq|\langle n|\rho|n-1\rangle|\leq\sqrt{\langle n|\rho|n\rangle}\sqrt{\langle n-1|\rho|n-1\rangle}\,,$$

hence

$$\begin{aligned}\sum_{n\geq n_0}|\Re\langle n|\rho|n-1\rangle| &\leq \sum_{n\geq n_0}\sqrt{\langle n|\rho|n\rangle}\sqrt{\langle n-1|\rho|n-1\rangle} \\ &\leq \sqrt{\left(\sum_{n\geq n_0}\langle n|\rho|n\rangle\right)\left(\sum_{n\geq n_0}\langle n-1|\rho|n-1\rangle\right)} \\ &\leq 1\,.\end{aligned}$$

Hence

$$\frac{f(\mathbb{K}(\rho))-f(\rho)}{\varepsilon\cos^2(\frac{u}{2})} \leq \varepsilon(\gamma^2-1)+2\frac{\gamma}{\sqrt{n_0}}\,,$$

which is negative for $n_0=\mathrm{int}\left(\left(\frac{2\gamma}{\varepsilon(1-\gamma^2)}\right)^2\right)+1$.

5.2.3.3 Proof of Lemma 5.2

Take $A>0$ and consider a sequence $(\rho_k)_{k\geq 0}\in\mathcal{V}_A$. We want to prove that there exists $\rho_\infty\in\mathcal{V}_A$ and a subsequence $\left(\rho_{q(k)}\right)_{k\geq 0}$ which converges strongly towards ρ_∞. To this aim, we start by proving that there exists $\rho_\infty\in B_{\mathcal{O}_{HS}}$ ($B_{\mathcal{O}_{HS}}$ is the unit ball of $\mathcal{O}_{HS}$), such that the sequence $\left(\rho_{q(k)}\right)_{k\geq 0}$ converges weakly to ρ_∞. We then prove that $\rho_\infty\in\mathcal{V}_A$, and finally that the convergence is strong.

We have $\mathcal{V}_A\subset\mathcal{D}\subset B_{\mathcal{O}_{HS}}$, hence $(\rho_k)_{k\geq 0}$ is a bounded sequence of $\mathcal{O}_{HS}$. Moreover, $\mathcal{O}_{HS}$ is a Hilbert space, it is therefore reflexive. According to [Brezis 1983, th III.27], we can extract a subsequence $\left(\rho_{q(k)}\right)_{k\geq 0}$ which converges for the weak topology to some $\rho_\infty\in B_{\mathcal{O}_{HS}}$. To lighten notations, we assume with no loss of generality that $q(k)=k$ for all k. This is equivalent to [Brezis 1983, prop III.5], for all $h\in\mathcal{O}_{HS}$, $\mathrm{Tr}\left(h^\dagger\rho_k\right)\to\mathrm{Tr}\left(h^\dagger\rho_\infty\right)$. In particular, we have for all m,n, $\rho_k^{mn}\to\rho_\infty^{mn}$, where we note $\langle m|\rho|n\rangle=\rho^{mn}$.

Let us now prove that $\rho_\infty\in\mathcal{V}_A$.

We start by proving that $\rho_\infty \geq 0$. For all $|\psi\rangle \in \mathcal{H}$, $|\psi\rangle\langle\psi| \in \mathcal{O}_{HS}$, and hence $\langle\psi|\rho_k|\psi\rangle \to \langle\psi|\rho_\infty|\psi\rangle$. And $\rho_k \geq 0$, hence for all $|\psi\rangle \in \mathcal{H}$, $\langle\psi|\rho_k|\psi\rangle \geq 0$, and hence $\rho_\infty \geq 0$.

Moreover, for all k, ρ_k is self-adjoint, hence, ρ_∞ is self-adjoint.

Next we show that $\mathrm{Tr}\,(\rho_\infty) = 1$. For all k, $\sum_{n=0}^{\infty} \rho_k^{nn} = 1$. Take $\varepsilon > 0$, $N > 0$ and $k > 0$. We have

$$|\sum_{n=0}^{N} \rho_\infty^{nn} - 1| \leq \sum_{n=0}^{N} |\rho_\infty^{nn} - \rho_k^{nn}| + \sum_{n \geq N} \rho_k^{nn} \; .$$

Since $\rho_k \in \mathcal{V}_A$, $\sum_{n=0}^{\infty} \sigma_n \rho_k^{nn} \leq A$. Moreover, for all n, $\sigma_n \rho_k^{nn} \geq 0$ hence $\sum_{n \geq N} \sigma_n \rho_k^{nn} \leq A$. For $N > n_0$, we have $\sigma_n > \sigma_N > 0$ for all $n > N$, and hence $\sum_{n \geq N} \rho_k^{nn} \leq A/\sigma_N$. From this we conclude that

$$|\sum_{n=0}^{N} \rho_\infty^{nn} - 1| \leq \sum_{n=0}^{N} |\rho_\infty^{nn} - \rho_k^{nn}| + A/\sigma_N \; .$$

We have $\sigma_n \to \infty$, hence there exists $N_\varepsilon > 0$ such that for all $N > N_\varepsilon$, $A/\sigma_N < \varepsilon/2$. We take $N > N_\varepsilon$. Since for all n, $\lim_{k \to +\infty} |\rho_\infty^{nn} - \rho_k^{nn}| = 0$, there exists $k_{\varepsilon,N} > 0$ such that for all $k > k_{\varepsilon,N}$, $\sum_{n=0}^{N} |\rho_\infty^{nn} - \rho_k^{nn}| \leq \varepsilon/2$. We therefore have

$$|\sum_{n=0}^{N} \rho_\infty^{nn} - 1| \leq \varepsilon \; ,$$

and hence $\mathrm{Tr}\,(\rho_\infty) = 1$.

Finally, we prove that $\sum_{n=0}^{\infty} \sigma_n \rho_\infty^{nn} \leq A$. Take $N \geq 0$ and $k > 0$.

$$\begin{aligned} \sum_{n=0}^{N} \sigma_n \rho_\infty^{nn} &= \sum_{n=0}^{N} \sigma_n (\rho_\infty^{nn} - \rho_k^{nn}) + \sum_{n=0}^{N} \sigma_n \rho_k^{nn} \\ &\leq \sum_{n=0}^{N} \sigma_n (\rho_\infty^{nn} - \rho_k^{nn}) + A \; . \end{aligned}$$

For all $\varepsilon > 0$, $\exists k_{\varepsilon,N}$ such that for all $k > k_{\varepsilon,N}$, $\sum_{n=0}^{N} \sigma_n (\rho_\infty^{nn} - \rho_k^{nn}) < \varepsilon$. Hence

$$\sum_{n=0}^{N} \sigma_n \rho_\infty^{nn} \leq \varepsilon + A \; ,$$

and hence $\sum_{n=0}^{\infty} \sigma_n \rho_\infty^{nn} \leq A$.

We have proven that $(\rho_k)_{k \geq 0}$ converges weakly to $\rho_\infty \in \mathcal{V}_A$. Let us now prove

that this convergence is strong. Take $N > 0$,

$$\begin{aligned}\mathrm{Tr}\left((\rho_\infty - \rho_k)^2\right) &= \sum_{m,n\geq 0} |\rho_\infty^{mn} - \rho_k^{mn}|^2 \\ &= \sum_{m,n<N} |\rho_\infty^{mn} - \rho_k^{mn}|^2 + \sum_{m,n>N} |\rho_\infty^{mn} - \rho_k^{mn}|^2 \\ &\qquad + 2\sum_{n=0}^{N}\sum_{m\geq N} |\rho_\infty^{mn} - \rho_k^{mn}|^2 \ . \quad (5.70)\end{aligned}$$

Notice that we have, for any two complex numbers x and y: $|x-y|^2 \leq 2(|x|^2 + |y|^2)$.

For any bounded positive self adjoint operator ρ, there exists a unique positive self adjoint bounded operator $\sqrt{\rho}$, such that $\sqrt{\rho}^2 = \rho$. For any m, n, we have:

$$|\rho_{mn}|^2 = |\langle m|\sqrt{\rho}\sqrt{\rho}|n\rangle|^2 \leq \rho_{mm}\rho_{nn} \ .$$

This is simply a Cauchy-Schwarz inequality in $\mathcal{H}$ for $\sqrt{\rho}|n\rangle, \sqrt{\rho}|m\rangle \in \mathcal{H}$.

From this we have:

$$\sum_{m,n>N} |\rho_\infty^{mn} - \rho_k^{mn}|^2 \leq \sum_{m,n>N} 2(\rho_\infty^{mm}\rho_\infty^{nn} + \rho_k^{mm}\rho_k^{nn}) \leq 4A^2/\sigma_N^2 \ ,$$

and

$$2\sum_{n=0}^{N}\sum_{m\geq N} |\rho_\infty^{mn} - \rho_k^{mn}|^2 \leq 8A/\sigma_N \ .$$

Take $\varepsilon > 0$, since $\sigma_N \to \infty$, there exists N_ε such that for all $N > N_\varepsilon$, $8A/\sigma_N + 4A^2/\sigma_N^2 \leq \varepsilon/2$. Now take $N > N_\varepsilon$ fixed. Since for all m, n $\lim_{k\to+\infty} \rho_k^{mn} = \rho_\infty^{mn}$, there exists $k_{N,\varepsilon}$ such that for all $k > k_{\varepsilon,N}$, $\sum_{m,n<N} |\rho_\infty^{mn} - \rho_k^{mn}|^2 \leq \varepsilon/2$. Hence $\mathrm{Tr}\left((\rho_\infty - \rho_k)^2\right) < \varepsilon$. This concludes the proof.

Chapter 6

Schrödinger cats and quantum error correction

Contents

Ce chapitre traite de la préparation d'états non classiques dans des circuits Josephson (section 6.2), et la correction d'erreur quantique (QEC) (section 6.3). Nous proposons une séquence de pulses qui permettrait la préparation de toute superposition d'états cohérents quasi-orthogonaux, et nous montrons comment ces opérations peuvent être utilisées pour la correction d'erreur autonome nécessitant seulement une cavité couplée à un qubit physique. Avant de décrire ces résultats, nous commençons par une rapide comparaison entre l'électrodynamique quantique en cavité et les circuits quantiques (section 6.1).

This chapter is concerned with the preparation of non-classical states in the context of Josephson circuits (section 6.2), and quantum error correction (QEC)

(section 6.3). We provide a detailed sequence of pulses which could prepare arbitrary superpositions of quasi-orthogonal coherent states in a cavity, and we show how these operations could be used for autonomous QEC requiring only a single cavity coupled to a single physical qubit. Before describing these results, we start with a brief section describing some differences and similarities between cavity QED and circuit QED (section 6.1).

6.1 From cavity QED to circuit QED

Up to this point, in this thesis, we have considered "real" atoms, coupled to "real" cavities. These atoms are real in the sense that they can be found in nature. In chapter 5 for instance, we described an experiment where Rb atoms interact with an electrical field confined in a microwave cavity. These systems, being simultaneously natural quantum systems, and described by a relatively simple theory, make them wonderful to explore the laws of quantum mechanics and understand how these intriguing laws carry out to our macroscopic world.

However, when working with natural systems, we are stuck with what nature has to offer. This can be problematic if we want a system with specific properties, such as frequency transitions or coupling strengths, or even more generally, if we want a specific Hamiltonian. As an example, in every experiment which aims to manipulate quantum states, an important quantity is the coupling strength between our controller and the system itself. The time needed to perform a state preparation decreases as the coupling increases. Since we always aim to perform the preparation in times much shorter than the lifetime, we always aim for large couplings. In the ENS experiment [Haroche 2006] for instance, this translated into increasing the coupling between the Rb atoms and the cavity mode. Indeed, a Rb atom in its ground state is very weakly coupled to a single photon in the cavity. In order to see any significant effect of one photon on the atom it was necessary to drive the Rb atoms into Rydberg states, which are states with a very large principle quantum number n (here $n = 50$). Preparing a Rb atom from its ground state to a Ryberg state is in itself a complex experiment.

The question then arises of whether there exists a class of quantum systems for which the properties can be easily engineered on demand. A field which offers such versatility is electrical engineering. Engineers have built basic electrical circuit elements such as inductors, capacitors, resistances, transistors, and so on, which they are able to assemble in order to obtain circuits with predefined properties. This way, we may engineer a huge range of technologies ranging from a radio to a computer processor. These electrical circuits as a whole, however, seem to obey to the laws of classical physics and electrodynamics. A long time dream has been to build systems combining engineering versatility and quantum behavior. This dream came to life not more than a decade ago when physicists in places like CEA Saclay, Yale and Santa Barbara started building big (on the micrometer scale) systems formed of capacitors, inductors and Josephson junctions. These systems were proven to have

a few collective degrees of freedom which obey to the laws of quantum mechanics [Devoret 2004].

The consequences of such new systems are huge. The ability to engineer systems with predefined Hamiltonians paves the way for quantum simulators, quantum computing and the observation of a variey of new effects. This embodies a complete change of paradigm. Instead of observing an intriguing effect on a natural system and trying to understand it by modeling it and finding its Hamiltonian, it is now possible to predict an interesting behavior produced by an imagined Hamiltonian, and "order" it for fabrication, and then observe it.

As theorists, this allows us to daydream about ideas and feel more confident that one may be able to put them into practice. After establishing the model of the system we consider and describing what behavior we should observe by performing a sequence of pulses, experimentalists can then translate this model into a circuit architecture. Properties such as couplings and frequencies can be obtained within a few percent uncertainty by carefully manufacturing the circuit. Tools such as "Maxwell", "HFSS" and more recently the "black box quantization" theory [Nigg 2012], are used to predict which Hamiltonian will be generated by a given architecture.

Recently, these engineered quantum circuits have reached coherence times which make them serious competitors to other systems such as trapped ions and cavities with Rydberg atoms. Lifetimes of several tens of microseconds for superconducting qubits and cavities in circuits have been reported, with couplings of several hundreds of MHz. This gives a coupling quality factor of the order of 10^4. This is of the same order as in the ENS experiment, where the cavity lifetime is ≈ 100 ms with a coupling of ≈ 50 kHz. Notice that although the coupling quality factor is of the same order, there is a three orders of magnitude difference in lifetimes and couplings. On the one hand, this makes all circuit QED experiments a thousand times faster than their cavity QED analogue: this is a huge advantage since measuring data on a quantum system necessarily requires averaging and hence performing the experiment tens of thousands of times. On the other hand, slower cavity QED experiments have made possible real time quantum feedback [Sayrin 2011], since processing information is much easier on the 100 microsecond time scale than on the 100 ns time scale.

Many experiments performed with trapped ions and cavities with Rydberg atoms have been reproduced in quantum circuits, such as the preparation of Fock states [Hofheinz 2008][Brune 1996] and quantum error correction [Reed 2012a][Schindler 2011]. Other experiments with quantum circuits don't seem possible at all with other systems. This is for instance the case of a recent experiment where it has been possible to measure the distortion of a coherent state into multi-component cat states and squeezed states due to the Kerr effect [Kirchmair *et al.* 2012].

In the spring of 2012, I had the immense pleasure of visiting Michel Devoret's and Rob Schoelkopf's groups in Yale. The work we present in this chapter was done during this visit. At the time of writing most of these ideas are still on the theoretical level, although some experimental data on the deterministic preparation of cat states has already been obtained, and we hope to report it in a few months.

The system we have in mind in this chapter is a set of superconducting qubits coupled to microwave cavities for which we propose some new experiments.

6.2 Deterministic protocol for mapping a qubit to coherent state superpositions in a cavity

We introduce a new gate that transfers an arbitrary state of a qubit into a superposition of two quasi-orthogonal coherent states of a cavity mode, with opposite phases. This qcMAP gate is based on conditional qubit and cavity operations exploiting the energy level dispersive shifts, in the regime where they are much stronger than the cavity and qubit linewidths. The generation of multi-component superpositions of quasi-orthogonal coherent states, non-local entangled states of two resonators and multi-qubit GHZ states can be efficiently achieved by this gate. This section reports the results we obtained in collaboration with G. Kirchmair, B. Vlastakis, R. Schoelkopf, M. Devoret and M. Mirrahimi. We have submitted a manuscript to Phys. Rev. Lett. and a preliminary version can be found on the ArXiv [Leghtas 2012b].

6.2.1 Introduction

In the field of quantum Josephson circuits, microwave resonators are extremely useful for performing readout, coupling multiple qubits and protecting against decoherence [Wallraff 2005, Majer 2007, Paik 2011]. In addition, using an oscillator as a memory to store a qubit state has been explored both theoretically and experimentally (see e.g [Gottesman 2001, Mariantoni 2011, Maître 1997]). The recent improvement in coherence times of microwave resonators with respect to superconducting qubits ([Megrant 2012, Reagor *et al.* 2012]) makes it particularly interesting to use a cavity as a quantum memory in this context.

In this section we introduce a new gate between a qubit and a cavity (qcMAP) which maps the qubit state onto a superposition of two quasi-orthogonal coherent states with opposite phases. This gate provides access to the large Hilbert space of the cavity, so that one can encode the information of a multi-qubit system on a single cavity mode and decode it back on the qubits. In particular, this gate can be employed to efficiently prepare any superposition of quasi-orthogonal coherent states (SQOCS) [Raimond 2010]. Furthermore, we show that this scheme can be easily adapted to prepare entangled states of two resonators, which would maximally violate Bell's inequality. Finally, the qcMAP gate offers a new method to use the cavity as a bus to perform multi-qubit gates and prepare arbitrary GHZ states.

Previously realized qubit-cavity encoding in superconducting qubits are based on a correspondence between the register's states and the cavity's Fock states [Hofheinz 2008]. These schemes are based on bringing the qubit into resonance with the cavity. The qcMAP gate does not require such real-time frequency tunings and hence avoids an extra decoherence channel. Additionally, in

contrast to the resonant regime, the time to prepare a SQOCS using the qcMAP gate does not increase with the amplitudes of the coherent components, but scales only linearly with the number of coherent components. Large SQOCS could hence be generated with high fidelities, exploring the decoherence of highly non-classical states [Brune 1996, Deléglise 2008].

We place ourselves in the strong dispersive regime, where both the qubit and resonator transition frequencies split into well-resolved spectral lines indexed by the number of excitations in qubit and resonator [Schuster 2007]. The resonator frequency ω_r splits into two well resolved lines ω_r^g and ω_r^e, corresponding to the cavity's frequency when the qubit is in the ground ($|g\rangle$) or the excited ($|e\rangle$) state. Through the same mechanism, the qubit frequency ω_q splits into $\{\omega_q^n\}_{n=0,1,2,\cdots}$ corresponding to the qubit frequency when the cavity is in the photon number state $|n\rangle$. Recent experiments have shown dispersive shifts that are about 3 orders of magnitude larger than the qubit and cavity linewidths [Paik 2011].

6.2.2 The qcMAP gate

The qcMAP gate relies on two operations which we detail in the following: the conditional cavity displacement, which we denote by D_α^g, and the conditional qubit rotation, which we denote by X_θ^0 (see Fig. 6.1(a)). An *un*conditional displacement D_α is obtained by applying a very short pulse, which displaces a coherent state by α regardless of the qubit state. A conditional displacement D_α^g can be realized in the strong dispersive limit: with a selective pulse of duration $T \gtrsim 1/\chi_{qr}$, we may displace the cavity by a complex amplitude α only if the qubit is in the ground state. For a coherent state $|\beta\rangle$, we have $D_\alpha^g|e,\beta\rangle = |e,\beta\rangle$, and $D_\alpha^g|g,\beta\rangle = e^{(\alpha\beta^\dagger - \alpha^\dagger\beta)/2}|g,\beta+\alpha\rangle$. Such a conditional displacement was first proposed in [Davidovich 1993] as part of a non-deterministic scheme to prepare a two-component superposition of coherent states. For the deterministic qcMAP gate, we combine this displacement with a conditional qubit rotation X_π^0. The conditional rotations X_θ^0 are simply achieved by applying a selective pulse at ω_q^0, performing an rotation of angle θ of the qubit state conditioned on the cavity being in its vacuum state. Such selective qubit rotations have been experimentally demonstrated in [Johnson 2010].

In order to map the state of the qubit to the cavity mode, we construct the qcMAP gate as follows. Starting from a qubit in $c_g|g\rangle + c_e|e\rangle$ and cavity in $|0\rangle$, a first conditional displacement $D_{2\alpha}^g$ entangles the qubit and the cavity, creating the state $c_g|g,2\alpha\rangle + c_e|e,0\rangle$. We choose $2|\alpha|$ to be large enough so that the non-orthogonality of the two coherent states $|\langle 2\alpha \mid 0\rangle|^2 = e^{-4|\alpha|^2}$ is negligible (of order 10^{-6} for $\bar{n} = |\alpha|^2 = 3.5$). A conditional π-pulse X_π^0 can then disentangle the qubit from the cavity leaving the qubit in $|g\rangle$ and the cavity in $c_g|2\alpha\rangle + c_e|0\rangle$. Finally, the unconditional displacement $D_{-\alpha}$ centers the superposition at the origin.

The qcMAP gate is well adapted to quantum information processing with a transmon qubit [Koch 2007] coupled to a microwave resonator. The Hamiltonian is

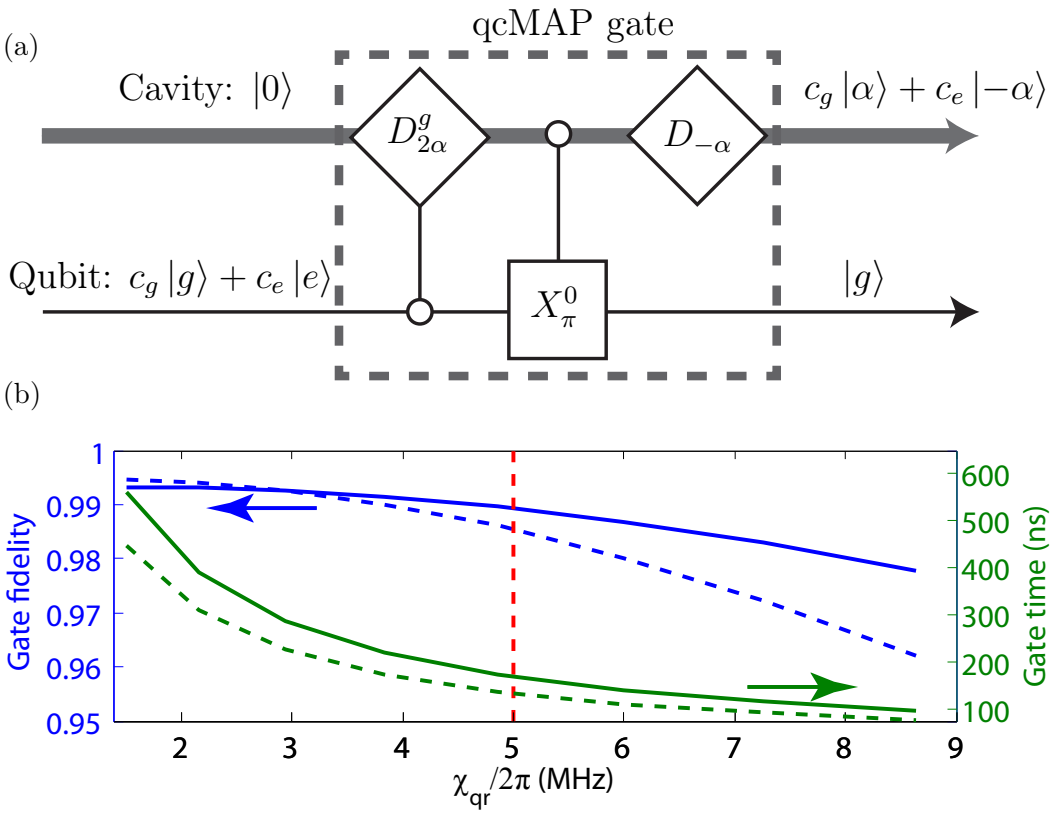

Figure 6.1: (a) The qcMAP gate comprises a conditional displacement of the cavity mode $D^g_{2\alpha}$ and a conditional rotation of the qubit X^0_π, mapping the qubit state to a superposition of two coherent states with opposite phases in the cavity. (b) Fidelity (blue) and gate time (green) of the qcMAP gate as a function of the dispersive coupling χ_{qr}, for two values 3.5 (solid line) and 7 (dashed line) of $\bar{n} = |\alpha|^2$. Increasing χ_{qr} decreases the gate time, however it also increases the cavity self-Kerr χ_{rr} which reduces the fidelity. This effect is more important for large coherent states, which explains the more important fidelity drop for $\bar{n} = 7$ photons. For $\bar{n} = 3.5$ photons, fidelities larger than 99% are obtained for χ_{qr} smaller than 5 MHz, with a gate time of ≈ 170 ns, much shorter than achievable coherence times.

well approximated by [Nigg 2012]

$$\frac{\mathbf{H}}{\hbar} = \omega_r \mathbf{a}^\dagger\mathbf{a} + \omega_q \mathbf{b}^\dagger\mathbf{b} - \frac{\chi_{rr}}{2}(\mathbf{a}^\dagger\mathbf{a})^2 - \frac{\chi_{qq}}{2}(\mathbf{b}^\dagger\mathbf{b})^2 - \chi_{qr}\mathbf{a}^\dagger\mathbf{a}\,\mathbf{b}^\dagger\mathbf{b}\,.$$

Here $\mathbf{a}$ and $\mathbf{b}$ are respectively the dressed mode operators of the resonator and the qubit ($|g\rangle$ and $|e\rangle$ are the first two eigenstates of $\mathbf{b}^\dagger\mathbf{b}$), ω_r and ω_q are their frequencies, χ_{qr} is the dispersive qubit-resonator coupling, and χ_{qq} and χ_{rr} the anharmonicities. Indeed, due to the coupling to a non-linear medium (the qubit), the cavity also inherits a Kerr effect that leads to the anharmonicity $\chi_{rr} = \chi_{qr}^2/4\chi_{qq}$ [Nigg 2012]. This nonlinearity can distort coherent states and sets a limit on the fidelity of the

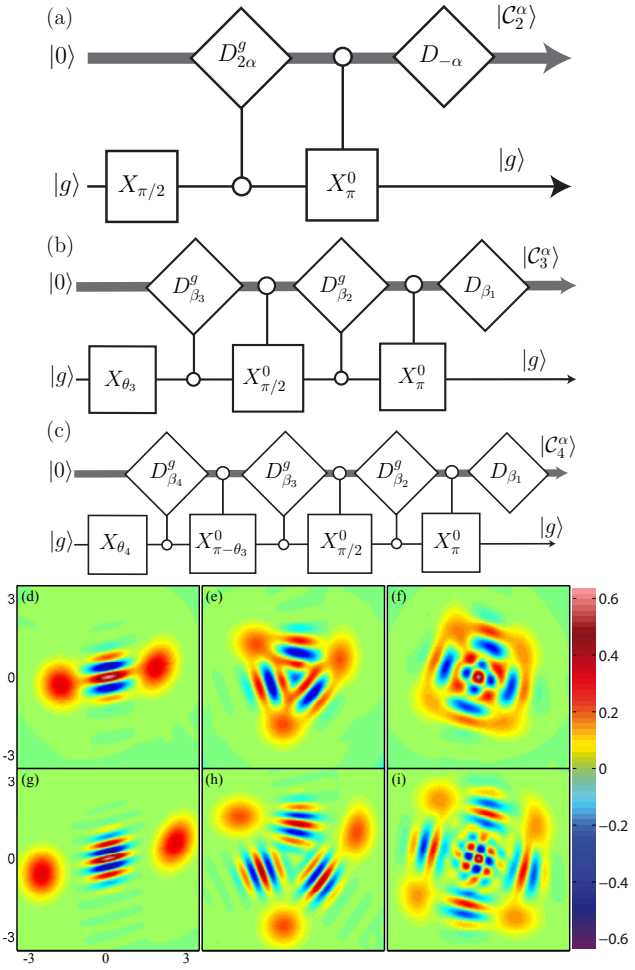

Figure 6.2: (a-c) Operations to prepare a 2 (a), 3 (b) and 4 (c) component SQOCS. $|\mathcal{C}_n^\alpha\rangle$ denotes a superposition of coherent states $|\alpha_1\rangle + \ldots + |\alpha_n\rangle$. In (b) and (c), $\beta_1 = \alpha_1$, $\beta_2 = \alpha_2 - \alpha_1$, $\beta_3 = \alpha_3 - \alpha_2$ and $\theta_3 = 2\arccos(1/\sqrt{3})$. In addition, in (c), $\beta_4 = \alpha_4 - \alpha_3$ and $\theta_4 = 2\arccos(1/2)$. (d-i) Wigner functions of the prepared states in presence of decoherence and the cavity self-Kerr. The upper figures correspond to $\bar{n} = 3.5$ photons in each coherent component and the lower ones correspond to 7 photons. We define the fidelity of the prepared state $|\psi_{\text{prep}}\rangle$ to the target $|C_n^\alpha\rangle$ as $F_{\text{prep}}(|C_n^\alpha\rangle) = |\langle\psi_{\text{prep}}|C_n^\alpha\rangle|^2$. We get $F_{\text{prep}}(|\mathcal{C}_2^\alpha\rangle) = 97.8\%$ (resp. 97.2%) for $\bar{n} = 3.5$ (resp. $\bar{n} = 7$) for a preparation time $T_{\text{prep}} = 170$ ns (resp. 135 ns). Similarly, $F_{\text{prep}}(|\mathcal{C}_3^\alpha\rangle) = 96.2\%$ (resp. 95.7%) and $T_{\text{prep}}(|\mathcal{C}_3^\alpha\rangle) = 320$ ns (resp. 225 ns); $F_{\text{prep}}(|\mathcal{C}_4^\alpha\rangle) = 91.9\%$ (resp. 91.5%) and $T_{\text{prep}}(|\mathcal{C}_3^\alpha\rangle) = 460$ ns (resp. 355 ns). Note the insensitivity of the preparation fidelity to the size of the coherent components. Due to the cavity self-Kerr, the components that are created earlier are deformed more than those created later.

gate.

While an unconditional cavity displacement D_α can be performed rapidly using a short pulse, the conditional cavity displacements D_α^g and qubit rotations X_θ^0 necessitate long pulses allowing one to selectively address the corresponding spectral line. In the qcMAP gate, X_π^0 transforms $|e,0\rangle$ to $|g,0\rangle$ while leaving $|g,2\alpha\rangle$ unchanged. To this end, we apply a pulse with a carrier frequency ω_q^0 and shape it such that it does not overlap with the spectral lines $\omega_q^n (= \omega_q^0 - n\chi_{qr})$ corresponding to the qubit frequencies when the cavity is in $|2\alpha\rangle$. Defining $\bar{n} = \langle\alpha|\mathbf{a}^\dagger\mathbf{a}|\alpha\rangle = |\alpha|^2$, the pulse length needs to be longer than a certain multiple of $1/4\bar{n}\chi_{qr}$. Here we take a Gaussian pulse of standard deviation $\sigma_t = 5/4\bar{n}\chi_{qr}$ and total length $6\sigma_t$ resulting in a π-pulse time of $15/2\bar{n}\chi_{qr}$ ($\approx$ 70ns for $\bar{n} = 3.5$ and $\chi_{qr}/2\pi = 5$MHz) for 99% fidelity. For the D_α^g operation, using a gaussian pulse to selectively address ω_r^g without driving $\omega_r^e = \omega_r^g - \chi_{qr}$ (the spectral lines are separated by χ_{qr} and not $4\bar{n}\chi_{qr}$) would require a relatively long time of $\approx 30/\chi_{qr}$. However, as detailed in section 6.2.6, D_α^g can be performed using two unconditional displacements and a waiting time between them; the whole operation time is significantly reduced to π/χ_{qr} ($\approx$ 100ns). The total gate time is $T_{\text{Gate}} \approx \frac{15+2\bar{n}\pi}{2\bar{n}\chi_{qr}}$ ($T_{\text{Gate}} \approx$ 170ns).

There is a compromise between decreasing the gate time with larger coupling strengths and increasing the undesirable effect of the cavity self-Kerr. The Kerr effect leads to a phase collapse of a coherent state with mean photon number $\bar{n}$ on a time scale of $T_{\text{collapse}} = \frac{\pi}{2\sqrt{\bar{n}}\chi_{rr}}$ [Haroche 2006, Section 7.2]. This phase collapse can be considered as an extra dephasing of the cavity and reduces the gate fidelity.

In Fig. 6.1(b), we compute the fidelity and time of the qcMAP gate in the presence of the cavity self-Kerr but without any decoherence. We take $\chi_{qq}/2\pi = 300$ MHz and vary χ_{qr}. The fidelity F of the gate $\mathcal{U}$ is defined as $F = \min_{c_g,c_e} |(c_g^\dagger\langle g,\alpha| + c_e^\dagger\langle g,-\alpha|)\,\mathcal{U}\,(c_g|g,0\rangle + c_e|e,0\rangle)|^2$. The gate fidelity and the gate time decrease with increasing χ_{qr}. The decrease in fidelity is slightly worse for higher $\bar{n}$ since the coherent state becomes more exposed to the cavity's nonlinearity. The maximum fidelity of $\approx 99.5\%$ is set by the fidelity of the conditional π-pulse which can be arbitrarily improved using longer pulses (at the expense of longer gate times). In presence of decoherence, one should increase the coupling strength (and therefore decrease the gate time) up to values that make the phase collapse due to the cavity self-Kerr comparable to other dephasing times.

6.2.3 Preparing arbitrary superpositions of coherent states in one and two cavity modes

One can tailor any SQOCS by applying a sequence of qcMAP gates (see [Raimond 2010] for another method based on the dynamical quantum Zeno effect, and [Lutterbach 2000] for a non deterministic scheme). The protocols to generate 2, 3 and 4-component SQOCS are given in Fig. 6.2(a-c). The master equation simulation of these preparation protocols lead to the Wigner functions shown in Fig. 6.2(d-i). The corresponding parameters are $\chi_{qr}/2\pi = 5$ MHz, $\chi_{qq}/2\pi = 300$ MHz and $\chi_{rr}/2\pi = 20$ kHz. The qubit relaxation and dephasing times

are $T_1 = T_2 = 20$ μs, and the cavity decay time is $T_{\rm cav} = 100\mu$s. Recent experiments with transmon qubits coupled to 3D resonators [Paik 2011, Rigetti 2012] indicate that such parameters are realistic. More details on the preparation scheme can be found in section 6.2.6. In particular, one notes the insensitivity of the fidelity to the size of the coherent components. The ability to prepare multi-component SQOCS also implies that the qcMAP gate can be used to store *multi*-qubit states in the resonator.

The qcMAP gate can also be used on a qubit coupled to two spatially separated cavities [Kirchmair *et al.* 2012] to prepare *non-local* mesoscopic superposition states of the form $|-\alpha,-\alpha\rangle + |\alpha,\alpha\rangle$. Such highly non-classical states achieve a maximum violation of Bell's inequality as soon as $|\alpha|^2 \approx 2$ [Haroche 2006, Section 7.6]. The preparation scheme is sketched in Fig. 6.3. As in the single-mode case, the sequence duration is set by the length of the selective operations. The two conditional displacements are performed simultaneously and their time is given by $\max(\pi/\chi_{qr_1}, \pi/\chi_{qr_2})$ (χ_{qr_1} and χ_{qr_2} being the dispersive coupling between the qubit and cavity modes). The conditional π-pulse is performed in a time of order $15/2\bar{n}(\chi_{qr_1} + \chi_{qr_2})$. Therefore, the preparation time for a non-local superposition is even shorter than the single-mode case. However, in addition to the cavity self-Kerr effects $\chi_{r_1r_1}$ and $\chi_{r_2r_2}$, we also have a cross-Kerr term $\chi_{r_1r_2}\mathbf{a}_1^\dagger\mathbf{a}_1\ \mathbf{a}_2^\dagger\mathbf{a}_2$ between the two modes ($\chi_{r_1r_2}$ given by $2\sqrt{\chi_{r_1r_1}\chi_{r_2r_2}}$ [Nigg 2012]). We simulate this scheme taking $\chi_{qr_1}/2\pi = 5$ MHz, $\chi_{qr_2}/2\pi = 4$ MHz, $\chi_{r_1r_2}/2\pi = 20$ kHz, $\chi_{r_1r_1}/2\pi = 20$ kHz, $\chi_{r_2r_2}/2\pi = 13$ kHz and $\chi_{qq}/2\pi = 300$ MHz, and coherence times of $T_1 = T_2 = 20$ μs for the qubit and $T_{\rm cav} = 100\mu$s for the two cavities. The entangled state $|\alpha,\alpha\rangle + |-\alpha,-\alpha\rangle$ with $|\alpha|^2 = 1.5$ is prepared with a fidelity of $\approx 96\%$ in 190 ns. By measuring the two-mode Wigner function at four points, as explained in [Banaszek 1999, Milman 2005, Sarlette 2012], we retrieved a Bell signal of 2.5, largely violating Bell's inequality (the maximum possible Bell signal is $2\sqrt{2}$).

6.2.4 Using the qcMAP gate to entangle qubits

We have shown that the qcMAP gate generates highly non-classical cavity field states, making it a promising tool to store multi-qubit states in the cavity [Gottesman 2001, Vitali 1998, Zippilli 2003]. An extension of the qcMAP gate uses the cavity as a bus to perform *multi*-qubit gates. As shown in Fig. 6.4(a), starting from state $c_g|g\rangle + c_e|e\rangle$ for one qubit, we use the qcMAP gate to map this state to a multi-qubit entangled state $c_g|gg\cdots g\rangle + c_e|ee\cdots e\rangle$. A first conditional displacement $D^g_{2\alpha}$ prepares $c_g|2\alpha, gg\cdots g\rangle + c_e|0, eg\cdots g\rangle$. The time for this operation is $\approx \pi/\chi_1$. Applying, in parallel, a conditional π-pulse X^0_π on $n_q - 1$ qubits, we prepare an (n_q+1)-body entangled state $c_g|2\alpha, gg\cdots g\rangle + c_e|0, ee\cdots e\rangle$. The time for this operation is fixed by the minimum dispersive coupling strength. Next, we perform a conditional displacement $D^{gg\cdots g}_{-2\alpha}$ disentangling the cavity from the qubits which are left in $c_g|gg\cdots g\rangle + c_e|ee\cdots e\rangle$, while the cavity is in vacuum. This conditional displacement can be performed in a very short time $\approx \pi/(\chi_1 + \cdots + \chi_{n_q})$, which decreases with the number of qubits. Such an operation can be compared to

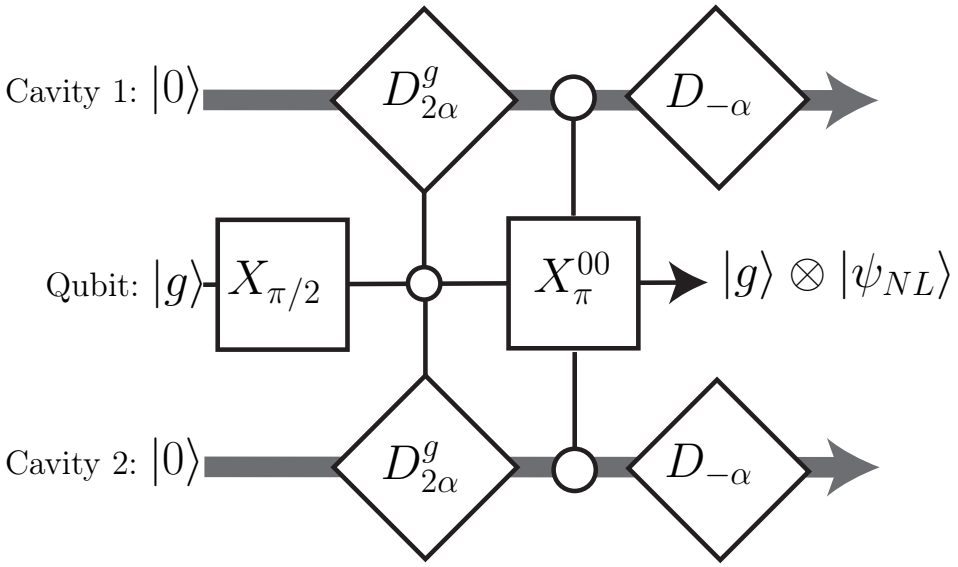

Figure 6.3: Protocol for preparing a non-local entangled state between two cavities that are dispersively coupled to a single qubit. Two simultaneous conditional displacements lead to a tripartite entanglement, preparing the state $|g, 2\alpha, 2\alpha\rangle + |e, 0, 0\rangle$; A π-pulse on the qubit, conditioned on both cavities being in vacuum, will then disentangle the qubit from the cavities leaving them in an entangled state $|\psi_{\rm NL}\rangle = (|-\alpha, -\alpha\rangle + |\alpha, \alpha\rangle)/N$, where N is a normalization constant. We obtain a fidelity of $\approx 96\%$ in 190ns, leading to a Bell signal of 2.5.

the joint readout of qubits in the strong dispersive regime [Filipp 2009, Chow 2010] where, by driving the cavity at a frequency corresponding to a particular joint state of qubits, one can measure its population with a high fidelity.

In Fig. 6.4(b), we plot the gate time and fidelity as a function of the dispersive coupling χ_{qr}. A limiting effect on the fidelity is the cavity self-Kerr which increases additively with the number of qubits. Despite this effect, for $\chi_{qr}/2\pi = 3$ MHz, we prepare a 5-qubit GHZ state with a $\approx 97.5\%$ fidelity in 300 ns. Furthermore, this gate can be performed between any subset of qubits coupled to the bus and does not require any qubit tunability or employment of higher excited states.

6.2.5 Summary and discussion

In conclusion, we have introduced the qcMAP gate which maps a qubit state to a superposition of two coherent states in a cavity. The qcMAP gate is then used to prepare 2, 3 and 4 component SQOCS, as well as a non-local mesoscopic field state superposition in two cavity modes.

Using this gate, the resonator could be used as a quantum "disc drive" to store *multi*-qubit states in a multi-component SQOCS. A SQOCS of maximum photon number $\bar{n}$ would be contained in a disc in phase space of radius $\sqrt{\bar{n}}$. In this disc, we

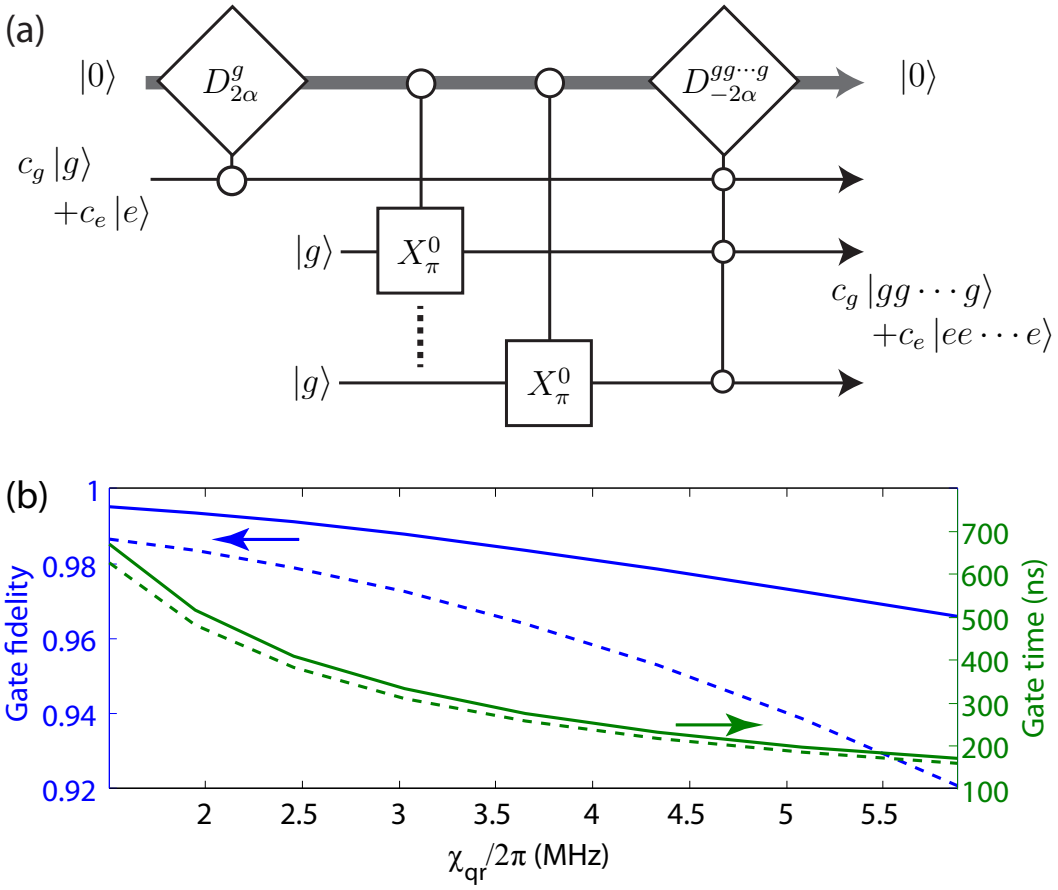

Figure 6.4: (a) The qcMAP gate can be used to map a single qubit state $c_g|g\rangle+c_e|e\rangle$ to a GHZ-type state $|\mathrm{GHZ}\rangle = c_g|gg\cdots g\rangle + c_e|ee\cdots e\rangle$ for an arbitrary number of qubits; The conditional rotations of qubits can be done in parallel and therefore the total preparation time does not increase with the number of qubits n_q (it actually slightly decreases with n_q since the conditional displacement $D^{gg\cdots g}_{-2\alpha}$ can be performed faster). (b) Gate fidelity (blue) and time (green) as a function of the dispersive coupling strength for 3 (solid lines) and 5 qubits (dashed lines); we take the same dispersive shifts $\chi_{qr}/2\pi = 3$ MHz for all qubits (not a necessary assumption) and $|\alpha|^2 = 3.5$. Like in Fig. 6.1, the simulation does not include decoherence but takes into account the cavity self-Kerr. For larger n_q, the cavity self-Kerr increases which leads to a drop in gate fidelity, particularly for high dispersive coupling strengths. We obtain fidelities in excess of 99% (resp. 98%) for $n_q = 3$ (resp. $n_q = 5$) with a gate time of 400 ns.

could fit coherent components which are at least separated by a minimal distance $\sqrt{m}$. Hence, the maximum non-orthogonality of two coherent components is e^{-4m}, which is a very small systematic storage error for moderate m (for $m = 2$, $e^{-4m} \approx 10^{-4}$). The number of coherent components we can fit in this disc is $\approx \bar{n}/m$ and

hence this $\bar{n}$ photon SQOCS could store a register of $\approx \log_2(\bar{n}/m)$ qubits. The effective decay rate of such a state would be $\bar{n}\kappa$ where κ is the decay rate of one photon.

Using the qcMAP gate, the cavity can also be used as a bus to perform a multi-qubit gate, preparing in particular, GHZ states. Finally, any multi-qubit gate can be performed by concatenating such qcMAP gates.

6.2.6 Detailed sequence for conditional displacements and preparation of superpositions of coherent states

In this section, we describe in detail the D_α^g operation and provide the full sequence of steps that prepares the two, three and four component superposition of quasi-orthogonal coherent states with performances announced in the section. Finally, a simple computation shows the first-order effect of the cavity self-Kerr on a coherent state.

While the conditional qubit rotation X_θ^0 is performed through long enough pulses ensuring a selective addressing of spectral lines, the conditional cavity displacement D_α^g is composed of two short unconditional displacements separated by a waiting time. This reduces the D_α^g operation time from $\approx 30/\chi_{qr}$ to $\approx \pi/\chi_{qr}$. We consider the rotating frame of the Hamiltonian $\omega_r a^\dagger a + \omega_q b^\dagger b - \frac{\chi_{qq}}{2}(b^\dagger b)^2$. We perform a first unconditional displacement D_β of the cavity through a very short pulse that displaces the cavity regardless of the qubit state. We wait for time T_{wait}, and apply a second unconditional displacement $D_{-\beta e^{i\chi_{qr}T_{wait}}}$. Neglecting the cavity self-Kerr, this sequence of operations leads to the following unitary evolution:

$$\begin{aligned}\mathcal{U} &= D_{-\beta e^{i\chi_{qr}T_{wait}}} e^{i\chi_{qr}T_{\text{wait}}a^\dagger a b^\dagger b} D_\beta \\ &= e^{-i|\beta|^2\sin(\chi_{qr}T_{wait})}|g\rangle\langle g| \otimes D_{\beta-\beta e^{i\chi_{qr}T_{wait}}} \\ &\qquad + |e\rangle\langle e| \otimes e^{-i\chi_{qr}T_{\text{wait}}a^\dagger a}.\end{aligned}$$

Taking $\alpha = \beta - \beta e^{i\chi_{qr}T_{wait}}$, we have

$$\begin{aligned}\mathcal{U}|g,0\rangle &= e^{-i|\beta|^2\sin(\chi_{qr}T_{wait})}|g,\alpha\rangle, \\ \mathcal{U}|e,0\rangle &= |e,0\rangle.\end{aligned}$$

Up to a phase term of $e^{-i|\beta|^2\sin(\chi_{qr}T_{wait})}$ that we can take into account in future qubit pulses, this is precisely the conditional displacement. In particular, taking $T_{\text{wait}} = \pi/\chi_{qr}$, we have a conditional displacement of $\alpha = 2\beta$ in a time of π/χ_{qr}.

In Figure 6.5, we provide the complete sequence of operations which generate superpositions of two, three and four quasi-orthogonal coherent components.

Let us finish by a simple computation showing the first order effects of the cavity self-Kerr. Considering a short time τ such that $\varepsilon = \chi_{rr}\tau/2 \ll 1$, we can show that the first order contribution of the cavity self-Kerr is simply an extra deterministic phase accumulation of the cavity's coherent states that we can take into account in future cavity displacements and qubit rotations. Indeed, the distortion of the

coherent states happens only as a second order term with respect to ε. Consider a coherent state $|\alpha\rangle$ of average photon number $\bar{n} = |\alpha|^2$. We define $|\psi_\varepsilon\rangle = e^{i\varepsilon(a^\dagger a)^2}|\alpha\rangle$ and we search for a coherent state of amplitude α_ε and global phase ϕ_ε: $e^{i\phi_\varepsilon}|\alpha_\varepsilon\rangle$, which is close to $|\psi_\varepsilon\rangle$ for small ε. We have $\langle\psi_\varepsilon|a|\psi_\varepsilon\rangle = \alpha e^{i\varepsilon}e^{\bar{n}(e^{2i\varepsilon}-1)} = \langle\alpha_\varepsilon|a|\alpha_\varepsilon\rangle$ for $\alpha_\varepsilon = \alpha e^{i\varepsilon}e^{\bar{n}(e^{2i\varepsilon}-1)} = \alpha e^{i\varepsilon(2\bar{n}+1)} + O(\varepsilon^2)$. In order to find ϕ_ε, we compute

$$\begin{aligned} e^{-i\phi_\varepsilon}\langle\alpha_\varepsilon|\psi_\varepsilon\rangle &= e^{-i\phi_\varepsilon}\langle\alpha|e^{i\varepsilon(-(2\bar{n}+1)a^\dagger a+(a^\dagger a)^2)}|\alpha\rangle + O(\varepsilon^2) \\ &= e^{-i\phi_\varepsilon}(1 - i\varepsilon\bar{n}^2) + O(\varepsilon^2) \end{aligned}$$

Taking $\phi_\varepsilon = -\varepsilon\bar{n}^2$, we get $e^{-i\phi_\varepsilon}\langle\alpha_\varepsilon|\psi_\varepsilon\rangle = 1 + O(\varepsilon^2)$. Therefore, as a first order approximation for the effect of the cavity self-Kerr, we have

$$e^{i\chi_{rr}\tau(a^\dagger a)^2/2}|\alpha\rangle \sim e^{-i\chi_{rr}\tau\bar{n}^2/2}|e^{i\chi_{rr}\tau(\bar{n}+\frac{1}{2})}\alpha\rangle.$$

In the simulations of this section, we took into account this extra coherent state rotation for the subsequent displacements. The overall phases were corrected by appropriately choosing the subsequence qubit pulse phases.

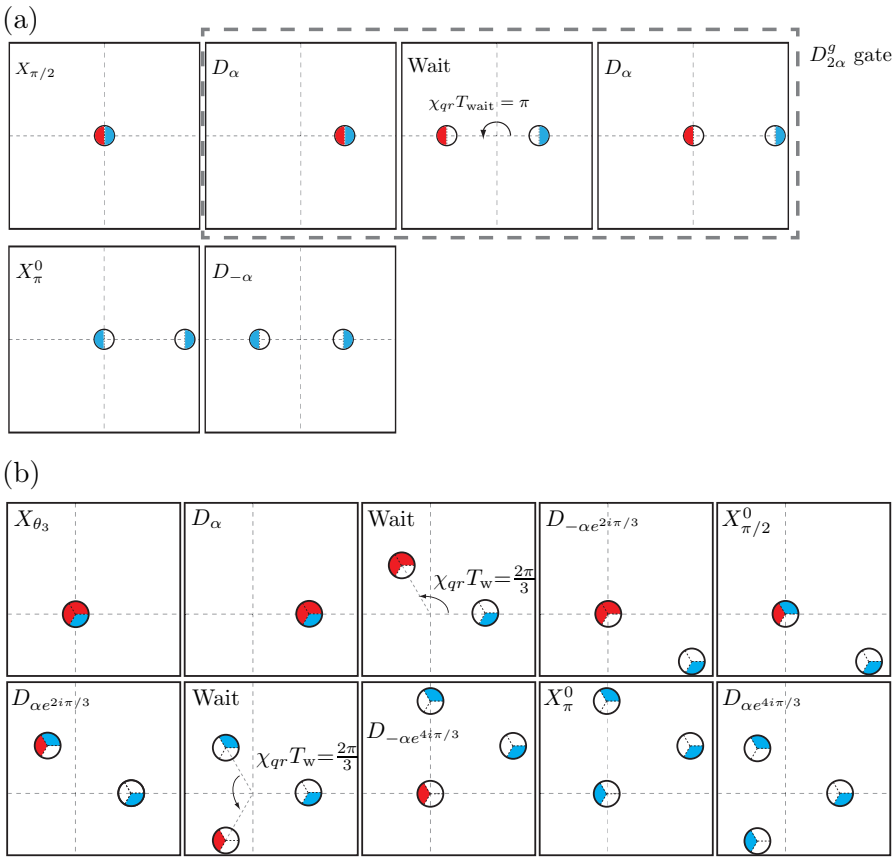

Figure 6.5: Detailed sequence to prepare a superposition of 2 (a) and 3 (b) quasi-orthogonal coherent states (SQOCS). See Fig. 6.6 for a 4 component SQOCS. Each frame is the Fresnel diagram of the field in the resonator. The two dotted lines represent two orthogonal quadratures, and intersect at 0. The frames are ordered from left to right and top to bottom. A circle of center α in the diagram refers to a coherent state of amplitude α. The fraction of the circle colored in blue [resp: red] corresponds to the population of the qubit which is in the ground state [resp: excited state]. Eg. frame 3 in (a) corresponds to state $\frac{1}{\sqrt{2}}(|g,\alpha\rangle + |e,-\alpha\rangle)$. In particular we represent $\frac{1}{\sqrt{2}}|g,\alpha\rangle$ with the right circle $(+\alpha)$, with a qubit in $|g\rangle$ (blue color) and a 50% population (half full). Fast (here considered instantaneous) displacements D_γ transform any coherent state $|\alpha\rangle$ to $|\alpha+\gamma\rangle$ regardless of the qubit state. The Fresnel diagram is in a rotating frame which leaves states of the form $|g,\alpha\rangle$ unchanged, while $|\psi(0)\rangle = |e,\alpha\rangle$ evolves as $|\psi(t)\rangle = |e,\alpha e^{i\chi_{qr}t}\rangle$. A selective pulse X^0_θ rotates the qubit state when the resonator is in the zero photon state $|0\rangle$. Graphically, this corresponds to changing a fraction of the color of a circle centered at 0. In (b), $\theta_3 = 2\arccos(1/\sqrt{3})$. A symbol in each frame n gives the operation performed to go from frame $n-1$ to n.

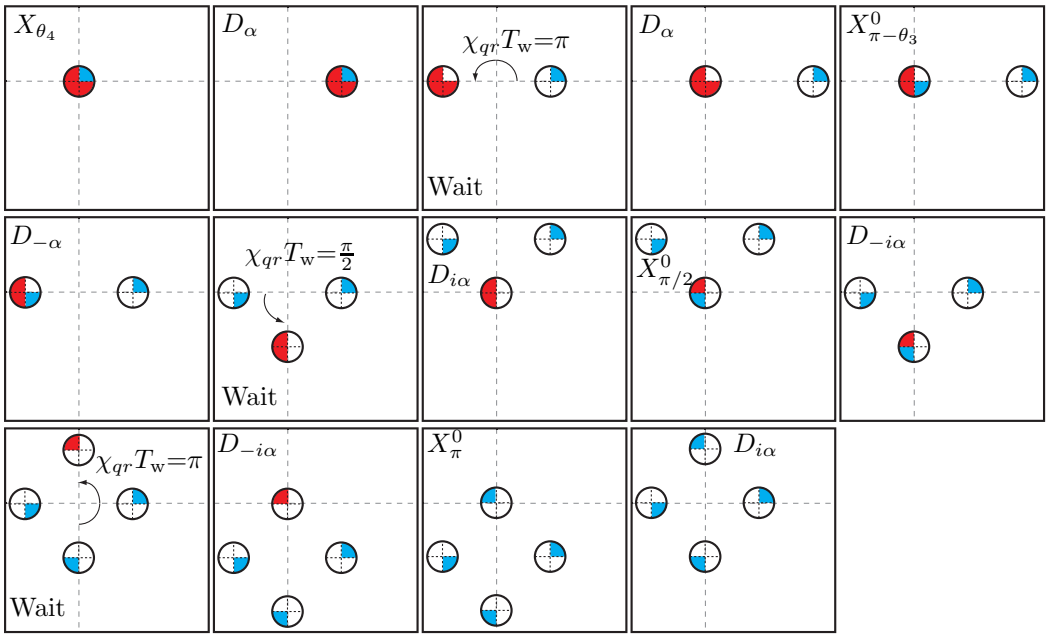

Figure 6.6: Detailed sequence to prepare a superposition of 4 quasi-orthogonal coherent states. We have $\theta_3 = 2\arccos(1/\sqrt{3})$ and $\theta_4 = 2\arccos(1/2)$. See caption of Fig. 6.5 for details on this diagrammatic representation.

6.3 Hardware-efficient autonomous quantum error correction

This section describes a very recent proposal we obtained in collaboration with G. Kirchmair, B. Vlastakis, R. Shoelkopf, M. Devoret and M. Mirrahimi [Leghtas 2012c].

We propose a new method to autonomously correct for errors of a logical qubit encoded in a cavity induced by energy relaxation of the qubit. This scheme encodes the logical qubit as a multi-component superposition of coherent states in a harmonic oscillator, more specifically a cavity mode. The sequences of encoding, decoding and correction operations employ the non-linearity provided by a single physical qubit coupled to the cavity. We layout in detail how to implement these operations in a practical system. This proposal directly addresses the task of building a hardware-efficient and technically realizable quantum memory.

6.3.1 Introduction

Long-lived coherence is a prerequisite for quantum computation. The last two decades have seen impressive improvements in the coherence times of qubits and cavities. The results of hardware improvement have been so substantial that the quality threshold needed for quantum error correction (QEC) [Shor 1995, Steane 1996] to be effective is within reach [Rigetti 2012]. Since the birth of QEC, many possible implementations have been proposed. We classify these QEC schemes as being either measurement based or autonomous. Measurement based QEC (MBQEC) consists of periodically measuring error syndromes and feeding back appropriate correction pulses conditioned on the measurement results [Chiaverini 2004]. In autonomous QEC (AQEC), however, no classical information needs to be extracted. Instead, it is sufficient to transfer the random errors to an ancillary quantum system which is then reset to remove the entropy [Schindler 2011, Reed 2012b]. Furthermore, continuous time implementations can be used for both MBQEC [Ahn 2002] and AQEC [Kerckhoff 2010].

All these methods encode the single logical qubit to be protected in a register of several physical qubits. While at least five physical qubits are needed to correct for single phase and bit flip errors of the register [Gottesman 1996], it has been shown that when the decoherence is due to a dominant quantum noise process such as amplitude damping, fewer resources might be needed. Indeed, [Leung 1997] propose a four-qubit code correcting for single amplitude damping errors.

In this section, we propose a QEC scheme which replaces the register of several qubits by a single high-Q cavity mode, coupled to a single physical qubit. The vastness of the Hilbert space of the harmonic oscillator, combined with the control provided by operations described in [Leghtas 2012b], allows this replacement. In our scheme, the logical qubit is encoded in a multi-component superposition of coherent states in the cavity mode, the coupled qubit bringing the non-linearity necessary for the manipulation of coherent states. This simple cavity-qubit system

is the standard building block of both circuit and cavity quantum electrodynamics (QED) experiments [Schoelkopf 2008]. Here, we show that this minimal hardware, together with an additional low-Q cavity mode used for qubit readout or qubit reset, is sufficient to correct for the dominant source of errors, namely photon damping in the high-Q cavity. Moreover, the number of independent quantum noise channels corrupting the logical information, would not increase with the number of encoded qubits, which represents an additional advantage of our protocol over a multi-qubit register. A cavity mode is thus a powerful hardware for protecting quantum information [Gottesman 2001, Vitali 1998, Zippilli 2003].

Previous proposals [Vitali 1998, Zippilli 2003] have suggested that states with a given photon number parity of a cavity mode (parity states) can be used to encode quantum information. There, stabilization of a parity manifold is obtained by a quantum non-demolition (QND) parity measurement and photon injection when needed. Such a scheme replaces the decoherence due to photon damping by a slower, unusual dephasing due to a drift in the parity manifold.

Here, we go a step forward towards a readily realizable quantum memory, by proposing a scheme for efficiently encoding a logical qubit in a particular cavity state that is fully protected against single quantum jumps due to photon damping. Depending on the experimental constraints, two approaches are possible. The first approach, a MBQEC scheme, keeps track of the quantum jumps by stroboscopic QND measurements of the photon number parity and corrects for the decay by an appropriate decoding and encoding operation sequence. The second approach, an AQEC scheme, transfers the entropy of the cavity state to an ancilla qubit and then removes this entropy by reseting the qubit state. All the encoding, decoding and correction operations of both approaches can be performed using tools that have been introduced in our recent paper [Leghtas 2012b].

6.3.2 Cavity logical 1 and logical 0, and MBQEC

An arbitrary qubit state $c_g|g\rangle+c_e|e\rangle$ (we denote by $|g\rangle$ and $|e\rangle$ the ground and excited state) is mapped into a multi-component coherent states $|\psi_\alpha^{(0)}\rangle = c_g|\mathbb{C}_\alpha^+\rangle + c_e|\mathbb{C}_{i\alpha}^+\rangle$, where

$$|\mathbb{C}_\alpha^\pm\rangle = \mathcal{N}(|\alpha\rangle \pm |-\alpha\rangle)\ , \quad |\mathbb{C}_{i\alpha}^\pm\rangle = \mathcal{N}(|i\alpha\rangle \pm |-i\alpha\rangle)\ .$$

$\mathcal{N}$ ($\approx 1/\sqrt{2}$) is a normalizing factor and $|\alpha\rangle$ denotes a coherent state of complex amplitude α, chosen such that $|\alpha\rangle, |-\alpha\rangle, |i\alpha\rangle, |-i\alpha\rangle$ are quasi-orthogonal. We have recently proposed a toolbox of operations which efficiently prepare these states $|\mathbb{C}_\alpha^\pm\rangle, |\mathbb{C}_{i\alpha}^\pm\rangle$ [Leghtas 2012b]. The logical 0: $|\mathbb{C}_\alpha^+\rangle$, and logical 1: $|\mathbb{C}_{i\alpha}^+\rangle$, have some remarkable properties: the state $|\psi_\alpha^{(0)}\rangle$ evolves, after a quantum jump due a photon loss, to $|\psi_\alpha^{(1)}\rangle = \mathbf{a}|\psi_\alpha^{(0)}\rangle / \left\|\mathbf{a}|\psi_\alpha^{(0)}\rangle\right\| = c_g|\mathbb{C}_\alpha^-\rangle + ic_e|\mathbb{C}_{i\alpha}^-\rangle$, where $\mathbf{a}$ is the annihilation operator. Furthermore, in absence of jumps during a time interval t, $|\mathbb{C}_\alpha^\pm\rangle$ and $|\mathbb{C}_{i\alpha}^\pm\rangle$ deterministically evolve to $|\mathbb{C}_{\alpha e^{-\kappa t/2}}^\pm\rangle$ and $|\mathbb{C}_{i\alpha e^{-\kappa t/2}}^\pm\rangle$, where κ is the cavity decay rate. Now, one can find a unitary transformation mapping $|\mathbb{C}_{\alpha e^{-\kappa t/2}}^-\rangle$ and $i|\mathbb{C}_{i\alpha e^{-\kappa t/2}}^-\rangle$ respectively to $|\mathbb{C}_\alpha^+\rangle$ and $|\mathbb{C}_{i\alpha}^+\rangle$. Therefore, whenever a jump is detected,

such a unitary transformation can restore the state independently of the superposition amplitudes c_g and c_e, thus undoing the action of decoherence. Moreover, the states $|\psi_\alpha^{(0)}\rangle$ and $|\psi_\alpha^{(1)}\rangle$ are eigenstates of the photon number parity operator $\mathbf{\Pi} = \exp(\mathbf{i}\pi\mathbf{a}^\dagger\mathbf{a})$, corresponding respectively to even and odd number of photons. Therefore, measuring continuously the parity observable reveals quantum jumps and can trigger the correction step.

Furthermore, one does not need to immediately correct when the parity measurement indicates a quantum jump. Indeed, continuing with a stroboscopic QND measurement of the parity observable, one can keep track of how many quantum jumps occured. If a second photon is lost, the state jumps to $|\psi_\alpha^{(2)}\rangle = \mathbf{a}^2|\psi_\alpha^{(1)}\rangle / \left\|\mathbf{a}^2|\psi_\alpha^{(1)}\rangle\right\| = c_g|\mathbb{C}_\alpha^+\rangle - c_e|\mathbb{C}_{i\alpha}^+\rangle$, which switches back the parity to even. A third jump gives $|\psi_\alpha^{(3)}\rangle = c_g|\mathbb{C}_\alpha^-\rangle - ic_e|\mathbb{C}_{i\alpha}^-\rangle$ with an odd parity. Finally, the fourth jumps reestablishes the initial state $\mathbf{a}^4|\psi_\alpha^{(0)}\rangle / \left\|\mathbf{a}^4|\psi_\alpha^{(0)}\rangle\right\| = |\psi_\alpha^{(0)}\rangle$.

We define the unitary operations $\mathcal{U}_{\text{encode}}$ and $\mathcal{U}_{\text{decode}}$ such that for all c_g and c_e,

$$\begin{aligned}\mathcal{U}_{\text{encode}} :&(c_g|g\rangle + c_e|e\rangle) \otimes |0\rangle \rightarrow |g\rangle \otimes (c_g|\mathbb{C}_\alpha^+\rangle + c_e|\mathbb{C}_{i\alpha}^+\rangle)\ .\\ \mathcal{U}_{\text{decode}} :&|g\rangle \otimes (c_g|\mathbb{C}_\alpha^+\rangle + c_e|\mathbb{C}_{i\alpha}^+\rangle) \rightarrow (c_g|g\rangle + c_e|e\rangle) \otimes |0\rangle.\end{aligned}$$

In section 6.3.4, we give a detailed pulse sequence which could inefficiently realize these operations. The stroboscopic QND parity measurements indicates at each time how many jumps have occurred, and hence, which orthogonal states encode the logical qubit. Similarly to $\mathcal{U}_{\text{decode}}$, one can consider 3 other decoding operations bringing back the new codewords to the qubit state $c_g|g\rangle + c_e|e\rangle$. Indeed, we will have four decoding operations denoted by $\mathcal{U}_{\text{decode}}^{(c)}$ for $c \equiv n_{\text{jumps}}$ (modulo 4) jumps detected. For example, if after a QND measurement time T_m, $n_{\text{jumps}} = 7$ parity changes are detected, we have $c = 3$, and $\mathcal{U}_{\text{decode}}^{(3)}$ is applied, thus transforming $|g\rangle \otimes (c_g|\mathbb{C}_{\alpha e^{-\kappa T_m/2}}^-\rangle - ic_e|\mathbb{C}_{i\alpha e^{-\kappa T_m/2}}^-\rangle)$ to $(c_g|g\rangle + c_e|e\rangle) \otimes |0\rangle$. The measurement time T_m should be chosen such that $|\pm\alpha e^{-\kappa T_m/2}\rangle$ and $|\pm i\alpha e^{-\kappa T_m/2}\rangle$ remain quasi-orthogonal. We may compute the overlap $\left|\langle\alpha e^{-\kappa T_m/2}|i\alpha e^{-\kappa T_m/2}\rangle\right|^2 = e^{-2|\alpha|^2 e^{-\kappa T_m}}$. For an overlap of, for instance, e^{-6}, we get $T_m = \log(|\alpha|^2/3)/\kappa$. A new cycle then starts by re-encoding the qubit state into $c_g|\mathbb{C}_\alpha^+\rangle + c_e|\mathbb{C}_{i\alpha}^+\rangle$, performing a QND parity measurement for time T_m, decoding and so on. An alternative can avoid decoding back to the qubit. We could apply, after each measurement time T_m, a correction operation which maps $|\psi_{\alpha e^{-\kappa T_w}}^{(c)}\rangle$ to $|\psi_\alpha^{(c)}\rangle$, thus re-pumping energy back into the damped state.

We denote $\varepsilon_{\text{meas}}$ the probability to make an erroneous measurement or to have a single jump or more during the measurement. Also, we denote by $\lambda_{\text{jump}} = \kappa\bar{n}$ the rate at which a quantum jump happens for the cavity state with an average number of $\bar{n}$ photons. If M is the number of measurements we perform during the time interval T_m (we assume $\lambda_{\text{jump}} T_m/M \ll 1$), the probability of having two jumps or more between two measurements is well approximated by $\varepsilon_{\text{wait}} = \frac{1}{2!}\frac{\lambda_{\text{jump}}^2 T_m^2}{M^2}$ (the number of jumps follows the Poisson law). The fidelity of the recovered state with respect to $c_g|g\rangle + c_e|e\rangle$ at the end of one encoding-measuring-decoding procedure is larger than

$F_{\rm QEC} \approx (1-\varepsilon_{\rm decode})\left((1-\varepsilon_{\rm meas})(1-\varepsilon_{\rm wait})\right)^M (1-\varepsilon_{\rm encode})$. Here, $(1-\varepsilon_{\rm decode})$ and $(1-\varepsilon_{\rm encode})$ represent the fidelities of the encoding and the decoding operations, taking into account various imperfections and in particular the decoherence during the operation time. Noting that $\varepsilon_{\rm wait}$ depends on the number of measurements M, in order to maximize $F_{\rm QEC}$, one should take $M \approx \kappa\bar{n}T_m/\sqrt{2\varepsilon_{\rm meas}}$. This corresponds to an equilibrium between the probability of an erroneous measurement, $\varepsilon_{\rm meas}$, and probability of having more than a single jump between two measurements, $\varepsilon_{\rm wait}$. In the limit where $2M\varepsilon_{\rm meas} = \kappa\bar{n}T_m\sqrt{2\varepsilon_{\rm meas}} \gg \varepsilon_{\rm decode}, \varepsilon_{\rm encode}$, the effective lifetime of the protected state is $\kappa_{eff} \approx \kappa\bar{n}\sqrt{2\varepsilon_{\rm meas}}$. One cycle of the measurement-based quantum error correction is performed in time $T_e + T_m + T_d$, this cycle can then be reiterated.

QND parity measurements have been previously performed through Ramsey-type experiments within the context of cavity QED with Rydberg atoms [Haroche 2007]. Such a measurement scheme can also be adapted to circuit QED experiments but necessitates a flux bias line which would allow to tune the qubit near and out of resonance with the cavity mode. Also, fast and reliable measurements would necessitate application of quantum limited amplifiers.

In order to avoid such further experimental complications, we propose in the next section an AQEC scheme which does not require any real-time measurement-based quantum feedback.

6.3.3 Autonomous QEC

AQEC is realized by using an auxiliary quantum system that we take here to be a qubit. The idea consists in finding a unitary operation $\mathcal{U}_{\rm correct}$ such that

$$\begin{aligned} \mathcal{U}_{\rm correct} : |g\rangle \otimes |\mathbb{C}^{\pm}_{\alpha e^{-\kappa t/2}}\rangle &\rightarrow \frac{1}{\sqrt{2}}(|g\rangle \pm |e\rangle) \otimes |\mathbb{C}^{+}_{\alpha}\rangle, \\ |g\rangle \otimes |\mathbb{C}^{\pm}_{i\alpha e^{-\kappa t/2}}\rangle &\rightarrow \frac{1}{\sqrt{2}}(|g\rangle \pm |e\rangle) \otimes |\mathbb{C}^{+}_{i\alpha}\rangle. \end{aligned} \tag{6.1}$$

This unitary operation transfers the entropy of the quantum system to be protected to the auxiliary one. Now, resetting the state of the auxiliary system, we can evacuate the entropy, restoring the initial total state. The AQEC scheme consists of encoding the qubit state $c_g|g\rangle + c_e|e\rangle$ in the state $|\psi^{(0)}_{\alpha}\rangle$ and performing the above unitary transformation followed by the reset of the auxiliary qubit in a stroboscopic manner. Assuming that at most one quantum jump can happen between two correction operations separated by time T_w, the state before the correction is given either by $|\psi^{(0)}_{\alpha e^{-\kappa T_w/2}}\rangle$ or $|\psi^{(1)}_{\alpha e^{-\kappa T_w/2}}\rangle$, and after the correction operation we have restored the initial state $|\psi^{(0)}_{\alpha}\rangle$. This whole process can be completed by a decoding step transferring the quantum information back onto the qubit (see Fig. 6.7).

We now quantify the performance of our AQEC scheme. Let $\rho^{(k)}_{\alpha}$ denote the projector onto the state $|\psi^{(k)}_{\alpha}\rangle$ for $k = 0, \cdots, 3$. The effect of the waiting time T_w between two corrections may be modeled by a Kraus operator

$$\mathbb{K}_w : \rho^{(0)}_{\alpha} \quad \rightarrow \quad p_0\rho^{(0)}_{\tilde{\alpha}} + p_1\rho^{(1)}_{\tilde{\alpha}} + p_2\rho^{(2)}_{\tilde{\alpha}} + p_3\rho^{(3)}_{\tilde{\alpha}} \ ,$$

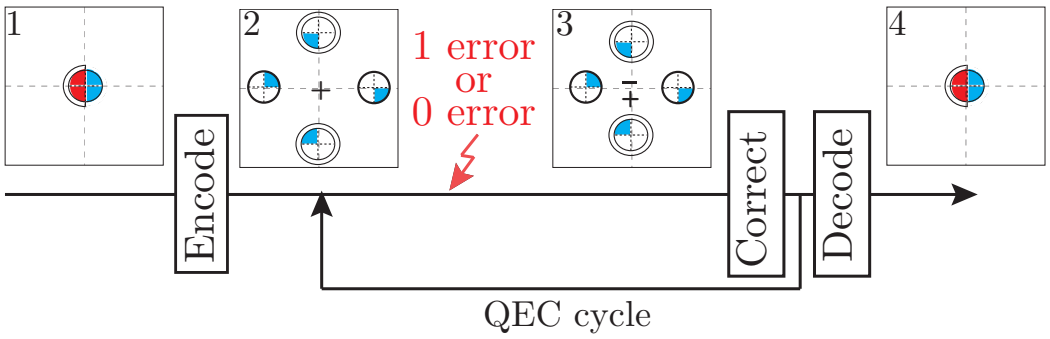

Figure 6.7: Our AQEC scheme is composed of three operations: encoding, correcting and decoding. The joint cavity-qubit state is represented by a generalized Fresnel diagram. Fresnel plane positions carry the description of the cavity mode, while colors carry the description of the qubit. Our protocol only requires that we represent superpositions of coherent states entangled with the qubit degrees of freedom. A circle whose center is positioned at α in the diagram corresponds to a coherent state component of amplitude α. For example, the diagram in frame 2 represents the state $c_g|C_\alpha^+\rangle + c_e|C_{i\alpha}^+\rangle = \mathcal{N}\left(c_g|g,\alpha\rangle + c_g|g,-\alpha\rangle + c_e|g,i\alpha\rangle + c_e|g,-i\alpha\rangle\right)$, where $\mathcal{N} \approx 1/\sqrt{2}$ is a normalization factor. Each component of this state corresponds to a circle whose color refers to whether the qubit is in $|g\rangle$ (blue) or $|e\rangle$ (red). The rim of each circle indicates whether the pre-factor is c_g (single line) or c_e (double line). Finally, the fraction of the colored disc represents the total weight $|\mathcal{N}c_{g,e}|^2$ of each coherent component. Here, quarter filled circles correspond to $|\mathcal{N}c_{g,e}|^2 = 1/4$. Initially (frame 1), the qubit is in $c_g|g\rangle + c_e|e\rangle$ and the cavity is in vacuum. The plus [resp: minus] sign in the 2 and 3 diagrams indicates whether the logical qubit is encoded in the pair $(|C_\alpha^+\rangle, |C_{i\alpha}^+\rangle)$ [resp: $(|C_\alpha^-\rangle, i|C_{i\alpha}^-\rangle)$]. A jump from a plus to a minus sign is induced by a photon loss error, which we aim to correct.

where $\tilde{\alpha} = \alpha e^{-\kappa T_w/2}$. For a Poisson process with a jump rate λ_{jump}, the probability of having k jumps during a time interval T_w is given by $\exp(-\lambda_{\text{jump}} T_w)\lambda_{\text{jump}}^k T_w^k/k!$. We denote p_k the probability of having k (modulo 4) jumps during the waiting time T_w. In the limit where $\varepsilon_{\text{jump}} := \lambda_{\text{jump}} T_w = \kappa T_w \bar{n} \ll 1$, we have $p_0 \approx 1 - \varepsilon_{\text{jump}} + \varepsilon_{\text{jump}}^2/2$, $p_1 \approx \varepsilon_{\text{jump}} - \varepsilon_{\text{jump}}^2$, $p_2 + p_3 \approx \varepsilon_{\text{jump}}^2/2$. The correction step consists of the joint unitary operation on the cavity-qubit system followed by a qubit reset. We model the effect of this operation by the Kraus operator $\mathbb{K}_c$, mapping both $|\psi^{(0)}_{\alpha e^{-\kappa T_w/2}}\rangle$ and $|\psi^{(1)}_{\alpha e^{-\kappa T_w/2}}\rangle$ to $|\psi^{(0)}_\alpha\rangle$. After N correction cycles and waiting times (each one taking a time $T_c + T_w$), we obtain a fidelity at time $t_N = N(T_c+T_w)$: $F_{\text{AQEC}}(t_N) = \left|\langle\psi^{(0)}_\alpha|(\mathbb{K}_c\mathbb{K}_w)^N|\psi^{(0)}_\alpha\rangle\right|^2$. We denote $(1-\varepsilon_{\text{correct}})$ the fidelity of the correction operation, taking into account various imperfections and particularly finite coherence times. Also, $\varepsilon_{\text{wait}} = \varepsilon_{\text{jump}}^2/2$ denotes the probability of having 2 or more jumps during the waiting time between two correction steps. We have $F_{\text{AQEC}}(t_N) \approx ((1-\varepsilon_{\text{correct}})(1-\varepsilon_{\text{wait}}))^N$. Assuming $T_c \ll T_w$, we obtain an effective decay rate $\kappa_{eff} \approx (\varepsilon_{\text{correct}} + (\kappa T_w \bar{n})^2/2)/T_w$. The latter is maximal for $T_w = \sqrt{2\varepsilon_{\text{correct}}}/\kappa\bar{n}$, which would lead to

$$\kappa_{eff} = \kappa\bar{n}\sqrt{2\varepsilon_{\text{correct}}}\,. \tag{6.2}$$

This is an improvement by a factor of $\sqrt{2\varepsilon_{\text{correct}}}$ with respect to the decay rate $\kappa\bar{n}$ of $|\psi^{(0)}_\alpha\rangle$ in absence of correction.

6.3.4 Encoding, decoding and correcting operations

We now show how we could perform the encoding, decoding and correcting operations in practice. We place ourselves in the strong dispersive regime, where both the qubit and the resonator transition frequencies split into well-resolved spectral lines indexed by the number of excitations in the qubit and the resonator [Schuster 2007]. The resonator frequency ω_r splits into two well resolved lines ω_r^g and ω_r^e, corresponding to the cavity's frequency when the qubit is in the ground ($|g\rangle$) or the excited ($|e\rangle$) state. Through the same mechanism, the qubit frequency ω_q splits into $\{\omega_q^n\}_{n=0,1,2,\cdots}$ corresponding to the qubit frequency when the cavity is in the photon number state $|n\rangle$. Recent experiments have shown dispersive shifts that are about 3 orders of magnitude larger than the qubit and cavity linewidths [Paik 2011].

The Hamiltonian of such a dispersively coupled qubit-cavity system is well approximated by

$$\mathbf{H}_0 = \omega_q \frac{\sigma_\mathbf{z}}{2} + \omega_c \mathbf{a}^\dagger\mathbf{a} - \chi\frac{\sigma_\mathbf{z}}{2}\mathbf{a}^\dagger\mathbf{a}\,,$$

where ω_q and ω_c are respectively the qubit and cavity frequencies, χ is the dispersive coupling, $\sigma_z = |e\rangle\langle e| - |g\rangle\langle g|$, and $\mathbf{a}$ is the cavity mode annihilation operator. This Hamiltonian may be written in an appropriate rotating frame as $\mathbf{H} = -\chi|e\rangle\langle e|\mathbf{a}^\dagger\mathbf{a}$. This dispersive coupling is called strong when $\chi \gg \kappa, 1/T_2$, where κ is the cavity decay rate and T_2 is the qubit dephasing time.

As detailed in [Leghtas 2012b] the strong dispersive qubit-cavity coupling allows one to efficiently perform conditional operations such as the conditional cavity

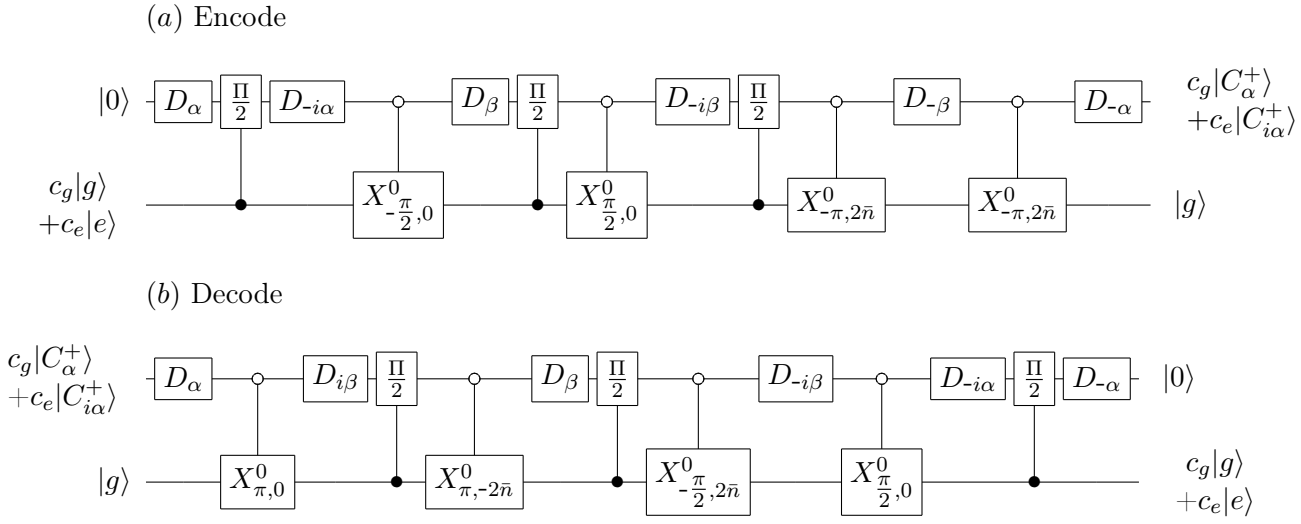

Figure 6.8: Sequence of operations which generate $\mathcal{U}_{\text{encode}}$ (a) and $\mathcal{U}_{\text{decode}}$ (b), mapping the qubit state to the cavity and back. D_α displaces the cavity state by an amplitude α regardless of the qubit state. Conditional operation Π [resp: $\frac{\Pi}{2}$] is realized by simply waiting for time π/χ [resp: $\pi/(2\chi)$]. This transforms states of the form $|e,\alpha\rangle$ to $|e,-\alpha\rangle$ [resp $|e,i\alpha\rangle$], and leaves $|g,\alpha\rangle$ unchanged. The conditional qubit rotation $X^0_{\theta,\eta}$ rotates the qubit state by $e^{\frac{\theta}{2}(e^{i\eta}|e\rangle\langle g|-e^{-i\eta}|g\rangle\langle e|)}$ only if the cavity is in the vacuum state $|0\rangle$. This is achieved by applying a long selective pulse exploiting the energy level dispersive shifts. We denote $\beta=\alpha(-1+i)$ and $\bar{n}=|\alpha|^2$.

displacements and the conditional qubit rotations. Long selective qubit pulses with carrier frequency ω_q^0 can rotate the qubit state conditioned on the cavity being in the vacuum state. Similarly, selective cavity pulses with carrier frequency ω_r^g [resp: ω_r^e] can coherently displace the cavity state conditioned to the qubit being in the ground [resp: excited] state. Furthermore, as explained in [Caves 2010, Leghtas 2012b], shorter operation times are obtained by replacing a conditional cavity displacement by two unconditional ones separated by a waiting time.

The operations involved in our QEC scheme rely on a qubit reset and three unitary transformations. The first one, D_α, displaces the cavity state by a complex amplitude α regardless of the qubit state. Second, the conditional operation Π [resp: $\frac{\Pi}{2}$] transforms states of the form $|e,\alpha\rangle$ to $|e,-\alpha\rangle$ [resp $|e,i\alpha\rangle$], and leaves $|g,\alpha\rangle$ unchanged. It is realized by simply waiting for time π/χ [resp: $\pi/(2\chi)$]. Third, a conditional qubit rotation $X^0_{\theta,\eta}$ rotates the qubit state by $e^{\frac{\theta}{2}(e^{i\eta}|e\rangle\langle g|-e^{-i\eta}|g\rangle\langle e|)}$ only if the cavity is in the vacuum state $|0\rangle$. This is achieved by applying a long selective pulse exploiting the energy level dispersive shifts. The reset operation sets the qubit state to $|g\rangle$ independently of the cavity state. This reset needs to be fast compared to χ to avoid re-entanglement of the qubit with the cavity mode. A possible scheme to perform such a fast reset is to rapidly tune (with a flux bias line) the qubit frequency to bring it into resonance with a low-Q cavity mode [Reed 2012b]. Another

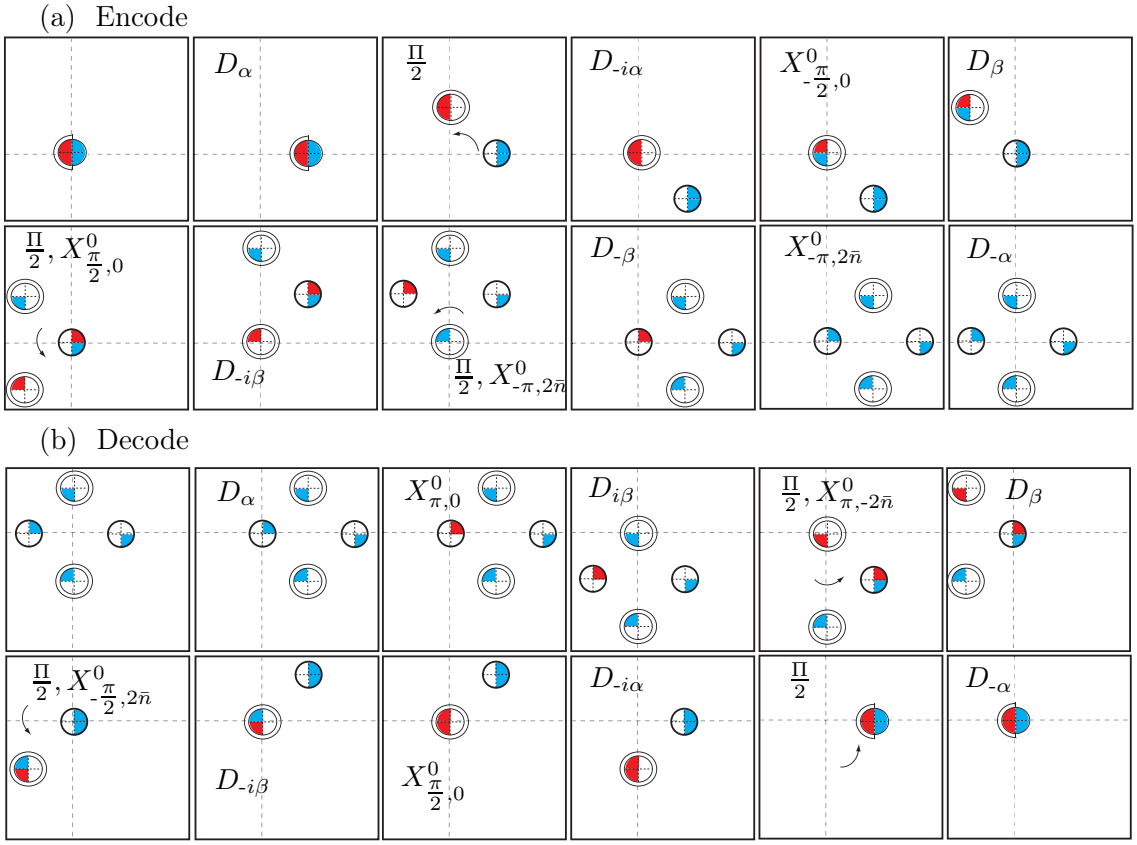

Figure 6.9: Diagrammatic equivalent of Fig. 6.8. The frames are ordered from left to right and top to bottom. The diagram notations are explained in Fig. 6.7. The symbol given in frame n corresponds to the operation performed to go from frame $n-1$ to n. All the possible operations are described in the caption of Fig. 6.8. The curved arrow corresponds to the rotation of the excited state component of the state.

(a) Transferring entropy from the cavity to the qubit, and qubit reset

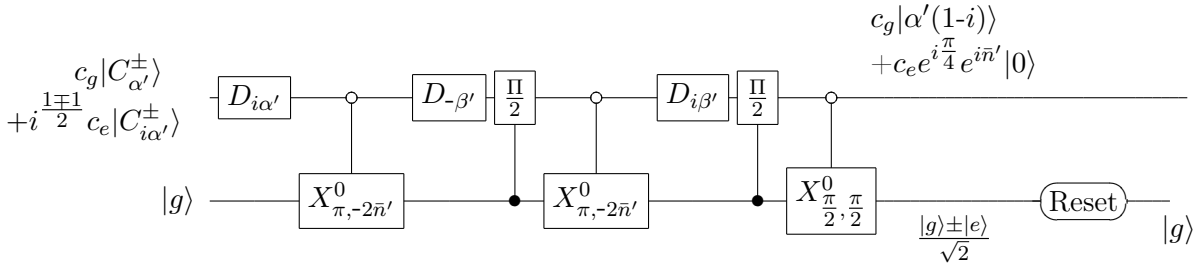

(b) Re-pumping energy into the cavity

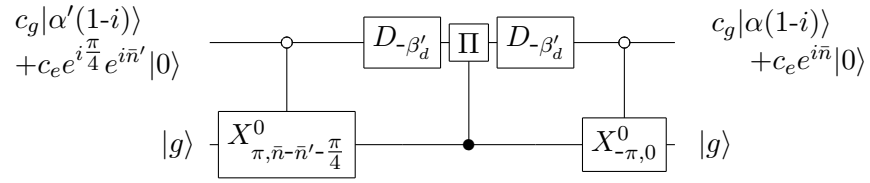

(c) Re-encoding the logical qubit into the cavity logical 0 and 1 states

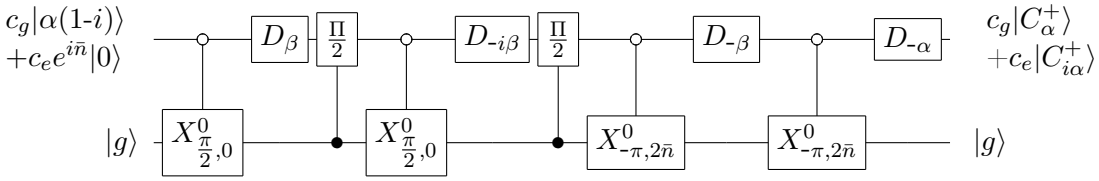

Figure 6.10: Full correcting sequence obtained by concatenating the three sequences of pulses (a-c). (a) First, the entropy is transferred from the cavity to the qubit, and then, the qubit is reset to its ground state. (b) Energy is re-pumped into the coherent component to compensate the deterministic decay due to damping during the waiting time T_w between two correction sequences. (c) The cavity state is mapped back onto the initial cavity logical 0 and logical 1. See the caption of Fig. 6.8 for a description of operations D_α, Π and $X^0_{\theta,\eta}$. Here, we denote $\alpha' = e^{-\kappa T_w/2}\alpha$ the damped amplitude after the waiting time T_w, $\bar{n}' = |\alpha'|^2$ and $\beta' = \alpha'(i-1)$. In order to compensate the damping during T_w, during the re-pumping step, we take $\beta'_d = (\beta' - \beta)/2$.

possibility, avoiding a flux bias line, is to perform a dynamical cooling cycle as proposed in [Leghtas 2012a]. See Fig. 6.8 and Fig. 6.10 for a detailed illustration of how combining all these operations leads to the encoding, decoding and correcting gates. A more geometrical representation is given in Fig. 6.9 and Fig. 6.11. For the correction sequence, unlike in (6.1) which suggests a qubit reset at the end of the correcting transformation, we find a shorter pulse sequence (see Figs. 6.10,6.11) which resets the qubit in the middle of the sequence.

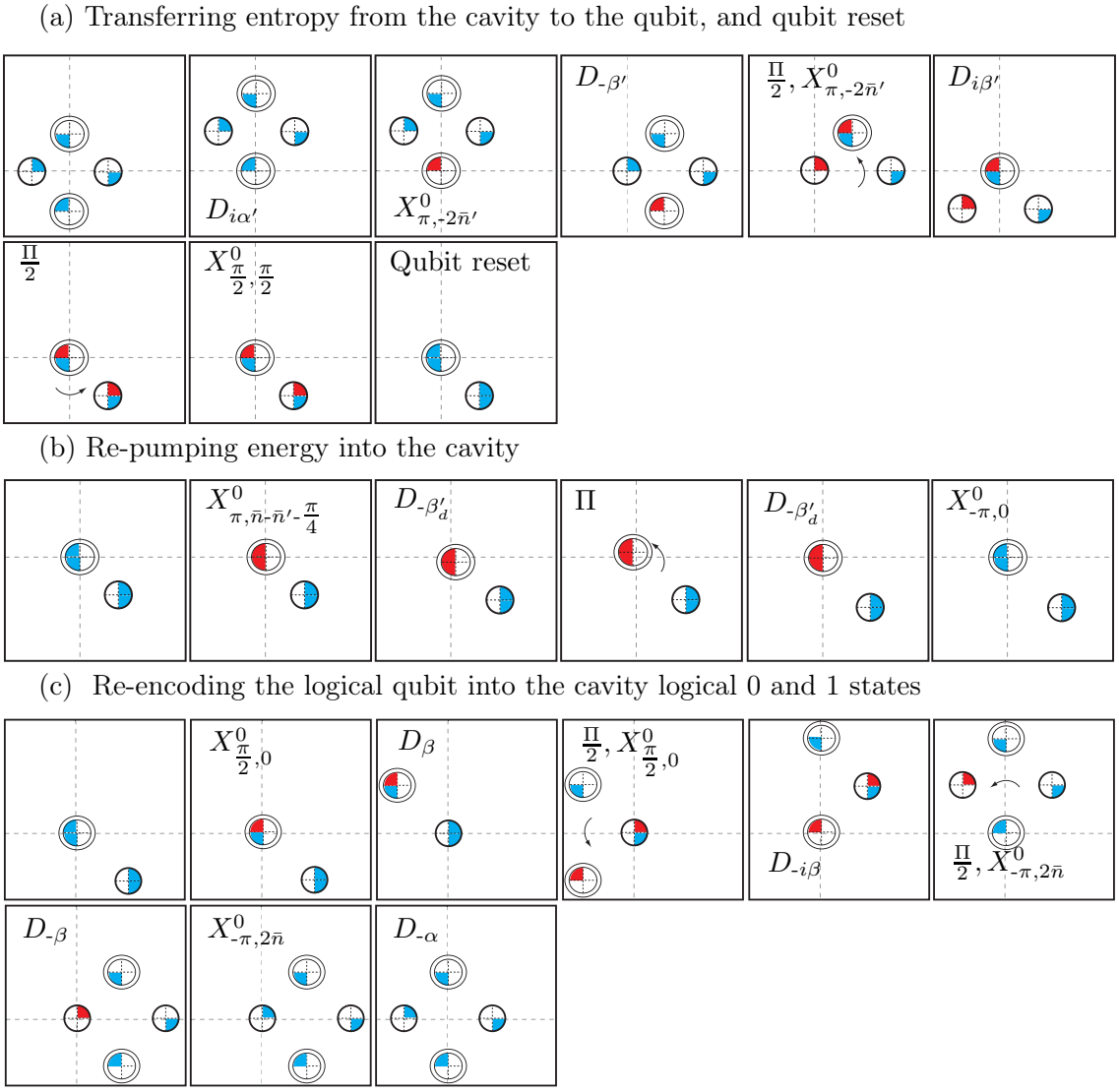

Figure 6.11: Diagrammatic equivalent of Fig. 6.10. See Fig. 6.7 for an explanation of the diagram notation. In the frame before last of (a), the error is encoded in the phase of the qubit superposition, and is not represented in this diagram. After qubit reset (last of frame of (a)), this phase information is erased.

6.3.5 Simulations

To numerically compute the fidelity of each operation, we simulate the corresponding sequence of pulses with a master equation taking into account the qubit and cavity decoherence. We take a qubit decay time T_1 and pure dephasing time T_2 of $T_1 = T_2 = 100$ μs and a cavity lifetime $T_{\text{cav}} = 1/\kappa = 2$ ms. The dispersive coupling strength is $\chi/2\pi = 40$ MHz and the mean photon number per coherent component is $\bar{n} = |\alpha|^2 = 4$. We get an encoding and decoding fidelity of $1-\varepsilon_{\text{encode}} = 1-\varepsilon_{\text{decode}} =$

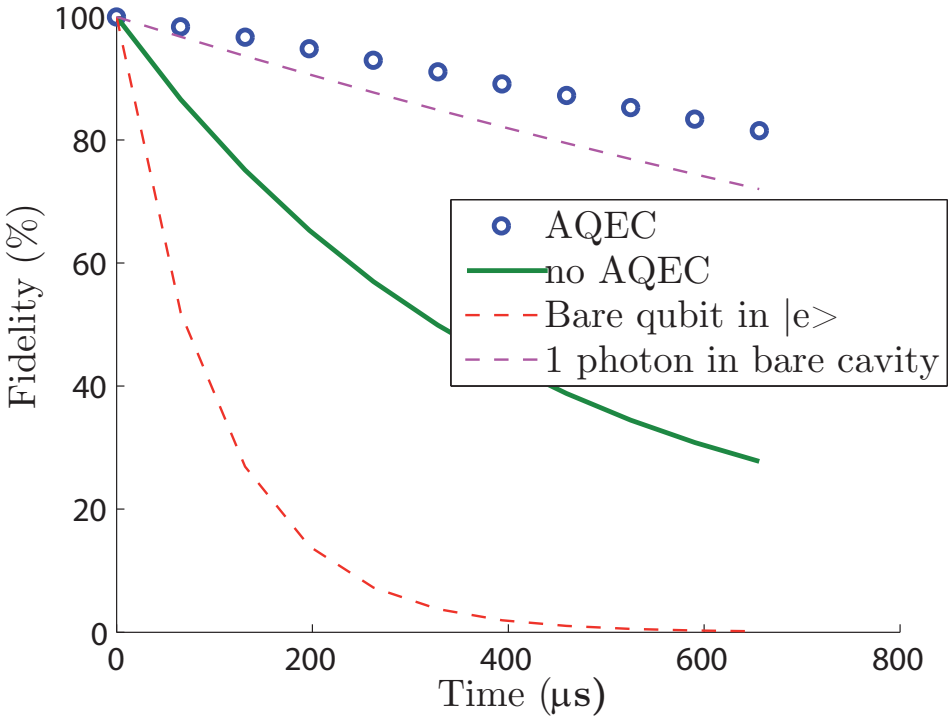

Figure 6.12: Fidelity of our AQEC scheme. The cavity state is initialized in state $|\psi_\alpha^{(0)}\rangle$. We represent the fidelity of the cavity state w.r.t $|\psi_\alpha^{(0)}\rangle$ in absence of the error correction sequence of Fig. 6.10 (green solid line) and after each correction sequence (blue open dots). These simulations take into account dominant sources of decoherence: cavity decay $T_{cav} = 2$ ms and qubit $T_1 = T_2 = 100$ μs. The decay rate of the bare qubit and cavity are plotted for comparison (red and magenta dashed lines).

99.65% for an operation time of $T_e = T_d = 231$ns, and a correcting fidelity of $1 - \varepsilon_{\text{correct}} = 99.23\%$ for an operation time of $T_c = 519$ ns. The optimal waiting time is $T_w = 65.6$ μs. This leads to an effective lifetime for the corrected state of $T_{cav}^{eff} = 4.1$ ms, within 1% agreement with the formula in (6.2). This represents a large improvement over the lifetime of the bare qubit $T_1 = 100$ μs, and of an uncorrected cavity $T_{cav}/\bar{n} = 500$ μs. There is even an improvement w.r.t a single photon lifetime of $T_{cav} = 2$ ms. Notice that a better correction gate fidelity could lead to an even larger improvement. This could be obtained by optimizing the pulse sequence for a specific experimental setting.

6.3.6 Conclusion

We have shown that it is possible to protect a logical qubit against relaxation by encoding it in a single cavity coupled to a single physical qubit, and driving them with simple control pulses. No control over the qubit frequency or the cavity-qubit coupling is necessary, as long as this coupling is in the strong dispersive regime.

Our theoretical prediction of the lifetime improvement is confirmed by numerical simulations of the proposed protocol. Also, additional control of the qubit frequency in real time could lead to simpler and faster operations with higher fidelities, by using ideas similar to those in [Caves 2010]. Finally, our scheme that corrects only for single jumps in the cavity, could be generalized to an n^{th} order correcting scheme by superposing $n+1$ quasi-orthogonal coherent states for each logical state zero and one.

Chapter 7

Conclusion

In this thesis, we tackle the problems of identification, state preparation and stabilization of quantum systems. We consider the context of an ensemble of atoms interacting with an electric field, Josephson circuits and cavity QED.

At the time of writing, two more experiments which we have proposed (not discussed in this manuscript) are currently being realized in the groups of Michel Devoret and Rob Schoelkopf at Yale:

The first experiment is on the stabilization of a two qubit Bell state by reservoir engineering. The system is composed of two 3D transmons which are strongly dispersively coupled to a microwave resonator. Simply by applying drives at well chosen frequencies and satisfying a few simple conditions, we could stabilize a state of the form $|ge\rangle + |eg\rangle$ with a fidelity above 90%. We predict a violation of Bell's inequality for arbitrarily large times. The experiment will be equipped with quantum limited amplifiers which would reveal single quantum trajectories dynamics, thus observing jumps and automatically triggered corrections. This would be the first experiment where an entangled pure state is stabilized, and where Bell's inequality is violated for arbitrarily large times.

The second experiment is on qubit cooling: qubits tend to be much hotter than their environment. We proposed a scheme to dynamically cool a qubit which is dispersively coupled to a cavity. The latter plays the role of a reservoir which stabilizes the qubit ground state. This scheme was experimentally tested and showed a reduction of temperature from 130 mK to 60 mK, in close agreement with our theory [Leghtas 2012a]. This experiment can also be viewed as a qubit reset with no fast qubit frequency tuning. A non-zero temperature is due to a coupling to an external environment. Dynamical cooling data could help us gain more information on the physics of this environment, which could help us increase coherence times.

We now list some future directions in the research subjects presented in this dissertation.

Stabilization by reservoir engineering seems to be perfectly adapted to the context of quantum systems, where measurement processing and latency in a feedback loop can be prohibiting. This idea was first proposed by Cirac, Zoller and co-workers [Poyatos 1996]. It would be useful to establish a mathematical foundation to reservoir engineering. For example: under which minimal assumptions can we insure the existence of an interaction Hamiltonian between the system and the reservoir in order to stabilize a target state, or more generally a manifold? Which set of initial states will converge to the limit set? What are the convergence rates? A

detailed mathematical analysis of such questions could lead to new tools to design experiments revealing some interesting behaviors.

Highly non-classical states could be prepared using the control laws we have proposed. These ideas emerged from a geometrical understanding of the dynamics of the system. Representations such as eigenvalue diagrams (chapter 4) and Q-functions (chapter 6) guided our intuition. Another approach to find these controls could be to use numerical methods [Mirrahimi 2005, Maday 2003, Khaneja 2005]. Although the latter may not reveal the underlying physics during the transfer from the ground to the target state, they could complete the preparation in shorter time, which could be of great interest to decrease sensitivity to decoherence.

We have proposed experiments where tailoring the interaction between a quantum system and its environment can stabilize highly non-classical states. This poses an intriguing question: do natural systems or even biological systems do the same? Can we imagine that some proteins interact with their environment in such a way that they are maintained in an entangled state? Could such a process be evolutionary advantageous? Some of these questions have been raised in the flourishing field of quantum biology [Engel 2007]. The Hilbert space of these systems is usually very large: a set of chromophores (qubits) coupled to a bath (resonators), which complicates numerically simulating them. Josephson circuits could serve as quantum simulators for these biological systems.

As coupling strengths and coherence times are rising, the span of operations we are able to do on these systems is widening. We have seen how the strongly dispersive regime offers the possibility to perform new operations. In particular this led us to proposing a full quantum error correction scheme using only one qubit and one cavity. Future circuit architectures will most certainly lead to new regimes paving the way for more possibilities. We hope that these ideas drawn from a merge of control theory and quantum physics will help guide the development of these future experiments.

Bibliography

[Aharonov 2007] D. Aharonov, W. van Dam, J. Kempe, Z. Landau, S. Lloyd and O. Regev. *Adiabatic quantum computation is equivalent to standard quantum computation*. SIAM J. Computing, vol. 37, no. 1, pages 166–194, 2007. (Cited on page 30.)

[Ahn 2002] C. Ahn, A.C. Doherty and A.J. Landahl. *Continuous quantum error correction via quantum feedback control*. Phys. Rev. A., vol. 65, 2002. (Cited on page 122.)

[Allen 1987] L. Allen and J.H. Eberly. Optical resonance and two-level atoms. Dover, 1987. (Cited on pages 31 and 34.)

[Altafini 2002] C. Altafini. *Controllability of quantum mechanical systems by root space decomposition of su(N)*. Journal of Mathematical Physics, vol. 43, no. 5, pages 2051–2062, 2002. (Cited on pages 3 and 11.)

[Averin 1998] D.V. Averin. *Adiabatic quantum computation with Cooper pairs*. Solid State Communications, vol. 105, no. 10, pages 659–664, 1998. (Cited on page 30.)

[Avron 1987] J.E. Avron, R. Seiler and L.G. Yaffe. *Adiabatic theorems and applications to the quantum hall effect*. Commun. Math. Phys., vol. 110, no. 1, pages 33–49, 1987. (Cited on page 31.)

[Avron 1999] J.E. Avron and A. Elgart. *Adiabatic theorem without a gap condition*. Commun. Math. Phys., vol. 203, no. 2, pages 445–463, 1999. (Cited on page 31.)

[Banaszek 1999] K. Banaszek and K. Wódkiewicz. *Testing Quantum Nonlocality in Phase Space*. Phys. Rev. Lett, vol. 82, page 2009, 1999. (Cited on pages 54, 81, 84, 87 and 115.)

[Barreiro 2011] J.T. Barreiro, M. Müller, P. Schindler, D. Nigg, T. Monz, M. Chwalla, M. Hennrich, C. F. Roos, P. Zoller and R. Blatt. *An open system quantum simulator with trapped ions*. Nature, vol. 470, pages 486–491, 2011. (Cited on pages 57 and 80.)

[Beauchard 2006] K. Beauchard and J.M. Coron. *Controllability of a quantum particle in a moving potential well*. Journal of Functional Analysis, vol. 232, pages 328–389, 2006. (Cited on pages 3 and 11.)

[Beauchard 2009] K. Beauchard and M. Mirrahimi. *Practical stabilization of a quantum particle in a one-dimensional infinite square potential well*. SIAM J. Control Optim., vol. 48, pages 1179–1205, 2009. (Cited on pages 3 and 11.)

[Beauchard 2010] K. Beauchard, J.M. Coron and P. Rouchon. *Controllability issues for continuous-spectrum systems and ensemble controllability of Bloch equations.* Communications in Mathematical Physics, vol. 296, pages 525–557, 2010. (Cited on page 31.)

[Beltrani 2007] V. Beltrani, J. Dominy, T.S Ho and H. Rabitz. *Photonic reagent control of dynamically homologous quantum systems.* J. Chem. Phys, vol. 126, no. 094105, 2007. (Cited on page 23.)

[Bennett 1984] C. H. Bennett and G. Brassard. *Quantum Cryptography: Public key distribution and coin tossing.* in Proceedings of the IEEE International Conference on Computers, Systems, and Signal Processing, Bangalore., page 175, 1984. (Cited on pages 2 and 10.)

[Bonnabel 2009] S. Bonnabel, M. Mirrahimi and P. Rouchon. *Observer-based Hamiltonian identification for quantum systems.* Automatica, vol. 45, no. 5, pages 1144 – 1155, 2009. (Cited on page 18.)

[Boscain 2002] U. Boscain, G. Charlot, J.P. Gauthier, S. Guérin and H.R. Jauslin. *Optimal control in laser-induced population transfer for two- and three-level quantum systems.* Journal of Mathematical Physics, vol. 43, no. 5, pages 2107–2132, 2002. (Cited on pages 3 and 11.)

[Boscain 2010] U. Boscain, F.C. Chittaro, P. Mason, R. Pacqueau and M. Sigalotti. *Motion planning in quantum control via intersection of eigenvalues.* Proc. 49th IEEE Conf. Decision and Control, pages 3028–3033, 2010. (Cited on page 32.)

[Boscain 2011] U. Boscain, F.C. Chittaro, P. Mason and M. Sigalotti. *Adiabatic control of the Schrödinger equation via conical intersection of eigenvalues.* Submitted to IEEE Transactions on Automatic Control, 2011. (Cited on page 31.)

[Brezis 1983] H. Brezis. Analyse fonctionnelle: théorie et applications. Masson, 1983. (Cited on pages 3, 11 and 104.)

[Brif 2010] C. Brif, R. Chakrabarti and H. Rabitz. *Control of quantum phenomena: past, present and future.* New Journal of Physics, vol. 12, no. 7, page 075008, 2010. (Cited on page 18.)

[Brune 1992] M. Brune, S. Haroche and J. M. Raimond. *Manipulation of photons in a cavity by dispersive atom-field coupling: Quantum-nondemolition measurements and generation of "Schrödinger cat" states.* Phys. Rev. A, vol. 45, page 5193, 1992. (Cited on page 55.)

[Brune 1996] M. Brune, E. Hagley, J. Dreyer, X. Maître, A. Maali, C. Wunderlich, J. M. Raimond and S. Haroche. *Observing the Progressive Decoherence of*

the "Meter" in a Quantum Measurement. Phys. Rev. Lett., vol. 77, pages 4887–4890, Dec 1996. (Cited on pages 55, 57, 109 and 111.)

[Carvalho 2001] A. R. R. Carvalho, P. Milman, R. L. de Matos Filho and L. Davidovich. *Decoherence, Pointer Engineering, and Quantum State Protection.* Phys. Rev. Lett., vol. 86, page 4988, 2001. (Cited on page 57.)

[Casagrande 2002] F. Casagrande, A. Lulli and V. Santagostino. *Coherently driven and coherently pumped micromaser.* Phys. Rev. A, vol. 65, page 023809, 2002. (Cited on page 62.)

[Caves 2010] C.M. Caves and A. Shaji. *Quantum-circuit guide to optical and atomic interferometry.* Optics Communications, vol. 283, pages 695–712, 2010. (Cited on pages 128 and 133.)

[Chambrion 2009] T. Chambrion, P. Mason, M. Sigalotti and U. Boscain. *Controllability of the discrete-spectrum Schrödinger equation driven by an external field.* Annales de l'Institut Henri Poincare. Annales: Analyse Non Lineaire/Nonlinear Analysis, vol. 26, no. 1, pages 329–349, 2009. (Cited on pages 3 and 11.)

[Chelkowski 1990] S. Chelkowski, A. D. Bandrauk and P. B. Corkum. *Efficient molecular dissociation by a chirped ultrashort infrared laser pulse.* Phys. Rev. Lett., vol. 65, no. 19, pages 2355–2358, 1990. (Cited on page 30.)

[Chiaverini 2004] J. Chiaverini, D. Leibfried, T. Schaetz, M.D. Barrett, R.B. Blakestad, J. Britton, W.M Itano, J.D. Jost, E. Knill, C. Langer, R. Ozeri and D.J. Wineland. *Realization of quantum error correction.* Nature, vol. 432, no. 7017, pages 602–605, 2004. (Cited on page 122.)

[Chow 2010] J.M. Chow, L. DiCarlo, J.M. Gambetta, A. Nunnenkamp, L.S. Bishop, L. Frunzio, M.H. Devoret, S.M. Girvin and R.J. Schoelkopf. *Detecting highly entangled states with a joint qubit readout.* Phys. Rev. A, vol. 81, page 062325, 2010. (Cited on page 116.)

[Coron 2007] J.M. Coron. *Control and Nonlinearity.* Mathematical surveys and monographs, vol. 136, 2007. (Cited on pages 3 and 11.)

[D'Alessandro 2008] D. D'Alessandro. Introduction to quantum control and dynamics. Chapman & Hall/CRC, 2008. (Cited on pages 2, 10 and 27.)

[Davidovich 1993] L. Davidovich, A. Maali, M. Brune, J. M. Raimond and S. Haroche. *Quantum switches and nonlocal microwave fields.* Phys. Rev. Lett., vol. 71, page 2360, 1993. (Cited on pages 55 and 111.)

[de Matos Filho 1996] R.L. de Matos Filho and W. Vogel. *Even and Odd Coherent States of the Motion of a Trapped Ion.* Phys. Rev. Lett., vol. 76, page 608, 1996. (Cited on pages 55 and 57.)

[Deléglise 2008] S. Deléglise, I. Dotsenko, C. Sayrin, J. Bernu, M. Brune, J.M. Raimond and S. Haroche. *Reconstruction of non-classical cavity field states with snapshots of their decoherence*. Nature, vol. 455, pages 510–514, 2008. (Cited on pages 55, 59 and 111.)

[Devoret 2004] M. H. Devoret and J.M. Martinis. Quantum Information Processing, vol. 3, page 163, 2004. (Cited on pages 57, 89 and 109.)

[Doherty 2000] A.C. Doherty, S. Habib, K. Jacobs, H. Mabuchi and S.M. Tan. *Quantum feedback control and classical control theory*. Phys. Rev. A, vol. 62, page 012105, Jun 2000. (Cited on pages 4 and 12.)

[Dotsenko 2009] I. Dotsenko, M. Mirrahimi, M. Brune, S. Haroche, J.M. Raimond and P. Rouchon. *Quantum feedback by discrete quantum nondemolition measurements: Towards on-demand generation of photon-number states*. Phys. Rev. A, vol. 80, no. 1, page 013805, Jul 2009. (Cited on pages 4 and 12.)

[Dowling 2008] J.P. Dowling. *Quantum Optical Metrology*. Contemporary physics 49, 125, 2008. (Cited on page 54.)

[Engel 2007] G. S. Engel, T. R. Calhoun, E. L. Read, T. Ahn, T. Manal1, Y. Cheng, R. E. Blankenship and G. R. Fleming. *Evidence for wavelike energy transfer through quantum coherence in photosynthetic systems*. Nature, vol. 446, page 782, 2007. (Cited on page 136.)

[Favard 1935] J. Favard. *Sur les polynomes de Tchebicheff*. Comptes-rendus de l'Académie des Sciences de Paris, vol. 200, pages 2052–2053, 1935. (Cited on pages 31 and 46.)

[Filipovicz 1986] P. Filipovicz, J. Javanainen and P. Meystre. *Quantum and semi-classical steady states of a kicked cavity mode*. J. Opt. Soc. Am. B, vol. 3, page 906, 1986. (Cited on page 63.)

[Filipp 2009] S. Filipp, P. Maurer, P.J. Leek, M. Baur, R. Bianchetti, J.M. Fink, M. Göppl, L. Steffen, J.M. Gambetta, A. Blais and A. Wallraff. *Two-Qubit State Tomography Using a Joint Dispersive Readout*. Phys. Rev. Lett., vol. 102, page 200402, 2009. (Cited on page 116.)

[Giovannetti 2004] V. Giovannetti, S. Lloyd and L. Maccone. *Quantum-Enhanced Measurements: Beating the Standard Quantum Limit*. Science, vol. 306, page 1330, 2004. (Cited on pages 10 and 54.)

[Giovannetti 2006] V. Giovannetti, S. Lloyd and L. Maccone. *Quantum Metrology*. Phys. Rev. Lett., vol. 96, page 010401, Jan 2006. (Cited on pages 2 and 10.)

[Goda 2008] K. Goda, O. Miyakawa, E. E. Mikhailov, S. Saraf, R. Adhikari, K. McKenzie, R. Ward, S. Vass, A. J. Weinstein and N. Mavalvala. *A quantum-enhanced prototype gravitational-wave detector*. Nature Physics, vol. 4, page 472, 2008. (Cited on page 54.)

[Gottesman 1996] D. Gottesman. *Class of quantum error-correcting codes saturating the quantum Hamming bound*. Phys. Rev. A, vol. 54, pages 1862–1868, 1996. (Cited on page 122.)

[Gottesman 2001] D. Gottesman, A. Kitaev and J. Preskill. *Encoding a qubit in an oscillator*. Phys. Rev. A, vol. 64, page 012310, 2001. (Cited on pages 110, 115 and 123.)

[Grover 1997] L. K. Grover. *Quantum Mechanics Helps in Searching for a Needle in a Haystack*. Phys. Rev. Lett., vol. 79, pages 325–328, Jul 1997. (Cited on pages 1 and 9.)

[Guérin 1997] S. Guérin. *Complete dissociation by chirped laser pulses designed by adiabatic Floquet analysis*. Phys. Rev. A, vol. 56, no. 2, pages 1458–1462, 1997. (Cited on page 31.)

[Guérin 2002] S. Guérin, S. Thomas and H. R. Jauslin. *Optimization of population transfer by adiabatic passage*. Phys. Rev. A, vol. 65, no. 2, page 023409, 2002. (Cited on page 51.)

[Haroche 2006] S. Haroche and J.M. Raimond. Exploring the Quantum. Oxford University Press, 2006. (Cited on pages 5, 12, 13, 54, 55, 57, 59, 62, 75, 85, 91, 94, 108, 114 and 115.)

[Haroche 2007] S. Haroche, M. Brune and J.M. Raimond. *Measuring the photon number parity in a cavity: from light quantum jumps to the tomography of non-classical field states*. Journal of Modern Optics, vol. 54, page 2101, 2007. (Cited on page 125.)

[Hofheinz 2008] M. Hofheinz, E.M. Weig, M. Ansmann, R.C. Bialczak, E. Lucero, M. Neeley, A.D. O'Connell, H. Wang, J.M. Martinis and A.N. Cleland. *Generation of Fock states in a superconducting quantum circuit*. Nature, vol. 454, pages 310–314, 2008. (Cited on pages 109 and 110.)

[Hulet 1983] R.G. Hulet and D. Kleppner. *Rydberg atoms in "circular" states*. Phys. Rev. Lett., vol. 51, pages 1430–1433, 1983. (Cited on page 31.)

[Iaconis 1998] C. Iaconis and I.A. Walmsley. *Spectral phase interferometry for direct electric-field reconstruction of ultrashort optical pulses*. Opt. Lett., vol. 23, no. 10, pages 792–794, 1998. (Cited on page 18.)

[James 2010] M.R. James and J.E. Gough. *Quantum Dissipative Systems and Feedback Control Design by Interconnection*. Automatic Control, IEEE Transactions on, vol. 55, no. 8, pages 1806 –1821, aug. 2010. (Cited on pages 4 and 12.)

[Jaynes 1963] E.T. Jaynes and F.W. Cummings. *Comparison of quantum and semiclassical radiation theories with application to the beam maser*. in Proceedings of IEEE., vol. 51, pages 89 – 109, 1963. (Cited on pages 6 and 14.)

[Johnson 2010] B.R. Johnson, M.D. Reed ad A.A. Houck, D.I. Schuster, L.S. Bishop, E. Ginossar, J.M. Gambetta, L. DiCarlo, L. Frunzio, S.M. Girvin and R.J. Schoelkopf. *Quantum non-demolition detection of single microwave photons in a circuit.* Nature Physics, vol. 6, pages 663–667, 2010. (Cited on page 111.)

[Judson 1992] R.S. Judson and H. Rabitz. Phys. Rev. Lett., vol. 68, no. 10, 1992. (Cited on pages 3 and 11.)

[Jurdjevic 1972] V. Jurdjevic and H.J. Sussmann. *Control systems on Lie Groups.* J. diff. eq., vol. 12, pages 313–329, 1972. (Cited on pages 3, 11 and 25.)

[Kato 1966] T. Kato. Perturbation theory for linear operators. Springer, 1966. (Cited on pages 27, 46, 47, 48, 49 and 50.)

[Kerckhoff 2010] J. Kerckhoff, H.I. Nurdin, D.S. Pavlichin and H. Mabuchi. *Designing quantum memories with embedded control: photonic circuits for autonomous quantum error correction.* Physical Review Letters, vol. 105, page 040502, 2010. (Cited on page 122.)

[Khalil 2001] H.K. Khalil. Nonlinear systems. Prentice Hall, 2001. (Cited on page 46.)

[Khaneja 2005] N. Khaneja, T. Reiss, C. Kehlet, T. Schulte-Herbrüggen and S. J. Glaser. *Optimal control of coupled spin dynamics: design of NMR pulse sequences by gradient ascent algorithms.* Journal of Magnetic Resonance, vol. 172, no. 2, pages 296 – 305, 2005. (Cited on page 136.)

[Kirchmair *et al.* 2012] G. Kirchmair *et al.* in preparation, 2012. (Cited on pages 109 and 115.)

[Koch 2007] J. Koch, T.M. Yu, J. Gambetta, A.A. Houck, D.I. Schuster, J. Majer, A. Blais, M.H. Devoret, S.M. Girvin and R.J. Schoelkopf. *Charge-insensitive qubit design derived from the Cooper pair box.* Phys. Rev. A, vol. 76, page 042319, 2007. (Cited on page 111.)

[Kraus 1983] K. Kraus. States, effects and operations: fundamental notions of quantum theory. Springer, Berlin, 1983. (Cited on page 60.)

[Krauter 2011] H. Krauter, C. A. Muschik, K. Jensen, W. Wasilewski, J. M. Petersen, J. I. Cirac and E. S. Polzik. *Entanglement Generated by Dissipation and Steady State Entanglement of Two Macroscopic Objects.* Phys. Rev. Lett., vol. 107, page 080503, Aug 2011. (Cited on pages 57 and 80.)

[Kuhr 2007] S. Kuhr, S. Gleyzes, C. Guerlin, J. Bernu, U. B. Hoff, S. Deléglise, S. Osnaghi, M. Brune, J.M. Raimond, S. Haroche, E. Jacques, P. Bosland and B. Visentin. *Ultrahigh finesse Fabry-Pérot superconducting resonator.* Applied Physics Letters, vol. 90, no. 16, page 164101, 2007. (Cited on pages 82 and 87.)

[LeBris 2007] C. LeBris, M. Mirrahimi, H. Rabitz and G. Turinici. *Hamiltonian identification for quantum systems: well-posedness and numerical approaches*. ESAIM, vol. 13, no. 2, pages 378 – 395, 2007. (Cited on pages 3, 11 and 18.)

[Leghtas 2009] Z. Leghtas, M. Mirrahimi and P. Rouchon. *Parameter estimation of a 3-level quantum system with a single population measurement*. Proc. IEEE. 48th CDC, pages 3816 –3820, 2009. (Cited on page 18.)

[Leghtas 2011] Z. Leghtas, A. Sarlette and P. Rouchon. *Adiabatic passage and ensemble control of quantum systems*. Journal of Physics B: Atomic, Molecular and Optical Physics, vol. 44, no. 15, page 154017, 2011. (Cited on pages 6, 14 and 30.)

[Leghtas 2012a] Z. Leghtas, K. Geerlings, S. Shankar, M. Mirrahimi and M.H. Devoret. *Stabilizing manifolds of quantum states by reservoir engineering*. APS march meeting, 2012. (Cited on pages 130 and 135.)

[Leghtas 2012b] Z. Leghtas, G. Kirchmair, B. Vlastakis, M.H. Devoret, R. Schoelkopf and M. Mirrahimi. *Deterministic protocol for mapping a qubit to coherent state superpositions in a cavity*. Submitted to Phys. Rev. Lett. preliminary version: http://arxiv.org/abs/1205.2401, 2012. (Cited on pages 7, 15, 110, 122, 123, 127 and 128.)

[Leghtas 2012c] Z. Leghtas, G. Kirchmair, B. Vlastakis, R. Schoelkopf, M.H. Devoret and M. Mirrahimi. *Hardware-efficient autonomous quantum error correction*. Preliminary version: http://arxiv.org/abs/1207.0679, 2012. (Cited on pages 7, 15 and 122.)

[Leghtas 2012d] Z. Leghtas, G. Turinici, H. Rabitz and P. Rouchon. *Hamiltonian identification through enhanced observability utilizing quantum control*. IEEE Transactions on Automatic Control., vol. 57, page 2679, 2012. (Cited on pages 6, 14, 17 and 18.)

[Leung 1997] D.W. Leung, M.A. Nielsen, I.L. Chuang and Y. Yamamoto. *Approximate quantum error correction can lead to better codes*. Phys. Rev. A, vol. 56, pages 2567–2573, 1997. (Cited on page 122.)

[Li 2006] J.S. Li and N. Khaneja. *Control of inhomogeneous quantum ensembles*. Phys. Rev. A, vol. 73, no. 3, page 030302, 2006. (Cited on pages 3, 11 and 31.)

[Li 2009] J.S. Li and N. Khaneja. *Ensemble control of Bloch equations*. IEEE Transactions on Automatic Control, vol. 54, no. 3, pages 528 –536, 2009. (Cited on page 31.)

[Lutterbach 2000] L. G. Lutterbach and L. Davidovich. *Production and detection of highly squeezed states in cavity QED.* Phys. Rev. A, vol. 61, page 023813, Jan 2000. (Cited on page 114.)

[Maas 1999] D.J. Maas, C.W. Rella, P. Antoine, E.S. Toma and L.D. Noordam. *Population transfer via adiabatic passage in the rubidium quantum ladder system.* Phys. Rev. A, vol. 59, no. 2, pages 1374–1381, 1999. (Cited on pages 31 and 37.)

[Maday 2003] Y. Maday and G. Turinici. *New formulations of monotonically convergent quantum control algorithms.* The Journal of Chemical Physics, vol. 118, no. 18, pages 8191–8196, 2003. (Cited on page 136.)

[Maday 2006] Y. Maday, J. Salomon and G. Turinici. *Monotonic time-discretized schemes in quantum control.* Numerische Mathematik, vol. 103, no. 2, pages 323–338, 2006. (Cited on pages 3 and 11.)

[Maître 1997] X. Maître, E. Hagley, G. Nogues, C. Wunderlich, P. Goy, M. Brune, J. M. Raimond and S. Haroche. *Quantum Memory with a Single Photon in a Cavity.* Phys. Rev. Lett., vol. 79, pages 769–772, Jul 1997. (Cited on page 110.)

[Majer 2007] J. Majer, J.M. Chow, J.M. Gambetta, J. Koch, B.R. Johnson, J.A. Schreier, L. Frunzio, D.I. Schuster, A.A. Houck, A. Wallraff, A. Blais, M.H. Devoret, S.M. Girvin and R.J. Schoelkopf. *Coupling superconducting qubits via a cavity bus.* Nature, vol. 449, page 443, 2007. (Cited on page 110.)

[Mariantoni 2011] M. Mariantoni, H. Wang, T. Yamamoto, M. Neeley, R.C. Bialczak, Y. Chen, M. Lenander, A.D. OÕConnell E. Lucero, D. Sank, M. Weides, J. Wenner, Y. Yin, J. Zhao, A.N. Korotkov, A.N. Cleland and J.M. Martinis. *Implementing the Quantum von Neumann Architecture with Superconducting Circuits.* Science, vol. 334, pages 61–65, 2011. (Cited on page 110.)

[Megrant 2012] A. Megrant, C. Neill, R. Barends, B. Chiaro, Y. Chen, L. Feigl, J. Kelly, E. Lucero, M. Mariantoni, P.J.J. O'Malley, D. Sank, A. Vainsencher, J. Wenner, T.C. White, Y. Yin, J. Zhao, C.J. Palmstrom, J.M. Martinis and A.N. Cleland. *Planar superconducting resonators with internal quality factors above one million.* Appl. Phys. Lett., vol. 100, page 113510, 2012. (Cited on page 110.)

[Messiah 1958] A. Messiah. Quantum mechanics. Wiley and Sons (New York), 1958. (Cited on pages 31 and 48.)

[Messiah 1964] A. Messiah. Mécanique quantique. Dunod Paris, 1964. (Cited on pages 91 and 92.)

[Milman 2005] P. Milman, A. Auffeves, F. Yamaguchi, M. Brune, J. M. Raimond and S. Haroche. Euro. Phys. J. D, vol. 32, pages 233–239, 2005. (Cited on pages 55, 80, 84 and 115.)

[Mirrahimi 2005] M. Mirrahimi, P. Rouchon and G. Turinici. *Lyapunov control of bilinear Schrödinger equations.* vol. 41, pages 1987–1994, 2005. (Cited on pages 3, 11 and 136.)

[Molmer 1993] K. Molmer, Y. Castin and J. Dalibard. *Monte Carlo wave-function method in quantum optics.* J. Opt. Soc. America B, vol. 10, page 524, 1993. (Cited on page 73.)

[Monroe 1996] C. Monroe, D. M. Meekhof, B. E. King and D. J. Wineland. *A "Schrödinger Cat" Superposition State of an Atom.* Science, vol. 272, page 1131, 1996. (Cited on page 55.)

[Myatt 2000] C. J. Myatt, B. E. King, Q. A. Turchette, C. A. Sackett, D. Kielpinski, W. M. Itano, C. Monroe and D. J. Wineland. *Decoherence of quantum superpositions through coupling to engineered reservoirs.* Nature (London), vol. 403, page 269, 2000. (Cited on page 55.)

[Nagao 1993] T. Nagao and M. Wadati. *Level statistics of discrete Schrödinger equations and orthogonal polynomials.* J. Physical Society of Japan, vol. 62, no. 1, pages 46–52, 1993. (Cited on page 45.)

[Nielsen 2000] M.A. Nielsen and I.L. Chuang. Quantum computation and quantum information. Cambridge University Press, 2000. (Cited on pages 30, 85 and 100.)

[Nigg 2012] S.E. Nigg, H. Paik, B. Vlastakis, G. Kirchmair, S. Shankar, L. Frunzio, M.H. Devoret, R. Schoelkopf and S. Girvin. *Black-box superconducting circuit quantization.* 2012. submitted, preprint at arXiv:1204.0587. (Cited on pages 109, 112 and 115.)

[Nussenzweig 1993] P. Nussenzweig, F. Bernardot, M. Brune, J. Hare, J.M. Raimond, S. Haroche and W. Gawlik. *Preparation of high-principal-quantum-number "circular" states of rubidium.* Phys.Rev. A, vol. 48, no. 5, pages 3991–3995, 1993. (Cited on pages 30 and 31.)

[Oreg 1984] J. Oreg, F.T. Hioe and J.H. Eberly. *Adiabatic following in multilevel systems.* Phys.Rev. A, vol. 29, no. 2, pages 690–697, 1984. (Cited on page 31.)

[Ourjoumtsev 2007] A. Ourjoumtsev, H. Jeong, R. Tualle-Brouri and P. Grangier. *Generation of optical "Schrödinger cats" from photon number states.* Nature (London), vol. 448, page 784, 2007. (Cited on page 57.)

[Paik 2011] H. Paik, D.I. Schuster, L.S. Bishop, G. Kirchmair, G. Catelani, A.P. Sears, B.R. Johnson, M.J. Reagor, L. Frunzio, L.I. Glazman, S.M. Girvin,

M.H. Devoret and R.J. Schoelkopf. *Observation of High Coherence in Josephson Junction Qubits Measured in a Three-Dimensional Circuit QED Architecture.* Phys. Rev. Lett., vol. 107, page 240501, 2011. (Cited on pages 110, 111, 115 and 127.)

[Petersen 2010] J. Petersen, R. Mitrić, V. Bonači ć Koutecký, J.P. Wolf, J. Roslund and H. Rabitz. *How Shaped Light Discriminates Nearly Identical Biochromophores.* Phys. Rev. Lett., vol. 105, page 073003, Aug 2010. (Cited on page 21.)

[Pielawa 2007] S. Pielawa, G. Morigi, D. Vitali and L. Davidovich. *Generation of Einstein-Podolsky-Rosen-Entangled Radiation through an Atomic Reservoir.* Phys. Rev. Lett., vol. 98, page 240401, Jun 2007. (Cited on page 57.)

[Poyatos 1996] J.F. Poyatos, J.I. Cirac and P. Zoller. *Quantum Reservoir Engineering with Laser Cooled Trapped Ions.* Phys. Rev. Lett., vol. 77, page 4728, 1996. (Cited on pages 4, 12, 57 and 135.)

[Raimond 2010] J.M. Raimond, C. Sayrin, S. Gleyzes, I. Dotsenko, M. Brune, S. Haroche, P. Facchi and S. Pascazio. *Phase Space Tweezers for Tailoring Cavity Fields by Quantum Zeno Dynamics.* Phys. Rev. Lett., vol. 105, page 213601, 2010. (Cited on pages 110 and 114.)

[Ramakrishna 1995] V. Ramakrishna, M.V. Salapaka, M. Dahleh, H. Rabitz and A. Peirce. *Controllability of molecular systems.* Phys. Rev. A, vol. 51, no. 2, pages 960–966, 1995. (Cited on pages 3 and 11.)

[Rauschenbeutel 2001] A. Rauschenbeutel, P. Bertet, S. Osnaghi, G. Nogues, M. Brune, J. M. Raimond and S. Haroche. *Controlled entanglement of two field modes in a cavity quantum electrodynamics experiment.* Phys. Rev. A, vol. 64, page 050301, Oct 2001. (Cited on page 80.)

[Reagor *et al.* 2012] M. Reagor *et al.* in preparation, 2012. (Cited on page 110.)

[Reed 2010a] M. D. Reed, L. DiCarlo, B. R. Johnson, L. Sun, D. I. Schuster, L. Frunzio and R. J. Schoelkopf. *High-Fidelity Readout in Circuit Quantum Electrodynamics Using the Jaynes-Cummings Nonlinearity.* Phys. Rev. Lett., vol. 105, page 173601, Oct 2010. (Cited on pages 4 and 12.)

[Reed 2010b] M. D. Reed, B. R. Johnson, A. A. Houck, L. DiCarlo, J. M. Chow, D. I. Schuster, L. Frunzio and R. J. Schoelkopf. *Fast reset and suppressing spontaneous emission of a superconducting qubit.* Applied Physics Letters, vol. 96, no. 20, page 203110, 2010. (Cited on pages 57 and 89.)

[Reed 2012a] M. D. Reed, L. DiCarlo, S. E. Nigg, L. Sun, L. Frunzio, S. M. Girvin and R. J. Schoelkopf. *Realization of three-qubit quantum error correction with superconducting circuits.* Nature, vol. 482, pages 382–385, 2012. (Cited on page 109.)

[Reed 2012b] M.D. Reed, L. DiCarlo, S.E. Nigg, L. Sun, L. Frunzio, S.M. Girvin and R.J. Schoelkopf. *Realization of three-qubit quantum error correction with superconducting circuits.* Nature, vol. 482, pages 382–385, 2012. (Cited on pages 122 and 128.)

[Rempe 1990] G. Rempe, F. Schmidt-Kaler and H. Walther. *Observation of sub-Poissonian photon statistics in a micromaser.* Phys. Rev. Lett., vol. 64, page 2783, 1990. (Cited on page 57.)

[Rigetti 2012] C. Rigetti, S. Poletto, J.M. Gambetta, B.L.T. Plourde, J.M. Chow, A.D. Corcoles, J.A. Smolin, S.T. Merkel, J.R. Rozen, G.A. Keefe, M.B. Rothwell, M.B. Ketchen and M. Steffen. *Superconducting qubit in waveguide cavity with coherence time approaching 0.1ms.* 2012. arXiv:1202.5533. (Cited on pages 115 and 122.)

[Rosenbluh 1991] M. Rosenbluh and R.M. Shelby. *Squeezed optical solitons.* Phys. Rev. Lett., vol. 66, page 153, 1991. (Cited on page 55.)

[Sanders 2007] J. Sanders, F. Verhulst and J. Murdock. Averaging methods in nonlinear dynamical systems. Springer, New York, 2007. (Cited on pages 25, 26 and 34.)

[Sarlette 2011] A. Sarlette, J. M. Raimond, M. Brune and P. Rouchon. *Stabilization of Nonclassical States of the Radiation Field in a Cavity by Reservoir Engineering.* Phys. Rev. Lett., vol. 107, page 010402, Jul 2011. (Cited on pages 57, 58, 60, 62, 63, 65, 79 and 89.)

[Sarlette 2012] A. Sarlette, Z. Leghtas, M. Brune, J. M. Raimond and P. Rouchon. *Stabilization of nonclassical states of one- and two-mode radiation fields by reservoir engineering.* Phys. Rev. A, vol. 86, page 012114, 2012. (Cited on pages 6, 14, 53, 54 and 115.)

[Sayrin 2011] C. Sayrin, I. Dotsenko, X. Zhou, B. Peaudecerf, T. Rybarczyk, S. Gleyzes, P. Rouchon, M. Mirrahimi, H. Amini, M. Brune, J.M. Raimond and S. Haroche. *Real-time quantum feedback prepares and stabilizes photon number states.* Nature, vol. 477, page 73, 2011. (Cited on pages 4, 12 and 109.)

[Schindler 2011] P. Schindler, J.T. Barreiro, T. Monz, V. Nebendah, D. Nigg, M. Chwalla, M. Hennrich and R. Blatt. *Experimental Repetitive Quantum Error Correction.* Science, vol. 332, page 1059, 2011. (Cited on pages 109 and 122.)

[Schirmer 2010a] S.G. Schirmer and F.C. Langbein. *Quantum system identification: Hamiltonian estimation using spectral and Bayesian analysis.* Communications, Control and Signal Processing (ISCCSP), 2010 4th International Symposium on, pages 1 –5, march 2010. (Cited on page 19.)

[Schirmer 2010b] S.G. Schirmer and D. Oi. *Quantum system identification by Bayesian analysis of noisy data: Beyond Hamiltonian tomography.* Laser Physics, vol. 20, pages 1203–1209, 2010. (Cited on page 19.)

[Schoelkopf 2008] R. J. Schoelkopf and S. Girvin. *Wiring up quantum systems.* Nature, vol. 451, pages 664–669, 2008. (Cited on page 123.)

[Schuster 2007] D.I. Schuster, A.A. Houck, J.A Schreier, A. Wallraff, J.M. Gambetta, A. Blais, L. Frunzio, J. Majer, B. Johnson, M.H. Devoret, S.M. Girvin and R. J. Schoelkopf. *Resolving photon number states in a superconducting circuit.* Nature, vol. 445, pages 515–518, 2007. (Cited on pages 111 and 127.)

[Shapere 1989] A. Shapere and F. Wilczek. Geometric phases in physics. World Scientific, 1989. (Cited on page 90.)

[Shapiro 2009] E.A. Shapiro, V. Milner and M. Shapiro. *Complete transfer of populations from a single state to a preselected superposition of states using piecewise adiabatic passage: Theory.* Phys. Rev. A, vol. 79, no. 2, page 023422, 2009. (Cited on page 31.)

[Shor 1994] P. W. Shor. *Algorithms for quantum computation: discrete logarithms and factoring.* In Proceedings, 35th Annual Symposium on Foundations of Computer Science, IEEE Press, Los Alamitos, CA, 1994. (Cited on pages 1 and 9.)

[Shor 1995] P. Shor. *Scheme for reducing decoherence in quantum memory.* Phys. Rev. A, vol. 52, pages 2493–2496, 1995. (Cited on page 122.)

[Slosser 1989] J.J. Slosser, P. Meystre and S.L. Braunstein. *Harmonic oscillator driven by a quantum current.* Phys. Rev. Lett., vol. 63, page 934, 1989. (Cited on pages 57 and 62.)

[Solano 2003] E. Solano, G.S. Agarwal and H. Walther. *Strong-Driving-Assisted Multipartite Entanglement in Cavity QED.* Phys. Rev. Lett., vol. 90, page 027903, 2003. (Cited on page 55.)

[Steane 1996] A. Steane. *Error Correcting Codes in Quantum Theory.* Phys. Rev. Lett, vol. 77, no. 5, 1996. (Cited on page 122.)

[Sugny 2007] D. Sugny, C. Kontz and H. R. Jauslin. *Time-optimal control of a two-level dissipative quantum system.* Phys. Rev. A, vol. 76, page 023419, Aug 2007. (Cited on pages 3 and 11.)

[Szegö 1967] G. Szegö. Orthogonal polynomials. American Mathematical Society, 1967. (Cited on pages 31 and 46.)

[Tan 1999] S.M. Tan. *A computational toolbox for quantum and atomic optics.* J. Opt. B, vol. 1, page 424, 1999. (Cited on page 79.)

[Teufel 2003] S. Teufel. Adiabatic perturbation theory in quantum dynamics. Springer, 2003. (Cited on pages 31, 46, 48, 50, 89 and 90.)

[Thomas 2005] S. Thomas, S. Guérin and H. R. Jauslin. *State-selective chirped adiabatic passage on dynamically laser-aligned molecules.* Phys. Rev. A, vol. 71, no. 1, page 013402, 2005. (Cited on pages 40 and 41.)

[Turinici 2001] G. Turinici and H. Rabitz. *Quantum wavefunction controllability.* Chemical Physics, vol. 267, no. 1-3, pages 1–9, 2001. (Cited on pages 3 and 11.)

[Turinici 2003] G. Turinici and H. Rabitz. *Wavefunction controllability for finite-dimensional bilinear quantum systems.* J. Phys. A, vol. 36, no. 10, page 2565, 2003. (Cited on page 27.)

[Turinici 2004] G. Turinici, V. Ramakhrishna, B. Li and H. Rabitz. *Optimal discrimination of multiple quantum systems: controllability analysis.* J. Phys. A, vol. 37, no. 1, page 273, 2004. (Cited on page 21.)

[Verstraete 2009] F. Verstraete, M. Wolf and I. Cirac. *Quantum computation, quantum state engineering, and quantum phase transitions driven by dissipation.* Nature physics, vol. 5, pages 633–636, 2009. (Cited on pages 4 and 12.)

[Villas-Bôas 2003] C.J. Villas-Bôas, F.R. de Paula, R.M. Serra and M.H.Y. Moussa. *Proposal to produce long-lived mesoscopic superpositions through an atom driven field interaction.* Journal of Optics B: Quantum and Semiclassical Optics, vol. 5, no. 5, page 391, 2003. (Cited on page 55.)

[Vitali 1998] D. Vitali, P. Tombesi and G.J. Milburn. *Quantum-state protection in cavities.* Phys. Rev. A, vol. 57, pages 4930–4944, 1998. (Cited on pages 115 and 123.)

[Vitanov 2001] N.V. Vitanov, T. Halfmann, B.W. Shore and K. Bergmann. *Laser-induced population transfer by adiabatic passage techniques: a review.* Annu. Rev. Phys. Chem., vol. 52, pages 763–809, 2001. (Cited on pages 31 and 36.)

[Wallraff 2005] A. Wallraff, D.I. Schuster, A. Blais, L. Frunzio, J. Majer, M. H. Devoret, S. M. Girvin and R. J. Schoelkopf. *Approaching Unit Visibility for Control of a Superconducting Qubit with Dispersive Readout.* Phys. Rev. Lett., vol. 95, page 060501, 2005. (Cited on page 110.)

[Warren 1993] W.S. Warren, H. Rabitz and M. Dahleh. *Coherent control of quantum dynamics: the dream is alive.* Science, vol. 259, pages 1581–1589, 1993. (Cited on page 18.)

[Weiner 2000] A.M. Weiner. *Femtosecond pulse shaping using spatial light modulators.* Review of Scientific Instruments, vol. 71, no. 5, pages 1929–1960, 2000. (Cited on page 34.)

[Werlang 2008] T. Werlang, R. Guzmán, F. O. Prado and C. J. Villas-Bôas. *Generation of decoherence free displaced squeezed states of radiation fields and a squeezed reservoir for atoms in cavity QED.* Phys. Rev. A, vol. 78, page 033820, Sep 2008. (Cited on page 57.)

[Will 2010] S. Will, T. Best, U. Schneider, L. Hackermüller, D.S. Lühmann and I. Bloch. *Time-resolved observation of coherent multi-body interactions in quantum phase revivals.* Nature (London), vol. 465, page 197, 2010. (Cited on page 55.)

[Wiseman 1993] H. M. Wiseman and G. J. Milburn. *Quantum theory of optical feedback via homodyne detection.* Phys. Rev. Lett., vol. 70, pages 548–551, Feb 1993. (Cited on pages 4 and 12.)

[Wiseman 1994] H.M. Wiseman. *Quantum theory of continuous feedback.* Physical Review A, vol. 49, pages 2133–50, 1994. (Cited on pages 4 and 12.)

[Wiseman 2009] H. Wiseman and Milburn G.J. Quantum measurement and control. Cambridge University Press, 2009. (Cited on pages 2 and 10.)

[Yatsenko 2002] L. P. Yatsenko, S. Guérin and H. R. Jauslin. *Topology of adiabatic passage.* Phys. Rev. A, vol. 65, no. 4, page 043407, 2002. (Cited on page 30.)

[Yurke 1986] B. Yurke and D. Stoler. *Generating quantum mechanical superpositions of macroscopically distinguishable states via amplitude dispersion.* Phys. Rev. Lett., vol. 57, page 13, 1986. (Cited on page 55.)

[Zhu 1998] W. Zhu, J. Botina and H. Rabitz. *Rapidly convergent iteration methods for quantum optimal control of population.* Journal of Chemical Physics, vol. 108, no. 5, pages 1953–1963, 1998. (Cited on pages 3 and 11.)

[Zippilli 2003] S. Zippilli, D. Vitali, P. Tombesi and J.M. Raimond. *Scheme for decoherence control in microwave cavities.* Phys. Rev. A, vol. 67, page 052101, 2003. (Cited on pages 115 and 123.)

[Zurek 1981] W.H. Zurek. *Pointer basis of quantum apparatus: Into what mixture does the wave packet collapse?* Phys. Rev. D, vol. 24, page 1516, 1981. (Cited on page 57.)

[Zurek 2003] W.H. Zurek. *Decoherence, einselection, and the quantum origins of the classical.* Rev. Mod. Phys., vol. 75, page 715, 2003. (Cited on page 57.)

Préparation et stabilisation de systèmes quantiques

Résumé: Cette thèse s'intéresse au problème de préparation et de stabilisation de systèmes quantiques. Nous considérons des modèles correspondant à des expériences actuelles en électrodynamique quantique en cavité, circuits Josephson, et de contrôle quantique cohérent par laser femtoseconde. Nous posons les problèmes dans le contexte de la théorie du contrôle et nous proposons des lois de commande qui préparent ou stabilisent des états cibles. En particulier, nous nous intéressons à des états cibles qui n'ont pas d'analogue classique: des états superpositions et intriqués. De plus, nous proposons une commande pour la stabilisation d'un sous-espace de l'espace des états, contribuant ainsi au domaine de la correction d'erreur quantique. Ces résultats ont été obtenu en étroite collaboration avec des expérimentateurs. Des mesures expérimentales préliminaires sont en bon accord avec certaines prédictions théoriques de cette thèse.
Mots clés: Contrôle quantique, préparation d'états, stabilisation, dissipation contrôlée, rétroaction quantique autonome, chat de Schrödinger, contrôle adiabatique, identification d'Hamiltonian, dimension infinie, fonction de Lyapunov.

Quantum state engineering and stabilization

Abstract: This thesis tackles the problem of preparing and stabilizing highly non classical states of quantum systems. We consider specific models based on current experiments in cavity quantum electrodynamics, Josephson circuits and ultra-fast coherent quantum control. The problem is posed in the framework of control theory where we search for a control law which prepares or stabilizes a desired target state. Of particular interest to us are target states with no classical analog: superposition and entangled states. More generally, we propose a scheme for the stabilization of a manifold of quantum states, thus introducing some new ideas for autonomous quantum error correction in a cavity. Close collaborations with experimentalists helped us in the design of control protocols which are readily employable in the laboratory. Experimental demonstrations are currently being implemented and preliminary measurements are in good agreement with the theory introduced in this thesis.
Keywords: Quantum control, state engineering, state stabilization, reservoir engineering, autonomous quantum feedback, Schrödinger cat state, adiabatic control, Hamiltonian identification, infinite dimensional, Lyapunov function.

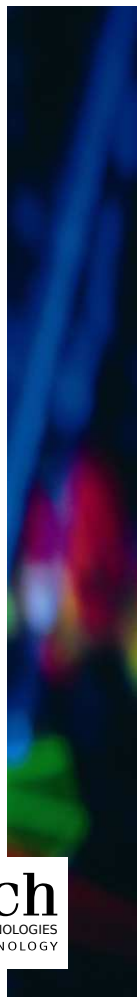

MINES ParisTech

ParisTech
INSTITUT DES SCIENCES ET TECHNOLOGIES
PARIS INSTITUTE OF TECHNOLOGY